UNIVERSITY OF SOUTHAMPTON

Paleomagnetic and Rock Magnetic Constraints on the Geodynamic Evolution of Sakhalin (NW Pacific)

Thesis submitted

by

Richard Weaver

for the degree

of

Doctor of Philosophy

FACULTY OF SCIENCE

SCHOOL OF OCEAN AND EARTH SCIENCE

26 July, 2002

UNIVERSITY OF SOUTHAMPTON

ABSTRACT

FACULTY OF SCIENCE
SCHOOL OF OCEAN AND EARTH SCIENCE

Doctor of Philosophy

PALEOMAGNETIC AND ROCK MAGNETIC CONSTRAINTS ON THE GEODYNAMIC EVOLUTION OF SAKHALIN (NW PACIFIC)

by Richard Weaver

Sakhalin is located in a tectonically complex region on the NW Pacific margin. Ancient subduction and accretion phases have affected Sakhalin, but Neogene to present-day deformation appears to have been accommodated by strike-slip faults, which transect Sakhalin from north to south. Fundamental questions are addressed in this study regarding the location of plate boundaries, the timing of the transition between tectonic regimes, the structural mechanisms of the transition, and the geodynamic evolution of Sakhalin. Paleomagnetic declination data from Sakhalin indicate rapid phases of Miocene clockwise vertical-axis crustal rotations. The data contradict published kinematic models that have been proposed to account for deformation in east and southwest Sakhalin. Analysis of paleomagnetic inclinations suggests that Sakhalin has remained near present-day latitudes throughout the Tertiary. Magnetic fabrics of Tertiary sedimentary rocks in Sakhalin have lineations that are regionally consistent and correspond to the direction of tectonic transport. Temporally consistent fabric orientations within regional structural domains are consistent with a plate model that includes the Okhotsk Sea, Eurasian, Amurian, Northern Honshu, Pacific, and North American plates. Many localities sampled in Sakhalin have been remagnetized. In most cases the mechanism for remagnetization is uncertain, although rock magnetic properties and microtextural relationships of Miocene mudstones from Okhta River indicate that a synfolding chemical remagnetization is carried by late diagenetic, nodular, pyrrhotite, which formed during a fluid migration event. Magnetic fabrics, paleomagnetic declinations, and remagnetization observations indicate significant Miocene or post-Miocene tectonic events, which may be associated with opening of the Japan Sea, Kuril Basin, and Tatar Strait Basin.

Declaration

I declare that this thesis is my own work and that my co-authors of submitted and published manuscripts have contributed in an advisory capacity. Appropriate acknowledgements are made in the text for the use of any results and diagrams that have previously been presented elsewhere. This thesis was completed wholly during full-time registered postgraduate canditature at the University of Southampton and is not substantially the same as any other work that has been, or is being, submitted for a degree or other qualification to any other university.

Richard Weaver

July 26, 2002

Acknowledgements

Many people have supported me greatly throughout this project. First of all, I want to thank Andrew Roberts for absolutely superb supervision and friendship throughout this project. His efforts reading my various manuscripts, advice on scientific writing, and probing questions, such as, "What age are these rocks?", and, "That's a bit visually jarring, isn't it?!" when asked to inspect yet another diagram, have given me confidence, a lot of insight, and many things to smile about. I thank David Macdonald and Rachel Flecker for giving me great feedback on papers that I have worked on and they have always given me encouragement.

After two successful field seasons, arranged by Cambridge Arctic Shelf Programme, in the Sakhalin bleakness, there are many people who made it memorable. David and Rachel with their lively and often amusing around-the-fire chats and stories. Andy for the '*Archbishop of Canterbury*' and teaching the ins-and-outs of paleomagnetic sampling in freezing cold streams. Sarah for being a good student friend and liquid consumption specialist. Eric for meticulous structural measurements, abnormally low heart rate, and excessive mineral-water intake, and Christine for calm organization, translation, and French chique. Fieldwork would not have been possible without logistical support from the Sakhalin Geological Expedition. I would particularly like to thank Pavel Kovtunovich for the partridge soup, '*bruces and sheilas*', and carrying large amounts of equipment, and Pietr Shegay for carrying even more stuff for paleomagnetic sampling. Zhenia Rasshchepkina for salmon fish cakes and 100 Russian words, and Vladimir Galversen for his cool and calm approach to field geology.

At home, technical support by Kevin Padley in the laboratory at the SOC was greatly appreciated. Wildly imaginative conversations about science fiction helped to break up many long days of measurements. I would like to thank my family for their support throughout, and acknowledge my many house mates and friends in the boat club for external relief. In the final lonely months, morning coffees with Dom Taunton and several late evening chats with Mike Sanders were great and kept me on an even keel.

Graduate School of the
Southampton Oceanography Centre

This PhD dissertation by

Richard Weaver

has been produced under the supervision of the following persons:

Supervisors:

Dr. Andrew P. Roberts (University of Southampton)

Dr. Rachel Flecker (Cambridge Arctic Shelf Programme, University of Cambridge, and University of Bristol)

Prof. David I. M. Macdonald (Cambridge Arctic Shelf Programme and University of Aberdeen)

Chair of Advisory Panel:

Prof. Alan E. S. Kemp (University of Southampton)

Member of Advisory Board:

Dr. Stephen Roberts (University of Southampton)

Examiners:

Dr. Tim A. Minshull (University of Southampton)

Dr. Ellen Platzman (University College London)

Contents

Bibliography

Chapter 4 Weaver, R., A. P. Roberts, R. Flecker, D. I. M. Macdonald, and L. M. Fot'yanova, Geodynamic implications of paleomagnetic data from Tertiary sediments in Sakhalin, Russia (NW Pacific), *J. Geophys. Res.*, 108, 2066, doi: 10.1029/ 2001JB001226, 2003.

Chapter 5 Weaver, R., A. P. Roberts, R. Flecker, and D. I. M. Macdonald, Tertiary geodynamics of Sakhalin (NW Pacific) from anisotropy of magnetic susceptibility fabrics and paleomagnetic data, manuscript submitted for publication, 2003.

Chapter 6 Weaver, R., A. P. Roberts, and A. J. Barker, A late diagenetic (synfolding) magnetization carried by pyrrhotite: Implications for paleomagnetic studies from magnetic iron sulphide-bearing sediments, *Earth Planet. Sci. Lett., 200*, 371-386, 2002.

1

Introduction

1. Rationale

The Sakhalin-Okhotsk Sea region of the NW Pacific margin remains a frontier region for geological and geophysical research (Figure 1.1). Even first-order features such as the locations of plate boundaries are uncertain (Figure 1.2a). The region is tectonically complex: Tertiary deformation in Sakhalin was accommodated by right-lateral transpression along N-S-trending strike-slip faults [*Jolivet et al.,* 1992; *Fournier et al,* 1994], whilst Mesozoic accretionary complex rocks exposed in Sakhalin indicate an ancient period of subduction [*Kimura,* 1994]. Lack of seismicity in the area means that the present-day plate tectonic configuration is difficult to determine (Figure 1.2a) [*DeMets,* 1992a; *Riegel et al.,* 1993; *Seno et al.,* 1996; *Takahashi et al.,* 1999], and the positions of boundaries between the Pacific, Eurasian, Okhotsk Sea, North American, and possible Northern Honshu and Amurian plates are not always clear [*Seno et al.,* 1996; *Takahashi et al.,* 1999]. It is also not clear exactly how the plates have evolved and interacted, and it is even not clear with which of these plates Sakhalin has evolved. Furthermore, deep-sea drilling has not been carried out in the Okhotsk Sea, which means there is a lack of important geological data, particularly regarding the age of the Okhotsk Sea sedimentary basins and the basement composition. The sedimentary basins are of interest for hydrocarbon exploration [*Lindquist,* 2000]. This paleomagnetic and rock magnetic study of Late Cretaceous–Tertiary sedimentary rocks from Sakhalin (Figure 1.2), provides new quantitative constraints on the tectonic evolution of the region.

1.1. Paleomagnetism

Paleomagnetism is an extremely useful tool for tectonic studies because paleomagnetic declinations reveal the amount of vertical-axis rotation of crustal blocks. Paleomagnetic declination data have successfully revealed vertical-axis rotations and have provided constraints on the timing and structural style of deformation in a number of regional tectonic studies, e.g., in New Zealand, California, Nevada, the Aegean Sea,

Israel, Bolivia, and the Philippines [*Ron et al.,* 1984; *Hornafius,* 1985; *Kamerling and Luyendyk,* 1985; *Luyendyk et al.,* 1985; *Nelson and Jones,* 1987; *Kissel and Laj,* 1988; *Fuller et al.,* 1989; *Roberts,* 1995a; *Lamb,* 2001]. The paleolatitude of crustal blocks can be constrained by the analysis of paleomagnetic inclination data [*Debiche et al.,* 1987; *Pechersky et al.,* 1997; Levashova et al., 1997, 1998; *Bazhenov et al.,* 1999; *Kravchinsky et al.,* 2002]. Apparent polar wander paths (APWPs) for stable continental and oceanic plates provide reference directions with which paleomagnetic data can be compared [*Besse and Courtillot,* 1991; *Gordon and Van der Voo,* 1995]. Thus, comparison of inclination data from Sakhalin with APWPs from the surrounding continents may provide constraints on the regional tectonic evolution. Until now only two small-scale paleomagnetic studies have been carried out in Sakhalin. *Takeuchi et al.* [1999] considered Tertiary paleomagnetic declination data from three localities in southwest Sakhalin, and suggested that clockwise vertical-axis rotations occur in 100-km-scale crustal blocks arranged in a domino formation. *Kodama et al.* [2000] used paleomagnetic data for magnetobiostratigraphic correlation of a Late Cretaceous sequence in south Sakhalin. These studies provide the only paleomagnetic constraints on the tectonic evolution of Sakhalin.

1.2. Rock magnetism

In paleomagnetic studies, it is important to establish that the natural remanent magnetization (NRM) is primary and that it is representative of the time-averaged geomagnetic field when the sediment was deposited [*Butler,* 1992]. Secondary magnetizations due to the chemical alteration of primary magnetic minerals can obscure and severely affect paleomagnetic results [*Van der Voo,* 1993]. Therefore, rock magnetic measurements provide valuable information about the magnetic mineralogy and the reliability of the paleomagnetic signal [*Dunlop,* 1995]. Rock magnetic measurements can help identify magnetic minerals, their grain sizes, and the effects of magnetic interactions among magnetic particles [*Dunlop,* 1995; *Dunlop and Özdemir,* 1997]. Primary and

secondary minerals can often be distinguished and the timing of remagnetization events may be established, e.g., due to tectonic events leading to mobilization of fluids or through diagenetic alteration [*McCabe and Elmore,* 1989; *Jackson,* 1990; *Channell and McCabe,* 1994].

Magnetic susceptibility is a rock-magnetic parameter, which can be measured to assess the relative contribution of ferrimagnetic (remanence-bearing), and paramagnetic and diamagnetic (rock-forming) minerals to the total susceptibility [*Banerjee et al.,* 1981; *Rochette,* 1987; *Hrouda and Kahan,* 1991; *Richter and Van der Pluijm,* 1994]. The magnetization of a rock depends on the alignment and distribution of minerals and can be anisotropic [e.g., *Fuller,* 1963]. The magnetic anisotropy can be quantified by measuring the anisotropy of magnetic susceptibility (AMS) or the anisotropy of anhysteretic or isothermal remanent magnetization (AARM or AIRM) [*Jackson,* 1991; *Borradaile and Henry,* 1997]. The AMS method is useful for identifying different phases of deformation in complex tectonic regions, because AMS fabrics can be related to tectonic stresses and strain [e.g., *Kissel et al.,* 1986; *Borradaile,* 1991; *Housen et al.,* 1995; *Sagnotti et al.,* 1999].

1.3. Aims

The overall aim of this work is to provide constraints on the tectonic evolution of the Sakhalin-Okhotsk Sea region. Based on paleomagnetic and rock magnetic techniques, the specific aim is to address fundamental questions regarding the geodynamic evolution of Sakhalin. 1) With which plates has Sakhalin interacted and evolved? 2) When did the transition from subduction to strike-slip tectonics occur in Sakhalin and what structural mechanism caused the transition? 3) Through what kinematic mechanisms did deformation take place? 4) Have there existed discrete domains of coherent rotational deformation?

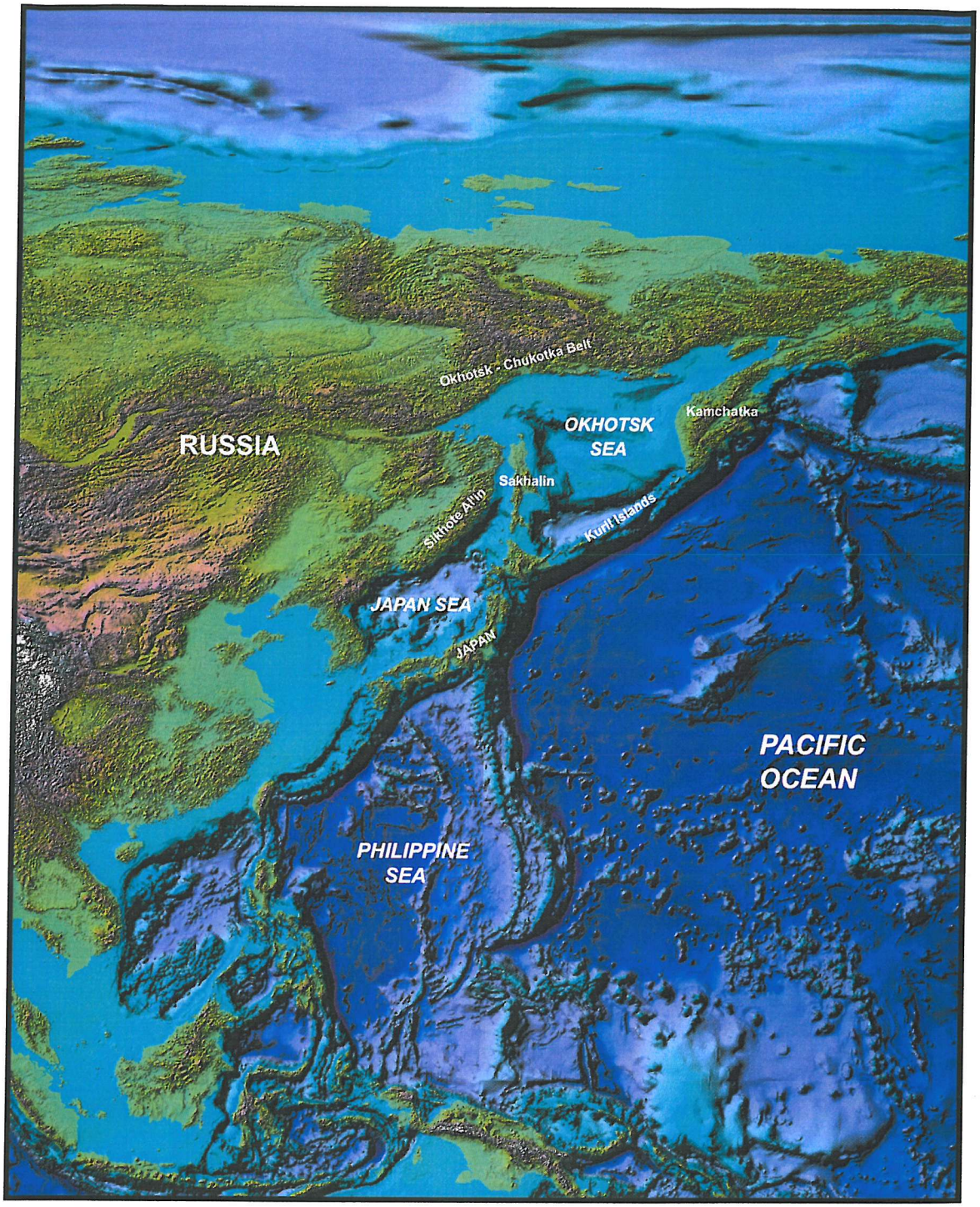

Figure 1.1. Regional topographic and bathymetric map of the Sakhalin-Okhotsk region and the northwest Pacific (provided by R. Flecker, Cambridge Arctic Shelf Programme, 2000).

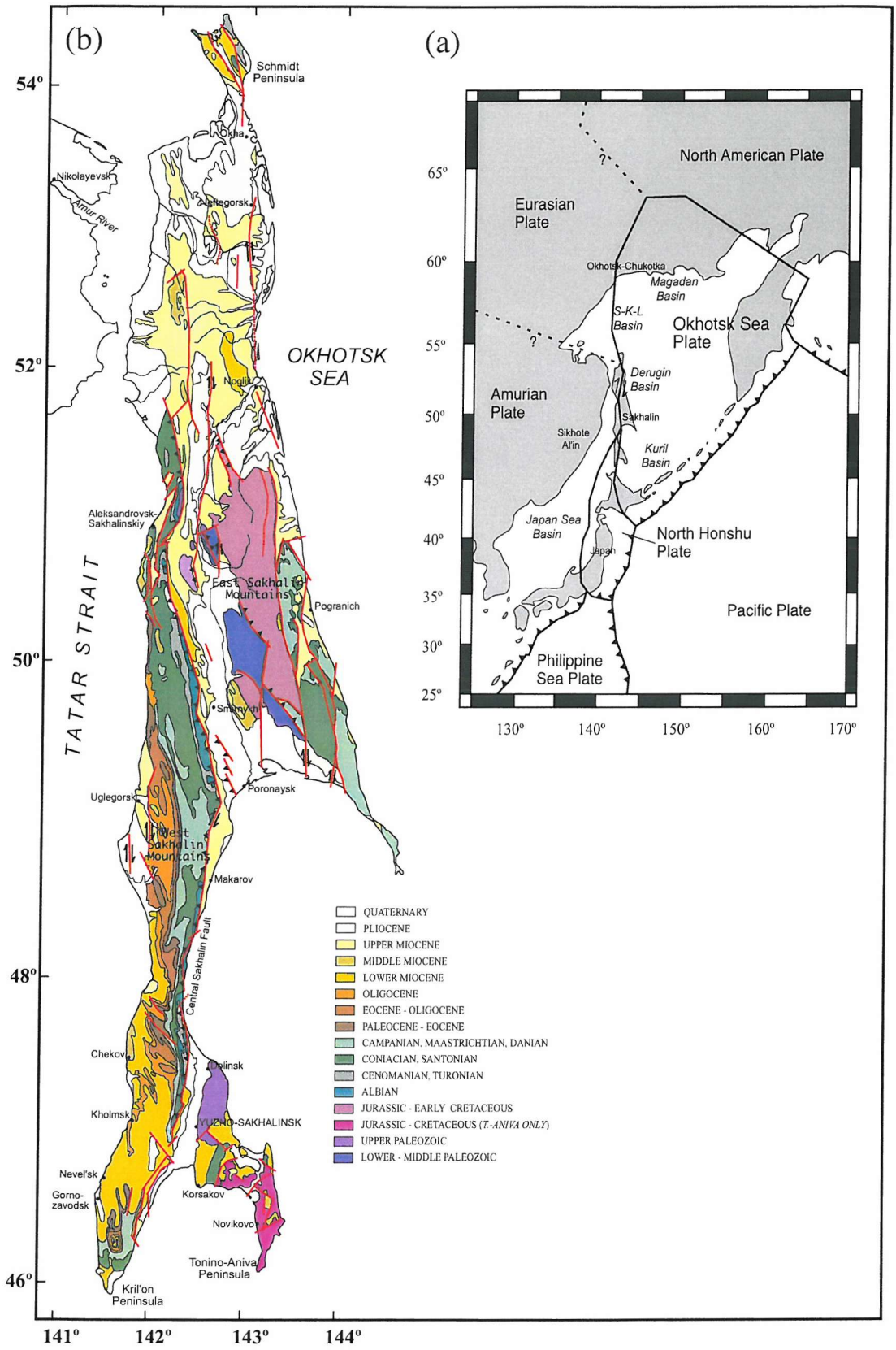

Figure 1.2. (a) Sketch map of the Okhotsk Sea region showing peripheral basins and plate boundaries proposed by *Takahashi et al.* [1999]. S-L-K: Shantar-Kashevarov-Lianskiy. (b) Geological map of Sakhalin. Compiled from various sources [*Vereshchagin,* 1969; *Rozhdestvenskiy,* 1982; *Kharakhinov,* 1983; *Fournier et al.,* 1994; *Ivashchenko et al.,* 1997].

2

Regional Geological Background

2. Regional Geology and Geodynamic Background

In order to appreciate the present level of understanding of regional tectonic evolution, a chronological summary of geological events from the Mesozoic to the Quaternary is presented in this chapter. It is important to point out that there are fundamental difficulties with Russian biostratigraphic correlation and dating because the Russian stratigraphic system has a different basis to the western system. For example, a poorly-dated stratigraphic section may be correlated to a different section of the same facies elsewhere with a much tighter age control [*R. Flecker and S. Inger,* Cambridge Arctic Shelf Programme, pers. comm., 1999]. This approach ignores lateral facies variations, and, therefore, the Russian literature may contain mis-dated geologic sections. In this study, the basic mappable unit is referred to as a "suite", which is consistent with Russian literature.

2.1. Jurassic - Early Eocene

2.1.1. Sakhalin Island Arc

Northeastern Russia is made up of many accreted terranes [*Parfenov and Natal'in,* 1986; *Zonenshain et al.,* 1990; *Zonenshain and Kuzmin,* 1997]. Sakhalin was also affected by accretionary events. Amongst the oldest mapped rocks on Sakhalin are Permian allochtonous rocks, which are part of the Susunay Complex on the Tonino-Aniva Peninsula (Figure 1.2b) [*Kimura et al.,* 1992a,b]. Within the southern part of the subduction complex, Triassic-Jurassic cherts, metavolcanics, and Cretaceous sands and clays typically exist in a sheared mass [*Zonenshain et al.,* 1990; *Kimura et al.,* 1992b; *D. I. M. Macdonald,* Cambridge Arctic Shelf Programme, *and Y. Mikhaelovitch,* Sakhalin Geological Expedition, pers. comm., 1999]. Greenschist- and blueschist-facies accretionary complex metamorphic rocks are also identified in the East Sakhalin Mountains and on the east Schmidt Peninsula to the north [*Zonenshain et al.,* 1990; *Voronova and Wardell,* 1991; *Kimura et al.,* 1992a]. Cretaceous sediments observed in

west Sakhalin (Figure 1.2b) are considered to be fore-arc basin deposits [*Zyabrev*, 1996; *Flecker et al.*, 1998]. Sandstones in the fore-arc basin indicate a volcanic arc provenance, with paleocurrent directions that clearly indicate that the source area lies to the west [*Zyabrev*, 1996]. The corresponding magmatic arc is thought to be the late Cretaceous-early Eocene (80–50 Ma) Sikhote Al'in volcanic belt on the Russian mainland [*Zonenshain et al.*, 1990; *Natal'in*, 1993]. Age relations of the mapped suites in the Susunay Complex and the East Sakhalin Mountains, thrust faults that dip to the west, and eastward-directed paleocurrents in the fore-arc basin are all consistent with westward subduction (Figure 1.2b, 2.1) [*Kimura et al.*, 1992a; *Flecker et al.*, 1998; *Macdonald and Flecker*, 1998].

During the latest Cretaceous and early Paleogene, considerable deformation occurred in the eastern Sakhalin and Hokkaido accretionary complexes [*Kimura*, 1994]. Rapid underplating [*Platt*, 1986] due to high influx of sediment to the trench caused the uplift of high-pressure and high-temperature metamorphic rocks, which caused doming and deformation in the accretionary complex and fore-arc basin [*Kimura*, 1994]. Deformation may also have been accommodated by collision of the "East Sakhalin Island Arc" (Figure 2.1) with Sikhote Al'in [*Zonenshain et al.*, 1990]. In Sakhalin, a widespread unconformity is present in the uppermost Cretaceous, which testifies to a marked period of deformation [*Macdonald and Flecker*, 1998].

The subducting plate in Sakhalin during the late Cretaceous seems to have been the Kula Plate [*Maruyama and Seno*, 1986; *Zonenshain et al.*, 1987; *Zonenshain et al.*, 1990], although more recent studies suggest that an Okhotsk Sea Plate, which could have contained far travelled "Okhotia" terranes proposed by *Zonenshain et al.* [1987], may have been subducting simultaneously in north Sakhalin and Chukotka [*Kimura*, 1994; *Baranov and Pristavakina*, 1997; *Gorbatov et al.*, 2000]. In Hokkaido, there is evidence of a reversal of subduction polarity in the mid-Cretaceous, but such a reversal appears not to have occurred in Sakhalin [*Kinimani and Kontani*, 1983; *Maruyama and Seno*, 1986]. The Kula-Pacific ridge subducted beneath northeast Asia at around 60 Ma, before

Pacific Plate subduction commenced in the region [e.g., *Maruyama and Seno,* 1986; *Maeda,* 1990]. At around the same time the exotic Okhotia massifs [*Zonenshain and Kuzmin,* 1997] had accreted to the Asian continent to the north, and new subduction zones became established south of the Okhotia massifs east of Sakhalin and Kamchatka [*Maruyama and Seno,* 1986; *Zonenshain et al.,* 1987; *Zonenshain and Kuzmin,* 1997]. This is consistent with a change in direction of Kula Plate motion at around 55 Ma [*Lonsdale,* 1988]. The lesser Kuril arc probably formed at the southern end of the Okhotia massifs with the onset of subduction [*Maeda,* 1990]. Details of the timing and mechanism of these plate transitions, and details of the terrane trajectories, remain unresolved because of the absence of paleomagnetic data sets. *Kimura et al.* [1983] suggested that oblique collisional tectonics may have commenced in the Paleogene.

2.1.2. Mongol-Okhotsk Suture

The Mongol-Okhotsk Suture and the Amur Suture (Figure 2.2) to the west of Sakhalin are remnants of Mesozoic accretion on the east of the Russian continent [*Parfenov and Natal'in,* 1986; *Natal'in,* 1993]. The Mongol-Okhotsk suture stretches across southeastern Siberia from the northern Okhotsk Sea in the east to northern Mongolia in the west (Figure 2.2). The suture formed during the Late Jurassic to Early Cretaceous by collision of the Bureyinskiy Massif with the Siberian Platform [*Zonenshain et al.,* 1990; *Natal'in,* 1993; *Bazhenova et al.,* 1995]. A wide belt of Jurassic greenschist metamorphics can be identified from west to east [*Zonenshain et al.,* 1990]. Evidence of intraplate magmatism is manifest in numerous granitic batholiths in the northern part of the belt, which probably formed in response to crustal thickening and subsequent formation of melts [*Zonenshain et al.,* 1990]. Magmatic arc volcanics in the Uda-Murgalsk belt in the northeast range in age from 200-70 Ma [*Natal'in,* 1993]. The massifs to the south of the suture consist of accreted exotic blocks with ages ranging from Devonian to Triassic. These rocks have been juxtaposed at the margin of the suture, evidently through continental collision [*Zonenshain et al.,* 1990; *Natal'in,* 1993]. The

"Amur microcontinental plate" or Amurian Plate is commonly used to refer to the collection of accreted terranes in the area south of the Mongol-Okhotsk suture [*Zonenshain et al.,* 1990; *Natal'in,* 1993; *Worrall et al.,* 1996]. The considerable width of the Amurian Plate-Siberian Craton continent-continent margin (Figure 2.2) indicates that a large amount of oceanic crust must have been subducted [*Bazhenova et al.,* 1995; *Van der Voo et al.,* 1999]. Intraplate magmatism, which becomes younger from Permian in the west to Early Cretaceous in the east, suggests a northeastward oblique collision between plates [*Zonenshain et al.,* 1990; *Bazhenova et al.,* 1995]. A recent paleomagnetic study of exotic and stable blocks from the Baikal region supports the geological evidence of a Mongol-Okhotsk ocean betweeen Amuria and Siberia during the Permian to Early Cretaceous [*Kravchinsky et al.,* 2002].

2.1.3. Amur Suture

A second suture, the Amur suture, formed to the southeast in the Sikhote Al'in region in the Cretaceous (Figure 2.2) [*Natal'in,* 1993]. A volcanic chain lies to the northwest of the suture together with an accretionary wedge of mélange and imbricate-stacked Early Cretaceous turbidites [*Natal'in,* 1993]. Subsequent accretion of terranes, which constitute much of Sikhote Al'in, caused suturing along the active margin [*Natal'in,* 1993; *Bazhenova et al.,* 1995]. Late Cretaceous-Paleogene volcanic rocks in Sikhote Al'in were emplaced during a separate subduction event [*Zonenshain et al.,* 1990; *Bazhenova et al.,* 1995]. A schematic reconstruction of these events, as proposed by *Bazhenova et al.* [1995], is shown in Figure 2.3.

2.1.4. Okhotsk

Along the northern margin of the Okhotsk Sea, the Okhotsk-Chukotka volcanic belt (Figure 1.1, 1.2a) was active in the Late Cretaceous [*Zonenshain,* 1990]. The belt marks the ancient active continental margin in northeast Russia, and geochemical evidence indicates that it had similar characteristics to the present-day Andean active

margin [*Zonenshain et al.,* 1990]. Dredged samples from the Academy of Sciences Rise and the Institute of Oceanology Rise in the centre of the Okhotsk Sea suggest that the basement may be part of a Cretaceous to early Paleogene island arc complex [*Savostin et al.,* 1983; *Baranov and Pristavakina,* 1997]. Angular clasts and poor sorting in sea-floor samples indicate that there may be a proximal sediment source, although the possibility of glacial deposition cannot be ruled out. The surrounding arc terranes could also have acted as a source [*Baranov and Pristavakina,* 1997]. *Worrall et al.* [1996] speculated that the basement highs in the Okhotsk Sea represent a southern extension of the northeast Russian terranes, which accreted against east Asia in the Mesozoic. *Zonenshain et al.* [1987] suggested that "Okhotia" exotic blocks arrived at the margin at around 70-50 Ma. An extensive drilling program is necessary to resolve these issues.

2.2. Mid Eocene

The northward collision of the Indian Plate with the Eurasian Plate during the middle Eocene was a major tectonic event [e.g., *Yin and Harrison,* 2000]. Thrust tectonics in the Himalayas, sinistral strike-slip deformation in China, and pull-apart extensional tectonics in the Baikal region in Russia are thought to have originated from the northward collision of India into Asia [*Tapponnier and Molnar,* 1976, 1977, 1979; *Peltzer and Tapponnier,* 1988]. The resultant deformation has been modelled through analogue indentation and extrusion models [*Tapponnier and Molnar,* 1976; *Tapponnier et al.,* 1982; *Peltzer and Tapponnier,* 1988]. It has also been proposed that the Baikal shear zone could be connected eastward by a left-lateral strike-slip fault (Figure 2.4) to the Stanovoi fault and the Shantar and Lianskiy fault systems (Figure 1.2a) in the northern Okhotsk Sea [*Worrall et al.,* 1996]. A system of N-S-striking dextral strike-slip faults, such as the faults that transect Sakhalin, has been reproduced in other India-Eurasia collision models and it has been suggested that many of the marginal sedimentary western Pacific basins formed due to these faults [*Jolivet et al.,* 1990; *Worrall et al.,* 1996]. However, a conflicting fault geometry in the northeast Baikal rift

zone, which comprises NE-trending *en echelon* normal fault segments, suggests that strike-slip fault propagation to the east is unlikely to have occurred [*Tapponnier and Molnar,* 1979; *San'kov et al.,* 2000]. Furthermore, satellite images do not clearly indicate an eastward continuation of the Baikal fault system [*Tapponnier and Molnar,* 1979]. The plastic deformation model proposed by *Molnar and Tapponnier* [1977] suggests a gradual change in stress that might explain the lack of observable deformation in northeast Asia. *Zonenshain and Savostin* [1981] suggested that the Baikal rift deformation does not extend further to the east because of the rigid motion of the Amurian plate toward Siberia. The large number of (micro-)plates and tectonic blocks (with different affinities) that interact in northeast Asia suggests that both plastic and rigid plate characteristics probably contributed to the overall deformation [*Parfenov and Natal'in,* 1986; *Molnar,* 1988]. Such complexity in northeast Asia may explain contradictions regarding the timing of basin formation and the interpretations of deformation mechanisms [*Worrall et al.,* 1996; *Allen et al.,* 1998; *Flecker and Macdonald,* 2002].

Problems with the suggested mechanism for the opening of the Japan Sea emphasizes the complexities concerning interpretations of timing of the faulting and basin formation [*Otofuji et al.,* 1991; *Jolivet and Tamaki,* 1992]. Extensive paleomagnetic data from Tertiary formations in NE and SW Japan indicate rapid vertical-axis rotations that were most likely associated with opening of the Japan Sea [*Otofuji et al.,* 1991, 1994]. NE Japan rotated about 46° counterclockwise between 20 and 12 Ma, whilst SW Japan rotated around 40° clockwise between 16.1 and 14.2 Ma (Figure 2.5). Vertical-axis rotations on this scale cannot be expected to occur solely due to motion on N-S-trending strike-slip faults along the Pacific margin (Figure 2.6) [*Jolivet et al.,* 1994]. At minimum, conjugate fault sets should be generated to satisfy basic kinematic requirements for vertical-axis rotations in *en echelon* fault zones [*Nur et al.,* 1989]. Furthermore, if these faults were generated as a result of a middle Eocene India-Eurasia collision [*Jolivet et al.,* 1990], there is about 25 m.y. of time before deformation

manifested itself along the Pacific margin in the proposed pull-apart origin of the Japan Sea [*Jolivet et al.,* 1991, 1994]. Further south, the formation of the marginal Bohai Basin in China pre-dates the India-Eurasia collision [*Allen et al.,* 1998]. Trench roll-back at the Pacific-Eurasia plate boundary is the preferred mechanism to explain the development of the Bohai Basin [*Watson et al.,* 1987; *Allen et al.,* 1998]. It is questionable, therefore, whether far-field effects of the India-Eurasia collision could have had a significant influence on events in NE Asia and the Pacific margin [*Jolivet et al.,* 1990; *Worrall et al.,* 1996]. It appears that local plate interactions, such as oblique collision of the Okhotsk Sea Plate with the Eurasian Plate, may have had a much greater influence on deformation in the region than the India-Eurasia collision event.

The wider impact of the India-Eurasia collision is also questioned by *Norton* [1995]. A substantial 60° change in trend occurred on the Emperor-Hawaii hotspot tracks at 43 Ma, a time that is often linked with major geological events (e.g., the India-Eurasia collision) [*Engebretsen et al.,* 1984; *Worrall et al.,* 1996]. Oceanic fracture zone data presented by *Norton* [1995] were used to show that the "43 Ma event" does not actually exist. Based on the fracture zone data, there appears to be no change in relative plate motion of the Pacific Plate, which suggests that the Hawaii seamount bend is probably due to a non-stationary hotspot [*Molnar and Stock,* 1987; *Norton,* 1995; *Tarduno and Cottrell,* 1997]. It is therefore inappropriate to attribute widespread geological events to a "43 Ma reshuffle", and a wider geodynamic link between the Pacific Plate, Eurasia, and India, through the India-Eurasia collision, appears unlikely. Consistent evidence from geodynamic models suggests that the India-Eurasia collision has had negligible influence on the global plate configuration [*Richards and Lithgow-Bertelloni,* 1996].

2.3. Late Eocene – Early Oligocene

In Sakhalin, late Eocene-early Oligocene conglomerate clasts with an accretionary complex origin appear to have had a source to the west [*Macdonald and Flecker,* 1998]. This suggests that the clasts were not derived from the uplifted local

Jurassic-Cretaceous complexes in east Sakhalin, but must have been channelled from Sikhote Al'in to the west [*Flecker and Macdonald,* 2002]. A fan-delta or a fluvial braided plain depositional environment has been interpreted for the central-western areas of Sakhalin, and paleocurrent data indicate that sediment supply was consistently from the west [*Macdonald and Flecker,* 1998].

Worrall et al. [1996] suggested that formation of the Magadan basin in the northern Okhotsk Sea (Figure1.2a) commenced in the late Eocene. This is based on syn-deformational relationships identified in seismic sections, in which the presence of listric boundary faults (with a WNW trend) were also interpreted [*Worrall et al.,* 1996]. However, it is possible that the listric shape of these faults is not real. The majority of seismically active faults are planar with dips between 30° and 60°. The listric shape can only occur as a result of subsequent fault activity and interaction [*Allen and Allen*, 1990; *Jackson*, 1987]. Poor migration of the seismic traces could account for a misleading curved shape to deep reflectors [*Sheriff and Geldart*, 1995]. The quality of the seismic data is not clear and there are few well ties to provide additional information. The timing of formation of this basin is therefore uncertain.

2.4. Late Oligocene

Biosiliceous mudstones were extensively deposited in Sakhalin during the late Oligocene and appear to be associated with relatively high sea levels [*Macdonald and Flecker*, 1998]. These sediments are hydrocarbon source rocks which are the subject of ongoing exploration in the region.

A basaltic-andesite sample from Aleksandrovsk-Sakhalinskiy (Figure 1.2b) was found to have a subduction-related signature based on petrographic and geochemical data [*Flecker and Macdonald,* 1997]. These rocks are likely to have formed from contaminated mantle lithosphere in a supra-subduction zone setting [*Flecker and Macdonald*, 1997]. The results indicate that subduction may have continued under Sakhalin beyond the Cretaceous, through the Paleogene and possibly into the Neogene

[*Flecker and Macdonald,* 1997]. This contradicts the views of *Worrall et al.* [1996] who suggested that the volcanics were related to extension and that subduction ceased at the Cretaceous-Tertiary boundary. Tuffaceous rocks crop out further south at Kholmsk [*Macdonald and Flecker*, 1998], which might indicate that subduction persisted in the area.

Syn-deformational sedimentation is thought to have been ongoing in the Magadan Basin in the late Oligocene (Figure 1.2a), and NE-trending extensional faults were probably active (possibly from the latest Eocene) in the Shantar-Kashevarov-Lianskiy sedimentary basins in the northwest Okhotsk Sea [*Worrall et al.,* 1996]. The basins have been interpreted to have a pull-apart origin, with a "lazy S" pattern of the bounding faults [*Allen and Allen*, 1990; *Worrall et al.,* 1996]. There is evidence of extensional tectonics in other parts of the region, notably around Japan, where paleostress indicators point to dextral transtension [*Jolivet et al.,* 1991; *Worrall et al.,* 1996].

Initial rifting of the Kuril Basin in the southern Okhotsk Sea (Figure 1.2a) may have commenced at the end of the late Oligocene, and is often assumed to be closely related to opening of the Japan Sea [*Kimura and Tamaki,* 1986; *Fournier et al.,* 1994; *Jolivet et al.,* 1994]. Seismic velocity data and moderate heat flow values from the Kuril Basin suggest that it is underlain by oceanic crust [*Baranov and Pristavakina,* 1997]. Ocean drilling has not been carried out in the Kuril Basin and linear marine magnetic anomalies have not been identified, which means that the timing of rifting of this back-arc basin is highly uncertain [*Baranov and Pristavakina,* 1997]. *Maeda* [1990] suggests that the Kuril Basin opened in the early Miocene because west-directed subduction of the Pacific Plate was ongoing in central Hokkaido. Seismic reflection data from the northern part of the Okhotsk Sea have been interpreted to indicate an early Miocene unconformity, which may have been connected with rifting and opening of the Kuril Basin [*Baranov and Pristavakina,* 1997]. However, because the seismic stratigraphy has been correlated to only a selection of drilled cores from the region [*Baranov and*

Pristavakina, 1997], ambiguity remains concerning the age of many reflectors, particularly in areas distant from drilled wells, such as the Kuril Basin.

2.5. Early Miocene

The timing of opening of the Japan Sea is indicated by the oldest age of oceanic basalts in the area. ^{40}Ar-^{39}Ar dating indicates an age of 24-17 Ma for this event [*Tamaki et al.,* 1992]. The tectonic regimes were transpressional in Sakhalin and Hokkaido, with transtension in south Japan where the Pacific Plate was subducting under the Eurasian Plate [*Jolivet et al.,* 1991; *Fournier et al.,* 1994]. It is likely that this was a late phase of subduction ("Mariana" type) with weak coupling between plates, which would have allowed extension in the back-arc region [*Uyeda,* 1982].

According to *Worrall et al.* [1996], activity began on N-S-trending, near-vertical strike-slip faults during the early Miocene in the Sakhalin offshore area. This constrains the geometries of sedimentary basins located to the north and east of Sakhalin. The Derugin Basin (Figure 1.2a) is an example where dextral strike-slip faults were interpreted to cross-cut the pre-existing Shantar-Kashevarov-Lianskiy faults, thereby causing tectonic inversion of the sediment pile [*Worrall et al.,* 1996]. There is no convincing onshore evidence of such an inversion in Sakhalin [*R. Flecker,* University of Cambridge, pers. comm., 2000]. This provides further uncertainty concerning the age interpretations of *Worrall et al.* [1996].

During the Aquitanian in Sakhalin, further volcanic tuffs were deposited in southern areas and subduction-related andesites [*R. Flecker,* University of Cambridge, pers. comm., 2000] crop out in the far south of the island [*Macdonald and Flecker,* 1998; *Flecker et al.,* 1998]. Early Miocene fan-delta deposits are found in central-west Sakhalin and the source of sediment, which contains accretionary complex detritus, was located to the west [*Macdonald and Flecker*, 1998]. Around Makarov, there are andesitic volcanics and N-S-trending basalt intrusive rocks, which have been linked to rifting of the Japan Sea and opening of the Kuril Basin [*Takeuchi,* 1997]. K-Ar-dated samples from Chekov

and Makarov in Sakhalin [*Takeuchi,* 1997] together with samples from Uglegorsk (Sakhalin) and Hokkaido (Japan) suggest that the age of the igneous rocks becomes progressively younger toward the south. The apparent southward migration of volcanism has been explained by a corresponding southward displacement of the Kuril Basin spreading centre along dextral strike-slip faults that were active in Sakhalin [*Takeuchi,* 1997; *Takeuchi et al.,* 1999]. This interpretation of events assumes that the Kuril Basin opened with a NE-SW spreading axis due to subduction-induced tension in the back-arc region [*Uyeda,* 1982; *Takeuchi et al.,* 1999].

However, the mechanism(s) for the opening of the Kuril Basin are still unclear [e.g., *Baranov et al.,* 1997]. Normal faults that are usually associated with arc-parallel back-arc basin opening could not be identified in seismic sections [*Baranov and Pristavakina,* 1997], but dextral offsets along near-vertical fault segments on the northern margin of the Kuril Basin were observed, which led *Baranov and Pristavakina* [1997] to propose an alternative model involving NE-SW strike-slip and a pull-apart mechanism for the opening of the Kuril Basin. The pull-apart model is consistent with NW-SE-trending extensional faults in central and northern parts of the Okhotsk Sea and suggests that opening occurred by counterclockwise rotation of the Okhotsk Sea relative to east Sakhalin [*Baranov and Pristavakina,* 1997]. However, this model fails to accommodate the different types of crust underlying the Okhtosk Sea, which comprise the Okhotsk Sea Plate [e.g., *Savostin et al.,* 1983].

A different model for the Kuril Basin opening suggests that the Okhotsk Sea Plate rotated clockwise about a pole located to the south of Kamchatka, which caused tension and subsequent basin formation near the Okhotsk Sea Plate-Pacific Plate boundary [*Kimura and Tamaki,* 1986]. This model was proposed in order to explain the fan-shaped geometry of the Kuril Basin. Recent studies of present-day regional plate motions that are constrained by seismological data support the idea of rigid clockwise rotation of the Okhotsk Sea Plate, although the present-day pole of rotation is probably located in northern Sakhalin [*Kimura and Tamaki,* 1986; *Seno et al.,* 1996; *Heki et al.,*

1999; *Takahashi et al.,* 1999]. The actual opening mechanism for the Kuril Basin may require a combination of the kinematic elements outlined in the above models.

In the Burdigalian, there was a relatively low sea level [*Haq et al.,* 1987; *Macdonald and Flecker,* 1998]. Volcanism persisted in southern Sakhalin on the Kril'on Peninsula [*Macdonald and Flecker,* 1998]. Reworked volcaniclastics and pyroclastic flows in the same locality at Kuznetsova appear to have been deposited in a shallow marine environment, with westward directed paleocurrents, which suggests that the Tatar Strait was open at that time [*Flecker et al.,* 1998]. In areas protected from clastic sedimentation, biosiliceous rocks are dominant and relatively clean sands, which are thought to originate from the paleo-Amur River to the west, are found in the Dagi area [*Flecker et al.,* 1998; *Macdonald and Flecker,* 1998].

2.6. Middle Miocene

In central Sakhalin, on the southern fringe of the paleo-Amur delta plain, the Sertunay Suite was deposited, which appears to have excellent hydrocarbon reservoir potential [*Hyden et al.,* 1997]. A roughly NE-SW-trending high-standing linear structure in central Sakhalin, known as the Mingin structure, appears to have controlled the sediment distribution in northern Sakhalin and probably limited the southward progradation of the paleo-Amur delta [*Macdonald and Flecker,* 1998; *Flecker and Macdonald,* 2002]. North of the structure, accretionary complex material is seen in Amur detritus [*D. I. M. Macdonald,* University of Aberdeen, pers. comm., 2000]. Elsewhere, biosiliceous rocks are abundant [*Macdonald and Flecker,* 1998], and this sedimentation coincides with the Pacific Rim climatic optimum for biosiliceous productivity [*Ingle,* 1981]. A change in paleocurrent directions near Aleksandrovsk-Sakhalinskiy, from broadly eastward to WSW-ward, indicates that the delta distribution might be controlled by the Mingin structure [*Flecker et al.,* 1998; *Macdonald and Flecker,* 1998]. Gravity and magnetic anomalies also have dextral offsets across the Mingin structure [*Flecker and Macdonald,* 1998].

In the middle Miocene, dextral strike-slip motion initiated on N-S-trending faults, which run through Sakhalin and Hokkaido [*Fournier et al.,* 1994]. Significant fault systems include the Tym-Poronay-Hidaka shear zone, which extends through Sakhalin and into central Hokkaido, the East Sakhalin-Abashiri shear zone off the east coast of Sakhalin and the West Sakhalin Fault in the Tatar Strait [*Rozhdestvenskiy,* 1982; *Kharakhinov et al.,* 1985; *Worrall et al.,* 1996].

The Japan Sea continued to open throughout the middle Miocene [*Tamaki et al.,* 1992]. At 15 Ma, basin subsidence was at a maximum [*Ingle,* 1992] and rates of vertical-axis rotation of NE and SW Japan (based on paleomagnetic data) reached a maximum [*Otofuji et al.,* 1991, 1994]. The duration of the rotation, particularly for the SW Japan arc, is bracketed within a 1-2 Ma period in the middle Miocene [*Otofuji et al.,* 1991, 1994; *Otofuji,* 1996]. *Jolivet et al.* [1994] argued that this period was too short if rotation is assumed to have been directly caused by opening of the Japan Basin. This is because *Tamaki et al.* [1992] argued that opening of the Japan Basin commenced at 24 Ma, based on the age of oceanic basalts. There must have been additional local deformation within the Japan arc, in order to produce the observed large (up to 50°) and rapid vertical-axis rotations. This deformation has been ignored by *Otofuji et al.* [1991, 1994] and *Otofuji* [1996], who proposed a "bar door" opening mechanism for the Japan Sea (Figure 2.5), and *Jolivet et al.* [1994], who suggested a strike-slip fault-based mechanism (Figure 2.6). *Altis* [1999] proposed an Okhotsk-Eurasia indentation and extrusion model with block rotations in order to accommodate the rotation of SW Japan (Figure 2.7).

In central Hokkaido [*Kimura et al.,* 1983], significant mountain-building took place with compressional stresses arising from the Kuril arc junction [*Niitsuma and Akiba,* 1985]. Conglomerates, which were deposited as a result of this mountain-building phase, become younger from 15 to 13 Ma toward the south and indicate that the Kuril arc junction may have had a southward relative motion [*Niitsuma and Akiba,* 1985]. Volcanic rocks associated with the Kuril volcanic front also appear to young toward the south, which supports the idea of mobility of the Kuril arc [*Niitsuma and Akiba,* 1985;

Takeuchi, 1997]. An angular unconformity in east Hokkaido may indicate that the Kuril Basin opened between 15 and 12 Ma [*Niitsuma and Akiba,* 1985; *Jolivet et al.,* 1994]. *Maeda* [1990] suggests a rapid 16-15 Ma opening of the Kuril Basin. The most convincing evidence is based on the isotopic composition of basalts exposed in an extensional graben in northern Hokkaido, which indicates a characteristic back-arc composition [*Ikeda et al.,* 2000]. The age of the basalts suggest that the Kuril Basin opening had ceased by 9-7 Ma, but deep-sea drilling is required to verify the exact ages of the basin [*Ikeda et al.,* 2000]. The overall evidence points toward an arc-parallel spreading mechanism and southward migration of the ridge.

2.7. Late Miocene

Deformation continued in south Sakhalin and on the Schmidt Peninsula in the late Miocene [*Macdonald and Flecker,* 1998]. Biosiliceous sediments were deposited in abundance [*Flecker and Macdonald,* 1998; *Macdonald and Flecker,* 1998], while latest Miocene fan and delta deposits occur in the north and good reservoir sandstones crop out in the central part of the northern area [*Macdonald and Flecker,* 1998]. Good potential hydrocarbon source rocks occur on Schmidt Peninsula [*Hyden et al.,* 1997].

In the Japan Sea, the ^{40}Ar-^{39}Ar age of the youngest oceanic basalts is 11 Ma, which indicates the end of the opening of the Japan Sea [*Tamaki et al.,* 1992]. Basin subsidence ceased and western northeast Japan began to uplift [*Ingle,* 1992; *Jolivet and Tamaki,* 1992; *Fournier et al.,* 1994]. The stress regime in northeast Japan changed from being extensional with σ_{Hmax} trending NNE to an E-W-trending compressional regime, based on data from faults and dyke swarms [*Nakamura and Uyeda,* 1980; *Fournier et al.,* 1994]. The significantly reduced subsidence in Japan and E-W compression represents an early stage of Pacific Plate subduction with strong coupling between the downgoing and over-riding plates [*Uyeda,* 1982].

2.8. Pliocene – Quaternary

Oblique subduction of the Pacific Plate under the Kuril arc close to Japan is believed to have caused strain partitioning and detachment of a fore-arc sliver, with arc-parallel dextral strike-slip faults on the trench-side of the volcanic arc (Figure 2.8) [*Kimura,* 1986]. The fore-arc blocks appear to have been translated toward Japan and probably rotated in accordance with the partitioned component directions of the plate motion vector (Figure 2.8) [*Kimura,* 1986; *Beck,* 1989; *DeMets,* 1992a,b]. Such a mechanism might explain the uplift and collision tectonics in the Hidaka Mountains (NE Hokkaido) and is relatively common in zones of oblique subduction [*Kimura,* 1986; *Beck,* 1989]. Elsewhere in northern Japan, E-W compression persisted parallel to the convergence direction of the Pacific Plate [*Nakamura and Uyeda,* 1980; *Jolivet et al.,* 1994]. Rapid subsidence of the Kuril Basin during the Pliocene is thought to have occurred by downward bending of the crust due to Pacific Plate subduction-related compressional stresses [*Baranov et al.,* 2002].

The Sakhalin deltaic sediments pass upward into terrestrial facies in the Pliocene. This indicates that the delta was extending eastward, but exactly how far east cannot be constrained from onshore evidence [*Macdonald and Flecker,* 1998]. Positive gravity and magnetic anomalies indicate that there could be a structural buffer offshore of northeastern Sakhalin [*Flecker and Macdonald,* 1998], which would prevent sand deposition further east. Deformation in Sakhalin is ongoing and seismological evidence indicates dextral transpression on N-S-trending strike-slip faults [*Fournier et al.,* 1994]. The most recent earthquake in Sakhalin occurred near the northern town of Neftegorsk in 1995 and resulted in dextral strike-slip fault plane solutions [*Ivashchenko et al.,* 1997; *Arefiev et al.,* 2000].

2.9. Summary

A number of geological events are thought to have been significant in the overall development of the Sakhalin-Okhotsk Sea region. 1) Late Mesozoic subduction under

Sakhalin and subsequent uplift of accretionary complex rocks. 2) Ancient tectonic blocks that have been transported from the south to the Okhotsk Sea and northeast Russian margin. 3) Oligocene to Miocene opening of marginal basins, e.g., the Kuril, Magadan, Derugin, Tatar Strait, and Japan Sea basins. 4) Neogene activity on N-S-trending right-lateral strike-slip faults. 5) Present-day NE-SW-directed dextral transpression. However, it is unclear how these events are related to each other because the dynamic and kinematic mechanisms of the deformation have not been established. The most controversial points mentioned above concern the extent to which the deformation can be considered to be plastic or rigid. For instance, is the formation of basins along eastern Asia due to eastward extrusion due to the India-Eurasia collision and subsequent strike-slip faulting, or, have the Amurian and Okhotsk Sea plates behaved as rigid boundaries to such defromation? Did the opening of the Kuril Basin take place by rifting due to rigid rotation of the Okhotsk Sea Plate, or, did opening take place by lithospheric thinning parallel to the backarc and southward migration along the Sakhalin shear zone? Only two studies consider the deformation in Sakhalin, based on quantitative field data [*Fournier et al.,* 1994; *Takeuchi et al.,* 1999].

NE-SW-directed transpression in Sakhalin has been accommodated by large-scale N-S-trending strike-slip faults since the Neogene [*Fournier et al.,* 1994] and is thought to have occurred by relative motion of the Okhotsk Sea Plate and the Amurian Plate [e.g., *Altis,* 1999]. *Fournier et al.* [1994] identified a number of subsidiary NNE-SSW-striking right-lateral strike-slip faults in the East Sakhalin Mountains and proposed a model for the deformation that involves counterclockwise-rotating blocks [e.g., *Garfunkel,* 1989; *Piper et al.,* 1997]. However, the nature and strength of the lithosphere beneath Sakhalin and the Okhotsk Sea is not known, and, thus, it is not certain whether the crust is strong and whether friction-associated stresses can account for deformation at the proposed 200-300 km scale [*Sonder and England,* 1986; *Maggi et al.,* 2000]. The dimensions of the Sakhalin-Hokkaido shear zone are 1500 km in length by ~300-400 km in width, which suggests that plastic deformation might describe the deformation better than rigid body

deformation [*Sonder et al.,* 1986; *England and Jackson,* 1989]. *Altis* [1999, 2001] considers the Okhtosk Sea Plate to be a rigid obliquely indenting block that causes plastic deformation in Sakhalin and northern Japan. Calculations for plastic behaviour of the crust along a right-lateral transpressional shear zone, such as Sakhalin, predict that clockwise vertical-axis rotations should take place and that the amount of rotation should die away exponentially from the rigid boundary [e.g., *England and Jackson,* 1989]. This exponential behaviour has been observed in paleomagnetic data from an oblique subduction zone in Washington State [*England and Wells,* 1991] and from the Nevada continental transform boundary [*Nelson and Jones,* 1987], which may be analogous to the plate boundary in Sakhalin. An extensive paleomagnetic investigation throughout the Sakhalin shear zone can help to test these questions.

A second kinematic model suggests that Neogene deformation in southwest Sakhalin and Hokkaido took place by clockwise rotation of 100-km-scale discrete blocks in domino formation along NE-SE-striking strike-slip faults [*Takeuchi et al.,* 1999]. The right-lateral slip of rigid blocks on either side of the deformation zone gives rise to the rotation of the domino blocks within the zone in a manner that is similar to models for distributed deformation in Greece and California [e.g., *Luyendyk et al.,* 1980; *McKenzie and Jackson,* 1986, 1989; *Luyendyk and Hornafius,* 1987; *Jackson and Molnar,* 1990; *Luyendyk,* 1991; *Taymaz et al.,* 1991]. The domino-style blocks in such models may rotate passively in response to ductile shear of the underlying lithosphere [e.g., *McKenzie and Jackson,* 1983; *Lamb,* 1987], or, they may be forced to rotate by mechanical pinning of the domino boundaries and rotation axes [e.g., *McKenzie and Jackson,* 1986, 1989; *Ron et al.,* 1984; *Taymaz et al.,* 1991; *Little and Roberts,* 1997]. The different mechanisms give rise to different rotation rates [*McKenzie and Jackson,* 1983], which can be used to estimate the cumulative offset in shear zones such as Sakhalin [e.g., *Dickinson,* 1996]. In Sakhalin, such a calculation is useful to accurately determine the sand distribution of the Amur delta [*Flecker and Macdonald,* 2002]. The model proposed by *Takeuchi et al.* [1999] is poorly constrained because of limited paleomagnetic data. At

the edges of rotating domino blocks, areas of compression or extension are expected to develop [e.g., *Jackson and McKenzie,* 1989; *Bayasgalan et al.,* 1999], but supporting geological data are not documented [*Takeuchi et al.*, 1999]. Paleomagnetic data are extremely valuable for distinguishing between such models. The paleomagnetic data presented in this study provide important constraints that have implications for local- and regional-scale deformation and for the plate tectonic evolution of Sakhalin.

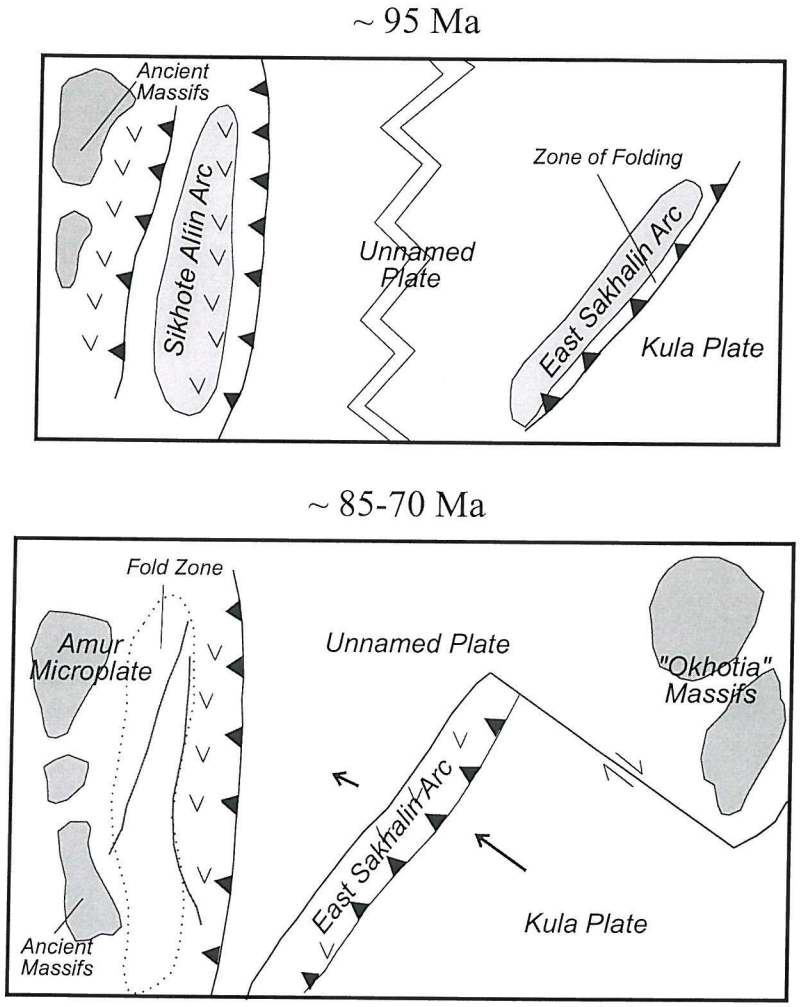

Figure 2.1. A possible schematic representation of the development of the Sikhote Al'in and Sakhalin belts. Modified after *Zonenshain et al.* [1990].

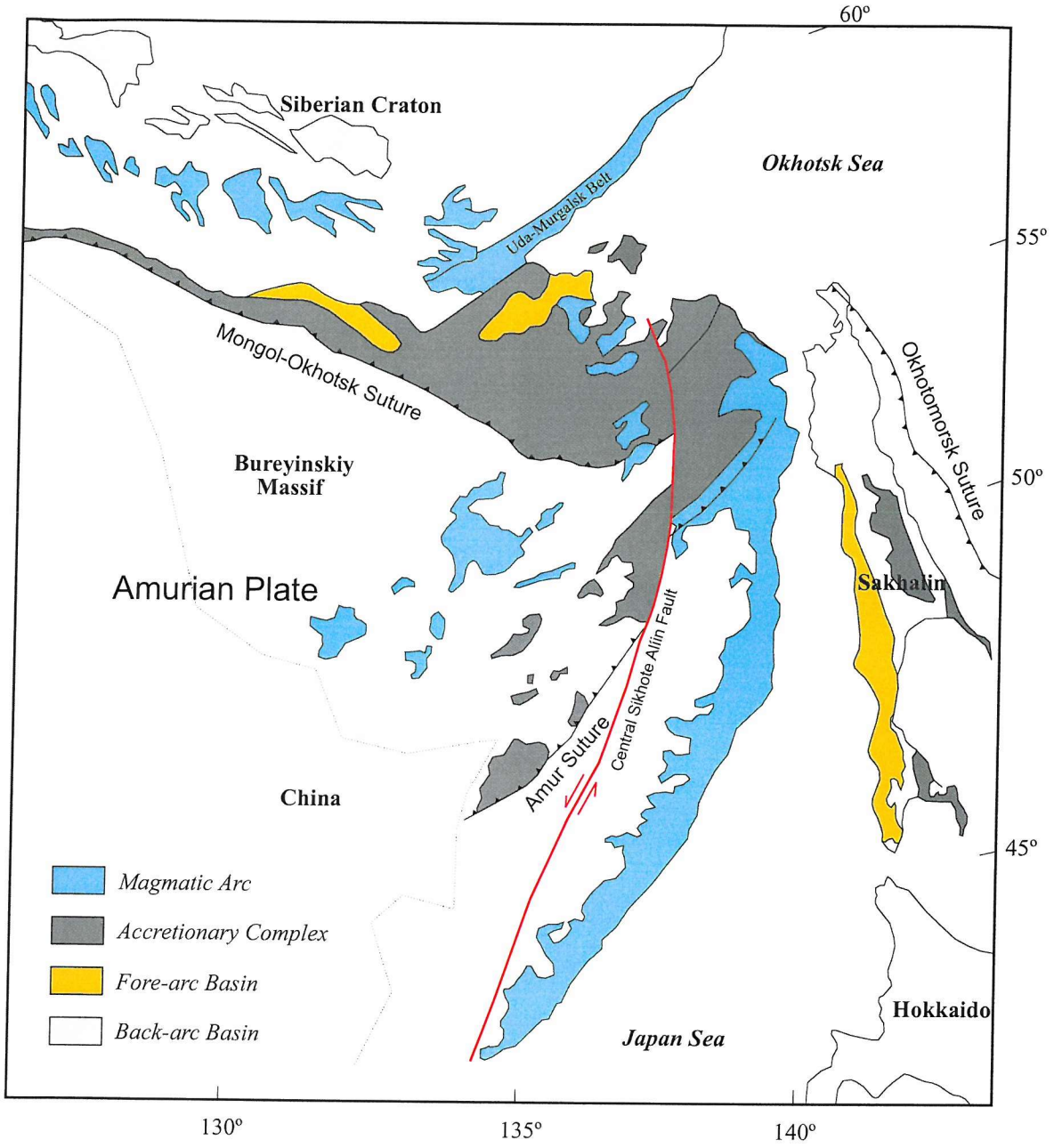

Figure 2.2. Map of major suture zones in southeastern Russia. Modified after *Natal'in* [1993].

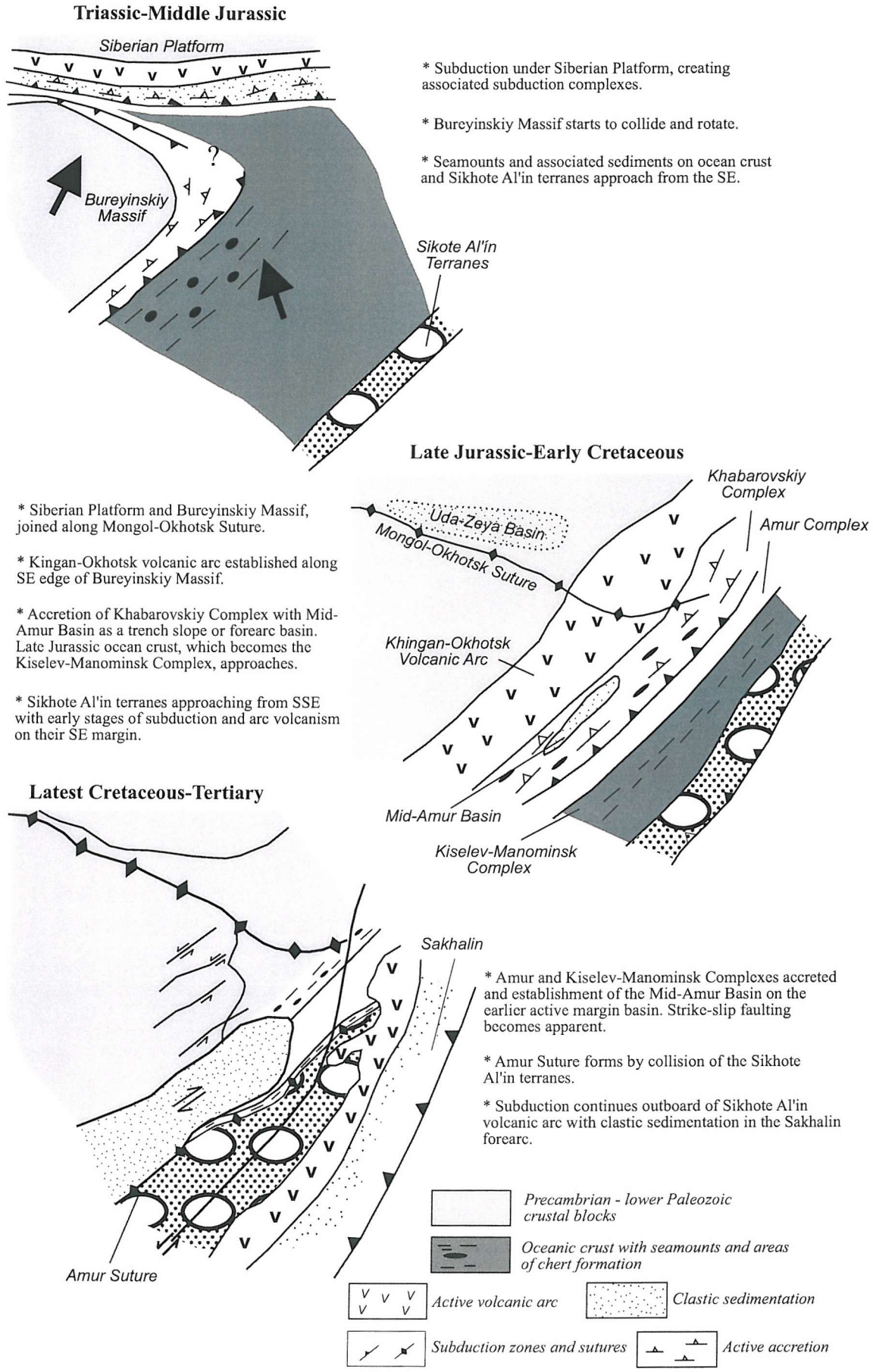

Figure 2.3. Sketch maps of the plate tectonic evolution in eastern Russia. After *Bazhenova et al.* [1995].

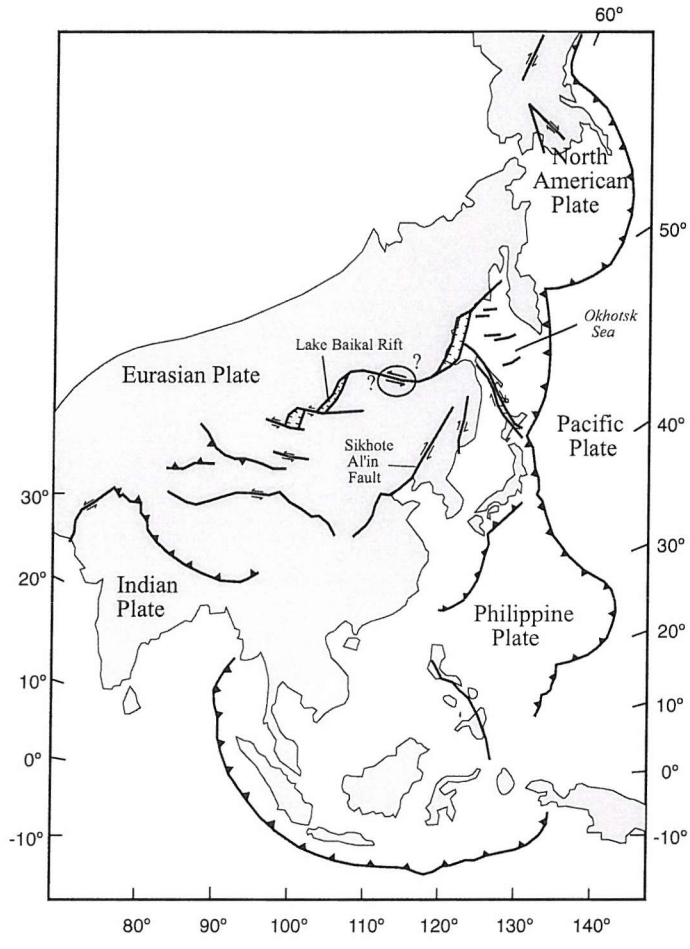

Figure 2.4. Plate tectonic map of NE Asia showing major fault patterns according to *Worrall et al.* [1996]. The circle indicates an area where the structural grain observed in the field is different from the dextral offsets implied here [*D. I. M. Macdonald,* University of Aberdeen, pers. comm., 2000].

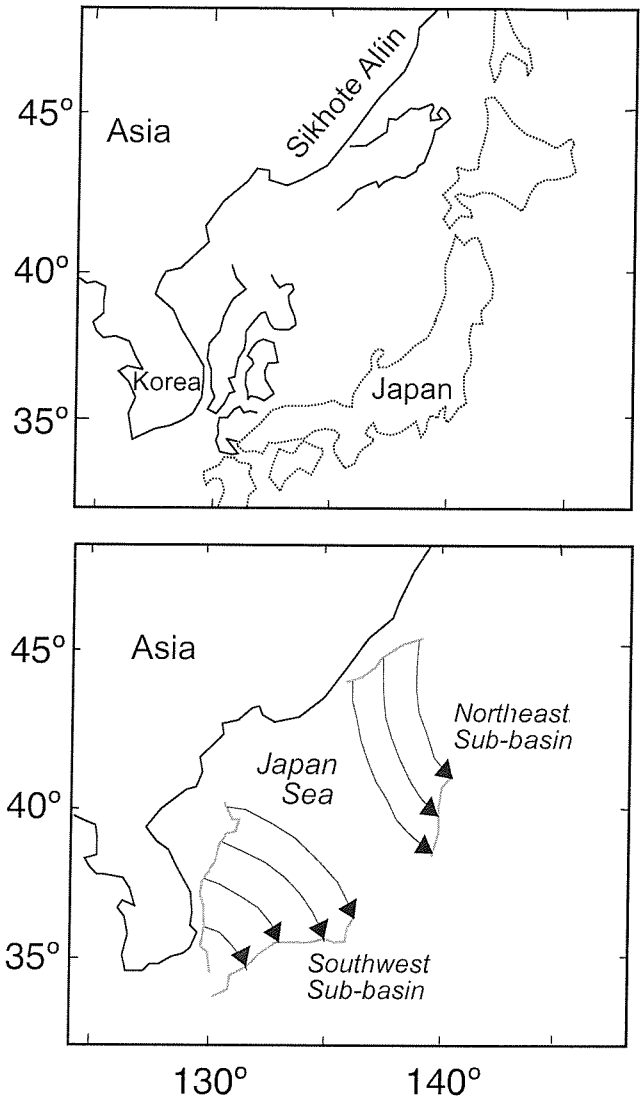

Figure 2.5. Fan-shaped "bar door" opening model for the Japan Sea after *Otofuji et al.* [1985].

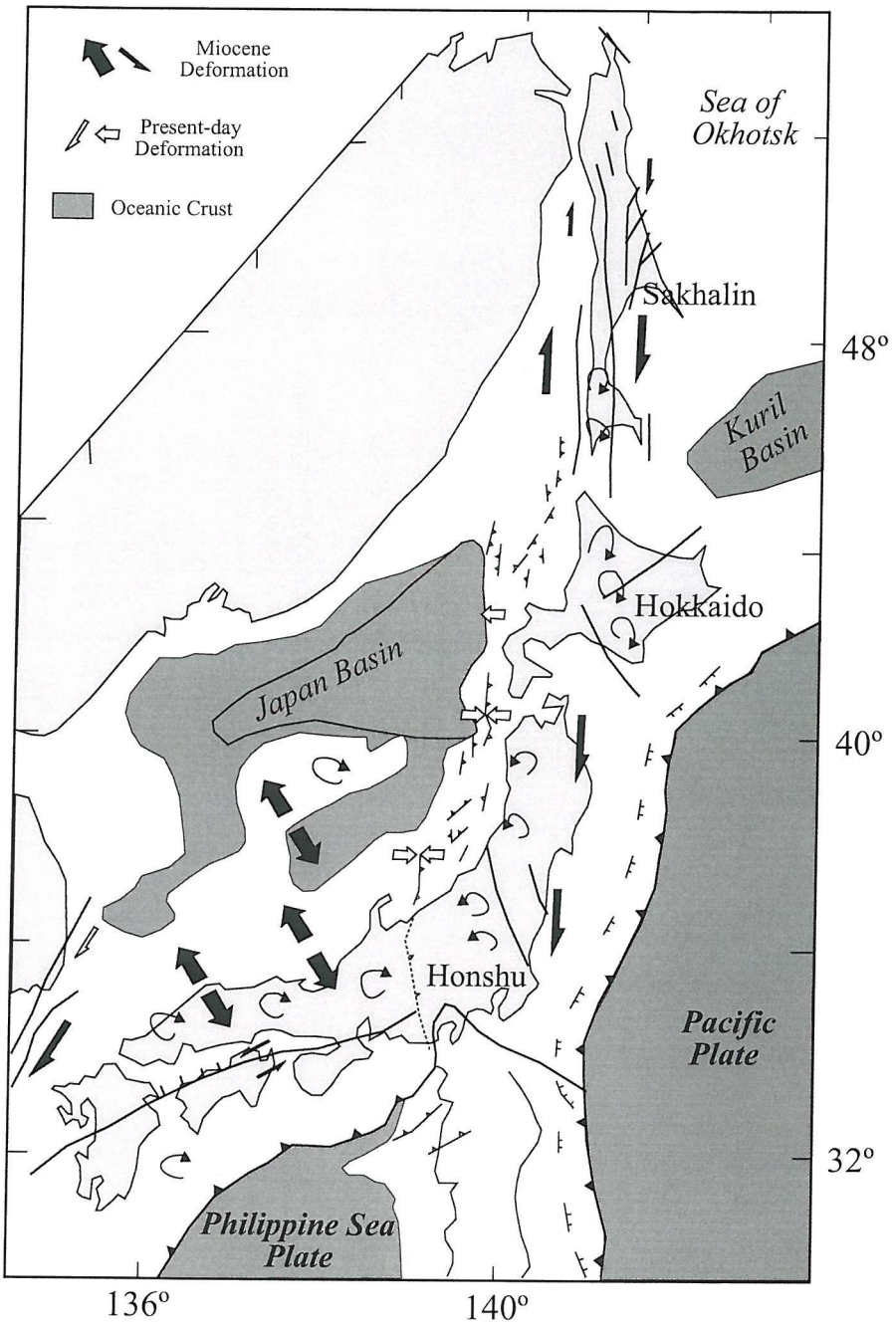

Figure 2.6. Tectonic model for opening of the Japan Sea proposed by *Jolivet et al.* [1995]. The Miocene and present-day stress fields are shown in bold and normal type, respectively. Paleomagnetic rotations are indicated.

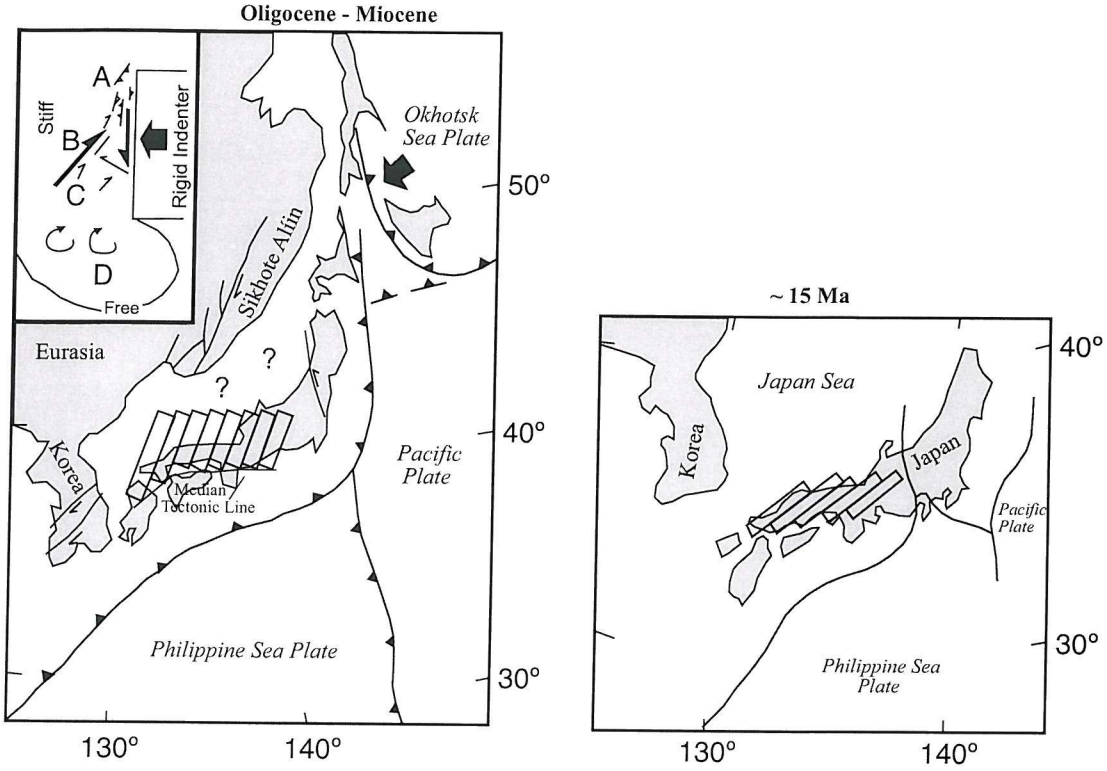

Figure 2.7. Tectonic model for opening of the Japan Sea. Modified after *Altis* [1999].

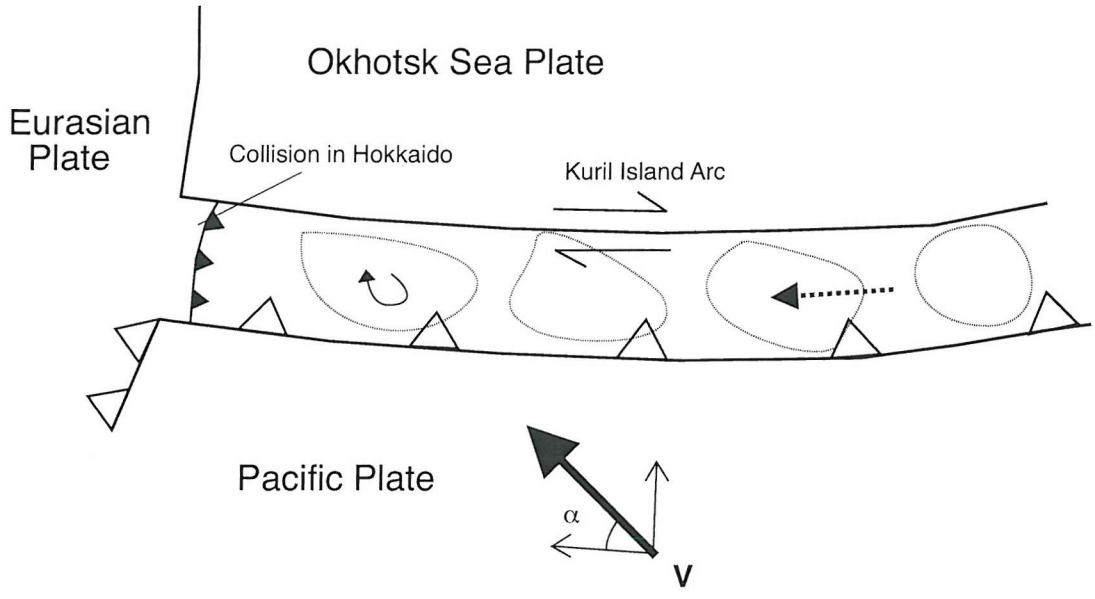

Figure 2.8. Mechanism for arc-parallel translation and rotation, which has been identified at the Kuril-Japan trench triple junction. The amount of rotation and arc-parallel transport is dependent upon the angle of obliquity, α, of the subducting Pacific Plate. Modified after *Kimura* [1986] and *Beck* [1989].

3

Paleomagnetic Theory and Methods

3. Paleomagnetic Theory and Methods

Rocks containing magnetic minerals can acquire a measurable magnetization due to exposure in the Earth's magnetic field. Paleomagnetic methods utilize this ability to provide information regarding the direction and intensity of the ancient geomagnetic field [e.g., *McElhinny,* 1973; *Butler,* 1992].

The Earth's magnetic field originates due to convection in the liquid outer core of the Earth and closely approximates a geocentric axial dipole (GAD) field when averaged over timescales of more than 10^4 years. At shorter timescales, a variable non-dipolar contribution to the field is significant. Polarity intervals have been recorded at longer timescales where the time-averaged magnetic north pole shifts from being coincident with geographic north to being coincident with the geographic south pole for extended periods of geological time. In the application of paleomagnetism to tectonics, only time-averaged GAD fields are considered. The geomagnetic field is described in terms of magnetic inclination (vertical component of magnetization) and magnetic declination (horizontal component of magnetization). There exists a simple relationship between the inclination, I, and the latitude, λ, of the observation site:

$$\tan I = 2\tan\lambda.$$

The time-averaged declination is expected to point toward true north or true south in a GAD field. Thus, measurement of the paleomagnetic declination and inclination of rocks can be compared with expected directions for a studied site and can provide useful tectonic, geodynamic, and kinematic information.

In order to use paleomagnetic data and evaluate the reliability of paleomagnetic results, by, for example, rock magnetic experiments, it is important to understand the magnetization processes involved. This chapter provides a summary of: 1) the theory of rock magnetism, 2) data analysis methods for paleomagnetism, and 3) rock magnetic methods used for determining magnetic mineralogy. In this chapter, bold lettering indicates the mathematical vector or tensor whilst italic lettering represents the scalar.

3.1. Magnetization

Some substances can only acquire a magnetization in the presence of an external magnetic field (induced magnetization), while others can retain a permanent magnetization even when an externally applied magnetic field is removed (remanent magnetization). The total magnetization of a material can, therefore, be regarded as the sum of the induced magnetization and the remanent magnetization, e.g. $M_{tot} = M_i + M_r$. In general, the magnetization of a substance depends on the bulk magnetic susceptibility, k, and the magnetic field, $\mathbf{H}$, through the relationship $\mathbf{M} = k\mathbf{H}$, which suggests that susceptibility is a scalar property and that magnetization is acquired in the direction of the applied field. In reality, however, magnetic susceptibility can be anisotropic and non-linear with field due to its dependence on, for example, temperature, stress, crystal shape, crystal lattice structure, and due to a finite number of electronic moments present in any given volume. Different types of magnetic behaviour occur according to the relative importance of the above factors to the magnetic susceptibility [e.g., *Butler,* 1992; *Dunlop and Özdemir,* 1997; *Tauxe,* 1998].

3.1.1. Induced Magnetization

Magnetic moments of electrons respond to an externally-applied field and create an induced magnetization. Diamagnetic behaviour is related to the orbit of electrons within an atom [e.g., *Tauxe,* 1998]. The centripetal orbital force gives rise to a small current, a magnetic moment, and a torque on the orbiting electron. Applying an external field causes a new force balance and a change in electronic orbital frequency (Larmor frequency), which is given as:

$$\omega_L = -q_e v_e \mu_0 H,$$

where q_e is the electron charge, v_e is the electron charge velocity, and μ_0 is the magnetic permeability of free space. This relationship indicates that the magnetization, M, must be

related to the magnetic field, H, by a negative constant of proportionality, i.e. the diamagnetic susceptibility is negative (Figure 3.1a). The diamagnetic susceptibility is small and practically independent of temperature. Upon removal of the applied field, the induced magnetization becomes zero.

Paramagnetic behaviour occurs due to the alignment of unpaired electronic spins in the presence of an applied magnetic field. In the absence of an external field and in the absence of exchange interactions (the ordering effect of neighbouring spins), the spins are randomly oriented and the magnetization is zero. Paramagnetic behaviour can be demonstrated by the statistical mechanical principles of Langevin theory (where exchange interactions are assumed to be negligible), which is based on a balance between thermal and magnetic energies [e.g., *Dunlop and Özdemir,* 1997; *Tauxe,* 1998]. The probability density of a given magnetic moment having magnetic energy (following the notation of *Tauxe* [1998]),

$$E_m = -m\mu_0 H \cos\alpha,$$

can be shown from statistical mechanics to be:

$$P(E) \propto e^{\left(\frac{-E_m}{kT}\right)},$$

where α is the angle between the magnetic moment and the external field, k is the Boltzmann constant, and T is temperature. Magnetization, M, is the net magnetic moment measured in the direction of the applied field. The saturation magnetization, M_s, is calculated by integrating over the total number of magnetic moments and is normalized over a given volume (v). The ratio of M/M_s is the Langevin function, which is given as:

$$L(a) = \coth a - \frac{1}{a},$$

where:

$$a = \frac{m\mu_0 H}{kT}.$$

When the magnetic energy, $\sim m\mu_0 H$, is 20-30 times larger than the thermal energy, kT, the Langevin function approaches saturation. When $kT >> m\mu_0 H$, for example, at room temperature, $L(a)$ is approximately linear with slope ~1/3, i.e.,

$$\frac{M}{M_S} \approx \frac{m_b \mu_0 H}{3kT}.$$

In order to take into account lattice defects and stress state, the function needs to be expressed in terms of the total number of moments, N, that contribute to the induced magnetization and saturation magnetization. The equation for the paramagnetic susceptibility, therefore, becomes:

$$\frac{M}{H} = \frac{N m_b^2 \mu_0}{3kvT}.$$

This indicates that paramagnetic susceptibility is positive (Figure 3.1.b) and larger in magnitude than diamagnetic susceptibility. An inverse, $1/T$, temperature dependence on paramagnetic susceptibility can be observed from the above equation.

3.1.2. Remanent Magnetization

Ferromagnetic behaviour is characterized by the acquisition of a remanent magnetization in the absence of an externally applied field (Figure 3.1d). Such behaviour occurs in crystals where exchange interaction between neighbouring electronic spin dipole moments is strong (in contrast to paramagnetism). The spins align themselves parallel or anti-parallel depending on the crystal structure. Different types ferromagnetic materials arise from the subtle differences in spin alignment, i.e. ferromagnetic, antiferromagnetic, spin-canted antiferromagnetic, defect antiferromagnetic, and ferrimagnetic. Spin alignment becomes increasingly random with increased temperature. Paramagnetic behaviour dominates above the characteristic Curie temperature for the

particular ferromagnetic material. Ferromagnetic behaviour can be considered to be a quasi-paramagnetic response to a large internal magnetic field. This can be described through paramagnetic "Langevin" principles which may be extended to incorporate expressions for an internal field and an external magnetic field.

The internal field (the Weiss molecular field) can be related to the magnetization of the substance by a constant (β). Applying this directly to the paramagnetic theory outlined above and following the notation of *Tauxe* [1998]:

$$\frac{M}{M_S} = L(a) = L\left(m_b \mu_0 \frac{(H + \beta M)}{kT}\right).$$

Above the Curie temperature, θ (T-$\theta > 0$), the behaviour is paramagnetic and only the external field is important, and βM is zero. In this case, the ferromagnetic susceptibility follows the Curie-Weiss law:

$$\frac{M}{H} = \frac{N m_b^{\,2} \mu_0}{3kv(T - \theta)}.$$

Below the Curie temperature, the external field is negligible relative to the internal Weiss molecular field:

$$\frac{M}{M_S} = L\left(\frac{m_b \mu_0 \beta M}{kT}\right) = L\left(\frac{\theta M}{T M_s}\right),$$

where the Curie temperature is:

$$\theta = \frac{N m_b^{\,2} \beta}{vk}.$$

This indicates that ferromagnetic susceptibility below the Curie temperature cannot be simply expressed. The remanent magnetization that is retained in the absence of an

external field is subject to magnetic hysteresis, which is fundamental to the measurement of ancient geomagnetic field directions in rocks.

3.2. Magnetic Anisotropy, Domains, and Hysteresis

3.2.1. Magnetic Anisotropy and Anisotropy Energy

Ferromagnetic particles, which may retain a magnetic moment in the absence of an applied field, have an internal magnetic anisotropy energy that acts to align the individual magnetic moments along the direction of minimum energy [e.g., *Dunlop and Özdemir,* 1997; *Tauxe,* 1998]. This direction coincides with a configuration of minimum charge distribution and a minimal internal "demagnetizing" field. These "easy" directions of magnetization give rise to magnetic anisotropy and to the blocking of moments in particular directions within a crystal. The magnetic anisotropy energy is the energy required to move a magnetic moment from one easy direction, through intermediate "hard" directions to the next easy direction. The magnetic field required to overcome this magnetic anisotropy energy is called the switching field or coercive field H_c (microscopic coercive force).

Different origins of anisotropy are responsible for the different types of anisotropy energy. 1) Shape anisotropy arises due to the physical shape of the grain where the anisotropy energy is magnetostatic. 2) Magnetocrystalline anisotropy results from crystal structure where the anisotropy energy is a magnetocrystalline energy. 3) Magnetostrictive anisotropy results from the state of stress and leads to a magnetostrictive anisotropy energy.

3.2.2. Magnetic Domains

The magnetostatic energy of a magnetic crystal that behaves as a single isolated magnetic dipole (single-domain (SD) grain) increases as the grain volume increases and a greater distribution of charge occurs over the grain surface [e.g., *Butler,* 1992; *Tauxe,* 1998]. At a certain grain size it becomes energetically more favourable for the

magnetization to be broken into several uniformly magnetized domains separated by domain walls. Grains with several domains are called multi-domain (MD) grains. The presence of several domains reduces the magnetic field and minimizes the charge distribution (i.e., the magnetostatic energy). A third category, pseudo single-domain (PSD) grains, exists in which particles only contain a few domains, which record ancient magnetizations in a similar manner to SD grains.

Exchange energy between spin moments in adjacent domains leads to the reversal of moments across the domain wall. A finite energy is associated with the domain wall region. Narrow domain walls exist in instances where the exchange energy is large because opposing spin moments are in close vicinity of each other. Wider walls occur when magnetocrystalline energy works to align the spins into the crystallographic easy direction. Moving domain walls requires less energy than switching SD moments. Therefore, MD grains have lower saturation remanence and coercivity compared to SD grains.

3.2.3. Magnetic Hysteresis

Hysteresis properties of magnetic particles can be investigated by applying a magnetic field and measuring the resulting magnetization at different field values. A hysteresis curve may be defined for ferromagnetic particles whereby an initial magnetic field is applied and increased from zero until the sample has reached saturation (where all the magnetic moments have aligned with the field). The magnetization is measured whilst the field is allowed to decay to zero and then applied in the opposite direction until the sample reaches negative saturation. Upon reduction of the applied field back to zero and further application of a field in the positive direction, the magnetization eventually reaches positive saturation at which point a hysteresis loop is defined [see *Tauxe,* 1998].

Several useful parameters can be obtained from hysteresis curves [e.g., *Butler,* 1992; *Verosub and Roberts,* 1995; *Tauxe,* 1998]. The maximum magnetization achieved is the saturation magnetization (M_s). The maximum remanence (saturation remanence)

that can be acquired by the sample is the magnetization, M_r, that remains in zero field after removing a saturating field. The coercive field required to switch the polarity of the net magnetic moment is the field value, H_c, at zero magnetization (the coercivity). The coercivity of remanence, H_{cr}, can also be estimated from hysteresis measurements. This is the magnitude of the field required for the remanent magnetization to be reduced from saturation to zero.

In MD grains, domain wall movements provide a more important mechanism for acquiring a remanent magnetization than switching of magnetic moments. Applying a field to a MD grain gives rise to preferential growth of domains parallel to the field. Domain walls may be destroyed in large fields, and eventually MD grains will reach saturation. The domains re-form and move back to their initial positions when the magnetic field is removed. However, domain walls take positions that are energetically most favourable in the vicinity of their initial positions, which leads to a small magnetic remanence. Only a small field is required to force the walls back to their zero moment positions and, consequently, MD particles have low coercivities [e.g., *Butler,* 1992].

Hysteresis parameters may be used to distinguish between SD, MD, or PSD grains, and different magnetic minerals. The ratios M_r/M_s and H_{cr}/H_c can be plotted against each other and have been used to determine the domain state of magnetite and titanomagnetite [*Day et al.,* 1977]. However, such plots (Day plots) have only limited use in practice because the shape of hysteresis curves depends on a number of factors such as magnetostrictive anisotropy, shape anisotropy, magnetocrystalline anisotropy, the bulk composition of the sample, and the size distribution of grains within any particular sample.

3.3. Natural Remanent Magnetization

The natural remanent magnetization (NRM) is the remanent magnetization acquired by a rock in the presence of the geomagnetic field. There are several mechanisms by which an NRM can be acquired. The NRM measured in a rock sample

often consists of several components of magnetization acquired through different physical processes [e.g., *Butler,* 1992], as described below.

3.3.1. Magnetic Relaxation and Viscous Remanent Magnetization

The stability of the remanent magnetization within a rock over time is vital for preserving information about the ancient geomagnetic field. Magnetic viscosity produces changes in magnetization with time at a constant temperature [e.g., *Néel,* 1955; *Dunlop and Özdemir,* 1997]. Within a randomly oriented population of magnetic particles in zero field, the thermal energy of an individual particle can become large enough to overcome the magnetic anisotropy energy and the moment can switch to its easy axis. In a zero field, these high-energy particles tend to become randomly oriented. The decay of remanent magnetization will be exponential with time [e.g., *Néel,* 1955]:

$$\mathbf{M}(t) = \mathbf{M}_0 e^{\left(\frac{-t}{\tau}\right)},$$

where t is time, $\mathbf{M}_0$ is the initial magnetization, and τ is the relaxation time. The relaxation time is the time taken for the remanence to decay to $1/e$ of its initial value. The relaxation time can be related to the ratio of magnetic anisotropy energy and thermal energy as follows:

$$\tau = \frac{1}{C} e^{\left(\frac{Kv}{kT}\right)},$$

where K is the anisotropy energy (containing the coercive force), which is dependent on the dominant type of anisotropy within the grain volume (v), and where C is a frequency factor, and kT is the thermal energy. Small changes in v and T lead to large changes in the relaxation time. The relaxation time can vary from the order of seconds to 10^9 years. Particles with relaxation times in the order of 10^2-10^3 seconds have high thermal energy, are unstable at short timescales, and have some paramagnetic characteristics. These

particles are known as superparamagnetic (SP) particles (Figure 3.1c). Magnetic particles that are responsible for carrying an ancient paleomagnetic signal have relaxation times of the order of geological time (i.e., 10^9 years).

Viscous remanent magnetizations (VRMs) can occur when the viscous moment-switching process occurs in the presence of a field such as the geomagnetic field. Particles that have had their moments switched by thermal energy re-align with the externally applied field. An exponentially increasing number of particles will have sufficient thermal energy to overcome the anisotropy energy barriers with time. Significant viscous components can be acquired by rocks due to exposure in recent fields. This can obscure the ancient component of magnetization acquired at the time of formation of the rock. Relatively low-coercivity MD grains typically carry such VRM components. The acquisition and relative significance of VRM components depends on grain sizes and origins of anisotropy energy of particles within the rock.

3.3.2. Blocking Temperatures and Thermal Remanent Magnetization

The relaxation time, τ, has a strong temperature dependence [e.g., *Néel,* 1955]. For a particular SD magnetic particle, there is a well-defined blocking temperature, T_b, at which the relaxation time increases from a very short timescale of 10^2-10^3 seconds to a long, geologically important, timescale. Between the blocking temperature and the Curie temperature, therefore, a particle will be superparamagnetic. Below the blocking temperature, a time-stable remanent magnetization may be acquired. In the case of a rock with a distribution of grain-sizes and anisotropy energies (and coercivities), a range of blocking temperatures is typically observed. Cooling increases τ until the magnetization is blocked and a thermal remanent magnetization (TRM) is acquired. Rocks that have cooled from high temperatures to below the blocking temperature, such as cooling lava flows, may acquire a TRM parallel to the Earth's field. Because of the complicated interdependence of coercivity, temperature, and relaxation time, it is difficult to establish

what type and what distribution of grains within a rock sample gives rise to a particular range of blocking temperatures and TRM components.

A mixed remanence acquisition mechanism between the viscous and thermal mechanisms may arise as a result of prolonged exposure of a rock to an elevated temperature below the Curie temperature. This type of NRM is a thermo-viscous magnetization (TVRM) which can be acquired naturally during metamorphism. Reduction of the relaxation time will occur due to the elevated temperature, but after cooling the relaxation time increases and a TVRM may be acquired [e.g., *Dunlop and Özdemir,* 1997].

3.3.3. Blocking Volumes and Chemical Remanent Magnetization

In a manner that is analogous to blocking temperatures, the relaxation time also depends on grain volume. At very small volumes, thermal energy dominates the magnetic anisotropy energy. At larger volumes, the magnetic anisotropy energy dominates. There is a critical blocking volume, v_b, above which particles can retain a remanence on geologically significant timescales. In nature, chemical reactions within a rock may allow magnetic minerals to grow in the presence of the geomagnetic field. Magnetic moments align themselves as they grow through the magnetic blocking volume and, consequently, a chemical remanent magnetization (CRM) is acquired [e.g., *McCabe and Elmore,* 1989; *Dunlop and Özdemir,* 1997].

3.3.4. Detrital Remanent Magnetization

Upon deposition of sedimentary rocks, a detrital or depositional remanent magnetization (DRM) may be acquired [e.g., *Verosub,* 1977]. As a magnetic particle settles through the water column, the geomagnetic field imparts a torque on the particle so that it aligns with the ambient magnetic field. In cases where the grains are near-spherical and the shape anisotropy is minimal, the field direction may be accurately preserved within the sediment.

However, post-depositional processes such as bioturbation may lead to realignment of grains after deposition to give rise to a post-depositional remanent magnetization (pDRM). The direction of magnetization can be affected by the shape of the magnetic particles and topography of the sediment-water interface. Particles with shape anisotropy have easy axes that rotate toward the bedding plane upon deposition and compaction, and a sloping or undulating interface can lead to imbrication of anisotropic particles. In some cases, a post-depositional inclination error can occur and can be corrected for [e.g., *Kodama,* 1997]. The magnetization becomes fixed at a particular depth that varies between sediments and depends on, for example, mineralogy. Processes that take place after deposition and before magnetization lock-in can alter the original alignment of the particles and give rise to a pDRM.

3.3.5. Isothermal Remanent Magnetization

Isothermal remanent magnetizations (IRMs) result from short-term exposure to a strong magnetizing field at a constant temperature. Grains with coercive force less than the applied field are affected. In nature, such a magnetization may occur from fields due to a lightning strike [e.g., *Butler,* 1992].

3.4. Display and Analysis of NRM

3.4.1. Plotting the Magnetic Vector

The three vector components measured in paleomagnetic studies are the magnitude, B, declination, D, and inclination, I, which combine to fully describe the geomagnetic field vector (Figure 3.2a) [e.g., *McElhinny,* 1973]. A frame of reference is chosen to describe these quantities. In a geological context, it is most meaningful to visualize the magnetic vector relative to the Earth's geographic reference frame. Declination is, therefore, defined as the angle between geographic north and the projection of the magnetic vector onto the horizontal plane. Declination is positive to the east of north and takes a value from 0° to 360° (Figure 3.2a). Inclination is defined as the

angle in the vertical plane between the magnetic vector and horizontal (Figure 3.2a). Inclination varies from –90° to +90° and is positive when the vector points downward, e.g., in regions where the dipole field lines point into the Earth such as in the northern hemisphere when the geomagnetic field is normally polarized. The Lambert northern hemisphere equal-area stereographic projection is used to display and interpret magnetic vector data (Figure 3.2b). This projection is naturally suited for plotting the direction of geomagnetic vectors following the conventions and definitions indicated above. Regions of equal area on a sphere (e.g., the Earth) will project as equal area regions on the stereographic plot, which enables easy assessment of data scatter. However, circles on a sphere will appear as ellipses in the two-dimensional plot. Different symbols are used for reversed (negative) and normal (positive) polarity magnetic inclinations.

In order to make meaningful plots of magnetic vector data from geological samples, a number of coordinate transformations need to be applied to the measured data. Three orthogonal vector components measured using a magnetometer allow the inclination, declination, and magnetization intensity to be determined in sample coordinates. Stereographic plots of raw data can be practically impossible to interpret in terms of their relationship to the geomagnetic field. By recording the azimuth of the sample with respect to geographic north and the dip of the sample's long axis relative to horizontal, the data can be converted to present-day geographic coordinates. However, a further coordinate transformation is usually required to correct for the bedding tilt of the sampled rock sequence. This transformation restores the data to stratigraphic coordinates of the ancient horizontal plane. In this form, the paleomagnetic data can be appropriately plotted and geologically interpreted using the equal area projection.

3.4.2. Demagnetization and Paleomagnetic Stability

The object of paleomagnetic studies is, usually, to plot and interpret the ancient primary NRM component at the time of rock formation. The presence of other more recent remanences comprising part of the NRM (such as a VRM or CRM) can obscure

the ancient signal. It is critical that secondary remanences are removed in order to identify reliable ancient magnetizations. Demagnetization methods allow different magnetization components to be identified and removed [*Zijderveld,* 1967]. Identification of different components relies on the principle that rock samples consist of particles and minerals with a distribution of coercivities or blocking temperatures and that the remanent magnetization components are acquired within discrete regions of the blocking temperature or coercivity spectra [e.g., *Hoffman and Day,* 1978]. Alternating field (AF) demagnetization and thermal demagnetization techniques are used to randomize moments by overcoming the coercive force and unblocking temperatures respectively.

AF demagnetization is carried out by exposing a rock sample to a sinusoidal linearly-decaying alternating magnetic field (Figure 3.3a). Only particles with coercivities less than the peak field value are affected by the AF signal. The magnetic moments of the particles align with the direction of the applied field. As the field is reduced, particles with coercivities between the peak field and the new field value become blocked with a direction corresponding to the direction of the AF (Figure 3.3b). As the AF decays to smaller and smaller values, particles with coercivities less than the peak field value become aligned in opposing directions, which cancel each other out over several AF cycles. Linear decay of the field to zero and symmetry of the field decay about the origin ensures that the net magnetic moment of the affected particles sums to zero (Figure 3.3).

Thermal demagnetization is carried out by heating a rock sample to an elevated temperature and then letting it cool back to room temperature in the presence of zero magnetic field. Magnetic moments of particles with blocking temperatures below the selected demagnetization temperature become randomized and get blocked upon cooling. The random moments cancel each other out and, thus, the net moment due to the affected particles is zero.

Progressive stepwise thermal and AF demagnetization of a sample allows different magnetization components to be revealed. This technique involves removing part of the NRM by demagnetization and measurement of the remaining NRM in successive steps until the NRM is completely removed (Figure 3.4a). Consecutive measurements typically indicate that the magnetic intensity decreases and that directions of the magnetization vector change as components with relatively low unblocking temperature or low coercivity are removed during progressive demagnetization (Figure 3.4a,b). Consistent directions (but with reduced intensity) upon measurement at several demagnetization steps suggest that a magnetic component has been isolated over the particular range of coercivities or unblocking temperatures.

Components that are easily removed at low temperatures or small AFs are low-stability components (Figure 3.4a,b). High-stability components are not easily removed. The highest stability component that may be resolved using stepwise demagnetization is the characteristic remanent magnetization, ChRM. The ChRM is not necessarily a primary component. Field strategies that include sampling different fold limbs, conglomerate pebbles, baked dyke-sediment contacts, and sampling at different stratigraphic levels allow field tests to be performed on the data, which help to constrain the age of the ChRM. Magnetic remanence carriers can be determined from rock magnetic experiments. Such methods combined with the analysis of demagnetization behaviour are generally required to unambiguously determine whether the ChRM is a primary component.

3.4.3. Vector Component Plots

The behaviour of the magnetic vector during demagnetization can be interpreted using vector component plots (Figure 3.4c). Vector component plots are constructed by projecting the (3-D) vector end-points into separate horizontal and vertical planes so that the data can be fully represented on a page in two dimensions [*Zijderveld,* 1967; *Dunlop,* 1979]. The distance from the origin of the plot to each projected data point is

proportional to the magnetic intensity. The vector is decomposed into a geographic reference frame, with a north component, $N = M \cos I \cos D$, an east component, $E = M \cos I \sin D$, and a vertical component $Z = M \sin I$. For the horizontal projection, the north versus east components are plotted. This indicates the magnetic declination of the vector at each demagnetization step. As different magnetization components are progressively removed, the angle of declination may change. In the same diagram, the vertical component is plotted in a similar manner with the *Up* component plotted versus *North*. This plot indicates the apparent inclination, which will generally change in value upon removal of low-stability components (Figure 3.4c). The axes of a vector component plot have two sets of labels according to whether one is looking at the vertical or horizontal components of the magnetization vector (Figure 3.4c).

By plotting the vectors after successive demagnetization steps, the different coercivity or blocking temperature components of magnetization may be revealed. Magnetization components with directional consistency over several demagnetization steps appear as straight lines for the corresponding data points in the vector component plot (Figure 3.4c). The coercivity or blocking temperature distribution may, therefore, be revealed (Figure 3.4b). In cases where the coercivity or blocking temperature spectra overlap, curved trajectories occur in the vector component plot as the lower-stability component is demagnetized. A ChRM component may be identified as a stable component that decays to the origin of the plot with magnetization equal to zero or with a magnetization that is too weak to measure.

3.5. Statistical Methods for Analyzing Paleomagnetic Vectors

A rigorous statistical framework is required to analyze paleomagnetic data and to obtain the best possible statistical estimate of the uncertainty associated with the identified primary direction of magnetization. There are numerous sources of uncertainty associated with paleomagnetic methods, for example, laboratory measurement uncertainty due to sample alignment errors and instrument noise, field measurement

uncertainties from sample orientation and orientation of rock units, uncertainty in the removal of secondary magnetization components, uncertainty due to the magnetization process, and uncertainty associated with secular variation of the geomagnetic field.

In order to obtain the best possible estimate of the orientation of stable magnetic components of a rock sample, a principal component least-squares analysis [*Kirschvink,* 1980] is usually applied to the data points plotted in vector component plots. For tectonic applications of paleomagnetism, secular variation of the Earth's magnetic field must be averaged out. Collection of numerous samples from stratigraphic sequences that span appropriate age ranges of $> 10^4$ years is required. Fisherian [*Fisher,* 1953] or bootstrapped [*Tauxe et al.,* 1991] statistical techniques can then be applied to the principal vector components of the samples, which allows calculation of the average paleomagnetic direction and provides a measure of the data scatter for a distribution of data on the surface of a sphere.

3.5.1. Principal Component Analysis

The principal component method considers the deviation of a sequence of data points from the average of the data set. This method may be applied to vector data representing a magnetic component isolated by progressive demagnetization [*Kirschvink,* 1980]. For any arbitrary vector in space, the variation of its three orthogonal components must be separately considered. The average of the equally weighted data points along each orthogonal direction is (following the notation of *Tauxe* [1998]):

$$\bar{x}_1 = \frac{1}{N}\left(\sum_1^N x_{1i}\right), \qquad \bar{x}_2 = \frac{1}{N}\left(\sum_1^N x_{2i}\right), \qquad \bar{x}_3 = \frac{1}{N}\left(\sum_1^N x_{3i}\right).$$

Calculating the data relative to the mean, the new coordinates become:

$$x'_{1i} = x_{1i} - \bar{x}_1, \qquad x'_{2i} = x_{2i} - \bar{x}_2, \qquad x'_{3i} = x_{3i} - \bar{x}_3.$$

These transformed components are substituted into the orientation tensor:

$$\mathbf{T}=\begin{pmatrix} \sum x_{1i}x_{1i} & \sum x_{1i}x_{2i} & \sum x_{1i}x_{3i} \\ \sum x_{1i}x_{2i} & \sum x_{2i}x_{2i} & \sum x_{2i}x_{3i} \\ \sum x_{1i}x_{3i} & \sum x_{2i}x_{3i} & \sum x_{3i}x_{3i} \end{pmatrix}.$$

For an arbitrary vector, all six independent components are non-zero. However, there exists a coordinate system where the vector is completely described by the three diagonal matrix components and where the off-axis terms are zero. The axes of the coordinate system are the eigenvectors of the matrix. In this case, because of the definition of the transformed components, the principal eigenvector, $\mathbf{V}_1$, obtained from the covariance matrix, $\mathbf{V}$, occurs in the direction of maximum data scatter. Eigenvectors $\mathbf{V}_2$ and $\mathbf{V}_3$ are orthogonal to each other and orthogonal to $\mathbf{V}_1$. The linear mathematical relationship is:

$$\mathbf{TV} = \tau\mathbf{V},$$

where:

$$\det|\mathbf{T} - \tau| = 0.$$

τ is the diagonal matrix containing the three eigenvalues. The eigenvalues of $\mathbf{T}$ indicate the variance associated with each eigenvector, and are used to quantify the fit of the principal eigenvector to the data. The maximum angular deviation (*MAD*) is defined as [*Kirschvink*, 1980]:

$$MAD = \tan^{-1}\left(\frac{\sqrt{(\sigma_2^2 + \sigma_3^2)}}{\sigma_1}\right),$$

where the standard deviation, σ, is:

$$\sigma_i = \sqrt{\tau_i}.$$

If a principal direction cannot be uniquely identified, the eigenvector $\mathbf{V}_3$, with least eigenvalue, τ_3, can be taken to be the pole of the best-fitting plane, which can be assumed to contain the principal component of the data.

In practice, principal component analysis may be used in conjunction with vector component plots [e.g., *Zijderveld,* 1967], which indicate the different components of magnetization that may need to be analyzed. The best-fit principal component determination of the mean declination and inclination can be indicated on a vector component diagram as a line-fit through the data points of the magnetization component of interest.

3.5.2. Fisher Statistics and Parametric Vector Analysis

A statistical method is required in paleomagnetism for calculating a mean paleomagnetic direction from a group of magnetic component vectors and for estimating the data scatter. It is often necessary to compare directions between different data sets. In such cases, it is useful to be able to quantify the differences and understand the statistical importance of the results. Statistical theories have been developed that may be used for the analysis of paleomagnetic unit vectors on a sphere [e.g., *Fisher,* 1953].

The Fisher statistical framework is a parametric method based on the probability of the paleomagnetic data set being drawn from the Fisher distribution, which is equivalent to a Gaussian normal distribution on the surface of a sphere. As for the Gaussian normal distribution, the standard deviation about the mean can be calculated for the Fisher distribution. The standard error in the mean provides a circular confidence limit within which a certain percentage of data points from the population are expected to appear. The Fisher probability density function is given as:

$$F = \frac{\kappa}{4\pi \sinh \kappa} e^{(\kappa \cos \alpha)},$$

where α is the angle between the unit vector and the mean direction, and κ is a precision parameter which tends to infinity ($\kappa \rightarrow \infty$) as the dispersion of the data population tends to zero. The mean direction is calculated by converting the vectors to unit vectors, summing

the individual directions, and scaling by the magnitude of the resulting vector (R). The cartesian coordinates of the mean direction, therefore, become:

$$\bar{x}_1 = \frac{1}{R}\left(\sum_i x_{1i}\right), \qquad \bar{x}_2 = \frac{1}{R}\left(\sum_i x_{2i}\right), \qquad \bar{x}_3 = \frac{1}{R}\left(\sum_i x_{3i}\right),$$

where the resultant vector magnitude is,

$$R = \left(\left(\sum_i x_{1i}\right)^2 + \left(\sum_i x_{2i}\right)^2 + \left(\sum_i x_{3i}\right)^2\right)^{\frac{1}{2}}.$$

The precision parameter κ of the Fisher distribution can be estimated for a finite set of directions:

$$\kappa \approx k = \frac{N-1}{N-R},$$

where N is the number of data points. The precision parameter, k, increases as R becomes similar in magnitude to N. A confidence limit within which the mean of the directional data set lies, can be calculated with a probability level p and confidence angle $\alpha_{(1-p)}$:

$$\alpha_{(1-p)} = \cos^{-1}\left(1 - \frac{N-R}{R}\left(\left(\frac{1}{p}\right)^{\frac{1}{(N-1)}} - 1\right)\right).$$

The 95% ($1-p = 0.95$) circular confidence limit is usually specified for paleomagnetic data sets. This is often approximated by:

$$\alpha_{95} \approx \frac{140}{\sqrt{kN}}.$$

The Fisher statistical framework allows quantitative comparison of parameters between different data sets, which is valuable for paleomagnetic purposes. However, the use of Fisher statistics is only valid if the paleomagnetic data set being considered is uni-

modal, spherically symmetric, and normally distributed (i.e., drawn from a Fisherian distribution). In reality, paleomagnetic data sets are generally bi-modal and contain a number of sources of uncertaintly, which suggests that the use of Fisher statistics may not always be appropriate.

3.5.3. Bootstrap Statistics and Non-Parametric Vector Analysis

Use of the statistical quantile-quantile (Q-Q) plot and estimation of the goodness-of-fit, by calculating the Kolmogorov-Smirnov parameter D, allows evaluation of a paleomagnetic data set to test whether it can be represented by a Fisher distribution [*Fisher et al.,* 1987]. In cases where the data set can not be assumed to have derived from a known distribution, such as the Fisher distribution, a non-parametric method may be applied. The non-parametric statistical bootstrap method allows calculation of uncertainties for unit vectors from non-Fisherian distributions [*Tauxe et al.,* 1991].

The bootstrap method is based on selection of a random number of N data points from the real data set under consideration. Using the selected data points, a new "bootstrapped" mean can be calculated for the randomly derived sub-data set. The method for calculating the bootstrapped mean may be carried out using the principal eigenvectors of the orientation matrix similar to the method descibed for principal component analysis. By repeatedly resampling the original data set in a random fashion and plotting the bootstrapped mean value from each sub-data set, the original data will be reflected by the distribution of mean directions of the sub-data sets. A data set with a large amount of scatter will lead to a bootstrap distribution that also contains a large amount of scatter. The new distribution can, thus, be regarded as the original distribution from which the actual data were derived. No assumption is made about the type of distribution from which the data originated. A large number of bootstrap (e.g., $> 10^3$) calculations are required so that the random sampling of the underlying data is truly random and not biased toward particular data points. This leads to a bootstrap

distribution where the original data are properly represented [e.g., *Tauxe et al.,* 1991; *Tauxe,* 1998].

In general, the bootstrap distribution will be elliptically distributed. Approximate 95% confidence limits may be calculated for paleomagnetic purposes by assuming that the distribution of the bootstrap means (but not necessarily the data) is the elliptical distribution on a sphere, which is known as the Kent distribution [*Kent,* 1982]. The Kent distribution can be written as:

$$F = c(\kappa,\beta)^{-1} e^{\left(\kappa\cos\alpha+\beta\sin^2\alpha\cos 2\phi\right)},$$

where α is the angle between the direction of the unit vector and the true mean direction that is estimated from the principal eigenvector, $\mathbf{V}_1$, of the orientation matrix, $\mathbf{T}$, ϕ is an angle measured from $\mathbf{V}_2$ in the plane perpendicular to $\mathbf{V}_1$, κ is a concentration parameter, and β is an ovalness parameter. When $\beta = 0$, the Kent distribution reduces to the Fisher distribution. Eigenvectors of the assumed Kent distribution are found in order to determine the appropriate directions and magnitudes of the deviation around the mean. The appropriate coordinate transformation of x into data coordinates x' is given as:

$$x' = \Gamma^T x,$$

where $\Gamma = (\gamma_1,\gamma_2,\gamma_3)$, which gives rise to the constrained eigenvectors of the orientation matrix ($\mathbf{T}$). The principal vector γ_1 is constrained to be parallel to the Fisher mean of the data, and the orientation of the vectors γ_2 and γ_3 are determined so that the off-axis terms of the orientation matrix $\mathbf{T}$ are minimized subject to the γ_1 constraint. The data mean may be calculated by the following parameters:

$$\hat{\mu} = \frac{1}{N}\sum_k x'_{k1}, \qquad \hat{\sigma}_2^2 = \frac{1}{N}\sum_k \left(x'_{k2}\right)^2, \qquad \hat{\sigma}_3^2 = \frac{1}{N}\sum_k \left(x'_{k3}\right)^2.$$

These parameters are related to the resultant vector magnitude, R, and eigenvalues τ_1 and τ_2 (by good approximation) in a way that is analogous to calculation of the Fisher mean:

$$\hat{\mu} = \frac{R}{N}, \qquad \hat{\sigma}_2^2 = \tau_2, \qquad \hat{\sigma}_3^2 = \tau_3.$$

The deviation about the major and minor axes of the 95% confidence ellipse are determined by calculating the ζ_{95} and η_{95} semi-angles and are given as:

$$\eta_{95} = \sin^{-1}\left(\sigma_3\sqrt{g}\right),$$
$$\zeta_{95} = \sin^{-1}\left(\sigma_2\sqrt{g}\right),$$

where:

$$g = -2\ln\left(\frac{0.05}{\left(N\hat{\mu}^2\right)}\right).$$

Because $\boldsymbol{\Gamma}$ is practically equivalent to $\mathbf{V}$, the eigenvectors of $\mathbf{V}$ give a good estimation of the direction of the semi-angles. The declination and inclination of these directions are therefore,

$$D_\zeta = \tan^{-1}\left(\frac{v_{22}}{v_{12}}\right),$$

$$I_\zeta = \sin^{-1} v_{32},$$

$$D_\eta = \tan^{-1}\left(\frac{v_{23}}{v_{13}}\right),$$

and:

$$I_\eta = \sin^{-1} v_{33}.$$

The tensor element notation, v_{12}, represents the x_1 component of the intermediate eigenvector ($\mathbf{V}_2$).

The bootstrap and Fisher statistical methods allow mean paleomagnetic directions of two data sets to be compared at a given level of confidence. Bootstrap distributions are analyzed to see if the confidence limits overlap in any of the three orthogonal directions defined by the confidence ellipse [e.g., *Tauxe,* 1998]. Such tests are important in geodynamic applications of paleomagnetism. The appropriate statistical method should be chosen subject to testing whether the paleomagnetic data sets derive from a Fisher distribution.

3.6. Statistical Methods for Analyzing Magnetic Susceptibility Tensors

The complex dependence of magnetization acquisition on, for example, temperature, stress, and crystal shape suggests that the magnetic susceptibility is not simply a scalar constant of proportionality between the applied magnetic field, **H**, and the magnetization (**M**). The general relationship between **H** and **M** may be written as three linear equations for the components of magnetization in an orthogonal coordinate system with axes, $\mathbf{X}_1$, $\mathbf{X}_2$, and $\mathbf{X}_3$, and susceptibility coefficients k_{ij} (following the notation of *Tauxe* [1998]):

$$M_1 = k_{11}H_1 + k_{12}H_2 + k_{13}H_3,$$
$$M_2 = k_{21}H_1 + k_{22}H_2 + k_{23}H_3,$$
$$M_3 = k_{31}H_1 + k_{32}H_2 + k_{33}H_3.$$

The susceptibility coefficients k_{ij} define the symmetric second-order anisotropy of magnetic susceptibility (AMS) tensor [e.g., *Hext,* 1963].

Measurement and evaluation of the magnetic suseptibility tensor in rocks may give an indication of the dominant type of anisotropy and can provide insight into the physical mechanisms that may have caused the measured anisotropy. AMS data have been used in geological contexts to determine different parameters such as paleocurrent

and paleowind directions [e.g., *Hamilton and Rees,* 1970; *Lagroix and Banerjee,* 2002], tectonic stress and strain [e.g., *Borradaile,* 1991; *Sagnotti et al.,* 1999], and directions of magmatic injections [e.g., *Knight and Walker,* 1988].

3.6.1. Determination of the AMS Tensor

There are six independent elements of the AMS tensor that need to be determined:

$$\begin{aligned} s_1 &= k_{11}, \\ s_2 &= k_{22}, \\ s_3 &= k_{33}, \\ s_4 &= k_{12} = k_{21}, \\ s_5 &= k_{23} = k_{32}, \\ s_6 &= k_{13} = k_{31}. \end{aligned}$$

A sample measurement scheme is designed where the measured susceptibility elements define a matrix, **K**, which are related to the six unknown elements, **s**, through the design matrix (**A**). The design matrix, **A**, and its transpose, $\mathbf{A}^T$, are derived from the known relationship between the different (chosen) measurement positions. A random error, δ, which has a zero mean value, may be associated with each measurement. This relationship may be expressed as:

$$K_i = A_{ij} s_j + \delta_i,$$

where the best-fitting mean values for **s** may be determined using linear algebra:

$$\bar{\mathbf{s}} = (\mathbf{A}^T\mathbf{A})^{-1}\mathbf{A}^T\mathbf{K} = \mathbf{B}\mathbf{K},$$

or in tensor notation:

$$\bar{s}_i = B_{ij} K_j.$$

It follows that the best-fitting mean value of **K** is:

$$\overline{K}_i = A_{ij}\overline{s}_j,$$

where the deviation of each component, δ_i, is:

$$\delta_i = K_i - \overline{K}_i.$$

It is possible to find an orthogonal coordinate system, **V**, where the off-axis terms are zero, which defines the eigenvectors of the susceptibility matrix. Eigenvalues, τ_i, defined by $\boldsymbol{\tau}$ are proportional to the magnitude of the diagonal elements s_1, s_2, and s_3. The eigenparameters are related to the susceptibility matrix by:

$$\mathbf{kV} = \tau\mathbf{V}.$$

The components of the eigenvectors are given by:

$$\mathbf{V} = \begin{pmatrix} v_{11} & v_{21} & v_{31} \\ v_{12} & v_{22} & v_{32} \\ v_{13} & v_{23} & v_{33} \end{pmatrix}.$$

The principal eigenvectors $\mathbf{V_1}$,$\mathbf{V_2}$, and $\mathbf{V_3}$ are the maximum, intermediate, and minimum susceptibilities, which are referred to as k_{max}, k_{int}, and k_{min}, respectively. Eigenvalues of the susceptibility sum to unity after scaling by their trace length. The parameters define a magnitude ellipsoid with semi-axes in the direction of the eigenvectors with lengths according to the eigenvalues.

Diamagnetic, paramagnetic, and ferromagnetic particles contribute to the bulk susceptibility of a rock sample and combine to define the shape of the anisotropy ellipsoid. The characteristic AMS ellipsoid may be classified according to different relationships among the three eigenvalues [e.g., *Jelinek,* 1978; *Tauxe,* 1998].

3.6.2. Linear Perturbation Statistical Method for Determining Errors Associated with the AMS Tensor

A statistical method for AMS data has been developed for measurement of multiple samples in a number of specific orientations that are evenly spaced over the unit sphere [e.g., *Hext,* 1963; *Jelinek,* 1976, 1978]. The method provides a quantifiable measure of uncertainty and data scatter, which is useful for comparing directions and detecting statistically significant differences between data sets.

Rotatable measurement designs such as this have near-spherical variance functions. The variance, in this instance, is related to the number of degrees of freedom, $n_f = N - 6$, associated with the chosen measurement scheme, where N is the total number of measurements, and is given as (following the notation of *Tauxe* [1998]):

$$\sigma^2 = \frac{\sum_i \delta_i^2}{n_f}.$$

The covariance matrix of **s** is therefore:

$$\mathbf{C} = \sigma^2 \left(\mathbf{A}^T \mathbf{A}\right)^{-1}.$$

Thus, based on determination of eigenvectors of the susceptibility tensor with an associated normally distributed random measurement error, a 95% confidence region may be defined for each eigenvector. Two-dimensional uncertainty ellipses tangential to the unit sphere and orthogonal to each eigenvector may be defined (Figure 3.5). The major and minor semi-axes of the uncertainty ellipse are aligned parallel with the two eigenvectors in the tangential plane. In the case where the uncertainty can be considered to be normally distributed, the expressions for the three confidence limits are simple:

$$\varepsilon_{12} = \tan^{-1}\left(\frac{f\sigma}{2(\tau_1 - \tau_2)}\right),$$

$$\varepsilon_{23} = \tan^{-1}\left(\frac{f\sigma}{2(\tau_2 - \tau_3)}\right),$$

$$\varepsilon_{13} = \tan^{-1}\left(\frac{f\sigma}{2(\tau_1 - \tau_3)}\right),$$

where:

$$f = \sqrt{2\left(F_{(2,n_f);(1-p)}\right)}.$$

The value F is a shape constant determined at the p probability level, with 2 and n_f degrees of freedom, which determines the extent to which the ellipsoid is statistically different from a sphere.

When dealing with multiple samples, perturbations, δ, from the mean may be large, which suggests that calculation of confidence regions based on data scatter due to simple random error is not accurate (because of large products in the covariance matrix). The mean anisotropy, **S**, for a number of samples, N_s, may be found by calculating a mean of the corresponding **s**-matrix element of each sample, e.g.:

$$\bar{S}_i = \sum_l s_{il},$$

where s_{il} is the i^{th} matrix element of the l^{th} sample. Calculation of a standard deviation for the mean of the data may then be calculated by analogy with the method for an individual sample, but with an increase in the number of degrees of freedom to $n_f = 6N_s - 6$. Thus, a 6×6 covariance matrix, **C**, arises with elements given by:

$$C_{jk} = \frac{1}{N_s}\sum_l \left(S_{lj} - \bar{S}_j\right)\left(S_{lk} - \bar{S}_k\right).$$

Transformation of the covariance matrix **C** into **C′** in eigenvector coordinates can be carried out by:

$$\mathbf{C}' = \mathbf{G}\mathbf{C}\mathbf{G}^T,$$

where **G** is the matrix:

$$\mathbf{G} = \begin{pmatrix} v_{11}^2 & v_{21}^2 & v_{31}^2 & 2v_{11}v_{21} & 2v_{21}v_{31} & 2v_{31}v_{11} \\ v_{12}^2 & v_{22}^2 & v_{23}^2 & 2v_{12}v_{22} & 2v_{22}v_{32} & 2v_{32}v_{12} \\ v_{13}^2 & v_{23}^2 & v_{33}^2 & 2v_{13}v_{23} & 2v_{23}v_{33} & 2v_{33}v_{13} \\ v_{11}v_{12} & v_{21}v_{22} & v_{31}v_{32} & v_{11}v_{22}+v_{21}v_{12} & v_{21}v_{32}+v_{31}v_{22} & v_{31}v_{12}+v_{11}v_{32} \\ v_{12}v_{13} & v_{22}v_{23} & v_{32}v_{33} & v_{12}v_{23}+v_{22}v_{13} & v_{22}v_{33}+v_{32}v_{23} & v_{32}v_{13}+v_{12}v_{33} \\ v_{13}v_{11} & v_{23}v_{21} & v_{33}v_{31} & v_{13}v_{21}+v_{23}v_{11} & v_{23}v_{31}+v_{33}v_{21} & v_{33}v_{11}+v_{13}v_{31} \end{pmatrix}.$$

A 2 × 2 covariance matrix, $\mathbf{W}_i$, for each eigenvector, $\mathbf{V}_i$, describes the variability of the mean:

$$\mathbf{W}_i = \begin{pmatrix} \dfrac{C'_{i+3,i+3}}{(\tau_i-\tau_j)^2} & \dfrac{C'_{i+3,k+3}}{(\tau_i-\tau_j)(\tau_i-\tau_k)} \\ \dfrac{C'_{i+3,i+3}}{(\tau_i-\tau_j)(\tau_i-\tau_k)} & \dfrac{C'_{i+3,k+3}}{(\tau_i-\tau_k)^2} \end{pmatrix}.$$

There are two eigenvalues, λ_m, of the covariance matrix, $\mathbf{W}_i$, which are related to the semi-axes of the confidence ellipses associated with each eigenvector (Figure 3.4) by:

$$\varepsilon_{im} = \tan^{-1}\left(\sqrt{f\lambda_m}\right),$$

where:

$$f = \frac{2(N-1)}{N(N-2)} F_{(2,N-2)}.$$

As in the calculation for an individual sample, F is a shape constant determined at the p^{th} probability level. The method of linear perturbation analysis applied to multiple samples provides a proper statistical framework (similar to the paleomagnetic vector framework) for analysis of AMS data from geological rock formations [*Jelinek,* 1976]. In geological applications, the bulk rock magnetic fabric may be investigated by analyzing AMS data.

3.7. Magnetic Mineralogy

It is important to have a detailed understanding of the type and grain-size distribution of magnetic minerals responsible for the remanent magnetization in a studied rock. The NRM may consist of different magnetic components, which do not necessarily yield ancient paleomagnetic directions. Paleomagnetic field tests, which are based on geological field relationships, are often helpful for determining whether a magnetization is ancient or recent. Rock magnetic experiments provide important additional information about the magnetic mineralogical characteristics of the rock samples.

Different remanence-bearing magnetic minerals possess different diagnostic physical properties such as the Curie temperature, magnetocrystalline anisotropy energy, low-temperature transition temperatures, saturation magnetization, coercivity, and high-temerature chemical alteration [e.g., *Dunlop and Özdemir,* 1997]. The most common remanence-bearing minerals are magnetite (Fe_3O_4), titano-magnetite ($Fe_{(3-x)}Ti_xO_4$), maghemite (γFe_2O_3), hematite (αFe_2O_3), goethite ($\alpha FeOOH$), pyrrhotite (Fe_5S_6 - $Fe_{11}S_{12}$), and greigite (Fe_3S_4). Several rock magnetic experiments are usually required to determine the remanence carriers because some experiments can be ambiguous due to non-uniqueness of some physical properties or due to the effects that the natural physical environment has had upon the minerals. Rock magnetic measurements are generally more effective than direct microscopic observations for determining the magnetic mineralogy because magnetic minerals are usually extremely small and are only present in rocks in extremely low concentrations.

3.7.1. Laboratory Induced Remanent Magnetizations

A remanent magnetization may be artificially imparted by deliberately subjecting samples to magnetic fields in the laboratory. Based on the analysis of such magnetizations, it is possible to determine a variety of magnetic properties.

An anhysteretic remanent magnetization (ARM) may be acquired by subjecting a sample to a linearly decaying AF (analogous to AF demagnetization) from a specified peak field whilst simultaneously applying a biasing DC field. This serves to progressively align all particles with coercivities below the peak AF in the direction of the DC field. The DC field is chosen so that it has a similar order of magnitude as the Earth's magnetic field (typically around 0.1 mT). Because the magnetizing field is small, SD and PSD particles will become magnetized and align with the DC field more efficiently than MD particles. SD and PSD grains are also more likely to faithfully record an ancient NRM in the Earth's field.

By applying a strong, short-term magnetization to a sample using an electromagnet at a constant temperature, a laboratory-induced IRM may be imparted to the sample. A strong field (usually between 0.9–3 T) is chosen so that the sample becomes magnetically saturated, and acquires a saturation IRM (SIRM), which is equivalent to M_r. All magnetic particles (including MD particles) that are capable of carrying a remanence will be affected by such a field. ARM and IRM measurements are the most commonly used in rock magnetic experiments [e.g., *Verosub and Roberts,* 1995; *Dunlop and Özdemir,* 1997].

3.7.2. Thermal Demagnetization of NRM (or ARM or IRM)

In addition to removing unwanted components of NRM for determining the ChRM of a sample, thermal demagnetization of an NRM, ARM, or IRM can provide mineral-specific high-temperature data. The point at which the magnetization becomes reduced to near zero values may give an indication of the magnetic mineral(s) responsible for the magnetiztion (i.e., the SD or PSD particles) [e.g., *Butler,* 1992]. For example, the Curie temperature is 580°C for magnetite and 680°C for hematite, which may be revealed by the characteristic decay of the magnetization at those temperatures. At high temperature steps, the remanence may become too weak to measure.

3.7.3. Thermomagnetic Curves

High temperature behaviour may also be investigated by heating a sample to elevated temperatures and by measuring the magnetization in steps whilst applying a constant magnetic field to the sample. Such measurements may be carried out using a variable field translation balance (VFTB) or Curie balance. All particles are magnetized in an applied field, including paramagnetic, diamagnetic, SD, PSD, and MD ferromagnetic particles. Magnetizing fields in such measurements are therefore usually kept at low values to ensure that the magnetization due to the remanence-bearing fraction is not masked by paramagnetic minerals.

Thermomagnetic curves may be used to determine Curie temperatures of the magnetic minerals. For Curie temperature determinations, it is important that the thermomagnetic curve is reversible by measuring the magnetization during cooling to room temperature. Cooling curves are useful for detecting thermal alteration of minerals. Performing several heating and cooling cycles to progressively higher peak temperatures can reveal the temperature at which the thermal alteration occurred.

3.7.4. Thermal Demagnetization of an IRM

Stepwise thermal demagnetization of an IRM enables investigation of the high-temperature properties of all remanence carriers (SD, PSD, and MD). The strong magnetization may allow minerals with low saturation remanence (e.g., goethite) to be detected more easily than by thermal demagnetization of an ARM. Results of thermal demagnetization of an IRM are less likely to be affected by thermal alteration because the mineral alteration products are not being actively magnetized by an applied field during measurement. Although strongly magnetic minerals may form at elevated temperatures during IRM or ARM thermal demagnetization experiments, they will not generally obscure the signal due to the remanence-bearing particles to the same extent as during thermomagnetic measurements. In addition, laboratory fields are relatively random and weak in magnetically shielded areas, which suggests that, in many instances,

the remanences acquired by alteration products should cancel out or not significantly affect the remanence. Furthermore, any contribution to the remanence from altered mineral products are likely to be less significant for thermal demagnetization of an IRM than for an ARM or NRM because of the relatively high intensity of the IRM.

High-temperature behaviour of different coercivity components may be investigated by carrying out thermal demagnetization of an IRM applied to a sample along three orthogonal axes [cf. *Lowrie,* 1990]. A strong (preferably saturating) field is applied first along one axis of the sample. A smaller field is then applied to the sample in a direction perpendicular to the original IRM. This causes particles with coercivities less than the applied field to re-align along the second axis. Finally, an IRM is imparted to the third orthogonal axis with a relatively low field value, which re-aligns the lowest coercivity fraction of grains within the sample. Thus, thermal demagnetization and measurement of these components provides mineralogical information regarding the discrete coercivity fractions.

High-temperature methods are powerful for determining the magnetic mineral composition of paleomagnetic samples, but are nevertheless restricted by the possibility of mineral alteration at elevated temperatures. Thermal alteration can be significant, even when laboratory fields are small, if there is production of new strongly magnetic minerals (e.g., magnetite) in large concentrations. For example, a sample composed predominantly of clay minerals, which commonly alter to form magnetite at elevated temperatures, could obtain a substantial magnetization in a well-shielded laboratory due to the large number of clay minerals. In many cases, rock magnetic experiments that are based on the analysis of magnetizations at room temperature are more appropriate indicators of magnetic mineralogy.

3.7.5. AF Demagnetization of NRM

The main purpose of AF demagnetization is to isolate the primary NRM component. However, in many cases, inspection of vector component diagrams indicates

magnetic components with discrete coercivity spectra. This is mostly used as a rapid screening method for identifying high or low-coercivity components. Such information can be used for constraining the interpretation of other rock magnetic results.

3.7.6. Partial ARM Acquisition Experiments

The measured ARM associated with a discrete coercivity window (e.g., 15-20 mT) is known as a partial ARM (pARM). A pARM may be determined for successive coercivity windows, which defines a pARM curve for the particular sample under investigation. The procedure for applying a pARM to a sample begins by AF-demagnetizing the sample from a peak field suitably chosen to ensure that the remaining magnetization after AF demagnetization becomes negligible. An ARM is then applied to the sample from a peak AF that corresponds to the desired upper limit of the pARM window. In order to obtain the pARM, the sample is AF demagnetized (with no bias field) from the peak AF that corresponds to the desired lower limit of the window. The remaining pARM may then be measured and plotted against the coercivity of the pARM window.

Partial ARM curves provide a method for investigating the contribution of each coercivity fraction to the ARM [*Jackson et al.*, 1988]. Peaked behaviour suggests that a well-defined population of particles is reponsible for the magnetization. This may be linked to particular minerals and grain sizes.

3.7.7. IRM Acquisition Experiments

Subjecting a paleomagnetic sample to stepwise increasing magnetizing fields and measuring the magnetization at each step allows the IRM acquistion behaviour to be determined. Such measurements allow aspects of the coercivity spectrum of the sample to be analyzed. The field at which saturation occurs may be defined and can be characteristic of particular types of magnetic minerals. Rates of increase in IRM with increasing field values vary depending on mineralogy.

3.7.8. Hysteresis Loops

Many useful parameters such as saturation magnetization, saturation remanence, coercivity, and coercivity of remanence may be obtained from hysteresis measurements, which help to identify magnetic minerals. However, the shape of magnetic hysteresis loops can also provide information regarding the distribution of particles within a paleomagnetic sample [*Roberts et al.,* 1995; *Tauxe et al.,* 1996].

In general, a rock sample will comprise SP, diamagnetic, paramagnetic, and ferromagnetic mineral phases with different grain sizes. Each type of magnetic mineral has characteristic hysteresis behaviour, which can lead to complex mixed loops that are made up by contributions from several end-member types (Figure 3.1). Particular mixtures may cause the hysteresis loops to take a distinctive shape. Typical shapes are the goose-necked, wasp-waisted, and pot-bellied hysteresis loops [*Roberts et al.,* 1995; *Tauxe et al.,* 1996]. A mixture of hematite with SD magnetite may lead to a goose-necked distortion of the loop. Wasp-waisted or pot-bellied loops have been observed for particular mixtures of SD and SP magnetite. Hysteresis loops may, therefore, contain important information about the carriers of magnetization and their grain sizes.

3.7.9. First Order Reversal Curve (FORC) Diagrams

In certain mixed particle magnetic systems, analysis of a single hysteresis loop may reveal information about the distribution of particles. In nature, however, mixtures of magnetic phases can be complex and there may be magnetic interactions between particles. As a result, it is likely to be difficult to determine the presence or absence of any given magnetic phase purely by analysis of a single hysteresis loop. FORC diagrams provide a means of using detailed hysteresis measurements to provide information about the entire magnetic assemblage rather than the bulk average properties provided by a single hysteresis loop.

A FORC diagram is obtained according to the following procedure. First, a sample is subjected to a saturating field, which is then ramped down to a chosen reversal field, H_a, such that only a certain proportion of the particles have had their magnetic moments switched into the opposite direction. The field is then increased from the reversal field, H_a (i.e., not the negative saturating field), until positive saturation is reached again (Figure 3.6a). The particle anisotropy energy barriers cause the affected fraction of grains to display hysteresis behaviour. Thus, partial hysteresis loops may be defined by cycling the magnetizing field between saturation and different successive reversal fields. The major hysteresis loop is the limiting envelope of several partial hysteresis loops. The magnetization curve, measured from the reversal field back to positive saturation, is the first order reversal curve (FORC) (Figure 3.6a).

The shape of the FORC will be distinct for different types of magnetic behaviour. The second derivative of the magnetization as a function of the reversal point H_a and the point of evaluation H_b along the reversal curve may be used to quantify the curvature of such curves. Evaluation at several points along different FORCs gives rise to a FORC distribution, which is given as:

$$\rho(H_a,H_b) \equiv -\frac{\partial^2 M(H_a,H_b)}{\partial H_a \partial H_b},$$

which is defined for $H_b > H_a$ [*Pike et al.*, 1999]. The distribution may be transformed into a more intuitive coordinate system, $\{H_c = (H_b-H_a)/2,\ H_u = (H_a+H_b)/2\}$, where H_c is the microscopic coercivity. Different FORCs may display different behaviour, which enables evaluation of different components of the mixed magnetic system by contouring the second derivative distribution in a FORC diagram against H_u and H_c (Figure 3.6b). A vertical spread of contours to high and low values of H_u occurs due to magnetic interaction effects between particles and the spread of the contours along the H_c axis is due to the coercivity of the measured particle distribution [*Pike et al.*, 1999; *Roberts et al.*, 2000].

3.7.10. Low-Temperature IRM Measurements

A further class of magnetic mineralogical data can be obtained from low-temperature measurements of an IRM. During such experiments, the magnetization is measured between low temperatures of about 5 K and room temperature (300 K). Low-temperature behaviour may be investigated by, for example, 1) cooling the sample in the presence of a constant magnetizing field (field-cooled (FC) curve) and measuring the magnetization upon heating back to room temperature, 2) cooling the sample in the absence of a field, applying an IRM to the sample at low temperature (zero-field-cooled (ZFC) curve), and measuring the magnetization during heating back to room temperature, or 3) applying an SIRM at room temperature and measuring the magnetization during low-temperature cooling and heating cycles (room-temperature (RT)-SIRM curve).

Low-temperature data can be used to identify magnetic transitions that are characteristic of particular magnetic minerals [e.g., *Dunlop and Özdemir,* 1997]. Low-temperature measurements can be particularly useful if high-temperature results are unreliable due to thermal alteration.

3.8. Summary

An understanding of magnetization processes and the origin of magnetic remanence is required for practical analysis of paleomagnetic data. Demagnetization techniques are used to isolate the ChRM component from paleomagnetic samples. Rock magnetic data provide evidence concerning the magnetic mineralogy and the grain-size distribution of particles. This allows assessment of whether the NRM and ChRM components are reliable indicators of the ancient geomagnetic field. A rigorous statistical framework enables appropriate mean paleomagnetic directions and mean AMS eigenvectors to be calculated and enables quantitative comparison with other data sets.

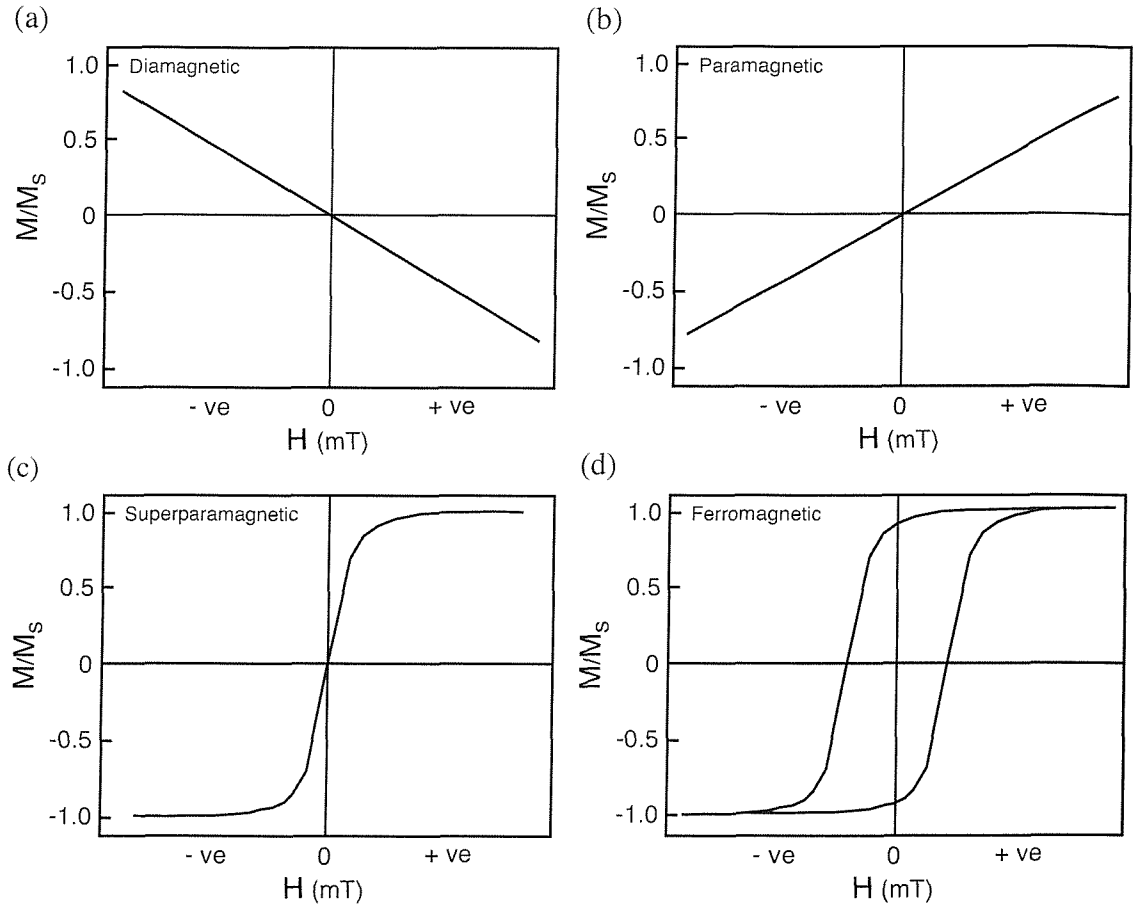

Figure 3.1. Characteristic hysteresis loops for end-member types of rock-forming magnetic minerals. (a) Diamagnetic behaviour. (b) Paramagnetic behaviour. (c) Superparamagnetic behaviour. (d) Ferromagnetic behaviour. For ferromagnetic materials, remanence properties will differ between minerals and amongst different coercivity or grain-size distributions.

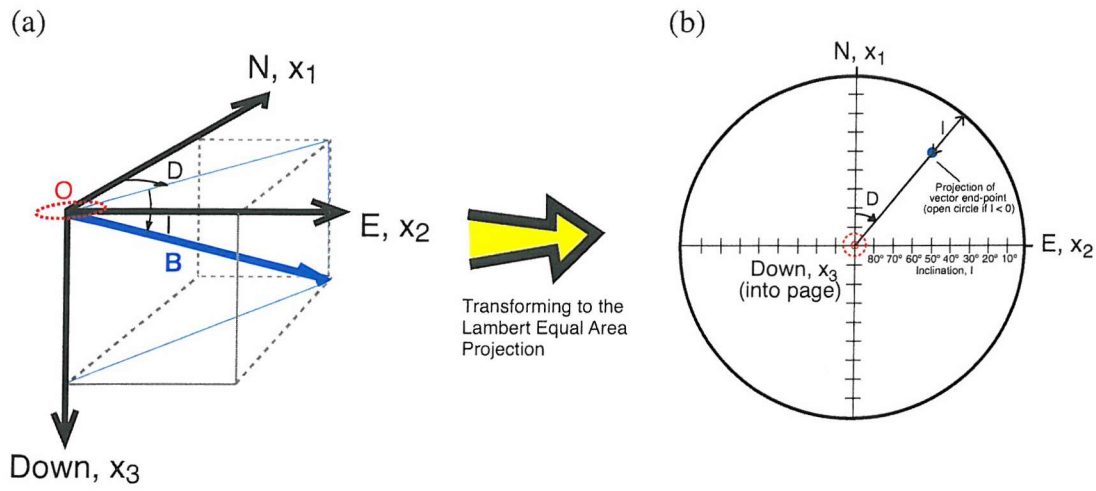

Figure 3.2. (a) Components of the geomagnetic field (**B**). The angle of declination (horizontal plane), *D*, and inclination (vertical plane), *I*, together with the magnetic intensity, combine to fully describe the field. (b) The Lambert equal area stereographic projection of the magnetic vector. Inclination is positive downward in the northern hemisphere. Positive inclinations are indicated by solid symbols. Open symbols are used for negative inclination values.

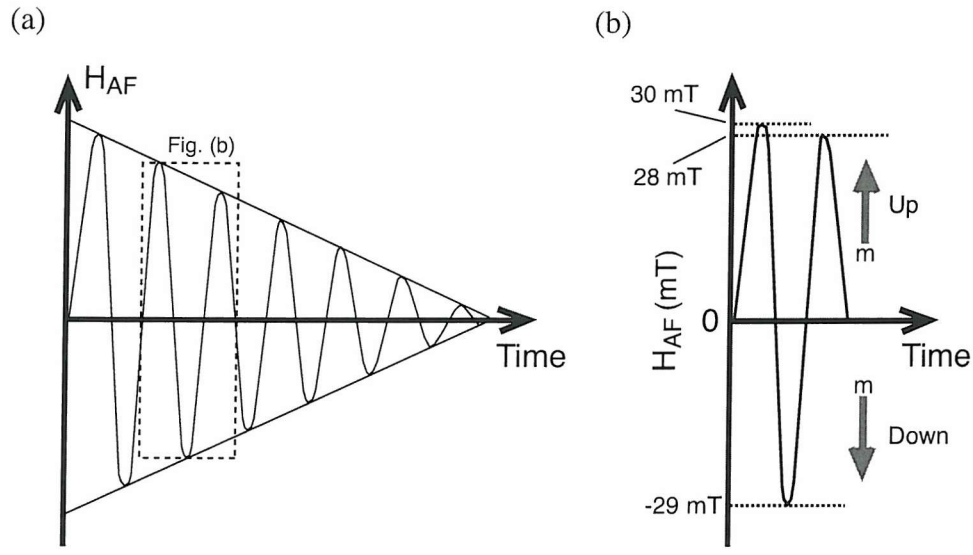

Figure 3.3. Schematic representation of AF demagnetization. (a) The sinusoidal waveform of the magnetic field decays linearly to zero from a peak AF. (b) Detailed view of part of the decaying waveform in Figure (a). At the first peak, the moments, *m*, are magnetized in the direction of the peak field. As the field is decreased from 30 to 29 mT, particles with coercive force between 30 and 29 mT become locked such that their net moment equals zero over the wave cycle. Modified after *Butler* [1992].

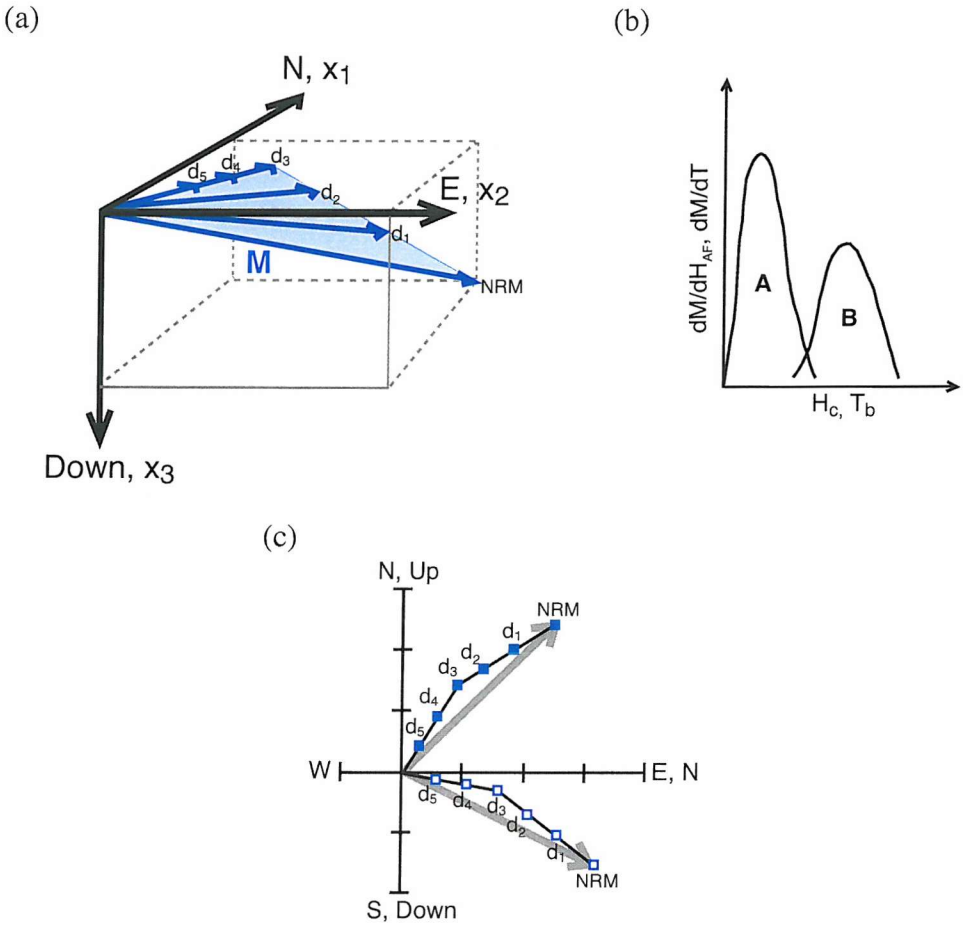

Figure 3.4. (a) Example of changes in a magnetization vector after successive demagnetization steps (d_1-d_6). The decrease in intensity after each step results in a shorter vector. Both the declination and inclination may change during demagnetization. Magnetization components may be identified from a constant declination and inclination over several demagnetization steps. (b) Schematic representation of a coercivity, H_c, or blocking temperature, T_b, distribution consisting of two magnetization components with slight overlap. Each component may have different declination and inclination values. The B-component is a high- stability T_b or H_c component, which may only be revealed after sufficient demagnetization and removal of component A. (c) Vector component diagram consisting of two well-defined components of magnetization. The diagram displays both the projection of declination (solid symbols) and inclination (open symbols) in the horizontal and vertical planes, respectively, for each demagnetization step. As the magnetization becomes weaker, the vector end-points plot closer to the origin. The resultant NRM vector is indicated by the grey arrow. The inclination is projected onto the vertical plane containing the north axis, which is indicated by a second label, *N*, on the x-axis of the diagram.

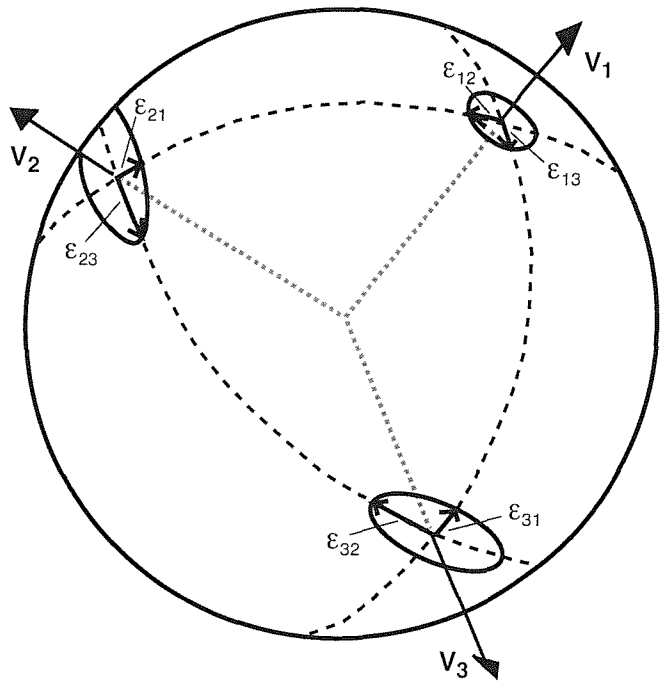

Figure 3.5. Uncertainty ellipses associated with the calculation of principal eigenvectors, **V**, and linear perturbation analysis of AMS tensor data. Uncertainty ellipses are tangential to the unit sphere. The semi-angles, ε_{im}, of the ellipses are defined to be parallel to the two orthogonal eigenvectors in the normal plane. Modified after *Tauxe* [1998].

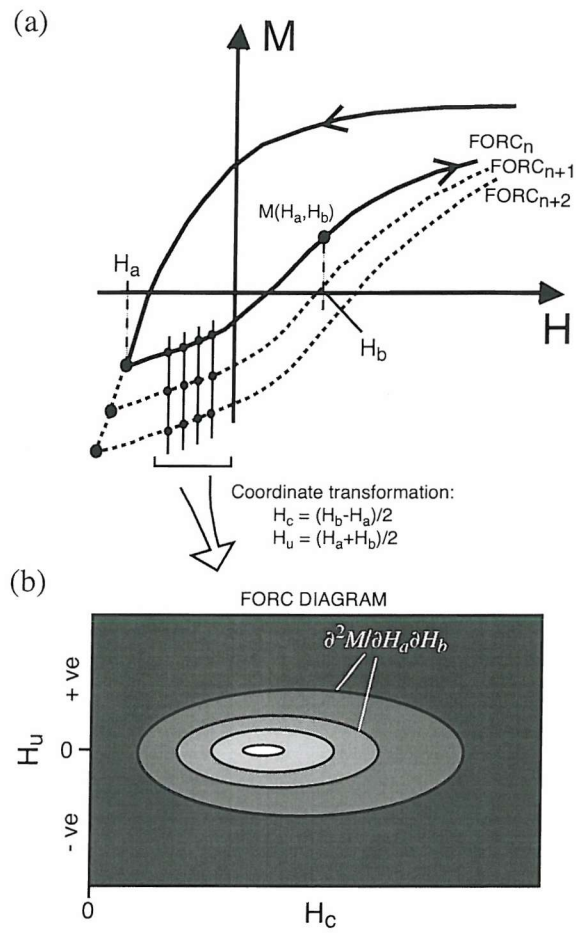

Figure 3.6. (a) Definition of a first-order reversal curve (FORC). The magnetic field, H, is ramped down from saturation to a reversal field value H_a. The FORC is the magnetization curve, M, measured from H_a back to positive saturation. Measurement of successive FORCs allows evaluation of the FORC distribution at several points to form a data array, which may be contoured in a FORC diagram. (b) Schematic representation of a FORC diagram. The FORC distribution is transformed into the $\{H_c,H_u\}$ coordinate system and is contoured for ease of interpretation. H_c is the microscopic coercive force. Lighter shades indicate higher values.

4

Geodynamic implications of paleomagnetic data from Tertiary sediments in Sakhalin, Russia (NW Pacific)

This chapter appeared in *Journal of Geophysical Research*, Volume 108 (B5), Weaver, R., A. P. Roberts, R. Flecker, D. I. M. Macdonald, and L. M. Fot'yanova, Geodynamic implications of paleomagnetic data from Tertiary sediments in Sakhalin, Russia (NW Pacific), 2066, doi: 10.1029/2001JB001226, Copyright (2003), with permission of the American Geophysical Union.

Abstract

N-S-trending right-lateral strike-slip faults, which were active in the Tertiary, transect Sakhalin, Russia, while Mesozoic fore-arc and accretionary rocks testify to an earlier period of subduction. Several kinematic models have been proposed for the region, but the details required to constrain these models, such as the timing of the transition from subduction to strike-slip tectonics in Sakhalin, are still unknown. Even first-order tectonic features, such as boundaries of the plates with which Sakhalin evolved during the Tertiary, are poorly known. Paleomagnetic results from around Sakhalin were obtained to constrain the geodynamic evolution of the region. Comparison of paleomagnetic inclination data with the apparent polar wander paths for the Eurasian, Pacific and North American plates suggests that Sakhalin probably evolved with the North American Plate, although a history including the Eurasian Plate cannot be ruled out. Paleomagnetic declination data suggest that significant clockwise vertical-axis rotation has occurred in Sakhalin since the mid-Paleocene. It is likely that this rotational deformation was accommodated by Tertiary activity on right-lateral strike-slip faults, which may be associated with the opening of the Japan Sea, Tatar Strait and Kuril Basin. These data contradict a published kinematic model for eastern Sakhalin, where anticlockwise vertical-axis rotations were predicted for Neogene basins in the East Sakhalin Mountains. Agreement is better, however, with published paleomagnetic data from southern Sakhalin, where clockwise vertical-axis rotations were documented.

4.1. Introduction

The plate configuration of the NW Pacific margin, around the Okhotsk Sea, is complex and the positions of boundaries between the Pacific, North American, Eurasian and Okhotsk Sea plates have not been precisely determined. This is partly due to the sparse distribution of seismic events, particularly in the NE part of the Asian continent [*Riegel et al.*, 1993; *Seno et al.*, 1996]. A wide zone of N-S-trending strike-slip faults, which crops out in Sakhalin, is considered to represent an active transform plate

boundary, but it is uncertain which plates are interacting in this area (Figures 4.1, 4.2) [*Seno et al.*, 1996]. The Tertiary geodynamic evolution of Sakhalin is also unclear. A Mesozoic accretionary complex in Sakhalin indicates a previous period of subduction (Figure 4.1c), but a transition to a dextral transpressive regime occurred some time in the Tertiary [*Kimura*, 1994]. Deep-sea drilling in the Okhotsk Sea could reveal vital geological data, particularly regarding the age of sedimentary basins, but this has not been carried out. In this study, we use paleomagnetic methods to address these first-order tectonic issues, and to develop an improved understanding of local tectonics. Paleomagnetic methods have proved valuable for constraining the geodynamic evolution of tectonically complex regions, such as the Philippines [*Fuller et al.*, 1989], the Aegean Sea [*Kissel and Laj*, 1988], New Zealand [*Little and Roberts*, 1997] and California [*Luyendyk et al.*, 1985]. Paleomagnetic work has been previously carried out on Tertiary rocks from three localities in southern Sakhalin [*Takeuchi et al.*, 1999], but no other paleomagnetic work has been reported on the Tertiary evolution of Sakhalin.

Several kinematic models for the NE Asian margin have been proposed which include Sakhalin and the Okhotsk Sea and suggest strike-slip deformation, pull-apart basin formation, and vertical-axis rotations of crustal-scale blocks [e.g., *Jolivet et al.*, 1995; *Worrall et al.*, 1996; *Takeuchi et al.*, 1999]. Much of the data on which these models are based are from Japan and the Japan Sea and it is not clear how Sakhalin has deformed. There are two models that suggest rotation of fault-bounded "domino" blocks in Sakhalin (Figure 4.3). *Fournier et al.* [1994] suggested that counterclockwise rotations would be expected for Neogene basins in eastern areas of Sakhalin (Figure 4.3a). More recent work by *Takeuchi et al.* [1999], based on paleomagnetic data from Hokkaido and southern Sakhalin, suggests that clockwise rotations have occurred, accommodated by 100-km-scale crustal blocks, which are part of a domino system that could extend southward to Hokkaido, Japan (Figure 4.3b). However, there are several problems with domino models. What happens at the edges of crustal blocks? With the fault geometries indicated in such models, triangular zones of compression or extension would be

expected at the boundaries of the blocks [e.g., *Luyendyk et al.*, 1980; *Hornafius et al.*, 1986; *Roberts*, 1995a; *Townsend and Little*, 1998; *Bayasgalan et al.*, 1999]. These structures are not evident in the field in Sakhalin. Also, rotations of more than 25° are theoretically impossible on a single set of faults [e.g., *Nur et al.*, 1989]. Evidence for multiple fault sets should therefore be expected to accommodate large-scale rotations.

Paleomagnetic data presented here should allow more accurate identification of rotated domains in Sakhalin, and may justify reconsideration of the existing kinematic models for evolution of the NE Asian margin. In this study, we aim to address the following questions. 1) With which plates has Sakhalin interacted and evolved? 2) When did the transition from subduction to strike-slip tectonics occur in Sakhalin? 3) By which structural mechanisms did the transition occur?

4.2. Geological Background and Sampling

4.2.1. Regional Geology

Sakhalin comprises two main tectonic zones separated by the N-S-trending Central Sakhalin Fault (Figure 4.1b). To the east, Mesozoic accretionary complex material has been uplifted [e.g., *Rikhter*, 1984; *Parfenov and Natal'in*, 1986]. These blueshist- and greenshist-facies metamorphic rocks are exposed in the East Sakhalin Mountains, NE Schmidt Peninsula, and on the Tonino-Aniva Peninsula in southern Sakhalin (Figure 4.1b,c) [*Vereshchagin*, 1969]. Small Tertiary depocentres, which may have pull-apart origins, also exist in these areas [*Worrall et al.*, 1996]. West of the Central Sakhalin Fault, there is a thick sequence of Mesozoic fore-arc sediments (Figure 4.1b,c) [*Parfenov and Natal'in*, 1986; *Zyabrev*, 1987]. The corresponding Mesozoic-Cenozoic volcanic arc is the East Sikhote Al'in Volcanic Belt [*Zonenshain et al.*, 1990; *Okamura et al.*, 1998] on the Russian mainland (Figure 4.1c).

Northeastern Russia is made up of a series of accreted terranes. Crustal blocks are defined and separated by magmatic arcs and accretionary complexes; arcs also stitch across earlier sutures [*Natal'in*, 1993]. The Mongol-Okhotsk Suture, which stretches

from the northern side of the Okhotsk Sea to SE Siberia, marks the Permian to Jurassic northeastward oblique collision of the Bureyinskiy Massif with the Siberian Craton (Figure 4.1c). A second suture, the Amur Suture, formed to the west of Sikhote Al'in in the Cretaceous by subsequent accretion of the Sikhote Al'in terrane. During accretion of Sikhote Al'in, subduction on the east side of the Russian mainland created the Late Cretaceous - Paleogene Sikhote Al'in volcanic arc. *Zonenshain et al.* [1990] suggested that oceanic subduction also occurred further east to give rise to the "East Sakhalin Arc". The unknown oceanic plate separating the "East Sakhalin Arc" from Sikhote Al'in was consumed through westward subduction. Late Cretaceous - early Eocene volcanic rocks in Sikhote Al'in are usually assumed to be associated with this subduction event and are the source of fore-arc sediments in the Sakhalin Trough [*Zonenshain et al.*, 1990].

Paleocene to Pliocene sediments were targeted for this paleomagnetic study (Figure 4.4). These sedimentary rocks occur in a variety of settings, including: 1) Tertiary terrestrial sequences, which mostly lie to the west of the West Sakhalin Mountains and date back as far as the Paleocene, 2) marine and continental sediments in the central valley and in small basins peripheral to the East Sakhalin Mountains; these are mostly of Oligocene and younger age, and 3) early Miocene-Pliocene sediments of the Amur delta in central northern areas (Figures 4.1b,c). Late Mesozoic and late Cenozoic tectonic events have caused strongly deformed sediments in the West Sakhalin Mountains [*Vereshchagin*, 1969] with NW-SE-trending mesoscale folds associated with late Cenozoic faulting [*Rozhdestvenskiy*, 1982; *Fournier et al.*, 1994].

4.2.2. Field Sampling

Dating and correlation of the Cenozoic sediments on Sakhalin are hampered by the predominance of continental and paralic strata. A relatively good lithostratigraphic framework has been constructed, constrained in part by biostratigraphic data from the successions deposited during episodic marine transgressions [*Menner et al.*, 1977; *Serova and Fot'yanova*, 1981; *Gladenkov*, 1988; *Zhidkova and Sal'nikov*, 1992;

Fot'yanova et al., 2001]. Recent isotopic dating of Tertiary volcanic rocks on Sakhalin [*Takeuchi*, 1997; *Okamura et al.*, 1998] broadly supports this framework, but the general accuracy of the chronostratigraphy, particularly in the continental parts of the succession, is difficult to judge.

The approximate stratigraphic range of paleomagnetic samples is indicated by vertical bars on the stratigraphic columns in Figure 4.4. At each locality, approximately 40 samples were taken from a number of beds within the stratigraphic sequence in order to obtain a mean paleomagnetic direction for which the geomagnetic secular variation has been adequately averaged. Paleomagnetic samples were collected from a diverse suite of Cenozoic rocks with a wide geographic distribution: southwest of the region dominated by strike-slip faulting, local to the Central Sakhalin Fault, and in the far east of Sakhalin (Figures 4.4, 4.5). A total of 1574 samples was collected from 28 localities around Sakhalin (Figure 4.5; Table 4.1). However, only 9 localities (160 samples) yielded reliable paleomagnetic data (Figure 4.5; Tables 4.1, 4.2); samples from 12 localities were remagnetized (see Appendix A), and samples from the other 7 localities were too weakly magnetized to provide reliable paleomagnetic data (see Appendix B). The localities that yielded reliable paleomagnetic results are listed in Table 4.1, which includes details of the local stratigraphy and structure.

4.3. Methods

4.3.1. Paleomagnetic Measurements

The natural remanent magnetization (NRM) of standard cylindrical samples (25-mm diameter × 22-mm height) was analyzed using a 2G Enterprises cryogenic rock magnetometer at the Southampton Oceanography Centre (SOC), U.K., and at the Istituto Nazionale di Geofisica e Vulcanologia (INGV), Rome, Italy. All analyzed samples were subjected to progressive demagnetization with a minimum of 10 steps until the samples were almost fully demagnetized and a characteristic remanent magnetization (ChRM) component was isolated, or until magnetometer noise levels were reached. The samples

measured at the SOC were individually measured in four orientations and then remeasured in four orientations in the opposite direction before averaging to ensure directional consistency and precision. It was not possible to follow this procedure at INGV, but the reproducability of results was checked and an accuracy of 1-2° was attained for consecutive runs. Pilot samples were measured from every locality using thermal and alternating field (AF) demagnetization techniques. Measurement of low-field magnetic susceptibility at each heating step indicated that thermal alteration occurred at elevated temperatures (above 350°C) in almost all samples. Where a ChRM was isolated prior to thermal alteration, the two techniques usually gave comparable results (Figure 4.6). AF demagnetization was therefore preferred for routine treatment, which was carried out using a tumbling demagnetizing system.

4.3.2. Paleomagnetic Analyses

Paleomagnetic data were interpreted by least-squares principal component analyses of vector component diagrams [*Kirschvink*, 1980]. Statistical treatment of the directional data was carried out using the non-parametric bootstrap method of *Tauxe et al.* [1991]. This statistical framework is ideal for small paleomagnetic data sets ($N < 25$), and makes no assumptions about the initial distribution from which the data were derived. This allows meaningful precision estimates at the 95% confidence level for data sets that are not fisherian. For fisherian data sets, the bootstrap calculations approximate the α_{95} estimates calculated following *Fisher* [1953]. For non-fisherian distributions instead of reporting α_{95} estimates, we report the 95% confidence limits for the semi-axes of the uncertainty ellipse (η_{95}, ζ_{95}) following *Tauxe et al.* [1991].

4.3.3. Magnetic Properties

A range of rock magnetic measurements was made to identify the magnetic mineral(s) responsible for the paleomagnetic signal at each locality. Approximately 5 representative samples from each locality were subjected to detailed rock magnetic

analyses. Anhysteretic remanent magnetizations (ARMs) were imparted to samples from each locality by applying a 0.1 mT DC bias field in the presence of a linearly decaying AF. Partial ARM (pARM) measurements were also made for progressively higher coercivity windows from 5 to 90 mT [e.g., *Jackson et al.,* 1988]. An ARM was first imparted for the range of coercivities up to the upper limit of the required coercivity window; the samples were then AF demagnetized up to the lower limit of the window. The portion of the ARM imparted between the upper and lower limits of the pARM window was then measured using a cryogenic magnetometer at the SOC. Between each pARM measurement, the samples were AF demagnetized at a peak field that was 5 mT higher than the upper limit of the previous step to ensure that the ARM was removed before the next measurement.

Low-temperature magnetic properties were analyzed using a Quantum Design Magnetic Properties Measurement System (MPMS-XL5) at the Institute for Rock Magnetism, Minnesota, U.S.A. Zero-field-cooling experiments were carried out by cooling a sample to 20 K in zero field, applying a field of 2.5 T and then switching off the field before measuring the low-temperature isothermal remanent magnetization (IRM) during heating back to 300 K. These measurements help with identification of the magnetic mineral(s) responsible for the NRM and help to assess the reliability of the ChRM in the samples. Thermomagnetic curves were obtained for bulk sediment samples using a variable field translation balance with a field of 76 mT and a heating rate in air of 10°C/min up to 700°C. Thermal alteration affected most samples at temperatures around 350°C and no mineralogically diagnostic data were obtained.

In addition, an impulse magnetizer was used to impart an IRM to a selection of 3-7 samples from each locality at increasing fields up to 0.8 T to assess the significance of magnetic remanence anisotropy. The field was applied at 45° to the bedding plane, to avoid any field impressed anisotropy [*Tauxe et al.,* 1990], and the IRM was then measured parallel (IRM_x) and perpendicular (IRM_z) to bedding.

The anisotropy of magnetic susceptibility (AMS) was measured using an AGICO Kappabridge KLY-3S magnetic susceptibility meter on samples from localities with well-defined paleomagnetic data. Measurements were made in rotational mode to evaluate the susceptibility in 3 orthogonal planes, at the INGV, Rome, Italy. The measurements allow evaluation of the percentage anisotropy, the shape of the anisotropy ellipsoid, and the dominant magnetic fabric. This can be important in sedimentary rocks where compaction can affect the orientation of magnetic grains at around the time of magnetization lock-in [*Blow and Hamilton*, 1978].

4.4. Results

4.4.1. West Sakhalin

4.4.1.1. Kitosiya River

Eight samples from Kitosiya River were subjected to thermal demagnetization. AF demagnetization was performed on the remaining samples. Thermal and AF demagnetization reveal the same component of magnetization (Figure 4.6a,b). A stable reversed polarity ChRM was found in 12 samples, and a normal polarity ChRM was identified in two samples (Figure 4.7a). A weak normal polarity viscous overprint is evident in some samples, probably due to exposure in the present-day geomagnetic field (Figure 4.6a). Rapid decay of the magnetization to near-zero levels at around 360°C suggests that a magnetic iron sulphide may be present in some of the samples. The Verwey-transition, which is identified by an anomaly at around 120 K in low-temperature data, indicates that magnetite is present (Figure 4.8). High relative pARM intensities below 20 mT, and a second peak at 30 mT, confirms that a range of magnetite grain sizes is likely to be present from pseudo single-domain (PSD) sizes of 2-3 μm, to multi-domain (MD) sizes of around 5–25 μm [*Jackson et al.*, 1988] (Figure 4.9). The paleomagnetic directions for the magnetite and inferred sulphide NRM components are indistinguishable and, therefore, it is likely that both components locked in at a similar time. The data are insufficient for a reversals test (Figure 4.7a), but the presence of

normal and reversed polarity data suggests that the sampled interval is thick enough to have enabled averaging of geomagnetic secular variation. The ChRM is interpreted as a primary magnetization, with a locality-mean direction of D = 218.6°, I = -56.4°, with α_{95} = 6.6° (Figure 4.7a; Table 4.2).

4.4.1.2. Okhta River

Samples from Okhta River have both stable normal and reversed polarity ChRM directions, which are usually isolated after removal of a secondary normal polarity component (Figure 4.6c). *Weaver et al.* [2002] demonstrated that the normal polarity samples carry a syn-folding magnetization, while the reversed polarity samples are consistent with a geocentric axial dipole direction at the site latitude. Based on detailed rock magnetic and electron microscopic investigations of polished sections, they showed that the syn-folding magnetization in the normal polarity samples is carried by pyrrhotite, which the evidence suggests formed in association with a late diagenetic fluid migration event. For the reversed polarity samples, thermal demagnetization appears to reveal the same component of magnetization identified with AF demagnetization, although the thermal data are noisier (Figure 4.6d). Low-titanium magnetite appears to be the primary remanence carrier because the NRM falls to near-zero values at around 550°C (Figure 4.6d). Low-temperature data contain evidence of a weak Verwey transition, which suggests that magnetite is present (Figure 4.8). Partial ARM data suggest that PSD magnetite grains probably carry the remanence in the reversed polarity samples from Okhta River (Figure 4.9). The reversed polarity ChRM and improved clustering after tilt correction (Table 4.2) suggests that these directions are primary. Locality-mean values are D = 179.7°, I = -66.2°, with α_{95} = 3.9° (Figure 4.7b; Table 4.2).

4.4.1.3. Kholmsk Pass

Useful paleomagnetic data were obtained for 38 samples from Kholmsk Pass. Stable magnetizations are discernable after removal of viscous magnetic overprints

which are present in many samples (Figure 4.6e,f). Thermal demagnetization of pilot samples suggests that a low-titanium magnetite is probably the magnetic carrier, because most of the NRM is removed below 550°C (Figure 4.6f). Data from pARM experiments show a peak at 30 mT, which is consistent with the presence of PSD magnetite (Figure 4.9). Furthermore, identification of the Verwey transition at around 120 K indicates that magnetite is present (Figure 4.8). The locality-mean ChRM is D = 3.4°, I = 73.1°, with η_{95} = 4.3° and ζ_{95} = 5.3° (Figure 4.7c). A bootstrap fold test [*Tauxe and Watson*, 1994] was carried out on the data from Kholmsk Pass (Figure 4.10a). This analysis reveals that maximum clustering occurs at around 80% unfolding, however, the 95% confidence limit on this direction ranges from 49% to 98% unfolding. The test is, therefore, inconclusive because the 95% confidence region eliminates the possibility of accurately constraining the timing of remanence aquisition. Slightly improved clustering after full tilt correction suggests that the ChRM is likely to be primary (Table 4.2).

4.4.1.4. Yar Stream/Vladimirovka River

Samples from Yar Stream and Vladimirovka River, located about 1 km east of the central fault region in south Sakhalin (Figure 4.5), were obtained from exposures of the early Miocene Kholmsk Suite. A stable ChRM component was revealed for some samples by AF demagnetization above 25 mT (Figure 4.6g). Thermal demagnetization was carried out on pilot samples, but mineral alteration was evident at around 300 - 400°C (Figure 4.6h). Both normal and reversed polarity ChRM directions were observed in 13 mudstone samples, some of which were from overturned beds (Figure 4.7d). Low-temperature IRM data and pARM acquisition data suggest that PSD magnetite is the dominant remanence carrier at this locality (Figures 4.8, 4.9). The tilt-corrected ChRM has a locality-mean direction of D = 169.5°, I = -56.7°, with α_{95} = 9.0° (Figure 4.7d; Table 4.2). A bootstrap fold test was carried out on the data, which indicates a best-clustering direction that includes the 100% unfolded direction (Figure 4.10b). The

reversed and normal polarity data also pass a bootstrap reversals test [*Tauxe et al.*, 1991]. The ChRM is therefore interpreted to be primary.

4.4.1.5. Onnay River

A stable normal polarity ChRM was identified in 21 samples from Onnay River (Figure 4.7e). Thermal and AF demagnetization data are comparable before thermal alteration occurs at 220°C (Figure 4.6i,j). A small amount of the NRM remains after AF demagnetization at 140 mT, which suggests that a high-coercivity magnetic mineral is present. However, a clear Verwey-transition indicates that magnetite is present (Figure 4.8). A pARM peak at 30 mT suggests that the magnetite occurs as PSD (~2-3 μm) grains (Figure 4.9). Random paleomagnetic directions were obtained from 11 pebble samples, which had similar lithology to the sampled suite, from an intraformational conglomerate at the top of the sampled sequence. This suggests that the magnetic remanence is ancient (i.e., it pre-dates the conglomerate). The resultant vector length, R, for the conglomerate data is 3.02, which is less than the critical value of $R_{95} = 5.29$ for $N = 11$ [*Watson*, 1956], above which non-randomness cannot be disproved at the 95% confidence level (Figure 4.10c). The locality-mean direction is $D = 14.1°$, $I = 60.7°$, with $\eta_{95} = 2.6°$ and $\zeta_{95} = 4.7°$ (Figure 4.7e).

4.4.2. Central Sakhalin

4.4.2.1. Malaya Orlovka River

Sixteen samples from Malaya Orlovka River yielded stable paleomagnetic directions. A reversed polarity ChRM is identified between 30 and 65 mT, after removal of a normal polarity overprint (Figure 4.6k). Thermal demagnetization experiments indicate thermal alteration of the magnetic minerals at around 350°C. Thermal and AF demagnetization results are similar before the onset of thermal alteration (Figure 4.6k,l). A clear peak is present at 30 mT in pARM acquisition plots, with rapid decay of the remanence in higher coercivity windows (Figure 4.9). It is therefore likely that the

remanence is dominated by PSD magnetite [*Jackson et al.*, 1988]. The data pass a bootstrap fold test (Figure 4.10d). A well-defined peak at 100% unfolding suggests that the ChRM is primary. The mean paleomagnetic direction for the locality is D = 176.5°, I = -48.9°, with α_{95} = 7.7° (Figure 4.7f).

4.4.3. Northeast Sakhalin

4.4.3.1. Dvoynoye River

At Dvoynoye River, paleomagnetic data from 12 samples have a stable high-coercivity ChRM. AF demagnetization had little effect in removing the NRM above 90 mT, so thermal demagnetization was carried out to remove the remaining NRM up to 700°C (Figure 4.6m). In other cases, the NRM was virtually removed at around 550°C (Figure 4.6n). The paleomagnetic direction isolated by AF demagnetization is identical to that isolated using thermal demagnetization (Figure 4.6m,n). A minor low-coercivity viscous component is observed in some samples possibly due to laboratory storage (Figure 4.6m,n). A Verwey transition indicates that magnetite is present in the samples (Figure 4.8) and a peak in the pARM data at 30 mT suggests that the magnetite occurs in the PSD size range (Figure 4.9). Thus, it appears that magnetite is the dominant remanence carrier, together with a high-coercivity mineral. The high-coercivity mineral is probably hematite since part of the remanence persists to 650-700°C. The hematite appears to be present in variable concentrations in different samples. All samples have reversed polarity and give a locality-mean direction of D = 211.8°, I = -54.2°, with α_{95} = 11.1° (Figure 4.7g; Table 4.2).

4.4.3.2. Chamgu River

For Chamgu River, 17 paleomagnetic samples yielded a stable ChRM above 25 mT (Figure 4.6o). A low-coercivity overprint with variable directions is also present. The overprint is probably a viscous magnetization acquired in the present-day geomagnetic field or in the laboratory. Thermal demagnetization below 300°C reveals

the same component of magnetization as AF demagnetization; thermal alteration occurs above this temperature (Figure 4.6p). Partial ARM data indicate a clear peak at 30 mT, which suggests that PSD magnetite is responsible for the NRM (Figure 4.9). A reversed polarity ChRM suggests that recent remagnetization has not occurred and the ChRM direction is interpreted as a primary magnetic component. The locality-mean paleomagnetic direction for the ChRM components calculated from these samples is D = 200.6°, I = -66.0°, with α_{95} = 7.4° (Figure 4.7h; Table 4.2).

4.4.3.3. Kongi River

Twenty samples from Kongi River yielded stable paleomagnetic directions. Most of the samples were from tuffaceous beds. A high-coercivity (25-120 mT) ChRM component has reversed polarity and is interpreted as a primary magnetization (Figure 4.6q). Viscous overprints are present in many samples below 25 mT. A Verwey transition at 120 K indicates the presence of magnetite (Figure 4.8). Similar results were obtained using AF and thermal demagnetization, although thermal alteration prevented heating above 360°C in tuffaceous samples (Figure 4.6q,r). Rapid thermal decay of the remanence below 360°C in tuffaceous samples (Figure 4.6r) is probably due to a titanomagnetite, although the AF demagnetization results also suggest the presence of a high-coercivity iron-oxide mineral such as hematite (Figure 4.6q). Partial ARM acquisition results indicate a peak at 30 mT, which, together with the thermal demagnetization data, suggests that PSD titanomagnetite is likely to be the primary NRM carrier (Figure 4.9). The mean paleomagnetic direction for the Kongi River locality is D = 205.0°, I = -55.7°, with η_{95} = 4.5° and ζ_{95} = 7.4° (Figure 4.7i; Table 4.2).

4.5. Discussion

Several kinematic models have been proposed for the evolution of NE Asia [e.g., *Otofuji et al.,* 1991; *Jolivet et al.,* 1994; *Altis,* 1999]. The models covering the Okhotsk Sea region are primarily derived using data from Japan and the Japan Sea. However,

because geological data are sparse for both Sakhalin and the Okhotsk Sea, the models are poorly constrained and inconsistent and the geodynamic evolution of this region remains unclear. Analysis of paleomagnetic data can help to constrain tectonic models in several ways. First, the data can constrain the timing of deformation. Second, they can help evaluate whether Sakhalin has evolved with the Pacific, North American, or Eurasian plates and they can help identify the position of plate boundaries, which are currently unclear (e.g., Figure 4.2). Third, the data can be used to delineate local domains with similar deformation history. Fourth, they can help define the structural style of deformation and, hence, provide insights into the tectonic evolution of the region. In the following, we discuss the geodynamic implications of paleomagnetic data from Sakhalin and the constraints they place on kinematic models of the regional dynamics.

4.5.1. Tertiary Paleolatitudinal Evolution of Sakhalin

4.5.1.1. Paleomagnetic Inclination Data

A Mesozoic accretionary complex in east Sakhalin indicates that the early geological evolution of Sakhalin was linked with the Pacific Plate, at least until the Eocene after final emplacement of an allochthonous terrane in southeast Sakhalin [*Bazhenov et al.,* 2001]. Currently, the Okhotsk Sea separates Sakhalin from the subducting Pacific Plate (Figure 4.1). Thus, there has been a transition within the Cenozoic between a geological evolution associated with the Pacific Plate to evolution with some other plate(s). Comparison of paleomagnetic inclination data for Tertiary rocks from Sakhalin with the APWP's for the Pacific, Eurasian, and North American plates (Figure 4.11) can help to constrain the timing of this transition. Inclination data from Oligocene beds at Kholmsk Pass are significantly different from the Pacific Plate APWP, and are in good agreement with the North American and Eurasian APWP's (Figure 4.11). This might suggest that the transition occurred by Oligocene time. However, data from Chamgu River and Okhta River have 95% confidence error bars that span the North American, Eurasian, and Pacific Plate APWP's. The data for the Kongi

River, Vladimirovka/Yar Stream, and Dvoynoye River localities plot within error of the Pacific Plate APWP, while mean inclination data from Onnay River and Kitosiya River plot directly in agreement with the Pacific path. Inclinations from Malaya Orlovka do not plot within error of any of the APWP's used for comparison in Figure 4.11, and are anomalously shallow. A number of depositional mechanisms can cause the long axes of naturally anisotropic magnetic remanence-bearing particles to rotate toward the bedding plane in a sediment [*Arason and Levi*, 1990]. Placing further constraint on the Tertiary evolution of Sakhalin appears to be difficult without testing for possible inclination shallowing within the studied sedimentary rocks.

4.5.1.2. Testing for Post-Depositional Inclination Shallowing

Initial investigation of inclination shallowing was carried out by measuring the anisotropy of magnetic susceptibility (AMS). In samples where the magnetic fabric is oblate, and the minimum susceptibility (k_{min}) is perpendicular to the bedding plane, an inclination correction can be applied if the susceptibility is dominated by ferrimagnetic minerals [*Hodych et al.*, 1999]. Alternatively, the anisotropy of ARM (AARM) can be measured to make such corrections [*Jackson et al.*, 1991; *Kodama*, 1997; *Tan and Kodama*, 1998]. In both cases, successful correction requires the average anisotropy of magnetic particles to be constant and small [*Hodych and Bijaksana*, 1993].

Samples from Dvoynoye River, Kongi River, and Malaya Orlovka River have oblate AMS ellipsoids and tilt-corrected magnetic fabrics with k_{min} axes close to vertical (Figure 4.12a). Samples from other localities have variable AMS ellipsoid shapes and are therefore unsuitable for direct AMS or AARM correction. There appears to be a significant correlation between tan I and the percentage anisotropy for three sites (Figure 4.12b). An AMS-based correction was made following the method of *Hodych et al.* [1999] where the inclination prior to flattening (I_F) is estimated by extrapolating the best-fit line to the point where $k_{min}/k_{max} = 1$. Comparison of inclination and I_F values for these localities suggests an inclination flattening of up to about 20° (Figure 4.12b). With this

method, it is assumed that the magnetic fabric is controlled by ferrimagnetic particles rather than by paramagnetic or diamagnetic matrix minerals. This assumption is not always valid and it is preferable to provide a more direct explanation for inclination shallowing by determining whether the remanence carrying grains are also anisotropic.

An alternative anisotropy test was performed by measuring an IRM parallel (IRM_x) and perpendicular (IRM_z) to the bedding plane to qualitatively evaluate the possibility of inclination shallowing. Inclination shallowing is manifest when IRM_z is less than IRM_x. The ratio IRM_z/IRM_x can be related to the amount of inclination shallowing by: $\tan I/\tan I_F = IRM_z/IRM_x$ [*Hodych and Buchan*, 1994]. For the majority of samples analyzed from Sakhalin, the value of IRM_z is lower than IRM_x for the entire range of applied fields (Figure 4.13). This suggests that the NRM-carrying fraction of grains is significantly anisotropic. The average IRM_z/IRM_x ratio for each sample was determined from the best-fit slope of IRM_z against IRM_x (Figure 4.13j). Only samples with a correlation coefficient of $R > 0.7$ were considered in our summary of IRM anisotropy data in Table 4.3. It is noteworthy that samples from Kholmsk Pass, where there is no discrepancy between the mean inclination value and the Eurasian and North American APWP's (Figure 4.11), have a mean IRM_Z/IRM_X ratio close to unity (Table 4.3; Figure 4.13c). Smaller ratios are found for all other localities, which indicates that inclination shallowing is likely to be significant (Table 4.3). More rigorous quantification of post-depositional inclination shallowing usually requires determination of the AARM tensor, sediment redeposition and electron microscopic analysis of grain size and shape to assess remanence anisotropy [*Jackson et al.*, 1991; *Kodama*, 1997; *Tan and Kodama*, 1998]. Such detailed analysis is beyond the scope of the present study. We simply indicate the likelihood of inclination shallowing with arrows on the data points in Figure 4.11, which suggest that these localities should have steeper mean inclinations.

4.5.1.3. Paleolatitude Implications of Tertiary Paleomagnetic Data from Sakhalin

The likelihood of significant inclination shallowing for many of the localities sampled in Sakhalin indicates that post-Paleocene evolution of Sakhalin with the Pacific Plate is improbable. The data are insufficient to enable us to distinguish whether Sakhalin evolved with the Eurasian or the North American plates. However, they do suggest that the sampled localities have remained near present-day latitudes since the mid-Paleocene (Figure 4.11). If this was the case, the attribution of late Cenozoic volcanism in the area to subduction-related processes [*Zonenshain et al.*, 1990] is incorrect.

4.5.2. Timing of Cessation of Subduction Beneath Sakhalin

Vertical-axis rotations, which are detectable by comparing measured paleomagnetic declinations with the expected APWP, are commonly associated with strike-slip fault systems [e.g., *Jackson and Molnar,* 1990*; Little and Roberts*, 1997]. The mean declinations from the localities sampled in Sakhalin are shown in Figures 4.5 and 4.14a. The data can be divided into two groups based on their common deformational history: 1) east Sakhalin (Figure 4.14b), and 2) localities in Sakhalin to the west of, and in the vicinity of, the Central Sakhalin Fault (Figure 4.14c). The expected declinations for the North American and Eurasian plates are also shown.

In east Sakhalin, there appears to have been approximately 10° of relative clockwise rotation from the middle Eocene to the early Miocene although the error bars of the adjacent data points overlap (Figure 4.14b). This is the earliest indication of a possible right-lateral strike-slip tectonic regime [*Fournier et al.,* 1994]. It suggests that Pacific Plate subduction had probably ceased by the onset of this rotation, which is consistent with Eocene accretion of a Pacific Plate allochtonous terrane in southeast Sakhalin [*Bazhenov et al.,* 2001]. This terrane accreted against Sakhalin on the Tonino-Aniva Peninsula (Figure 4.1b), approximately 400 km south of Dvoynoye River, which suggests that deformation associated with the docking of this relatively small (~10-km-

scale) terrane is unlikely to have caused the observed rotation at Dvoynoye River. No relative rotation is observed during the Miocene in east Sakhalin. A 25° clockwise-deviated declination observed at Kongi River suggests that the region has rotated clockwise since 8 Ma (Figure 4.14a,b).

If vertical-axis rotations are regionally coherent in west Sakhalin (Figure 4.14c), the data seem to suggest a period of clockwise rotation of up to ~40° from the mid-Paleocene to the late Oligocene. It is most likely that westward-directed subduction of the Pacific Plate under Sakhalin in the mid-Paleocene to Eocene [*Bazhenov et al.,* 2001] controlled deformation in both east and west Sakhalin. A terrane docking and indentation event in southern Sakhalin in the Eocene [*Bazhenov et al.,* 2001] may have resulted in a clockwise rigid body rotation at Kitosiya River (mid-Paleocene samples), where paleomagnetic results indicate significantly clockwise deflected declinations (Figure 4.14). However, the observed vertical-axis rotations may also be associated with strike-slip fault deformation, which seems to have begun after the middle Eocene in west Sakhalin (Figure 4.14c). Well-documented N-S-trending right-lateral strike-slip faults observed in Sakhalin [*Fournier et al.,* 1994] are likely to have accommodated such deformation. Clockwise relative rotation between the late Eocene and the late Oligocene in west Sakhalin (Figure 4.14c), and clockwise rotation sometime between the middle Eocene and the early Miocene in east Sakhalin (Figure 4.14b), suggests that a transition from subduction to strike-slip tectonics must have occurred by the late Eocene and that rotational deformation associated with strike-slip faulting affected Sakhalin as a whole. However, with existing data, it is not possible to precisely determine when the vertical-axis rotations commenced.

Different characteristics are evident for the Neogene evolution of west Sakhalin compared to east Sakhalin (Figure 4.14c). Counterclockwise rotation of around 35° appears to have occurred since the Oligocene before a rapid clockwise phase of rotation of about 40° in the Early Miocene (~20 Ma). Deformation in southwest Sakhalin, close

to the Central Sakhalin Fault, is complex. This is reflected in variable declination values near the Central Sakhalin Fault (Figure 4.5).

In view of the relatively sparse paleomagnetic data set from Sakhalin, it is difficult to determine to what extent Sakhalin may have deformed as a coherent region and to constrain the significance of deformation at various scales. Further sampling is required in both east and west Sakhalin and close to the central fault. Extensive sampling of well-dated Paleocene-Eocene rocks needs to be carried out to provide precise and independent constraints on the timing of the transition from subduction to strike-slip tectonics in Sakhalin.

4.5.3. The India-Eurasia Collision Model

Jolivet et al. [1990] and *Worrall et al.* [1996] suggested that the abundance of right-lateral fault systems along the NW Pacific margin was caused by the Eocene collision of India and Eurasia. This pattern of faulting has been reproduced in analog models, assuming that the eastern edge (the NW Pacific region) is a "free" boundary [*Tapponnier et al.*, 1982; *Peltzer and Tapponnier,* 1988]. The northern boundary of the deformed area in these models is a left-lateral strike-slip fault. *Worrall et al.* [1996] suggested that a continuous fault system links Magadan (northern Okhotsk Sea) westward to Lake Baikal.

There are several problems with this collision-driven model for deformation along the NW Pacific margin. 1) The concept of a "free" boundary clearly does not accurately represent the complex interactions of the Pacific Plate with the North American, Eurasian, and/or Okhotsk Sea plates. 2) The age of basins generated by dextral motion along the East Asian margin is not consistent with an India-Eurasia collision model. In some cases, the basins pre-date initial collision [*Allen et al.*, 1998]. 3) The case for a linking sinistral fault system from Baikal to Magadan, which would have partially reactivated the Mesozoic Mongol-Okhotsk suture (Figure 4.1c), is not tenable. In the area to the east of Lake Baikal, the mapped structural grain cross-cuts the trend of

the faults required to link to the Mongol-Okhotsk suture; no trace of the postulated linking fault has been found or is apparent in satellite photographs.

Our paleomagnetic data also suggest that the India-Eurasia collision model is unable to explain observed deformation patterns along the NW Pacific margin. For example, counterclockwise rotations are predicted, based on fault data, in Neogene basins in eastern Sakhalin (Figure 4.3a) [*Fournier et al.*,1994]. Such rotations would be consistent with deformation generated by extrusion resulting from the India-Eurasia collision [*Jolivet et al.,* 1994; *Worrall et al.,* 1996]. However, data from the Chamgu, Kongi and Dvoynoye rivers of east Sakhalin consistently indicate significant clockwise vertical-axis rotations (Figure 4.14b).

4.5.4. Deformation in Sakhalin Linked to Evolution of the Japan Sea

Initial opening of the Japan Sea has been dated by the ^{40}Ar-^{39}Ar technique at between 24 and 17 Ma [*Tamaki et al.,* 1992]. It is frequently assumed that the initial rifting of the Kuril Basin in the Okhotsk Sea (Figure 4.1a) may have been closely associated with the back-arc opening of the Japan Sea basin and a regional reorganization of interacting continental and oceanic blocks [e.g., *Jolivet and Tamaki*, 1992; *Takeuchi et al.,* 1999]. However, neither the age nor the oceanic nature of the crust in the Kuril Basin have been securely established, because it does not exhibit linear sea floor anomalies and has not been drilled.

In west Sakhalin, a rapid clockwise vertical-axis rotation event (20-50°), which is significant at the 95% confidence level, can be identified at around 20 Ma (Figure 4.14c). This is not seen in east Sakhalin (Figure 4.14b). The timing of this rotation coincides with opening of the Japan Sea (Figure 4.14c) and probably pre-dates the opening of the Tatar Strait further to the north near Aleksandrovsk (Figures 4.1b, 4.14c) [*Flecker and Macdonald,* 2002]. The observed clockwise rotations in southern Sakhalin might be associated with dextral strike-slip activity on the Central Sakhalin Fault, which continues southward to Hokkaido. In this instance, opening of the Japan Sea Basin would have

caused deformation in southern Sakhalin. In some models [*Takeuchi,* 1997; *Takeuchi et al.,* 1999], a mechanism for the observed right-lateral faulting and clockwise rotations in southern Sakhalin is provided by linked opening of the Japan Sea and Kuril Basin followed by southward motion of the Kuril ridge (Figure 4.3b).

A later phase of 25° of clockwise rotation is observed in east Sakhalin at about 8 Ma (Figure 4.14b). One possible cause of this may be the cessation of spreading in the Kuril Basin, which would have resulted in increased rates of dextral displacement on N-S-trending strike-slip faults along the east coast of Sakhalin and associated clockwise vertical-axis rotations of crustal-scale blocks. The declination data can therefore be interpreted to suggest that the Kuril Basin opened in the Miocene following inferred back-arc opening along an axis parallel to the arc. Spreading in the Kuril Basin, therefore, probably commenced around 24 - 20 Ma and ceased at about 10 - 8 Ma (Figure 4.14c).

4.5.5. Evidence for the Existence of an Okhotsk Sea Plate

On the basis of earthquake slip data (e.g., the 1995 Neftegorsk earthquake [*Ivashchenko et al.,* 1997], which indicates a transform boundary in northern Sakhalin), *Seno et al.* [1996] suggested that the Okhotsk Sea Plate currently rotates clockwise about a pole in the northern Okhotsk Sea. This gives a solution that takes into account thrust deformation in southern Sakhalin, which the "extrusion" model [*Jolivet et al.,* 1994; *Worrall et al.,* 1996] fails to do. Thus, the paleomagnetic data presented here are in agreement with the interpretations of *Seno et al.* [1996], who suggested that the inclusion of an Okhotsk Sea Plate gives a more realistic solution to the geodynamic evolution of the region. Since paleomagnetic data are not available from the Okhotsk Sea Plate, our Sakhalin data are compared with the North American and Eurasian APWP's (Figure 4.14).

4.5.6. Style of Deformation in Sakhalin

Takeuchi et al. [1999] suggested that domino-style deformation might accommodate clockwise vertical-axis rotations inferred from paleomagnetic data from southern Sakhalin (Figure 4.3b). Their paleomagnetic data are broadly consistent with the new data presented in this study, but they had insufficient data to constrain the details of their domino model (e.g., what happens at the edges of the blocks where they meet the bounding faults?). They also failed to document detailed field evidence for block rotation on either Sakhalin or Hokkaido. Such evidence includes triangular zones of compression and extension that would be expected, where the axes of rotation for the blocks in the deforming zone can be identified [*Roberts,* 1995a; *Townsend and Little,* 1998; *Bayasgalan et al.,* 1999]. However, triangular depocentres have been identified from isopach maps of the southern Tatar Strait [*Antipov et al.*, 1980]. *Jolivet et al.* [1994] suggested that these are small pull-apart basins which formed in a similar manner to those documented by *Lallemand and Jolivet* [1986] along the northwestern coast of Honshu, but it is possible that they represent the extensional zones expected to be generated by block rotation.

4.6. Conclusions

Paleomagnetic inclination data suggest that Sakhalin has remained near its present-day latitude for most of the Tertiary period and that it has evolved with either the Eurasian or the North American plates. Declination data support this interpretation.

Paleomagnetic declination data, when compared with the APWP's for the interacting plates, can be linked to a transition from subduction tectonics to a strike-slip regime in Sakhalin around the middle-late Eocene, but it is not possible to establish the exact timing of the transition. This interpretation is consistent with paleomagnetic data from an exotic terrane, which probably accreted against southeast Sakhalin in the Eocene [*Bazhenov et al.,* 2001]. Different phases of clockwise vertical-axis rotation are discernable for localities in southwest Sakhalin and also in central eastern Sakhalin. A

rapid clockwise rotation phase in the early Miocene in southwest Sakhalin may be linked to the onset of rifting in the Japan Sea, Kuril Basin and Tatar Strait. Further rotation in the latest Miocene, which only involved the eastern localities, might be associated with the end of opening in the Kuril Basin and a change of deformation style, with activity on eastern offshore faults in Sakhalin.

Paleomagnetic data are consistent with the block rotation model of *Takeuchi et al.* [1999], but the model remains relatively unconstrained by structural data. Deformation appears to be complex in the southwest and close to the Central Sakhalin Fault, while deformation in eastern areas appears to have been more uniform. Further structural domains may be identified with further sampling.

Our data are in conflict with the model of *Fournier et al.* [1994], which predicted counterclockwise rotations in east Sakhalin in response to extrusion at the east Asian margin in response to the India-Eurasia collision. Clockwise-deflected paleomagnetic declinations agree with a plate reconstruction model proposed by *Seno et al.* [1996], which suggests that the extrusion model is unrealistic and that plate boundary deformation is better described with a separate Okhotsk Sea Plate.

Acknowledgements

Fieldwork on Sakhalin was carried out as part of the CASP research program funded by Agip, Anadarko, Arco, BP, Exxon, JNOC, Mobil, Philips, and Texaco. RW gratefully acknowledges financial support from a U.K. NERC PhD studentship. APR, RF, DIMM, and LMF acknowledge support from a grant from the Royal Society of London. Field logistics were provided by SGRE in Yuzheno-Sakhalinsk; we are indebted to Vladimir Galversen, Pavel Kovtunovich, Zhenia Rasshchepkina, and Valeriy Gorbachov for their help and support. The authors thank the following people for their interest in and help with this research: Larisa Voronova, Christine Brouet-Menzies, Eric Blanc, Sarah Poynter, Mark Allen, and Simon Inger. We are grateful to Kevin Padley for technical support at the SOC, Fabio Florindo for assistance with measurements at the INGV, Rome, Italy, Mike Jackson for assistance at the IRM, Minneapolis, U.S.A., and Kaz Kodama for discussions and for providing a preprint of an unpublished manuscript. We thank an anonymous reviewer and associate editor Tim Rolph for constructive comments which helped to improve the manuscript.

Table 4.1. Sampling localities, geological suites, and description of local geology

Region	Locality and lat./long.	No. of samples	Description of strata and local structure
West	Kitosiya River 46.4°N, 141.9°E	15	**Suite**: Sinegorian Beds; **Age**: Early Paleocene; **Lithology and environment**: lagoonal/brackish mudstone and siltstone, intermittent marine sandstone, coal; **Structure**: dip 31°W/187°
	Okhta River 46.9°N, 142°E	31	**Suite**: Nevel'sk; **Age**: Early Miocene; **Lithology and environment**: marine mudstone and siltstone, volcanic clasts common; **Structure**: dip 50°W/180°
	Kholmsk Pass 47.1°N, 142.1°E	49	**Suite**: Takaraday; **Age**: Early Oligocene; **Lithology and environment**: marine siltstone and mudstone; **Structure**: core of large anticline, dip 28°W/158° to 2°SE/040°, flanked by: **Suite**: Arakay; **Age**: Oligocene; **Lithology and environment**: mudstone, siltstone, sandstone, volcaniclastics and conglomerate; **Suite**: Kholmsk; **Age**: Early Miocene; **Lithology and environment**: marine siltstone, sandstone, volcaniclastics and conglomerate
	Vladimirovka R. 47.1°N, 142.3°E	60	**Suite**: Kholmsk; **Age**: Early Miocene; **Lithology and environment**: marine mudstone, siltstone, sandstone, volcaniclastics and conglomerate; **Structure**: vertical-overturned strata close to CSF, dip 70°SE/020° to 80°NW/204°
	Onnay River 49.6°N, 142.2°E	47	**Suite:** Arakay; **Age**: Oligocene; **Lithology and environment**: marine siliceous mudstone, siltstone, sandstone and conglomerate; **Structure**: east limb of syncline, dip 40°W/193° to 80°W/193°
Central	M. Orlovka R. 49.7°N, 142.7°E	27	**Suite**: Nutov; **Age**: Miocene-Pliocene; **Lithology and environment**: marine/deltaic siltstone and sandstone; **Structure**: NW-trending syncline, dip 76°NE/330° to 22°SW/114°
East	Dvoynoye R. 50.1°N, 143.7°E	25	**Suite**: Lyukamen; **Age**: Eocene; **Lithology and environment**: marine mudstone and sandstone; **Structure**: dip 15°N/215°
	Kongi River 51.1°N, 143.4°E	46	**Suite**: Borsk; **Age**: Early Miocene; **Lithology and environment**: marine sandstone and volcaniclastics; **Structure**: dip 65°E/355°
	Chamgu River 50.9°N, 143.5°E	25	**Suite**: Borsk; **Age**: Early Miocene; **Lithology and environment**: marine siliceous mudstone; **Structure**: dip 48°W/175°

For locations, see Figure 4.5. CSF: Central Sakhalin Fault. Number of samples refers to the total number of analyzed samples. The number of samples with stable magnetizations are shown in Table 4.2.

Table 4.2. Paleomagnetic data from Tertiary rocks, Sakhalin

Locality	Age (Ma)	Suite Name	Strat. Thickness (m)	Average Bedding Dip (°)/Strike (°)	Lat. (°)	Long. (°)	Pol.	n	D_m (°)	I_m (°)	α_{95} (°)	k	Fshr?	η_{95} (°)	ζ_{95} (°)	D_m (°)	I_m (°)	α_{95} (°)	k	Fshr?	η_{95} (°)	ζ_{95} (°)
									Geographic coordinates							*Stratigraphic coordinates*						
West Sakhalin																						
Kitosiya River	64-60	Sinegorian Beds	~ 7.2	31 W/187	46.4	141.9	R + N	14	242.1	-34.0	6.6	37	Yes	-	-	218.6	-56.4	6.6	37	Yes	-	-
							N	2	-	-	-	-	-	-	-	-	-	-	-	-	-	-
							R	12	241.6	-32.5	7.2	37	Yes	-	-	219.7	-54.6	7.2	38	Yes	-	-
Okhta River	21-17	Lower Nevel'sk	~ 43	50 W/180	46.9	142.0	R	9	215.3	-60.0	5.8	81	Yes	-	-	179.7	-66.2	3.9	177	Yes	-	-
Kholmsk Pass	33-23	Takaraday, Arakay, Kholmsk	~ 16	28 W/158 to 2 SE/040	47.1	142.1	N	38	25.5	68.3	6.1	15	No	5.8	5.9	3.4	73.1	5.7	18	No	4.3	5.3
Yar/Vladimirovka River	23-15	Kholmsk	~ 500	70 SE/020 to 80 NW/204	47.1	142.3	R + N	13	148.0	17.2	16.7	7	No	5.6	11.9	169.5	-56.7	9.0	22	Yes	-	-
							N	6	321.6	10.7	17.1	16	No	5.1	17.5	353.1	61.0	20.2	12	Yes	-	-
							R	7	154.8	39.7	8.7	49	Yes	-	-	167.1	-53.1	7.3	69	Yes	-	-
Bykov ++	44-30	L. Due, Krasnopolev, Takaraday	-	-	47.3	142.5	N	63	-	-	-	-	-	-	-	16.7	55.6	8.9	40	Yes	-	-
Serpyanka River++	28-24	Arakay	-	-	47.3	142.4	N	53	-	-	-	-	-	-	-	31.8	52.2	13.1	20	Yes	-	-
Chekov++	24-16	Kholmsk, Nevel'sk	-	-	47.4	142.2	N	66	-	-	-	-	-	-	-	40.3	58.1	14.4	16	Yes	-	-
Onnay River	30-22	Takaraday, Arakay	~ 209	40 W/193	49.6	142.2	N	21	59.6	54.3	10.5	10	No	3.4	14.1	14.1	60.7	3.9	67	No	2.6	4.7
Central Sakhalin																						
Malaya Orlovka River	11-2	Nutov	~ 53	76 NE/330 to 22 SW/114	49.7	142.7	R	16	112.0	-32.6	15.3	7	No	5.6	19.0	176.5	-48.9	7.7	24	Yes	-	-
East Sakhalin																						
Dvoynoye River	47-41	Lyukamen	~ 304	15 NW/215	50.1	143.7	R	12	220.0	-57.5	14.6	12	No	7.9	10.0	211.8	-54.2	11.1	16	Yes	-	-
Chamgu River	24-20	Lower Borsk	~ 9.1	48 W/175	50.9	143.5	R	17	238.6	-28.9	7.4	24	Yes	-	-	200.6	-66.0	7.4	24	Yes	-	-
Kongi River	11-5	Upper Borsk	~ 17	65 E/355	51.1	143.4	R	20	121.7	-37.7	6.4	20	No	4.5	7.4	205.0	-55.7	6.4	27	No	4.5	7.4

++ Data from *Takeuchi et al.* [1999].

Table 4.3. Anisotropy of IRM data

Locality	n	IRMz/IRMx	Avg. Flattening (°)
Kitosiya River	6	0.900	6.5
Okhta River	3	0.820	4.1
Kholmsk Pass	6	0.957	1.0
Yar/Vlad. River	5	0.739	4.1
Onnay River	3	0.738	6.0
M. Orlovka River	6	0.669	9.8
Dvoynoye River	7	0.768	7.1
Chamgu River	6	0.447	12.4
Kongi River	5	0.735	8.1

The inclination flattening, I_F - I, was determined for each sample and divided by the no. of samples (n) to calculate the average flattening

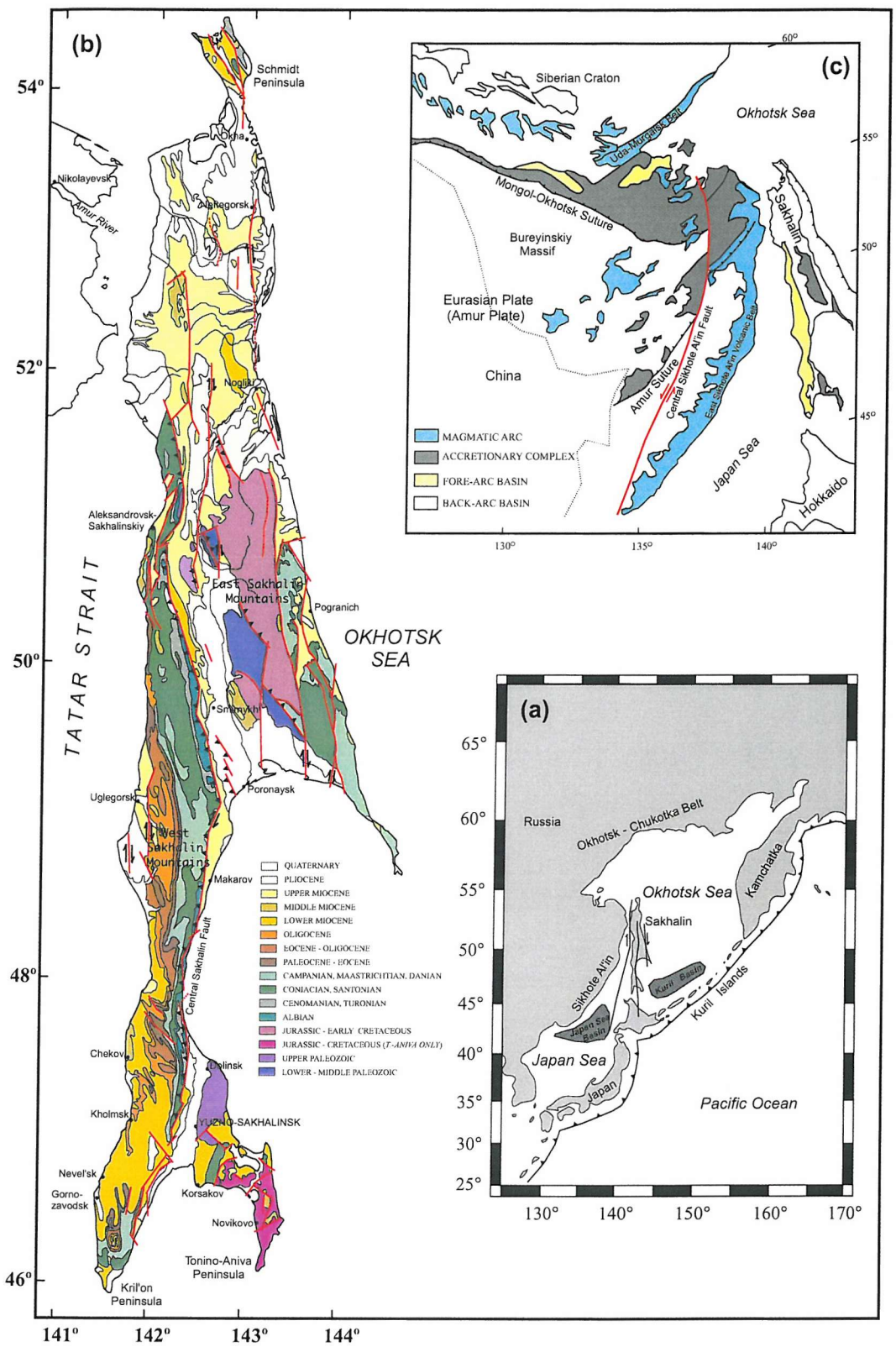

Figure 4.1. (a) Sketch map of the Okhotsk Sea region showing the N-S-trending faults across Sakhalin. Darker shading indicates the location of proven or postulated oceanic crust. Modified after *Seno et al.* [1996]. (b) Geological map of Sakhalin. Compiled from various sources [*Vereshchagin,* 1969; *Rozhdestvenskiy,* 1982; *Kharakhinov,* 1983; *Fournier et al.,* 1994; *Ivashchenko et al.,* 1997]. (c) Map of major suture zones and tectonostratigraphic units in southeastern Russia. Modified after *Natal'in* [1993].

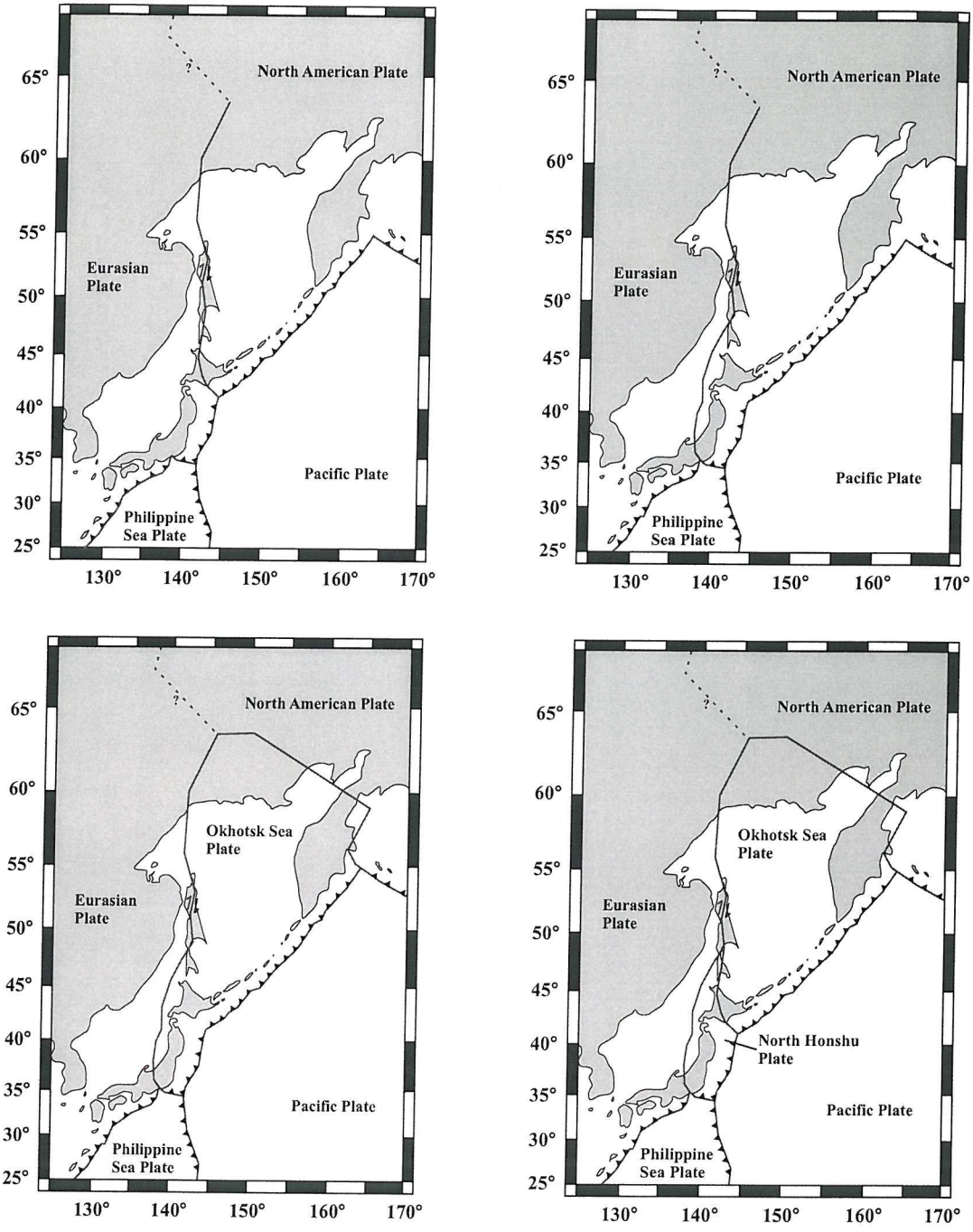

Figure 4.2. Possible plate configurations in NE Asia, after *Seno et al.* [1996]. The location of the boundary indicated by the dashed line is uncertain because of a lack of seismic activity in the region.

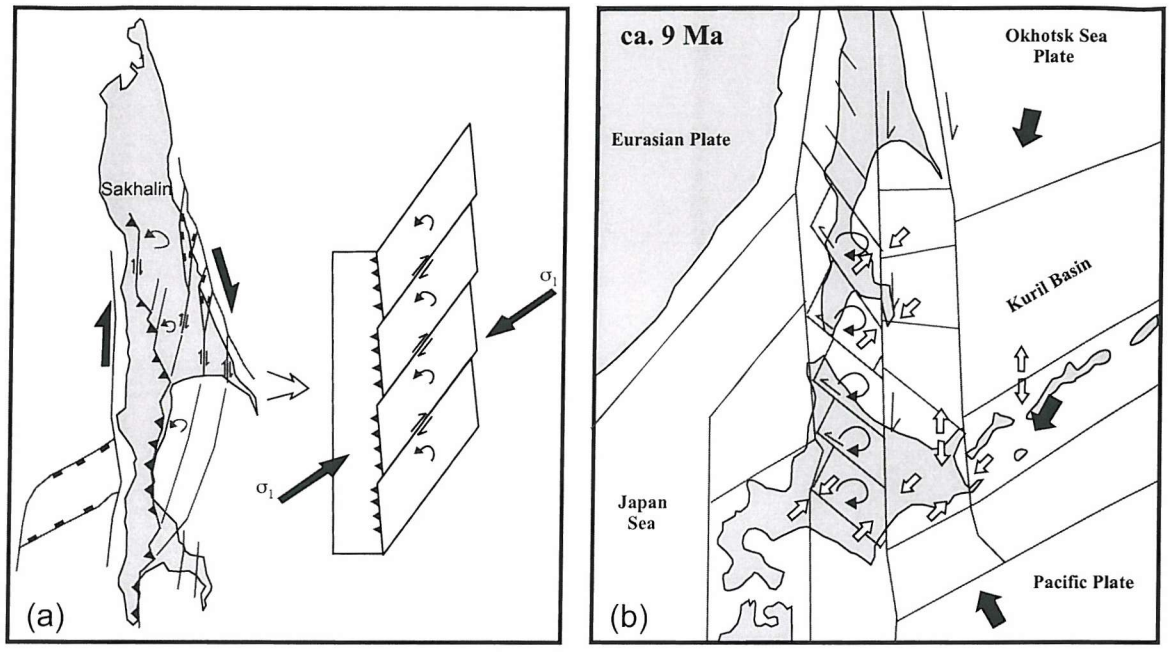

Figure 4.3. (a) Tectonic model for vertical-axis rotations in Sakhalin, as proposed by *Fournier et al.* [1994], showing counterclockwise block rotation during Neogene basin formation in eastern Sakhalin. (b) Tectonic model for vertical-axis rotations in Sakhalin and Hokkaido, as proposed by *Takeuchi et al.* [1999], showing clockwise block rotation during opening of the Japan Sea. The rotational mechanism has been linked to the synchronous opening of the Kuril Basin.

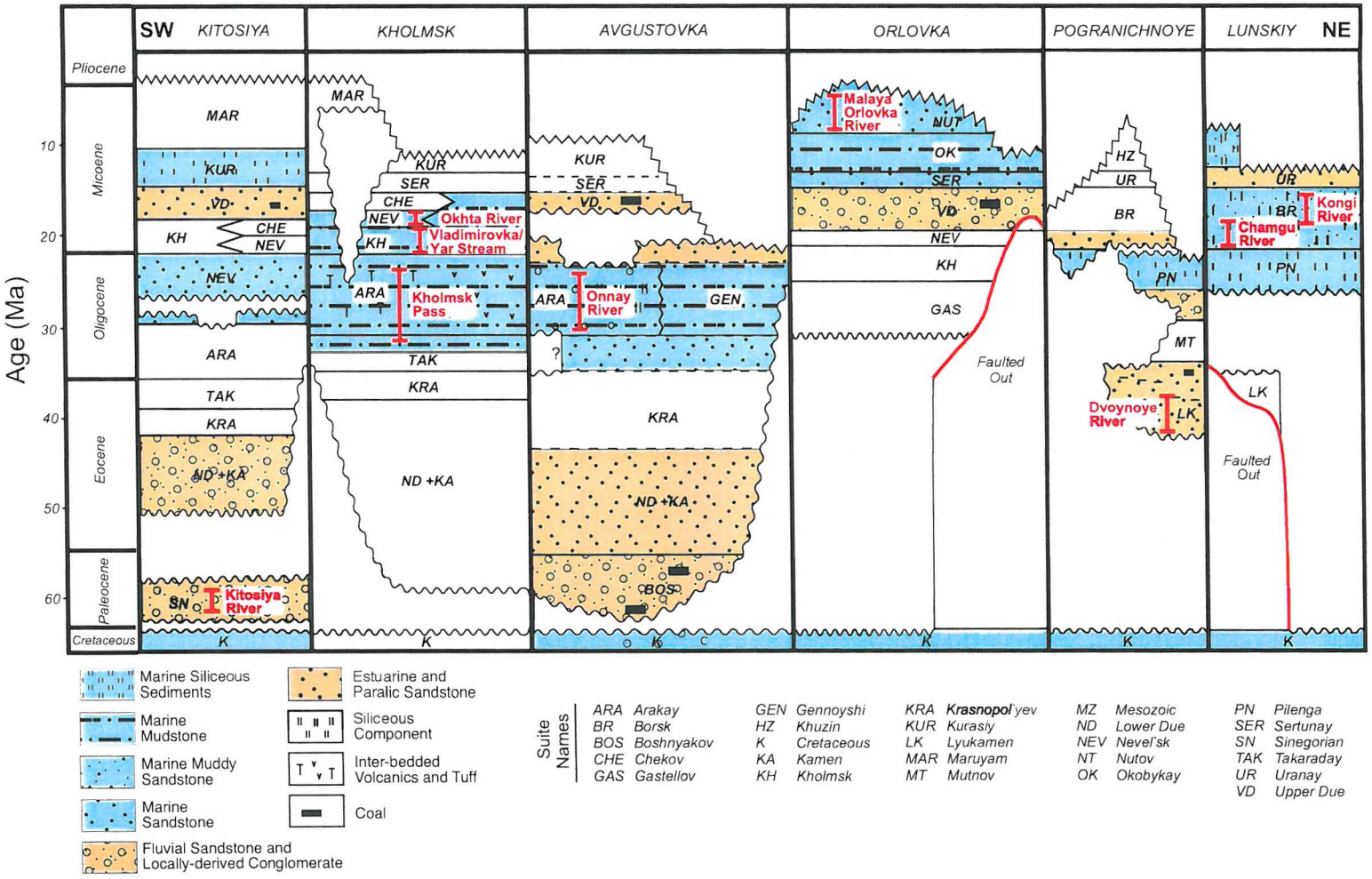

Figure 4.4. Stratigraphic sections of Sakhalin. Paleomagnetic sampling sites are indicated by vertical bars with names of the sampled localities. Only the samples taken from marine successions have well constrained ages. The ages of paralic and continental sediments are subject to much greater errors. The stratigraphic information is derived from *Vereshchagin et al.* [1969], *Gladenkov* [1988], *Menner et al.* [1977], *Serova and Fot'yanova* [1981], *Zhidkova and Sal'nikov* [1992], and *Fot'yanova et al.* [2001].

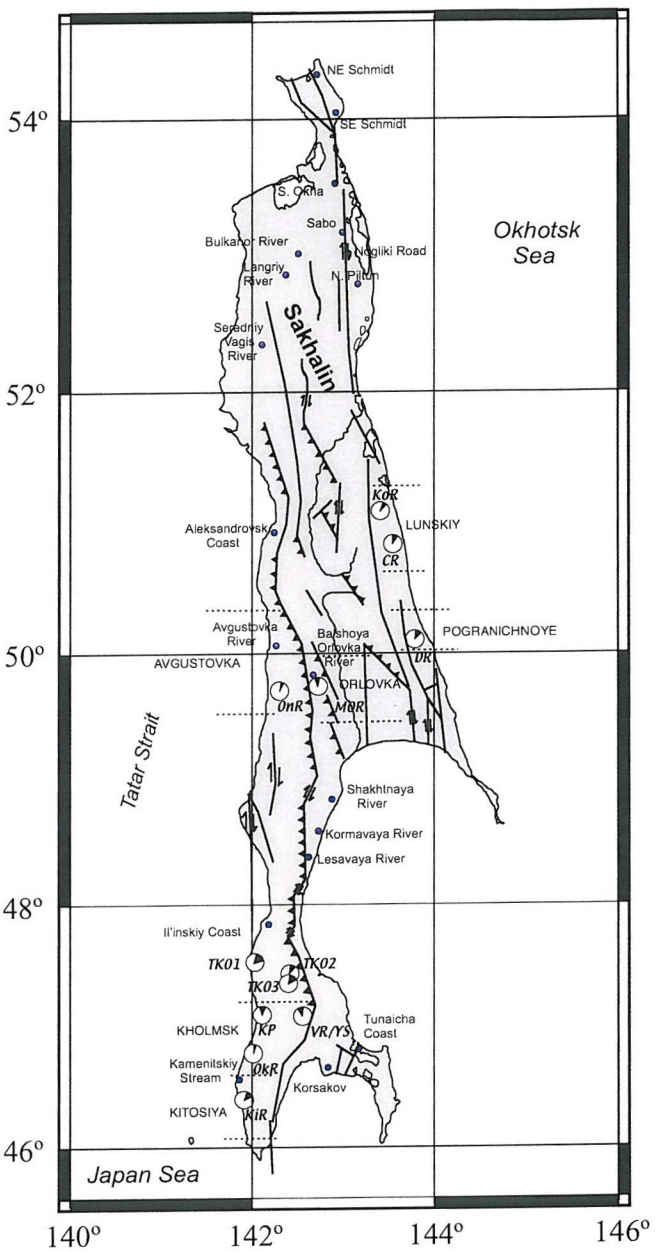

Figure 4.5. Paleomagnetic sampling localities in Sakhalin. Paleomagnetic declination data from the localities with reliable data are indicated, along with the associated 95% confidence limits. Abbreviations are as follows: KiR – Kitosiya River, OkR – Okhta River, KP – Kholmsk Pass, VR/YS – Vladimirovka River and Yar Stream, OnR – Onnay River, MOR – Malaya Orlovka River, DR – Dvoynoye River, CR – Chamgu River, KoR – Kongi River. Localities from *Takeuchi et al.* [1999] are indicated by TKO1, TKO2 and TKO3, respectively. Localities from which no useful paleomagnetic data were obtained are shown as small solid circles.

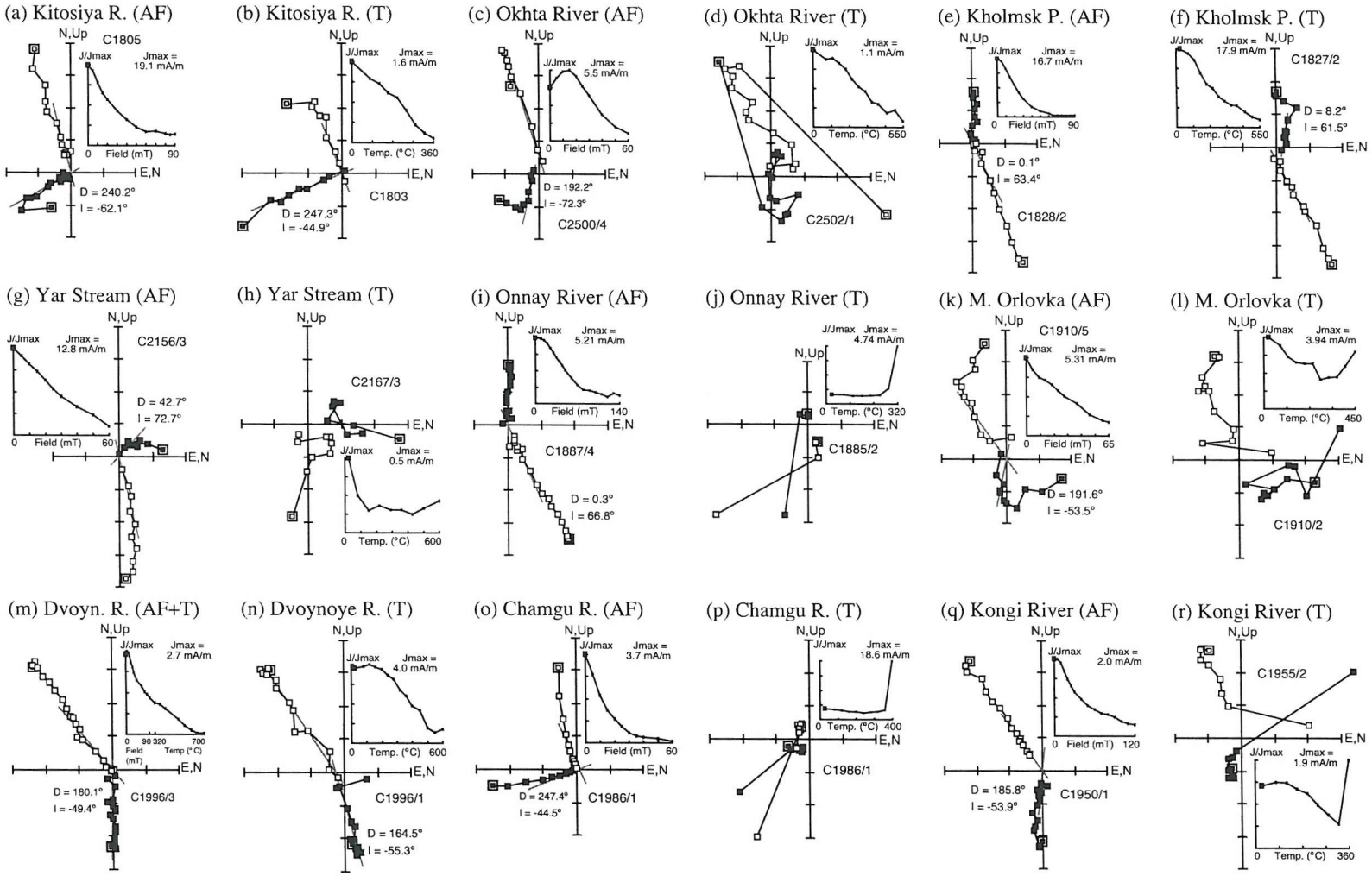

Figure 4.6. Vector component plots for representative samples from Sakhalin, with plots of magnetization decay on demagnetization. Lines represent least-squares best-fits to the ChRM vector [*Kirschvink,* 1980]. Open symbols represent projections onto the vertical plane (inclinations) and solid symbols represent projections onto the horizontal plane (declinations). All data are shown after structural tilt correction.

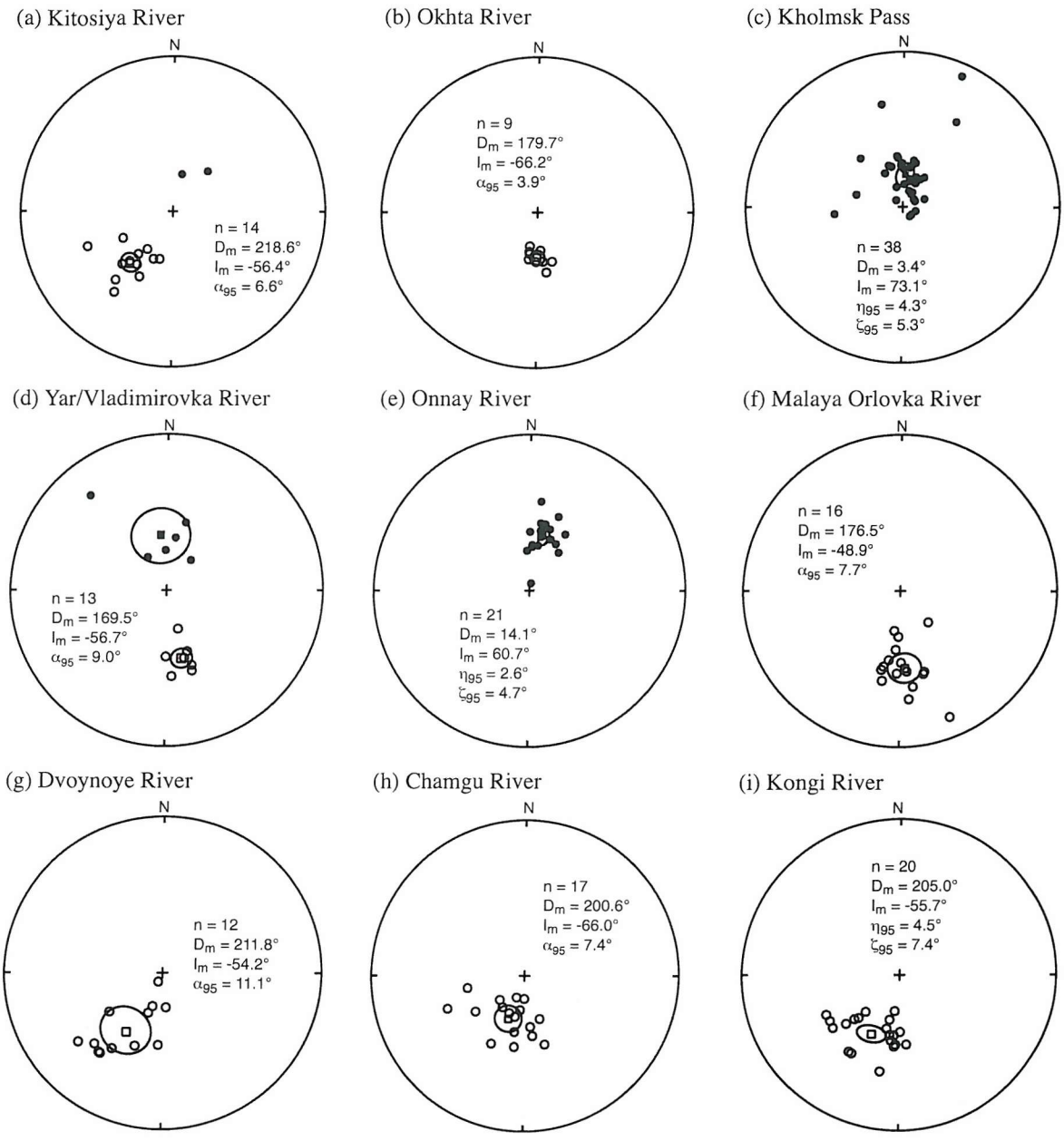

Figure 4.7. Equal area stereographic plots showing the site-mean remanence directions from Sakhalin. Reversed (solid symbols) and normal (open symbols) polarity sites are plotted in stratigraphic coordinates. The square represents the mean paleomagnetic direction (D_m = mean declination; I_m = mean inclination; n = number of samples with stable magnetizations). The ellipses represent the 95% confidence limit defined by the α_{95} value [see *Fisher*, 1953] or by η_{95} and ζ_{95} for the 95% confidence limits that define the minor and major semi-axes for confidence ellipses determined using bootstrap statistics for non-fisherian data sets [see *Tauxe et al.*, 1991].

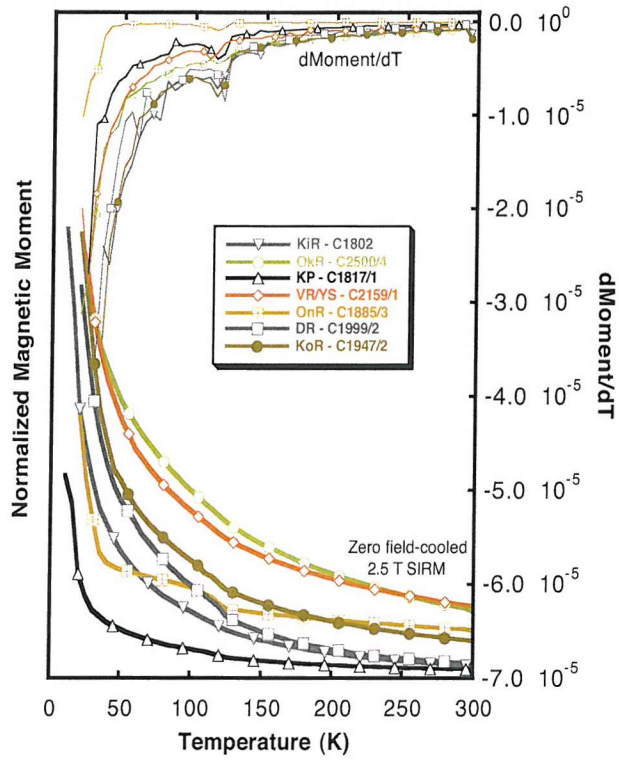

Figure 4.8. Low-temperature ZFC plots (normalized magnetic moment versus temperature), with the first derivative of the curves shown above. Data points are plotted at 5 K intervals and adjacent points are used to calculate the derivative. Different symbols are used to distinguish between samples (inset key). Errors associated with measurement uncertainty are negligible and only exist within the width of the lines. The Verwey transition, which is characteristic of magnetite, is detected at around 120 K for all samples.

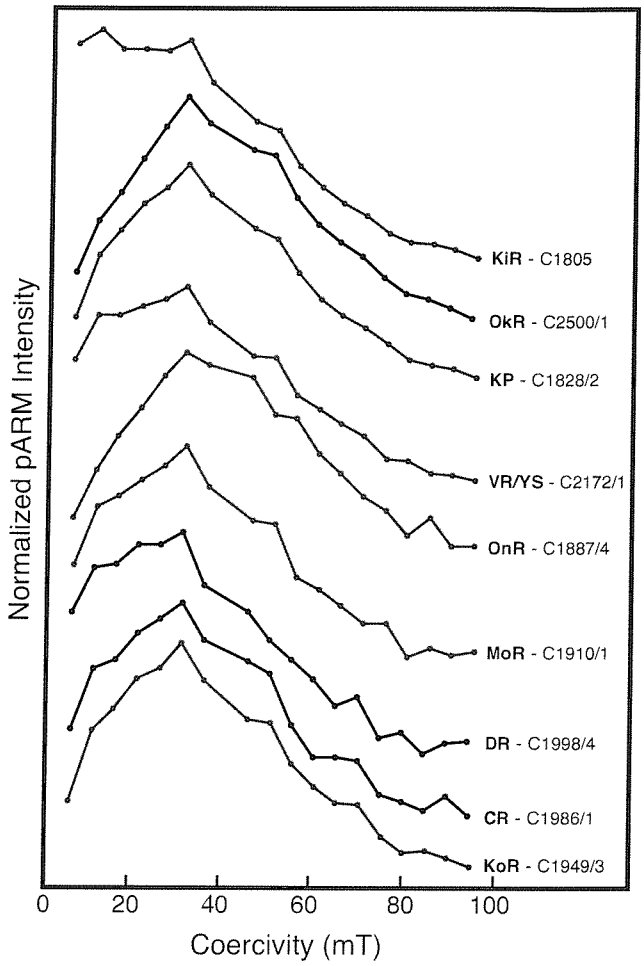

Figure 4.9. Partial ARM spectra for representative samples from all sampling localities (same abbreviations as in Figure 4.5). Peak values at around 30 mT suggest that PSD magnetite is the greatest contributor to the remanence [see *Jackson et al.*, 1988].

(a) Kholmsk Pass

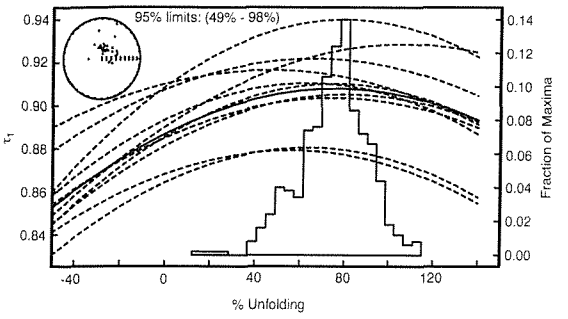

(b) Yar/Vladimirovka River

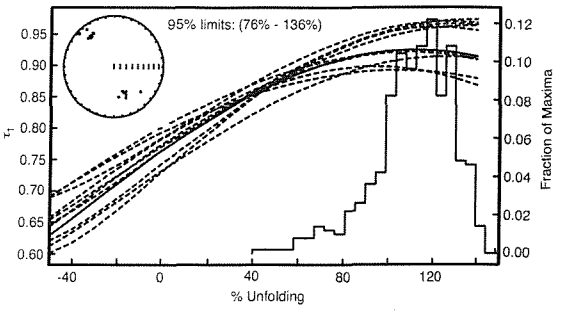

(c) Onnay River

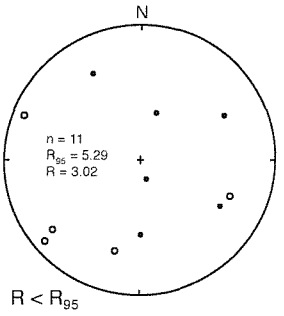

(d) Malaya Orlovka River

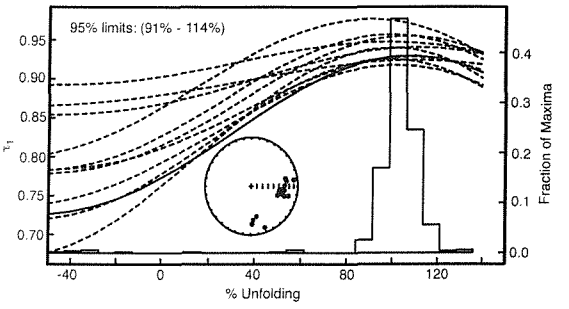

Figure 4.10. Paleomagnetic field tests. (a) and (b) Bootstrap fold tests following the method of *Tauxe and Watson* [1994] for data from Kholmsk Pass and Yar Stream/Vladimirovka River, respectively. The histograms indicate the distribution of bootstrapped means [*Tauxe,* 1998]. Principal eigenvalues of paleomagnetic data are plotted for varying percentages of structural unfolding (dashed lines). Equal-area projections of the paleomagnetic mean directions prior to unfolding are inset. (c) Conglomerate test for intraformational conglomerate at Onnay River (plotted in geographic coordinates). Randomness cannot be disproved at the 95% confidence level [*Watson,* 1956], and the test is passed. (d) Bootstrap fold test for data from Malaya Orlovka River.

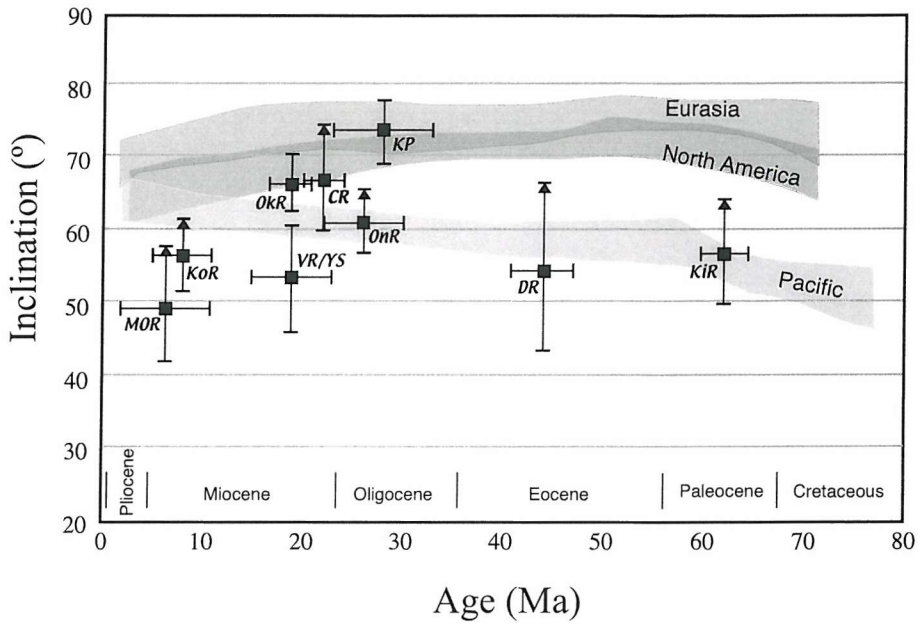

Figure 4.11. Inclination versus age for paleomagnetic data from Sakhalin compared with the Eurasian, North American [*Besse and Courtillot,* 1991], and Pacific [*Gordon and Van der Voo,* 1995] reference plates. The reference directions expected for a geocentric axial dipole (GAD) field are plotted as a shaded envelope for the latitudinal range of Sakhalin. Arrows indicate probable inclination shallowing; the inclinations should be steeper to be representative of the paleofield (see Figure 4.12, 4.13). Localities are indicated using the same abbreviations as in Figure 4.5.

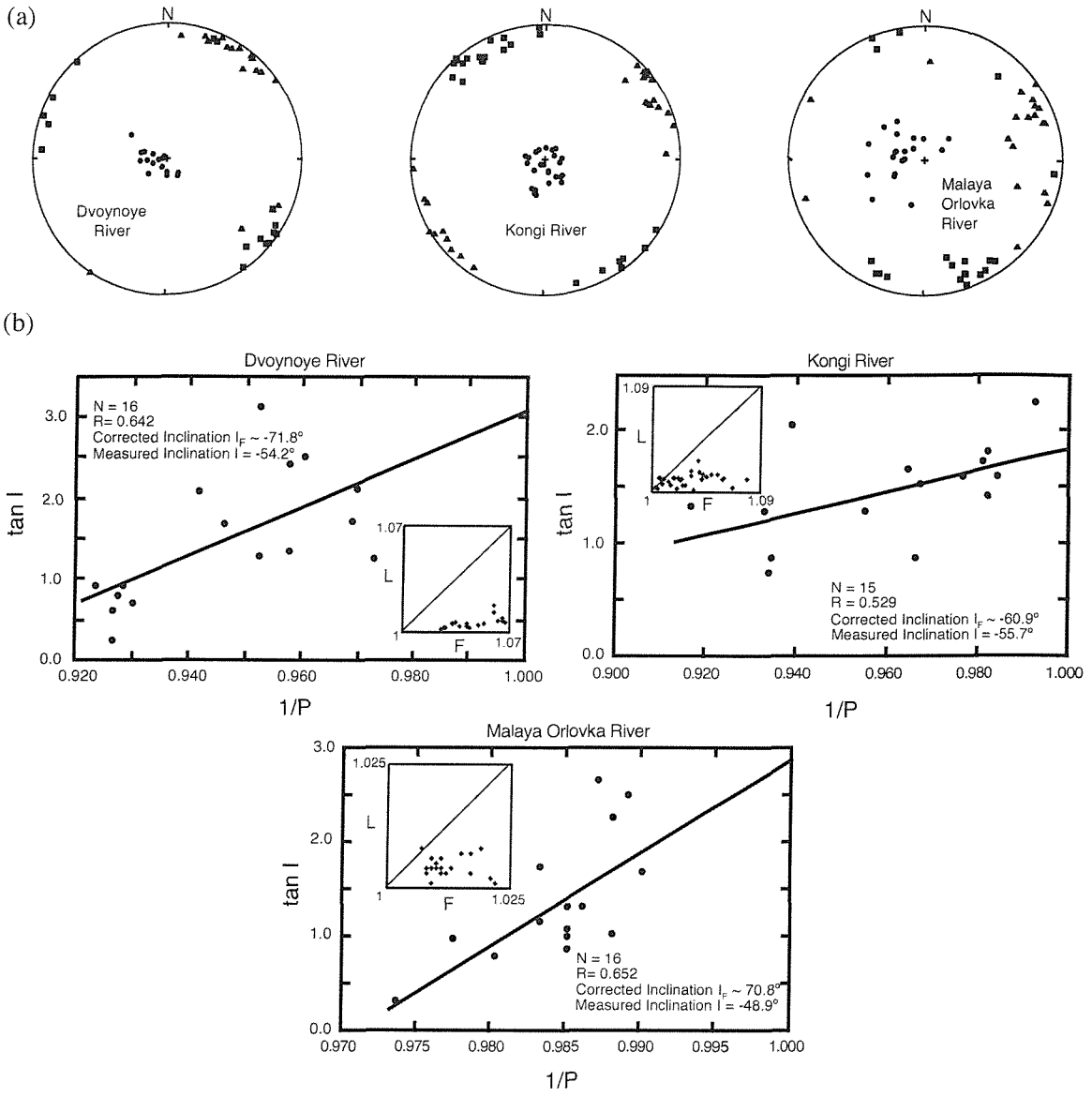

Figure 4.12. (a) Equal-area plots of magnetic fabrics for samples from Dvoynoye River, Kongi River and Malaya Orlovka River. Dots = k_{min}, triangles = k_{int}, and squares = k_{max}. (b) Prediction of the expected inclination for paleomagnetic samples for the three localities shown in (a), based on AMS parameters ($P = k_{max}/k_{min}$), following *Hodych et al.* [1999]. Oblate magnetic fabrics are indicated in the Flinn susceptibility plots (L versus F, where $L = k_{max}/k_{int}$ and $F = k_{int}/k_{min}$).

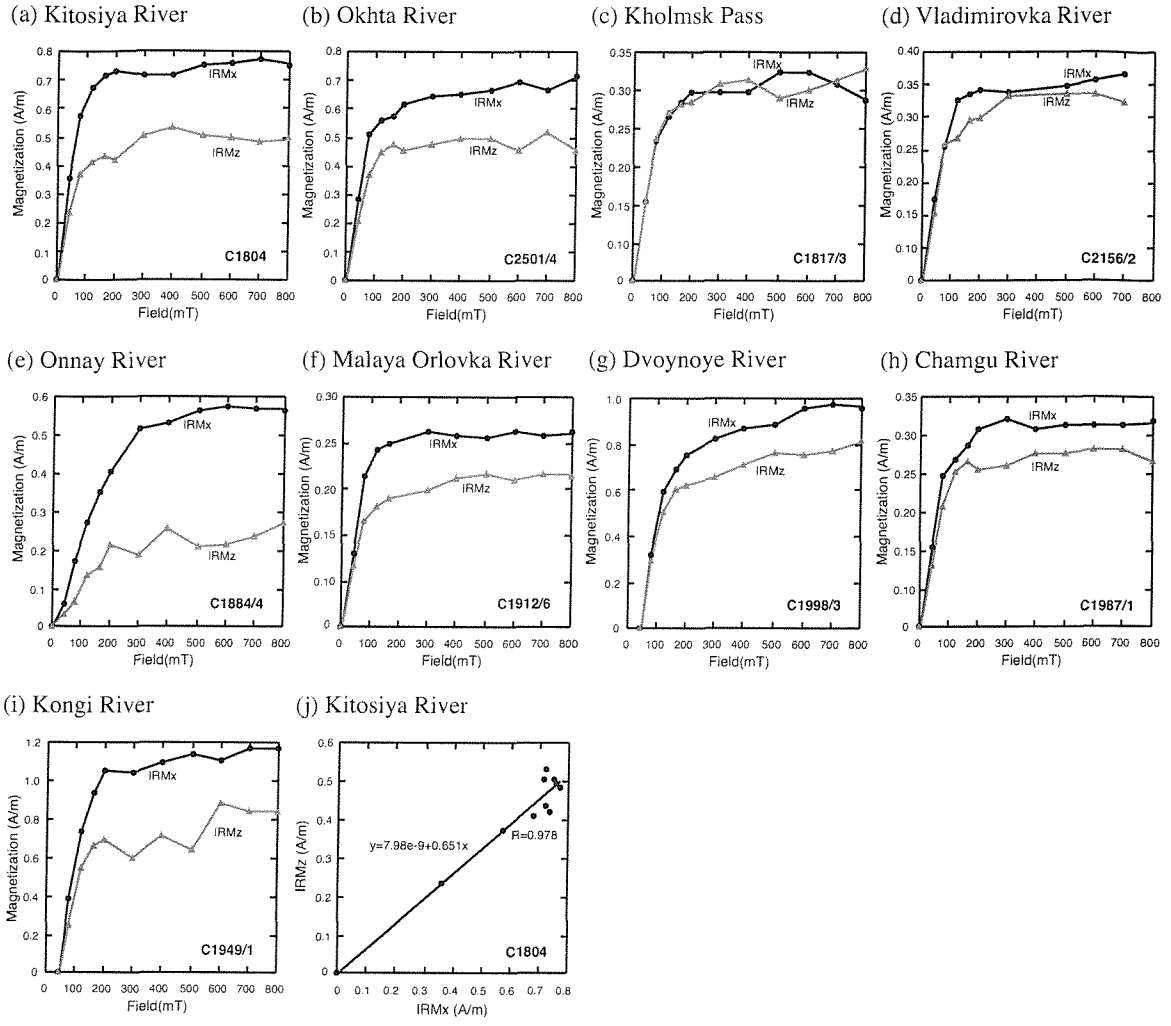

Figure 4.13. (a) – (i) IRM acquisition curves for bedding-normal components (IRM_Z) and bedding-parallel components (IRM_X) for all successful paleomagnetic sampling localities in Sakhalin. (j) The gradient of the best-fit correlation line of IRM_Z versus IRM_X was used to determine the IRM_Z/IRM_X ratio, which gives an estimate of inclination shallowing in the sediments [*Hodych and Buchan,* 1994].

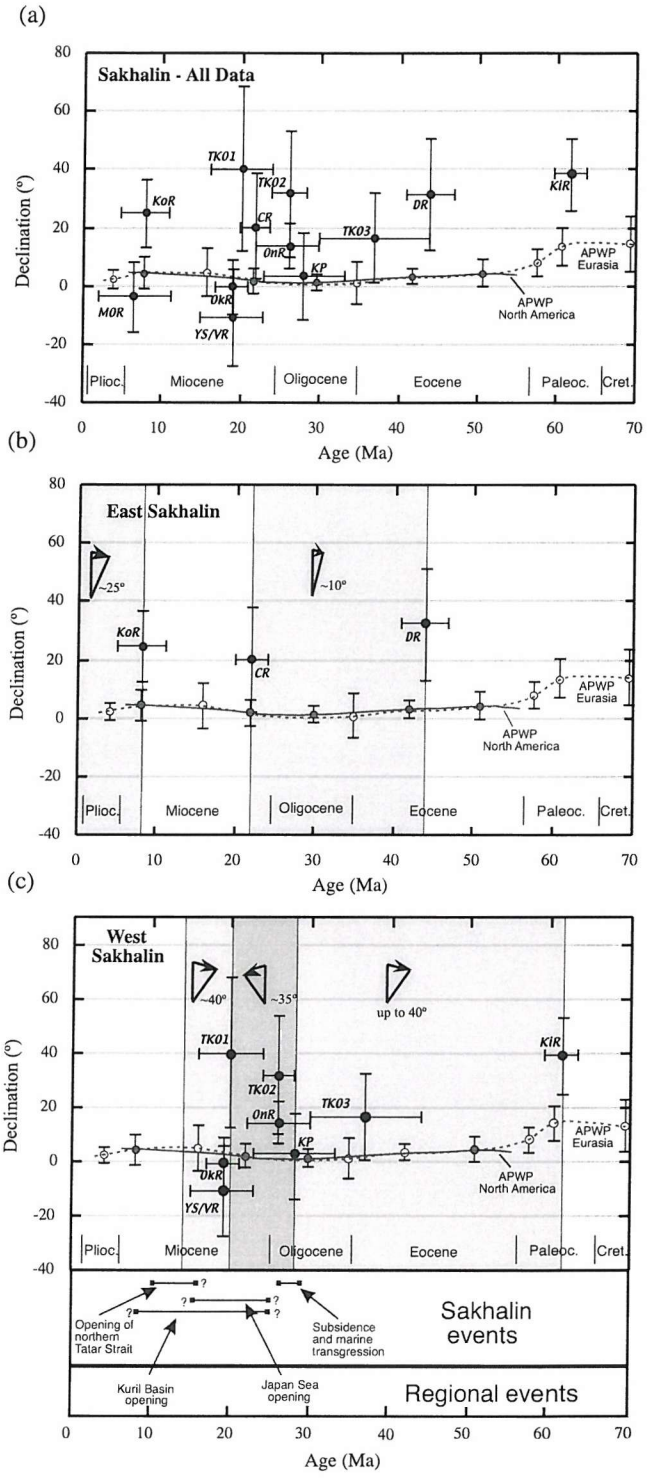

Figure 4.14. Declination versus age for paleomagnetic data from (a) Sakhalin, (b) east Sakhalin, and (c) west Sakhalin, with the expected North American Plate (solid line) and Eurasian Plate (dashed line) values shown for reference APWP's. The range of expected values is indicated for each pole position. Abbreviations for localities are as in Figure 4.5, with data from *Takeuchi et al.* [1999] indicated by TKO1, TKO2, TKO3. Sakhalin tectonic events are from *Flecker and Macdonald* [in press]; timing of Japan Sea opening is from *Tamaki et al.* [1992]. Kuril Basin opening is constrained by paleomagnetic data presented here and by *Takeuchi et al.* [1999]. "?" indicates uncertainty in the dating of tectonic events. Note that in Sakhalin this is particularly important when sediments are paralic because biostratigraphic constraints are potentially subject to large errors.

5

Tertiary geodynamics of Sakhalin (NW Pacific) from anisotropy of magnetic susceptibility fabrics and paleomagnetic data

This chapter has been submitted for publication as: Weaver, R., A. P. Roberts, R. Flecker, and D. I. M. Macdonald, Tertiary geodynamics of Sakhalin (NW Pacific) from anisotropy of magnetic susceptibility fabrics and paleomagnetic data.

Abstract

Sakhalin has been affected by several phases of Cretaceous and Tertiary deformation due to the complex interaction of plates in the northwest Pacific region. A detailed understanding of the strain provides constraints on the plate-scale processes controlling the formation and deformation of marginal sedimentary basins. Anisotropy of magnetic susceptibility (AMS) data are presented from fine-grained mudstones and siltstones from 22 localities in Sakhalin. AMS data reliably record strain tensor orientations close to the time of deposition of the sediments. Paleomagnetically determined vertical-axis rotations of crustal rocks allow rotation of the fabrics back to its original orientation. Results from southwest Sakhalin indicate a ~N035°E-directed net tectonic transport from the mid-Paleocene to the early Miocene, which is consistent with the present-day relative motion between the Okhotsk Sea and Eurasian plates. Reconstruction of the early-late Miocene AMS fabrics in east Sakhalin indicates a tectonic transport direction of ~N040°E. In west Sakhalin, the transport direction appears to have remained relatively consistent from the Oligocene to the late Miocene and has a different attitude of ~N080°E. This suggests local deflection of the stress and strain fields, which was probably associated with opening of the northern Tatar Strait. A northward-directed tectonic transport is observed in Miocene sediments in southeast Sakhalin, mid-Eocene sediments in east Sakhalin, and in late Cretaceous rocks of west and northern Sakhalin, which may be associated with ancient northwestward motion of the Pacific Plate.

5.1. Introduction

The geological evolution of Sakhalin, which lies on the northwest Pacific margin, has been complex, with evidence of several deformation phases. Neogene displacement along N-S-trending strike-slip faults suggests a right-lateral transpressive tectonic regime [*Fournier et al.,* 1994]. However, Mesozoic accretionary complex rocks and fore-arc basin sediments exposed in Sakhalin are associated with an ancient episode of

subduction [*Parfenov et al.,* 1981; *Richter,* 1984; *Kimura,* 1994]. The timing of the cessation of subduction beneath Sakhalin is currently poorly constrained with suggested estimates that range from Late Mesozoic [*Worrall et al.,* 1996] to Middle Miocene [*Zonenshain et al.,* 1990]. Interpretation of the ancient evolution of the area is further complicated by controversy over the present-day plate tectonic configuration of the NW Pacific, which probably involves interaction between the North American, Eurasian, Amurian, Northern Honshu, Okhotsk Sea, Pacific, and Philippine Sea Plates (Figure 5.1) [*Takahashi et al.,* 1999]. However, the location of many of the boundaries between these plates and even the existence of some of the plates remains uncertain [*Seno et al.,* 1996].

Several kinematic models have been suggested for the Cenozoic evolution of the east Asian margin. These models consider basin formation either to be the product of large-scale extrusion as a result of India-Eurasia collision [e.g., *Tapponnier et al.,* 1986; *Jolivet et al.,* 1990; *Worrall et al.,* 1996], or, of roll-back on the Pacific Plate [e.g., *Watson et al.,* 1987; *Northrup et al.,* 1995]. Regional studies have been used to test these models [e.g., *Allen et al.,* 1998]. In the northwest Pacific, these models are based primarily on data from Japan and the Japan Sea [*Otofuji et al.,* 1991; *Jolivet et al.,* 1994; *Altis,* 1999]. However, in the Sakhalin-Okhotsk Sea region, to the north of Japan (Figure 5.1), few data have been documented regarding the geodynamic and tectonic evolution and, therefore, the proposed geodynamic models are underconstrained [*Fournier et al.,* 1994; *Worrall et al.,* 1996; *Takeuchi et al.,* 1999].

Spatial and temporal variation of stress and strain fields are important to help identify and determine the location of past and present plate boundaries and provide constraints on regional geodynamic models. Stress is a fundamental tectonic body force, but it is inherently difficult to determine because only strain, which results from the acting stress, can be observed [e.g., *Ramsay and Lisle,* 2000]. At local scales, for instance, stress and strain become partitioned, which complicates interpretation of geological structures in the field (macrofabrics) and often makes it difficult to link such features with the regional compressive stress. These relationships are further complicated

if more than one phase of deformation has occurred. In southern Sakhalin, for example, published fault-analysis data [*Fournier et al.,* 1994] are ambiguous and indicate inconsistent paleostress orientations. A source of uncertainty with fault-derived paleostress data is the possibility of unidentified vertical-axis rotations of crustal blocks and the resulting deflection of fault trends. *Fournier et al.* [1994] pointed out that supporting paleomagnetic data are needed to provide a robust estimate of the paleostress in this region.

In the present study, anisotropy of magnetic susceptibility (AMS) data from Late Cretaceous – Pliocene rocks in Sakhalin are used to define a microscopic rock deformation fabric. The microscopic fabric orientation is used as a means for determining the direction of net tectonic transport [e.g., *Kissel et al.,* 1986; *Lee et al.,* 1990; *Sagnotti et al.,* 1994], which can be considered to be independent of the paleostress field or the finite strain history of the rocks [e.g., *Twiss and Moores,* 1992]. Magnetic rock fabrics can form in weakly-deformed sediments and they can provide important constraints on spatial and temporal directional differences in regional tectonic transport.

We combine AMS data with paleomagnetic data, which provide quantitative kinematic constraints for various regions in Sakhalin [*Takeuchi et al.,* 1999; *Weaver et al.,* 2003]. Paleomagnetic data suggest that:

1) Sakhalin remained around its present-day latitude for most of the Tertiary,
2) the transition from subduction tectonics to strike-slip tectonics may have occurred around the mid-Eocene, and
3) Sakhalin underwent rapid clockwise vertical-axis rotation phases (up to about 40°) in the Miocene, which may have been linked to rifting in the Japan Sea, Kuril Basin, and Tatar Strait.

These data allow the AMS fabrics and, therefore, the interpretation of tectonic transport directions, to be determined relative to geographic north.

5.2. Geological Setting and Fieldwork

Sakhalin is located to the east of mainland Russia along the western margin of the Okhotsk Sea (Figure 5.1). A north-south-trending system of active right-lateral strike-slip faults transects Sakhalin [*Ivashchenko et al.,* 1997]. The east and west regions of Sakhalin are separated by the Central Sakhalin Fault (Figure 5.2). Mesozoic accretionary complex rocks are exposed in east Sakhalin, in the East Sakhalin Mountains, Tonino-Aniva Peninsula and NE Schmidt Peninsula (Figure 5.2). Mesozoic fore-arc sediments crop out in west Sakhalin [*Parfenov and Natal'in,* 1986; *Zyabrev and Bragin,* 1987]. The associated volcanic arc is the Sikhote Al'in belt on the Russian mainland (Figure 5.1) [*Zonenshain et al.,* 1990; *Okamura et al.,* 1998]. Many phases of crustal accretion and uplift have affected northeastern Russia since the Permian and tectonic uplift of Sakhalin is thought to have been associated with a collisional phase [*Natal'in,* 1993]. Tertiary sediments in Sakhalin were deposited in small basins in the east, which were probably generated by strike-slip fault activity [*Worrall et al.,* 1996]. In north Sakhalin, thick successions of deltaic sediments accumulated in the early Miocene-Pliocene. These sediments are thought to have been derived from the paleo-Amur River (Figure 5.2) [*Varnavskiy et al.,* 1990], which drains the eastern side of the Siberian Craton. Tertiary sequences exposed along the West Sakhalin Mountains (Figure 5.2) date back to the Paleocene. Cenozoic faulting has resulted in further deformation and uplift throughout Sakhalin [*Rozhdestvenskiy,* 1982; *Kharakhinov et al.,* 1985].

Extensive sampling of Late Cretaceous to Tertiary fine-grained sediments was carried out in Sakhalin as part of a regional-scale tectonic study. Cylindrical paleomagnetic samples were collected from 28 localities; reliable paleomagnetic data were acquired from only 9 of these. AMS results are presented from 22 localities that have well-defined magnetic fabrics. The age, lithology, and bedding attitudes are listed for each sampled locality in Table 5.1.

5.3. Methods

AMS measurements were carried out using an AGICO KLY-3S magnetic susceptibility meter at the Istituto Nazionale di Geofisica e Vulcanologica (INGV), Rome, Italy. Low-field magnetic susceptibility of oriented cylindrical samples (h = 2.2 cm × d = 2.5 cm) was measured during rotation of each sample in 3 perpendicular planes. This method ensures accurate determination of the AMS to around 5×10^{-6} SI. The eigenvalues of the susceptibility (k_{max}, k_{int}, k_{min}) were calculated by solving the second rank symmetrical susceptibility tensor [e.g., *Tauxe,* 1998]. Eigenvectors were calculated and statistical treatment was carried out following the method of *Jelinek* [1978]. The mean susceptibility (k_{mean}), the degree of anisotropy, P', where:

$$P' = \exp\sqrt{2\left[\left(\ln k_{max} - \ln k_{mean}\right)^2 + \left(\ln k_{int} - \ln k_{mean}\right)^2 + \left(\ln k_{min} - \ln k_{mean}\right)^2\right]},$$

and the shape of the AMS ellipsoid (T):

$$T = \frac{2\left(\ln k_{int} - \ln k_{min}\right)}{\left(\ln k_{max} - \ln k_{min}\right)} - 1,$$

were used to characterize the anisotropy of individual samples [*Jelinek,* 1981]. Mean directions of the principal eigenvectors and eigenvalues are listed in Table 5.2.

Hysteresis measurements were carried out on representative samples from each locality using a Princeton Measurements Corporation vibrating sample magnetometer (μVSM) at the Institute for Rock Magnetism (IRM), Minneapolis, MN, USA. Samples were measured up to maximum fields of 1 T. Such data are useful for assessing the relative contribution of paramagnetic and ferrimagnetic minerals to the susceptibility.

5.4. Results

5.4.1. Rock Magnetic Results

Hysteresis loops for samples from throughout Sakhalin have clear positive slopes, which indicate a significant contribution from paramagnetic minerals (Figure 5.3). Mean susceptibility values that range from 26 to 403 μSI suggest that paramagnetic minerals dominate the susceptibility and that the ferrimagnetic fraction of grains are unlikely to be important when considering the magnetic fabric [*Rochette,* 1987; *Hrouda and Kahan,* 1991; *Borradaile and Henry,* 1997]. These observations suggest that paramagnetic matrix minerals define the AMS fabrics rather than the orientation distribution of ferrimagnetic minerals [*Borradaile and Henry,* 1997].

Rock magnetic data from localities where the natural remanent magnetization (NRM) was reliable for tectonic purposes (i.e. stable and not remagnetized) indicate the presence of pseudo single-domain (PSD) magnetite, and, at two localities, a ferrimagnetc iron sulphide mineral is present [*Weaver et al.,* 2002, 2003]. NRM intensities are generally low (10^{-7}-10^{-5} A/m).

5.4.2. Magnetic Fabrics

The majority of samples have an AMS fabric with a near-vertical clustering of k_{min}, together with k_{int}, and k_{max} axes that lie in the paleohorizontal (bedding) plane. This indicates a sedimentary origin of the fabrics [e.g., *Rees and Woodall,* 1975]. At each sampled locality, oblate fabrics (i.e. $T > 0$, $P' > 1.00$) are consistent with flattening due to compaction (Figure 5.4) [*Jelinek,* 1981]. Most samples have a weak anisotropy with $P' < 1.04$, the value of which is consistent between regions and suites containing different lithologies (Figure 5.4). This suggests that the degree of anisotropy is not strongly correlated to the amount of finite strain or to the lithology of the rocks [e.g., *Housen et al.,* 1995] (Table 5.1). Additionally, the majority of fabrics have a well-defined clustering of k_{max} directions (Table 5.2), which has been reported in areas of less intense deformation and tectonic strain [e.g., *Parés et al.,* 1999]. Anomalous AMS ellipsoids that

were measured in some samples (Figure 5.4) and the resulting scatter around the mean eigenvector directions, are probably due to subtle variations in the mineralogical composition [*Rochette,* 1987; *Rochette et al.,* 1992].

Evidence from sediments in Italy indicates that AMS lineations could be controlled by the direction of the maximum horizontal stress [*Mattei et al.,* 1997; *Sagnotti et al.,* 1999]. Regional coherence of AMS fabrics from mudrocks in Taiwan also suggests that lineation development may have been controlled by the regional stress [*Kissel et al.,* 1986; *Lee et al.,* 1990]. However, it remains uncertain whether fabrics from Sakhalin originate strictly in response to stress or strain [e.g., *Borradaile,* 1988; *Averbruch et al.,* 1992; *Aubourg et al.,* 1999], because, in most documented cases of AMS-determined paleostress orientations, deformation and folding has occurred virtually perpendicular to the maximum horizontal stress. In Sakhalin, there appears to be no consistent relationship between bedding strike and the orientation of k_{max} for any given age or region (Figure 5.5). This suggests that the k_{max} lineation is not directly related to the finite strain observed in the field (macrofabrics).

Alternatively, the observed fabrics may have formed due to paleocurrent alignment of sedimentary particles [*Hamilton and Rees,* 1970]. This appears unlikely, however, because of the spatial and temporal consistency of the AMS fabrics in samples from different sedimentary settings (Table 5.1; Figures 5.6-5.9).

The cumulative evidence from Sakhalin suggests that magnetic fabrics from different types of fine-grained sedimentary rocks developed early during a phase of plastic deformation in response to tectonic forces. Consistent magnetic fabrics probably represent the net tectonic transport direction. The deformation mechanism that created the fabric could be due to granular, or, cataclastic flow of material in the rock, or by dislocation glide along crystallographic glide planes. Anisotropic minerals may have chemically grown in the sediment in response to stress. However, it is unlikely that a chemical mineral growth has affected all the sediments equally from such varied sedimentary environments (see Appendix B). Electron microscopic observations also

indicate that the rocks have a clastic sedimentary matrix without obvious authigenic mineral growth textures. Therefore, mechanical alignment of "plate-like" minerals through, for example, dislocation glide, appears to be a more feasible mechanism for creation of the magnetic fabrics. AMS fabrics that have recorded both a vertical k_{min} axis and a k_{max} lineation in the horizontal plane are regarded as "early" tectonic fabrics. In such cases, a lineation forms in response to horizontal force components acting perpendicular to the lineation trend [e.g., *Parés et al.,* 1999].

5.5. Discussion

5.5.1. Tectonic Transport in Sakhalin

5.5.1.1. South Sakhalin

AMS-based fabric analyses from south Sakhalin are presented in Figure 5.6. Paleomagnetic data from Kitosiya River, Kholmsk Pass, and Vladimirovka River allow the fabric to be restored relative to north and allows a tectonic transport direction to be estimated from the mid-Paleocene to early Miocene (see white arrows in Figure 5.6). Counterclockwise back-rotation of the Kitosiya River fabric by 40°, gives a corrected transport direction of about N041°E. Clockwise rotation of the Vladimirovka data by 10° indicates a corrected direction of N040°E. Furthermore, the corrected data from Kholmsk Pass suggest N028°E-directed tectonic transport in the Oligocene, although the confidence ellipse associated with the AMS data is large. After correction, the fabric orientations are regionally consistent and suggest a net tectonic transport direction in south Sakhalin that has remained almost constant around N035±5°E since the Paleocene (Figure 5.6). Data from Il'inskiy Coast are within error of this estimate, but the amount of vertical-axis rotation at this locality is uncertain.

Magnetic fabric k_{int} orientations are closer to E-W in mid-late Miocene rocks at Kormavaya River and Shakhtnaya River (Figure 5.6). *Fournier et al.* [1994] noted that there is evidence for clockwise deflection of folds in the vicinity of the Central Sakhalin Fault, although the amount of rotation is not specified. This suggests that the mid-late

Miocene data might be in closer agreement with the localities to the southwest after correction for the inferred clockwise vertical-axis rotation (~20°).

The AMS fabrics observed at Tunaicha and Korsakov, both on the Tonino-Aniva Peninsula (Figure 5.2), indicate a clear E-W-trending lineation, which suggests a N-S-directed tectonic transport. This is in contrast to the fabrics elsewhere in south Sakhalin (Figure 5.6). It is difficult to explain such a difference in orientations from rocks of the same age by assuming a single tectonic regime and coherent deformation across the whole south Sakhalin region (Figure 5.6). Our observations suggest that these localities may have been part of a different crustal block. This possibility is discussed further below.

5.5.1.2. East Sakhalin

AMS data from early and mid-Miocene rocks at Chamgu River in east Sakhalin have k_{int} mean directions of N066°E and N069°E, respectively (Figure 5.7). At Kongi River, k_{int} from the Upper Borsk Suite clusters at around N057°E (Figure 5.7). The Miocene data are, therefore, within error of each other and are consistent with paleomagnetic results, which suggest that there was negligible relative rotation between these localities from the Eocene to the Miocene [*Weaver et al.,* 2003]. However, the paleomagnetic declinations are clockwise deflected by 20-30°, which yields a corrected k_{int} of ~N040±8°E at the Chamgu River and Kongi River localities (Figure 5.7).

The uncorrected k_{int} direction for Eocene sediments at Dvoynoye River (N028°E) is within error of the corrected k_{int} directions from Kongi River and Chamgu River (Figure 5.7). However, paleomagnetic data suggest that the Dvoynoye River locality has rotated 32° clockwise since the Eocene [*Weaver et al.,* 2003], which suggests a N-S-trending corrected transport direction (Figure 5.7). Therefore, there appears to be ~40° difference in fabric orientation, which suggests that the transport direction may have changed between the mid-Eocene and early Miocene.

5.5.1.3. West Sakhalin

Paleomagnetic data from Onnay River and Malaya Orlovka River allow magnetic fabrics to be corrected for vertical-axis tectonic rotations (Figure 5.8). After correction, the late Miocene magnetic fabric at Malaya Orlovka River has k_{int} = N077°E. This is consistent with data from North Aleksandrovsk, where k_{int} = N083°E. The AMS fabrics from Gennoyshi Suite (Oligocene) mudstone at Avgustovka and Aleksandrovsk-Due Coast yield a mean k_{int} direction of N109°E and N112°E, respectively (Figure 5.8). A similar k_{int} direction (k_{int} = N106°E) is obtained from the early Miocene (Upper Due) AMS data set from Aleksandrovsk (Figure 5.8). Thus, early Oligocene – early Miocene sediments have consistent k_{int} trends (~N110°E). In the early to mid-Miocene, the trends change to k_{int} ~N080°E. AMS data from different localities suggest that the direction of net tectonic transport remained relatively fixed spatially.

Paleomagnetic data [*Weaver et al.,* 2003] indicate that localities in west and southwest Sakhalin rotated clockwise by ~20-30° between the early Miocene and mid-Miocene. It is likely that the observed change in magnetic fabric orientation for west Sakhalin is due to a regional vertical-axis rotation event (with a fixed stress field) around the mid-Miocene. This is supported by the back-rotated magnetic fabric at Onnay River, which has a k_{int} direction within error of the mid-late Miocene fabric orientations (Figure 5.8).

Alternatively, the stress field could have changed orientation, which may have yielded a tectonic transport direction that changed from ESE-WNW to become ENE-WSW-trending in the early Miocene (Figure 5.8). In this case, the clockwise vertical-axis rotation observed at Onnay River could be interpreted as a local-scale rotational event. Without useful paleomagnetic data from Aleksandrovsk-Sakhalinskiy, this possibility cannot be ruled out.

AMS data from Late Cretaceous black shales from Aleksandrovsk-Due Coast suggest a k_{int} direction of N142°E (Figure 5.8). Assuming that these sediments belong to the same tectonostratigraphic block as the other Due Coast localities, the data seem to

indicate counterclockwise change in direction of the net tectonic transport of around 30° between the Late Cretaceous and the Early Oligocene.

5.5.1.4. North Sakhalin

AMS fabric data for mid-Miocene sediments from SE Schmidt Peninsula, North Sakhalin (Figure 5.9), indicate a NE-SW-trending transport direction (k_{int} = N024°E), which is consistent with transport directions determined elsewhere in Sakhalin (Figures 5.6-5.8), as well as paleostress trends expected for Neogene transpression [*Fournier et al.,* 1994]. On the NE Schmidt Peninsula, a late Cretaceous transport direction appears to trend directly N-S. This suggests an apparent clockwise rotation of around 25° of the NE Schmidt AMS fabric relative to SE Schmidt between the late Cretaceous and mid-Miocene (Figure 5.9), which could be due to a vertical-axis block rotation or to a change in transport direction. The significance of any relative rotation is uncertain in the absence of paleomagnetic data.

5.5.2. Geodynamic Significance of Tectonic Transport Estimates from Sakhalin

Magnetic fabric orientations from localities on the Kril'on Peninsula (Figure 5.2) in south Sakhalin are consistent and suggest a net transport direction of ~N035°E (Figure 5.6). The data suggest that this region has deformed coherently from the mid-Paleocene to late Miocene, which is consistent with paleomagnetic data that indicate consistent clockwise vertical-axis rotations during this period [*Takeuchi et al.,* 1999; *Weaver et al.,* 2003]. Oblique compression and deformation on Tertiary strike-slip faults probably accommodated this deformation [*Fournier et al.,* 1994].

A N-S to NNW-SSE direction of the net tectonic transport (regionally consistent AMS fabrics) in the Early Miocene on the Tonino-Aniva Peninsula suggests that this region belongs to a different tectonic block compared to the adjacent Kril'on Peninsula (Figure 5.6). Several ancient exotic terranes that originated from southerly latitudes have accreted onto the Tonino-Aniva Peninsula [e.g., *Zonenshain et al.,* 1990]. Paleomagnetic

data indicate that a Late Cretaceous island arc terrane travelled northward with the Pacific Plate and accreted onto Sakhalin in the mid-Eocene [*Bazhenov et al.*, 2001]. Some models of the NW Pacific and NE Asia suggest that plate or micro-plate boundaries divide the west and east parts of southern Sakhalin (Figure 5.1) [*Seno*, 1985; *Seno et al.*, 1996; *Takahashi et al.*, 1999]. Our analysis supports the suggestion that this region evolved independently as part of a different plate or micro-plate.

In west Sakhalin (Figure 5.8) and at Makarov further to the south (localities 6 and 7, Figure 5.6), the back-rotated orientation of the AMS fabric is consistently N080°E-N110°E from the Oligocene to late Miocene. This regionally coherent direction indicates a tectonic transport direction that is different to that of south Sakhalin, and suggests that these localities may belong to a different tectonic block, as some plate models suggest [e.g., *Takahashi et al.*, 1999]. Another possibility is that the E-W-directed opening of the Tatar Strait during this period [*Jolivet et al.*, 1994] could account for local deflection of the strain tensor in west Sakhalin. AMS data and paleomagnetic data indicate a phase of rapid clockwise vertical-axis rotation in the mid-Miocene, which may be linked to the opening of the Tatar Strait (Figure 5.8) [*Weaver et al.*, 2003].

Consistent fabrics from Miocene localities in east Sakhalin reveal a tectonic transport direction of around N040°E (Figure 5.7), which is similar to the direction obtained for Sakhalin. Miocene clockwise vertical-axis rotation observed in paleomagnetic data probably occurred through oblique compression along N-S-trending strike-slip faults that were active in the Neogene. AMS data from mid-Eocene sediments at Dvoynoye River indicate a N-S-directed net tectonic transport direction, which suggests that early deformation in this area may have been controlled by a Pacific-type motion similar to the Tonino-Aniva Peninsula and in contrast to southwest Sakhalin (Figure 5.6, 5.7). This remains uncertain in the absence of reliable paleomagnetic results for Tertiary sediments from the Tonino-Aniva Peninsula.

5.6. Conclusions

Magnetic fabrics observed in Late Cretaceous to Late Miocene sedimentary rocks from Sakhalin have clustered k_{max} axes in the bedding plane together with k_{min} axes normal to the bedding plane. After correction for paleomagnetically-determined vertical-axis rotations, the fabrics are regionally consistent and define regions, which have characteristic directions of net tectonic transport. Data from the Kril'on Peninsula in south Sakhalin indicate a consistent tectonic transport direction of around N035°E from the mid-Paleocene to the late Miocene. In west Sakhalin, magnetic fabrics indicate a tectonic transport direction of around N080°E, which was probably from the Oligocene (Figure 5.10). A rapid phase of clockwise rotation in the early-mid-Miocene may be linked with the opening of the Tatar Strait, which may explain the consistent E-W-oriented k_{int} axes of the magnetic fabrics and, thus, a different direction of transport for west Sakhalin. The direction of Miocene tectonic transport in east Sakhalin is around N040°E. In east Sakhalin and southwest Sakhalin, clockwise vertical-axis rotations appear to have been accommodated by oblique NE-SW compression along N-S-trending strike-slip faults. On the Tonino-Aniva Peninsula (early Miocene) and at Dvoynoye River (mid-Eocene) in east Sakhalin, a contrasting N-S-directed net tectonic transport suggests that the regions may have evolved with different tectonic blocks or micro-plates. The boundaries between the separate regions defined by the AMS data are consistent with present-day plate models [*Seno,* 1985; *DeMets,* 1992a; *Seno et al.,* 1996; *Takahashi et al.,* 1999].

In the transpressional Sakhalin shear zone, the AMS method for determining ancient transport directions from "early" tectonic fabrics is ideal because deformation is significantly oblique to the regional stress in a region where there have been several phases of deformation and vertical-axis rotations. Previous AMS studies have concentrated on regions where the regional compressive stress is near-perpendicular to the strain axes of macroscopic structures. In these cases, it is inherently uncertain whether the AMS develops as a result of stress or strain. In Sakhalin, the magnetic

fabrics appear to have been recorded during an early stage of plastic deformation in different lithological types of fine-grained clastic sediments that were deposited in different environments. This suggests that the AMS technique may be more generally applicable and not necessarily restricted to "undeformed" clay-rich sediments.

Acknowledgements. Fieldwork in Sakhalin was carried out as part of the Cambridge Arctic Shelf Programme research program funded by Agip, Anadarko, Arco, BP, Exxon, JNOC, Mobil, Philips, and Texaco. RW gratefully acknowledges financial support from a U.K. NERC Ph.D. studentship. APR, RF, and DIMM acknowledge support from a grant from the Royal Society of London. Field logistics were provided by Sakhalin Geological Research Expedition in Yuzhno-Sakhalinsk; we are indebted to Vladimir Galversen, Pavel Kovtunovich, Zhenia Rasshchepkina and Valeriy Gorbachov for their help and support. The authors are grateful to Fabio Florindo for assistance with measurements at the Istituto Nazionale di Geofisica e Vulcanologia, Rome, Italy, and to Mike Jackson for assistance at the Institute for Rock Magnetism, Minneapolis, U.S.A.

Table 5.1. Magnetic susceptibility and geological data from sampling localities in Sakhalin

Locality	Lat. (°)	Long. (°)	Suite	Age	Lithology	Avg. Bedding Dip (°)/Strike (°)	N	Range of k_{mean} SI	k_{mean} SI
Aleksandrovsk-Due	50.8	142.1	Gennoyshi	Oligocene	Marine siltstone	50 NE/328	15	1.74E-04 - 2.99E-04	2.23E-04
Aleksandrovsk-Due	50.8	142. 1	Krasnoyarkov	Late Cretaceous	Black shale	51 SW/026	16	2.03E-04 - 2.43E-04	2.30E-04
Aleksandrovsk-Due	50.8	142.1	Upper Due	Early Miocene	Lagoonal siltstone	13 NE/298	8	1.18E-04 - 2.36E-04	1.55E-04
Avgustovka	49.7	142.2	Gennoyshi	Oligocene	Marine siltstone	45 W/184	29	1.23E-04 - 2.90E-03	3.44E-04
Balshoya Orlovka	49.6	142.7	Upper Due	Early Miocene	Lagoonal siltstone	29 S/089	23	5.21E-05 - 2.13E-03	1.17E-03
Chamgu	50.9	143.5	Borsk	Early Miocene	Siliceous siltstone	48 W/175	27	9.39E-05 - 6.06E-04	1.70E-04
Chamgu	50.9	143.5	Khuzin	Mid-Late Miocene	Siliceous mudstone	10 NE/348	51	8.70E-05 - 1.24E-04	1.05E-04
Dvoynoye	50.1	143.7	Lyukamen	Middle Eocene	Marine mudstone	15 NW/215	17	1.74E-04 - 5.02E-04	3.29E-04
Il'inskiy	47.9	142.1	Kurasiy	Late Miocene	Siliceous mudstone	36 NE/ 317	43	1.75E-05 - 4.89E-05	3.11E-05
Kholmsk	47.1	142.1	Takaraday, Arakay, Kholmsk	Oligocene - Miocene	Marine volcaniclastic mudstone	28 W/158 to 2 SE/040	32	1.20E-04 - 1.35E-03	4.03E-04
Kitosiya	46.9	141.9	Sinegorian Beds	Early Paleocene	Marine mudstone	31 W/187	11	1.27E-04 - 2.80E-04	2.13E-04
Kongi	51.1	143.4	Borsk	Early Miocene	Sandy marine mudstone	65 E/355	25	1.61E-04 - 2.84E-04	2.12E-04
Kormovaya	48.7	142.7	Kurasiy-Maruyama	Mid-Late Miocene	Marine mudstone	65 E/357	38	1.03E-04 - 2.14E-04	1.40E-04
Korsakov	46.6	142.8	Kholmsk	Early Miocene	Siliceous mudstone	80 NW/226	18	1.18E-04 - 5.03E-04	1.75E-04
Malaya Orlovka	49.6	142.7	Nutovsk	Miocene - Pliocene	Mudstone	76 NE/330 to 22 SW/114	20	1.09E-04 - 2.07E-04	1.51E-04
NE Schmidt	54.2	142.8	Toninsk	Late Cretaceous	Marine mudstone	30 E/356	26	1.30E-04 - 2.91E-04	2.05E-04
North Aleksandrovsk	51.2	142.2	Sertunay, Okobykay	Middle Miocene	Mudstone	21 SE/058 to 34 NW/208	20	1.31E-04 - 2.18E-04	1.83E-04
Onnay	49.6	142.2	Arakay	Oligocene	Siliceous black siltstone	40 W/193	18	1.44E-04 - 3.60E-04	1.97E-04
SE Schmidt	54.0	142. 9	Pil'sk	Middle Miocene	Siliceous mudstone	57 SW/126 to 61 NE/340	32	1.06E-05 - 4.51E-05	2.62E-05
Shakhtnaya	48.8	142.8	Sertunay	Early-Mid Miocne	Mudstone	65 E/005	26	6.16E-05 - 1.80E-04	1.35E-04
Tunaicha	46.9	143.1	Kholmsk	Early Miocene	Siliceous mudstone	30 W/163	12	3.58E-05 - 1.63E-04	7.45E-05
Vladimirovka/Yar	47.1	142.3	Kholmsk	Early Miocene	Siliceous mudstone	70 SE/020 to 80 NW/204	50	1.05E-04 - 8.51E-04	2.01E-04

Table 5.2. AMS eigenparameter data from Sakhalin

Locality	Suite	N	k_{min}	D_{kmin} (°)	I_{kmin} (°)	k_{int}	D_{kint} (°)	I_{kint} (°)	k_{max}	D_{kmax} (°)	I_{kmax} (°)	ε_{12} (°)	ε_{13} (°)	ε_{23} (°)
Aleksandrovsk-Due	Gennoyshi	15	0.32690	45.7	63.0	0.33552	291.6	11.7	0.33758	196.4	23.9	6.4	5.4	6.5
Aleksandrovsk-Due	Krasnoyarkov	16	0.32873	191.1	85.6	0.33461	321.9	2.9	0.33666	52.0	3.3	9.5	3.3	3.9
Aleksandrovsk-Due	Upper Due	8	0.32963	318.0	78.4	0.33349	105.8	9.8	0.33688	196.8	6.1	6.4	4.6	7.9
Avgustovka	Gennoyshi	29	0.32682	322.9	80.5	0.33455	109.1	7.9	0.33862	199.8	5.2	8.2	5.3	6.0
Balshoya Orlovka	Upper Due	23	0.32349	210.3	79.4	0.33803	119.5	0.2	0.33848	29.4	10.6	67.2	4.4	5.9
Chamgu	Borsk	27	0.32882	15.7	81.5	0.33312	246.2	5.5	0.33807	155.5	6.6	7.5	5.6	9.9
Chamgu	Khuzin	51	0.33027	116.6	84.5	0.33463	248.6	3.7	0.33510	338.9	4.1	36.8	2.7	2.7
Dvoynoye	Lyukamen	17	0.32252	238.2	85.0	0.33811	28.3	4.4	0.33937	118.5	2.5	17.7	6.0	2.2
Il'inskiy	Kurasiy	43	0.32657	131.1	84.6	0.33566	230.0	0.8	0.33777	320.1	5.3	13.2	2.9	3.0
Kholmsk	Takaraday, Arakay, Kholmsk	32	0.33038	192.1	80.5	0.33450	30.5	9.0	0.33511	300.1	3.0	37.2	4.6	5.3
Kitosiya	Sinegorian Beds	11	0.32099	48.6	82.2	0.33853	260.5	6.7	0.34049	170.1	4.1	23.5	8.2	8.7
Kongi	Borsk	25	0.32479	171.7	85.2	0.33597	57.3	2.0	0.33924	327.1	4.4	9.2	5.0	4.0
Kormovaya	Kurasiy-Maruyama	38	0.33048	343.5	78.7	0.33406	84.3	2.1	0.33546	174.7	11.1	9.5	2.1	11.1
Korsakov	Kholmsk	18	0.32741	269.8	87.5	0.33552	152.8	1.1	0.33707	62.8	2.2	24.0	5.9	4.6
Malaya Orlovka	Nutovsk	20	0.33058	285.3	76.8	0.33416	74.1	11.4	0.33526	165.5	6.7	14.0	8.5	9.9
NE Schmidt	Toninsk	26	0.32680	190.9	74.7	0.33453	359.9	15.1	0.33867	90.7	2.8	9.9	4.6	5.5
North Aleksandrovsk	Sertunay, Okobykay	20	0.32923	149.1	82.7	0.33403	262.8	3.0	0.33674	353.1	6.7	12.7	6.3	11.3
Onnay	Arakay	18	0.32889	126.7	85.0	0.33453	303.2	5.0	0.33658	33.3	0.3	17.5	4.5	10.4
SE Schmidt	Pil'sk	32	0.33007	271.1	85.5	0.33464	24.2	1.7	0.33529	114.3	4.1	26.2	5.1	6.2
Shakhtnaya	Sertunay	26	0.32870	224.4	83.3	0.33472	77.2	5.7	0.33658	346.8	3.6	9.9	4.6	5.1
Tunaicha	Kholmsk	12	0.33000	210.6	71.4	0.33332	6.3	17.1	0.33668	98.5	7.2	6.7	7.7	11.3
Vladimirovka/Yar	Kholmsk	50	0.32480	239.7	83.4	0.33579	29.6	5.7	0.33941	119.9	3.3	10.3	2.6	5.1

ε_{12}, ε_{13}, and ε_{23} represent the 95% confidence semi-angles in the k_{max} - k_{int}, k_{max} - k_{min}, and k_{int} - k_{min} planes, respectively [*Jelinek*, 1978].

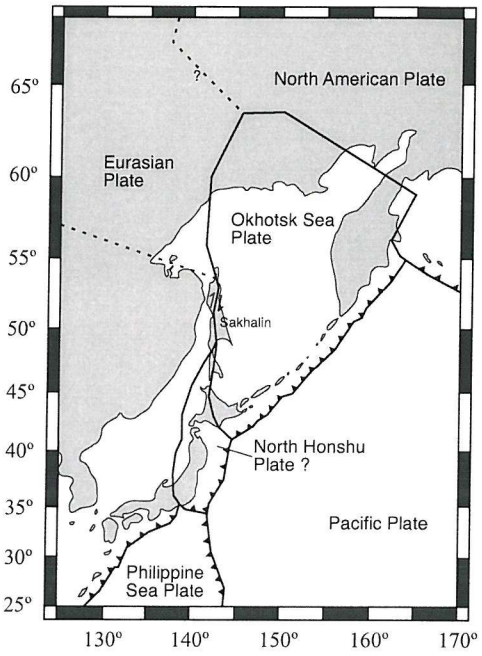

Figure 5.1. Plate configuration and location of Sakhalin in NE Asia. Modified after *Seno et al.* [1996] and *Takahashi et al.* [1999]. Dashed line indicates that the location of the plate boundary is uncertain.

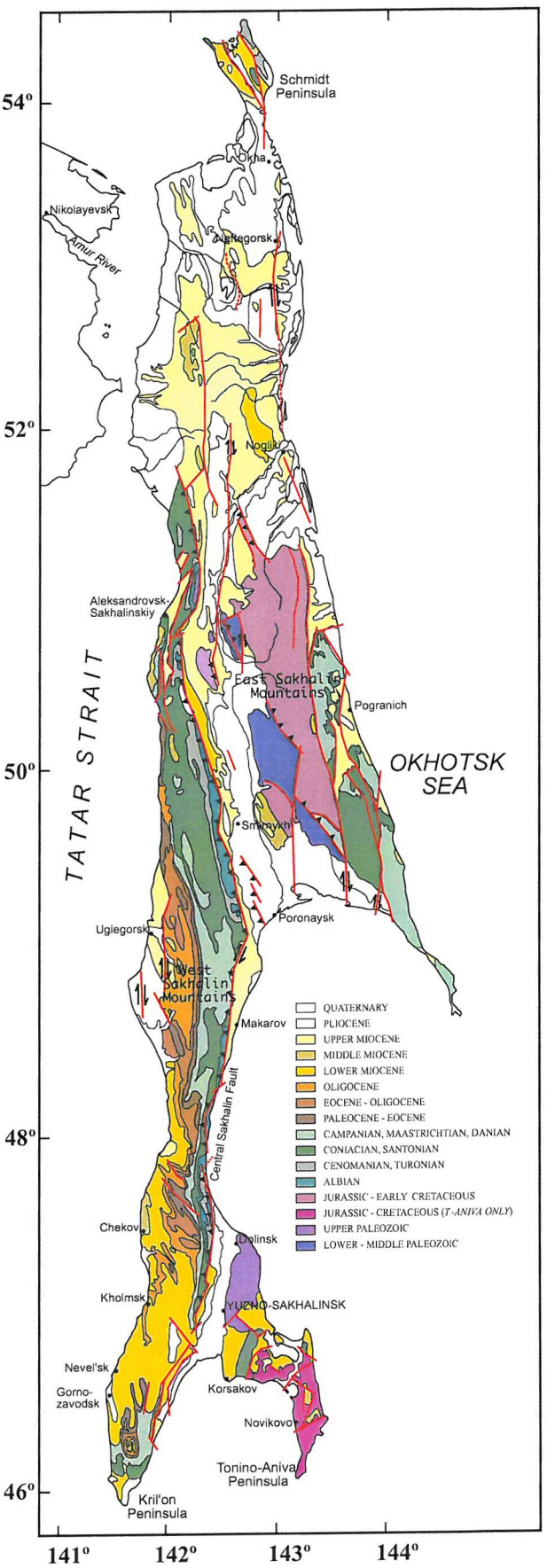

Figure 5.2. Geological map of Sakhalin. Compiled from various sources [*Vereshchagin,* 1969; *Rozhdestvenskiy,* 1982; *Kharakhinov,* 1983; *Fournier et al.,* 1994; *Ivashchenko et al.,* 1997].

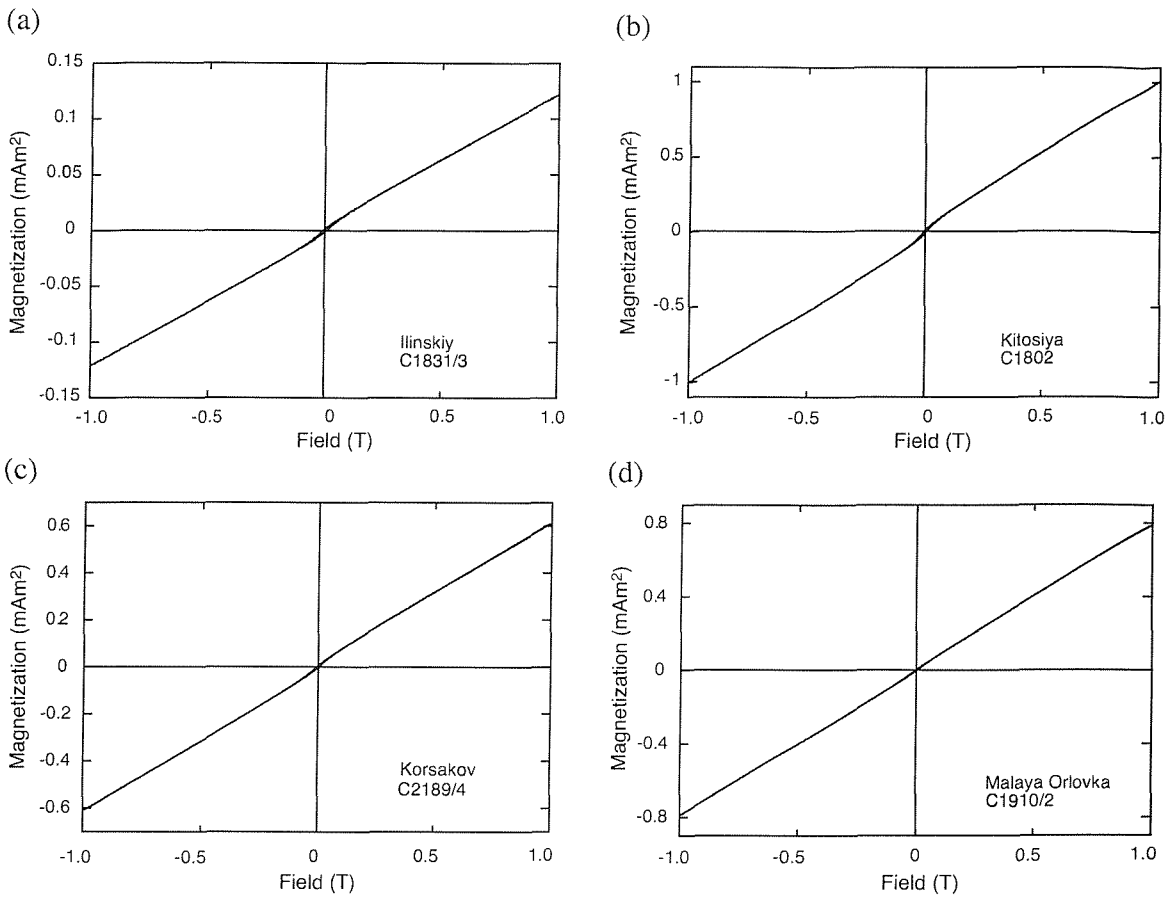

Figure 5.3. Hysteresis loops without paramagnetic slope correction indicate a significant fraction of paramagnetic grains for representative samples from Sakhalin. (a) Il'inskiy Coast (sample C1831/3). (b) Kitosiya River (sample C1802). (c) Korsakov (sample C2189/4). (d) Malaya Orlovka River (sample C1910/2).

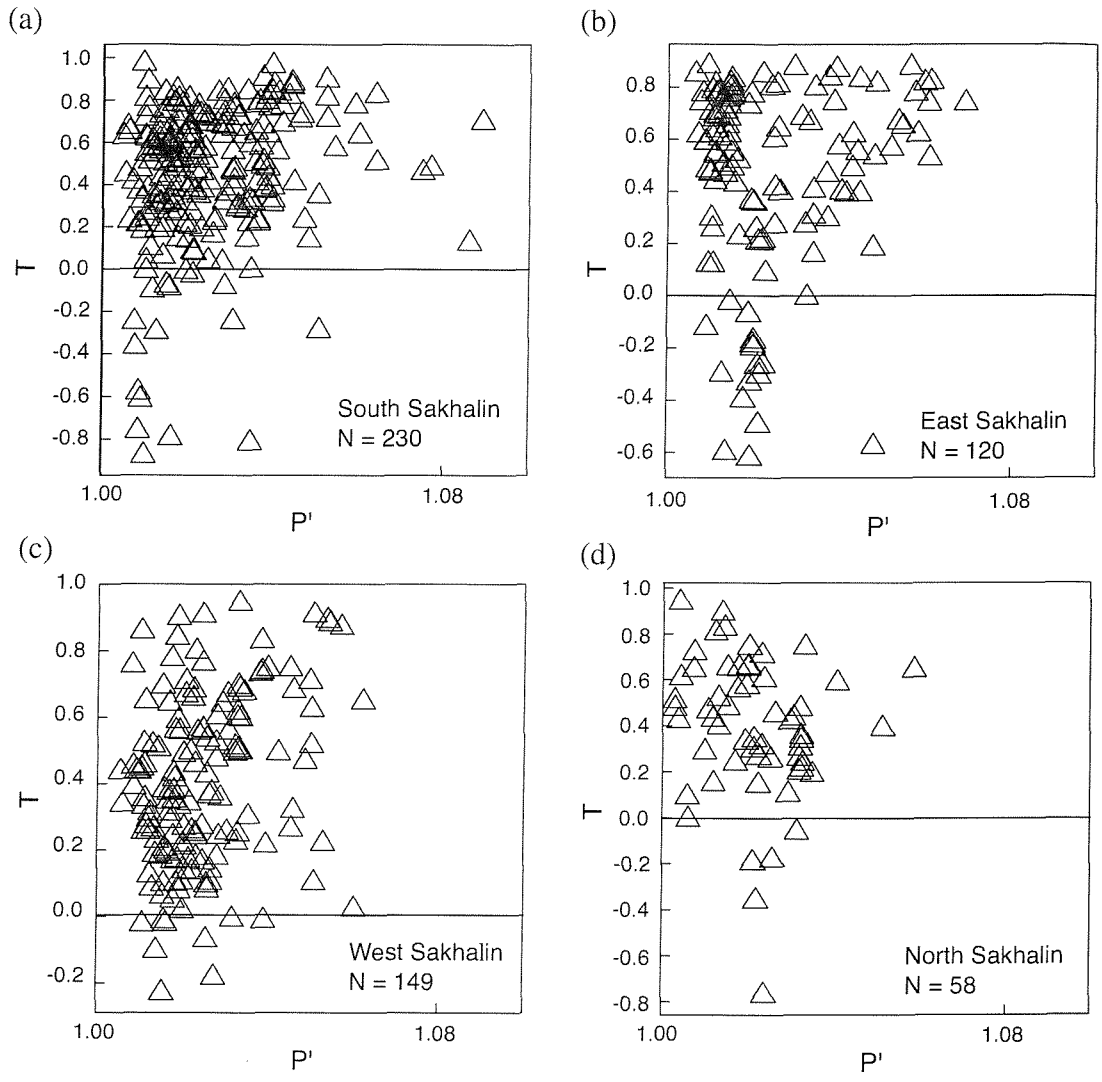

Figure 5.4. Anisotropy of magnetic susceptibility (AMS) plots for samples from Sakhalin [*Jelinek,* 1981]. *T* is the shape parameter of the AMS ellipsoid and ranges from –1 (prolate) to 0 (sphere) to +1 (oblate). *P'* is the corrected anisotropy degree which has values >+1 (sphere). (a) South Sakhalin, (b) East Sakhalin, (c) West Sakhalin, (d) North Sakhalin.

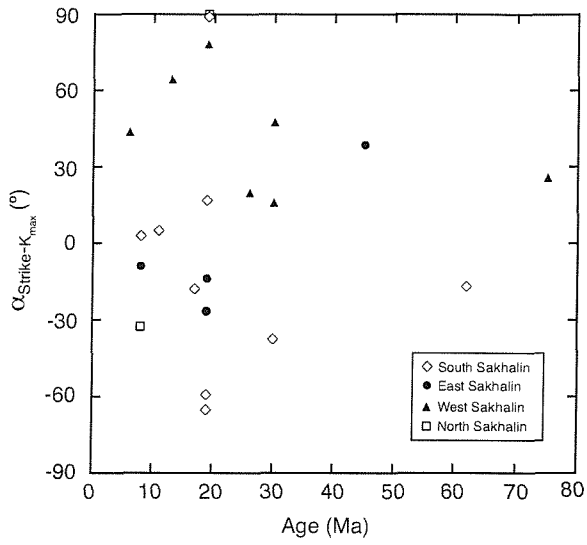

Figure 5.5. Dependence plot of k_{max} on the bedding strike versus age of the sampled sediments in Sakhalin. $\alpha_{strike-kmax}$ is the angle between the bedding strike and k_{max}. Intermediate angles of $\alpha_{strike-kmax}$ between 0° and 90° or between –90° and 0° suggest that neither the direction of k_{max} (the magnetic lineation) nor the direction of k_{int} is dependent on the strike of the bedding.

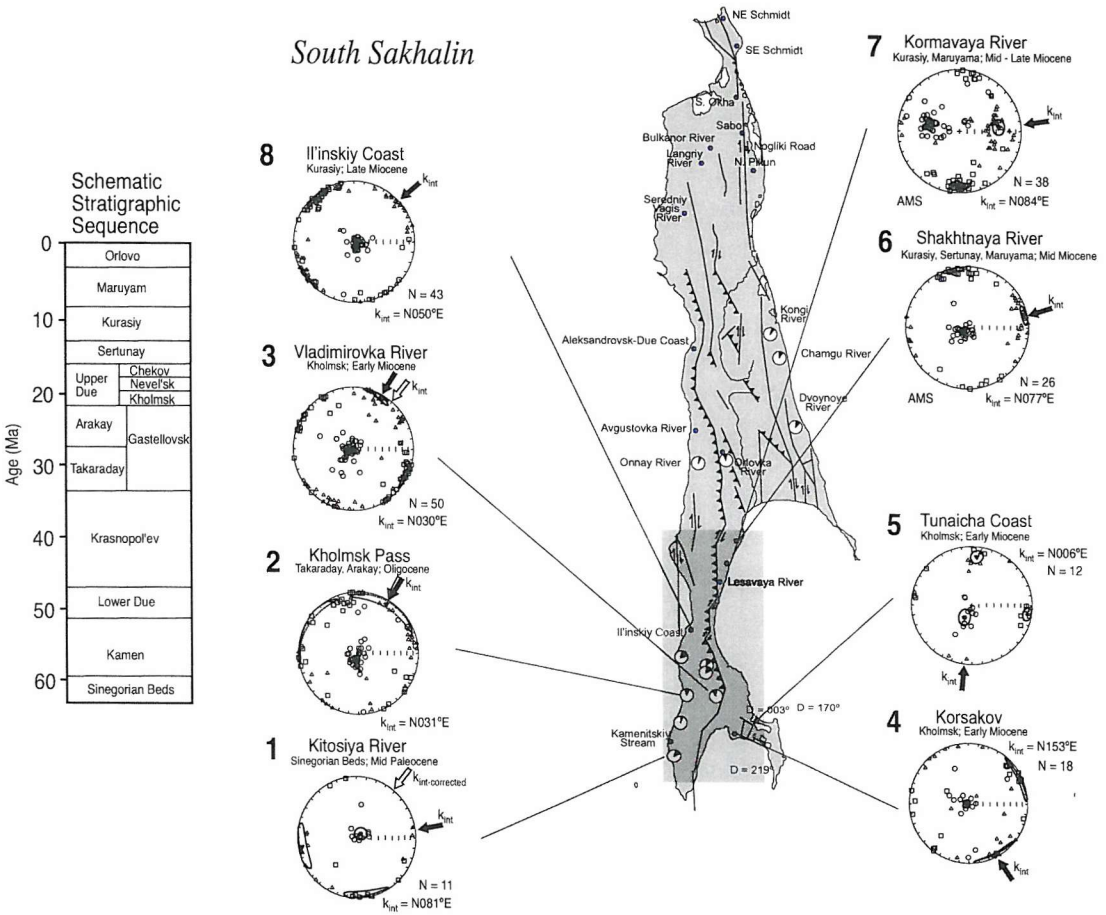

Figure 5.6. AMS fabrics from south Sakhalin. Solid arrows indicate the direction of k_{int} (uncorrected for vertical-axis rotation and perpendicular to lineation), which is the AMS-inferred direction of the net tectonic transport. White arrows indicate the transport direction determined from AMS data after correction for paleomagnetically determined vertical-axis rotations. Mean paleomagnetic declinations are indicated on the map for localities where reliable paleomagnetic data were obtained. Bold numbers indicate the age progression of the localities from 1-oldest to 8-youngest. k_{min} data points are indicated by circles, k_{int} data points are indicated by triangles, and k_{max} data points are indicated by squares.

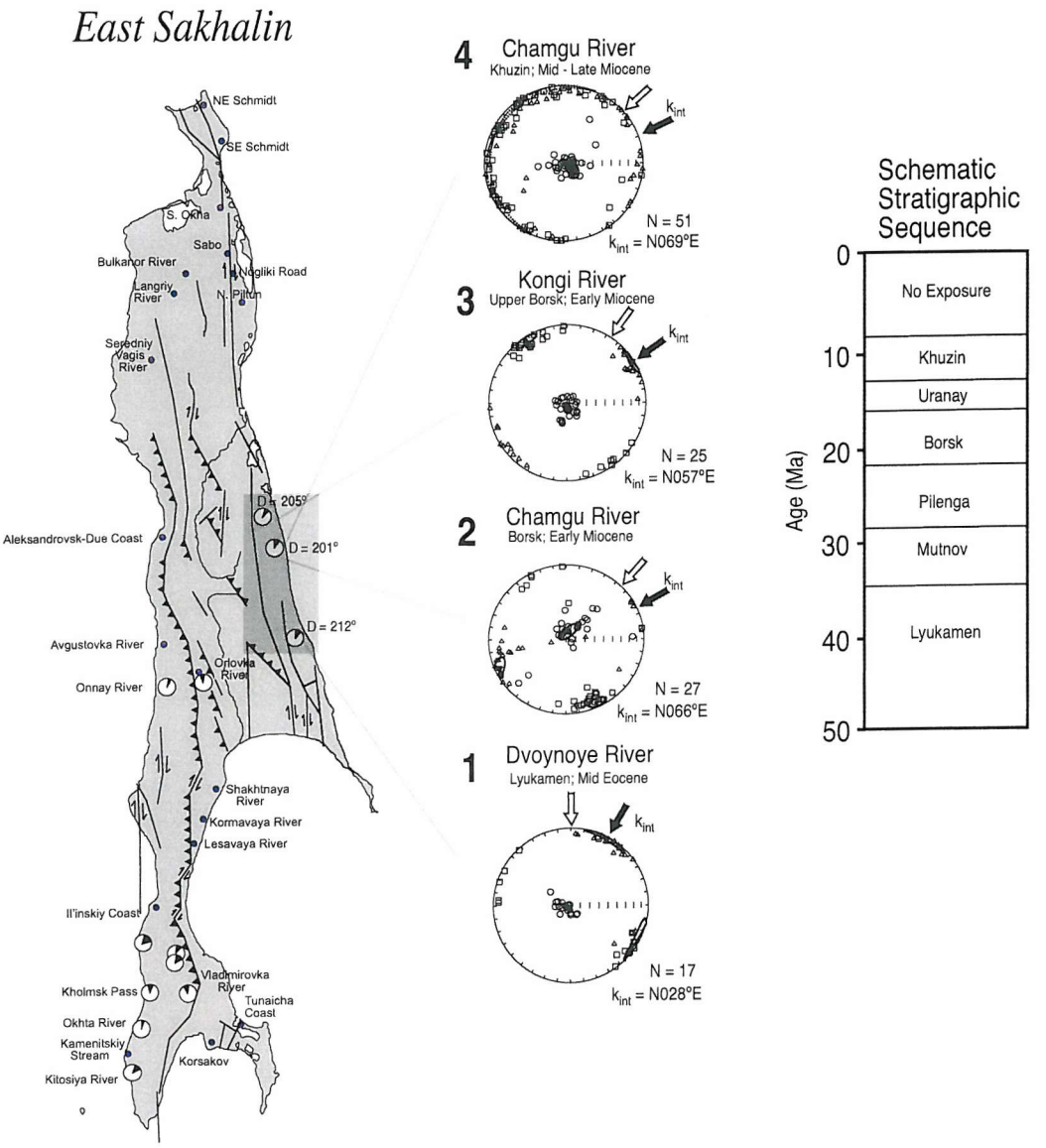

Figure 5.7. AMS fabric analyses from east Sakhalin. Conventions are the same as in Figure 5.6.

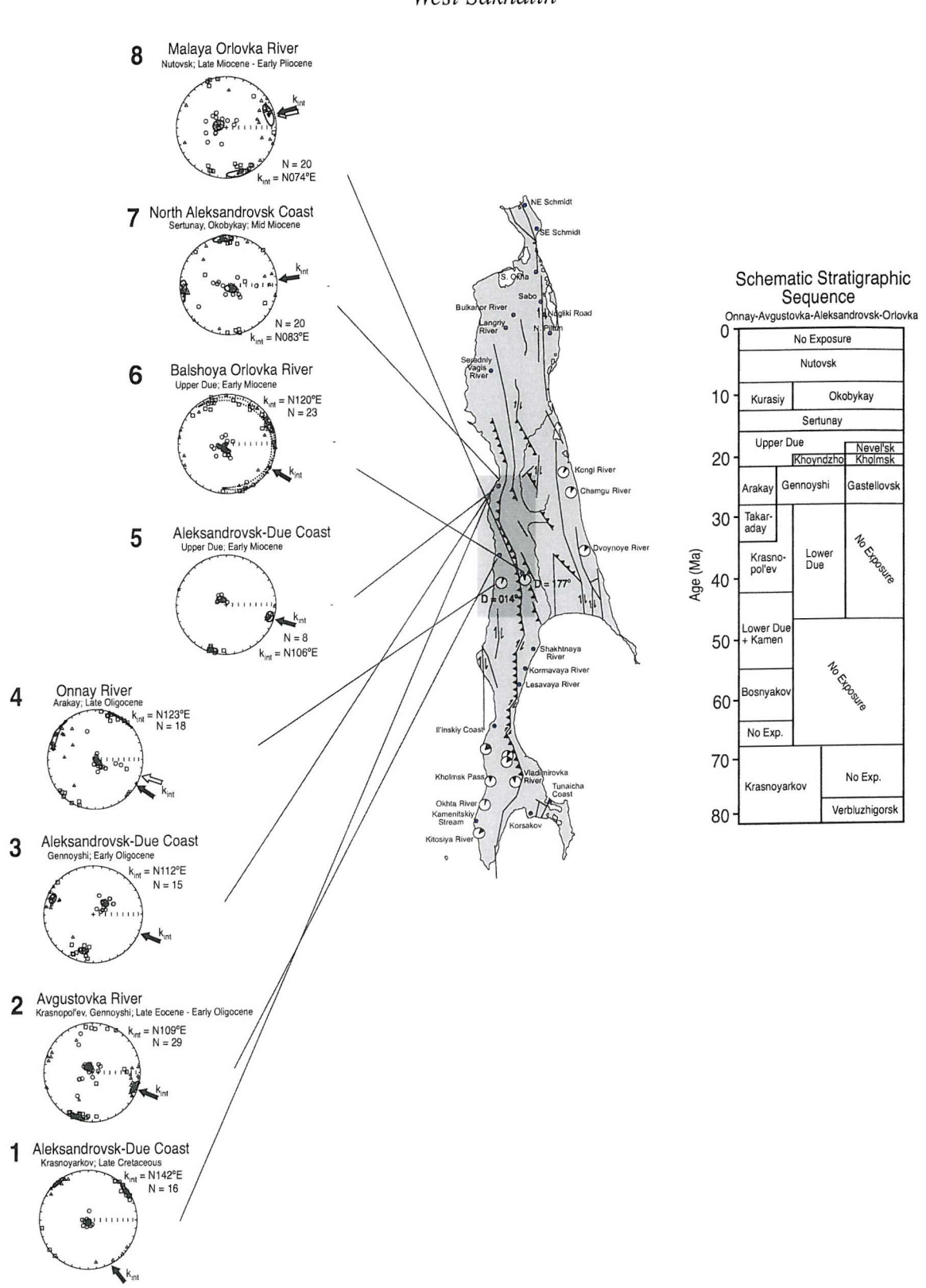

Figure 5.8. AMS fabric analyses from west Sakhalin. Conventions are the same as in Figure 5.6.

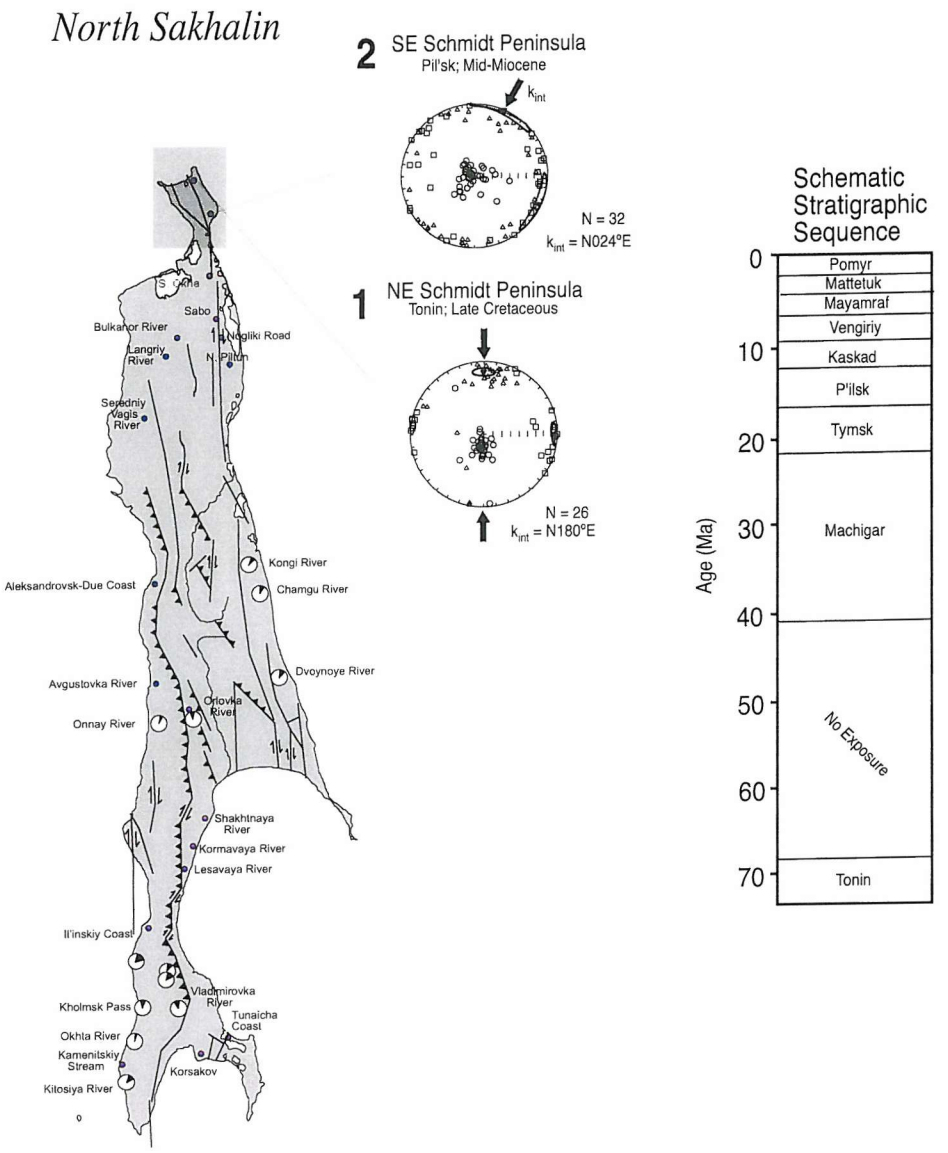

Figure 5.9. AMS fabric analyses from north Sakhalin. Conventions are the same as used in Figure 5.6.

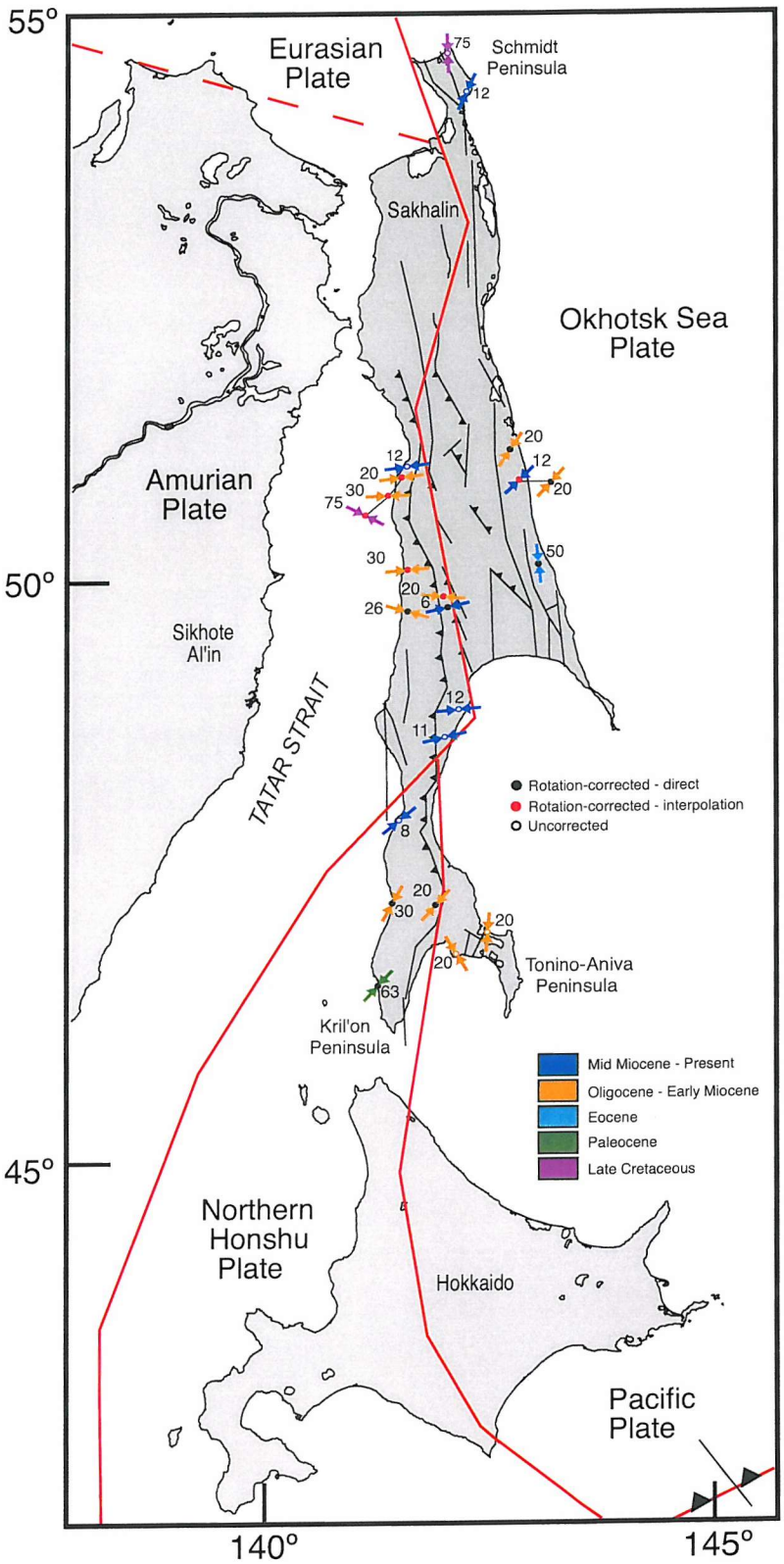

Figure 5.10. Interpretation of AMS fabric data from Sakhalin. Arrows indicate the direction of net.tectonic transport. Data are plotted after correction for paleomagnetically-determined vertical-axis rotations. Interpolated vertical-axis rotation corrections were applied at localities without directly useful paleomagnetic data. In west Sakhalin, 20° of regionally coherent clockwise vertical-axis rotation is assumed to have occurred in the early to mid-Miocene (see text). Present-day plate boundaries are derived from models proposed by *Seno* [1985], *DeMets* [1992a], *Seno et al.* [1996] and *Takahashi et al.* [1999].

6

A late diagenetic (synfolding) magnetization carried by pyrrhotite: Implications for paleomagnetic studies from magnetic iron sulphide-bearing sediments

This chapter appeared in *Earth and Planetary Science Letters*, Volume 200, Weaver, R., A. P. Roberts, and A. J. Barker, A late diagenetic (synfolding) magnetization carried by pyrrhotite: Implications for paleomagnetic studies from magnetic iron sulphide-bearing sediments, pages 371-386, Copyright (2002), with permission of Elsevier Science.

Abstract

Paleomagnetic, rock magnetic, and sedimentary micro-textural data from an early Miocene mudstone sequence exposed in Okhta River, Sakhalin, Russia, indicate the presence of pyrrhotite and magnetite at different stratigraphic levels. Sites that contain only magnetite have a reversed polarity characteristic remanent magnetization (ChRM) with a low-coercivity overprint, which coincides with the present-day geomagnetic field direction. Pyrrhotite-bearing sites have stable normal polarity ChRMs that are significantly different from the present-day field direction. After correction for bedding tilt, the ChRM data fail a reversals test. However, the normal polarity pyrrhotite ChRM directions become antipodal to the tilt-corrected magnetite ChRM directions and are consistent with the expected geocentric axial dipole field direction at the site latitude after 40% partial unfolding. These data suggest that the pyrrhotite magnetization was acquired during folding and after lock-in of the magnetite remanences. Electron microscope observations of polished sections indicate that fluid-associated halos surround iron sulphide nodules. Pyrrhotite is present in randomly oriented laths in and around the nodules, and the nodules do not appear to have been deformed by sediment compaction. This observation is consistent with a late diagenetic origin of pyrrhotite. Documentation of a late diagenetic magnetization in pyrrhotite-bearing sediments here, and in recent studies of greigite-bearing sediments, suggests that care should be taken to preclude a late origin of magnetic iron sulphides before using such sediments for geomagnetic studies where it is usually crucial to establish a syn-depositional magnetization.

5.1. Introduction

The ferrimagnetic iron sulphide minerals, greigite (Fe_3S_4) and monoclinic pyrrhotite (Fe_7S_8), have been reported to carry stable magnetizations in a variety of marine and lacustrine sedimentary environments [*Linssen,* 1988; *Snowball and Thompson,* 1990; *Kalcheva et al.,* 1990; *Tric et al.,* 1991; *Mary et al.,* 1993; *Roberts and*

Turner, 1993; *Hallam and Maher,* 1994; *Florindo and Sagnotti,* 1995; *Roberts et al.,* 1996; *Horng et al.,* 1998; *Richter et al.,* 1998; *Dinarès-Turell and Dekkers,* 1999]. Greigite forms under anoxic conditions, where bacterial sulphate reduction provides H_2S that reacts with detrital iron minerals to ultimately produce pyrite (FeS_2) [*Berner,* 1970, 1984]. In general, limited availability of sulphate is favourable for greigite formation, whereas higher concentrations of sulphate favour the production of the more stable pyrite [*Berner,* 1984; *Sweeney and Kaplan,* 1973; *Wilkin and Barnes,* 1997]. The formation of pyrrhotite in sediments is more unexpected because it is predicted to occur at pH > 11 [*Garrels and Christ,* 1965], which is beyond the range of values expected for sedimentary pore waters [*Stumm and Morgan,* 1981]. However, in the case of extremely low sulphur activity it is possible for pyrrhotite to form in sediments [*Garrels and Christ,* 1965]. Clear documentation of the presence of pyrrhotite in sediments suggests that this condition has sometimes been met [*Linssen,* 1988; *Mary et al.,* 1993; *Roberts and Turner,* 1993; *Horng et al.,* 1998; *Dinarès-Turell and Dekkers,* 1999]. Evidence of early diagenetic sulphidization reactions in reducing sedimentary environments has led to the conclusion, in many cases, that magnetic iron sulphide minerals formed during early burial and that they record a near-depositional chemical remanent magnetization (CRM) [*Linsen,* 1988; *Tric et al.,* 1991; *Mary et al.,* 1993; *Roberts and Turner,* 1993; *Hallam and Maher,* 1994].

In contrast to interpretations of early diagenetic pyrrhotite and greigite formation, several recent studies reveal the presence of contradictory magnetic polarities, even in adjacent samples, in sediments containing ferrimagnetic iron sulphide minerals [*Florindo and Sagnotti,* 1995; *Thompson and Cameron,* 1995; *Horng et al.,* 1998; *Richter et al.,* 1998; *Xu et al.,* 1998; *Dinarès-Turell and Dekkers,* 1999; *Jiang et al.,* 2001]. A recent study demonstrates that greigite may not always form as an early diagenetic precursor to pyrite; it can occur as a result of late diagenetic reactions [*Jiang et al.,* 2001]. Pyrrhotite has also recently been proposed as a late diagenetic phase in a model diagenetic pathway for the Trubi marls from Sicily [*Dinarès-Turell and Dekkers,* 1999], although the timing

of formation of the late diagenetic iron sulphide could not be established. In this study, we present results from Sakhalin, Russia, where the existence of pyrrhotite and the timing of pyrrhotite formation in a marine sedimentary sequence can be constrained by paleomagnetic and rock magnetic data as well as by sedimentary petrography. These results are discussed in terms of their implications for studies of geomagnetic field behaviour from sediments containing magnetic iron sulphide minerals.

6.2. Geological Setting

Sakhalin is located off the east coast of mainland Russia, north of Japan, on the western margin of the Okhotsk Sea (Figure 6.1). The west Sakhalin/Tatar Strait basin, which was originally a fore-arc basin between the Sikhote Al'in volcanic belt and the eastern Sakhalin accretionary complex [*Zyabrev and Bragin,* 1987; *Zonenshain et al.,* 1990; *Kimura,* 1994], contains a thick succession of shallow marine Cretaceous and Cenozoic sediments. Folding of these sequences occurred in response to right-lateral strike-slip deformation along the Central Sakhalin Fault (Figure 6.1) [*Rozhdestvenskiy,* 1982].

Paleomagnetic samples were taken from eight sites across a stratigraphic interval of ~70 m in an early Miocene sequence of marine mudstones of the lower Nevel'sk Suite for a study of regional tectonics [*Weaver et al.,* 2003]. The sampled sediments dip uniformly toward the west (21°W/182°) and are freshly exposed along Okhta River in southwest Sakhalin (Figure 6.1). The marine mudstones consist of feldspar-rich siliciclastic material with a composition and texture that indicates a provenance from local igneous sources [*Zonenshain et al.,* 1990]. The location of the sampled sequence is shown in Figure 6.1, along with a simplified stratigraphic column for southwest Sakhalin.

6.3. Methods

Oriented cylindrical paleomagnetic samples (10.8 cm^3) were collected in the field and the natural remanent magnetization (NRM) was measured using a 2G-Enterprises cryogenic magnetometer at the Southampton Oceanography Centre (SOC). Stepwise tumbling alternating field (AF) demagnetization was performed on the majority of samples using a Molspin AF demagnetizer because thermal demagnetization of pilot samples produced magnetic mineral alterations at elevated temperatures. For stably magnetized samples, AF and thermal demagnetization yielded similar results. AF demagnetization was preferred since the samples could be used for subsequent rock magnetic experiments. Characteristic remanent magnetization (ChRM) directions were identified from vector component diagrams using principal component analysis [*Kirschvink,* 1980]. ChRM directions were then analyzed using the statistics of *Fisher* [1953].

Low-temperature magnetic measurements were conducted to identify possible magnetic transitions, which are diagnostic of magnetic mineralogy [e.g., *Dekkers et al.,* 1989; *Rochette et al.,* 1990; *Moskowitz et al.,* 1993; *Roberts,* 1995b; *Housen et al.,* 1996; *Torii et al.,* 1996; *Moskowitz et al.,* 1998]. A Quantum Design Magnetic Properties Measurement System (MPMS-XL5) was used at the Institute for Rock Magnetism (IRM), Minnesota, U.S.A. Usually, three different measurement cycles were carried out for samples from each site. A zero-field-cooled (ZFC) cycle was applied first, where the samples were cooled from 300 K to 10 K in zero field. A saturation isothermal remanent magnetization (SIRM) was imparted using a 2.5 T field, which was switched off before measuring the SIRM at 5 K steps during warming back to 300 K. A field-cooled (FC) cycle was then applied, by cooling samples from 300 K to 10 K in a 2.5 T field. The field was then switched off at 10 K and the magnetization measured at 5 K intervals during warming back to 300 K. A room temperature SIRM (RT-SIRM) cycle was applied third, by imparting a 2.5 T SIRM at 300 K before switching off the field and measuring the magnetization at 5 K steps during cooling to 20 K and during warming back to 300 K.

Magnetic hysteresis loops and first-order reversal curve (FORC) diagrams [*Roberts et al.,* 2000] were acquired to assess the coercivity distributions of the magnetic assemblages in the samples. Measurements were made using a Princeton Measurements Corporation vibrating sample magnetometer (VSM) at the IRM, with maximum applied fields of 1 T. Measured hysteresis parameters include: M_r (saturation remanence), M_s (saturation magnetization), H_c (coercive force), and H_{cr} (coercivity of remanence). The instrument is sufficiently sensitive to enable acquisition of high quality data from relatively weakly magnetic bulk samples (sensitivity = 10^{-9} Am^2).

High-temperature magnetic behaviour was investigated using a variable field translation balance (VFTB) at the SOC. An applied field of 76 mT was used and the magnetization was measured during heating at 10°C/minute from room temperature to 700°C and during cooling back to room temperature. Measurements were all carried out in air because iron sulphides are thermally unstable and use of inert atmospheres can give rise to variable rates of thermal alteration and less diagnostic thermomagnetic behaviour [*Reynolds et al.,* 1994]. Thermal demagnetization of 3-axis IRMs [*Lowrie,* 1990] was carried out to determine the magnetic minerals in different coercivity components. Fields of 0.9 T, 0.3 T, and 0.12 T were applied to representative samples, along the *x*, *y*, and *z* axes, respectively.

Sediment micro-textures were studied in polished thin sections from representative samples using a LEO 1450VP scanning electron microscope (SEM) operated at 15 keV at the SOC. Elemental analyses were obtained from energy-dispersive X-ray spectra (EDS) generated from point analyses (2-3 μm beam diameter) of individual mineral grains, using a Princeton Gamma Tech (IMIX-PTS) system. X-ray diffraction (XRD) patterns were obtained using a Philips X-ray diffractometer (CoKα radiation) at the SOC to identify minerals.

6.4. Results

6.4.1. Rock Magnetism

Of the eight sites sampled at the Okhta River section, one is unstably magnetized, three are dominated by magnetite, three are dominated by pyrrhotite, and one has magnetic properties consistent with a mixture of magnetite and pyrrhotite (Table 6.1). In the following discussion, we present results from each of these groups in turn.

Vector-component diagrams from sites C2500-C2502 reveal a two-component NRM after AF demagnetization (Figure 6.2a,b). The low-coercivity magnetic component (0-20 mT) has normal polarity. A ChRM component with reversed polarity is present between 25 and 60 mT. The demagnetization trajectory suggests minimal overlap of the two components. The same ChRM component appears in thermally demagnetized samples, although the data are noisier (Figure 6.2b). The NRM is almost removed at 550°C, which suggests that low-titanium magnetite is present (Figure 6.2b). Low-temperature thermomagnetic curves contain evidence of a weak Verwey transition at ~120 K, as suggested by a small peak in the plot of the derivative of the magnetic moment with respect to temperature, which confirms the presence of magnetite (Figure 6.2c). The weak nature of the transition may result from surficial oxidation of the magnetite [*Özdemir et al.,* 1993]. Magnetic hysteresis parameters were determined for a bulk sediment sample (Figure 6.2d) and FORC diagrams have contours that close around a peak at H_c = 28 mT with little vertical spread of the contours (Figure 6.2e). This coercivity value is consistent with the presence of SD magnetite and lack of vertical spread of the contours suggests that interactions among magnetite particles is negligible [*Roberts et al.,* 2000]. Divergent contours that intersect the H_u axis indicate a fraction of multi-domain (MD) or pseudo single-domain (PSD) grains. An additional small peak around the origin of the FORC diagram indicates that superparamagnetic (SP) grains are present [*Roberts et al.,* 2000; *Pike et al.,* 2001]. Considered together, the rock magnetic evidence suggests that non-interacting magnetite, with a broad distribution of grain sizes, is the main magnetic mineral at these sites.

Contrasting rock magnetic characteristics are observed for sites C1876-C1878, which are situated higher in the sedimentary sequence than sites C2500-C2502 (Figure 6.1). Vector component diagrams typically display a single normal polarity remanence component, which appears to be stable at AFs up to 80 mT (Figure 6.3a). Thermal demagnetization indicates rapid thermal decay of the same component up to around 280°C, where thermal alteration starts to occur (Figure 6.3b). Low-temperature magnetic transitions are not clearly evident in the ZFC, FC, or RT-SIRM curves, although there is a small anomaly in the derivative of magnetization with respect to temperature and a separation of the ZFC and FC curves at around 30-40 K for samples from site C1878 (Figure 6.3c). The magnetic ordering temperature for siderite ($FeCO_3$) at 38 K [*Housen et al.,* 1996] and a magnetic transition for pyrrhotite (34 K) are known to occur in this temperature range [*Dekkers et al.,* 1989; *Rochette et al.,* 1990], so this anomaly is not necessarily indicative of the presence of pyrrhotite. However, observed coercivity of remanence values of 68.4 mT (Figure 6.3d), are similar to those reported for ferrimagnetic iron sulphides such as greigite or pyrrhotite [*Dekkers,* 1988; *Rochette et al.,* 1990; *Snowball,* 1991; *Roberts,* 1995b; *Horng et al.,* 1998; *Sagnotti and Winkler,* 1999]. FORC diagrams suggest that high-coercivity ($H_c \approx 60$ mT) single-domain (SD) particles are present with relatively strong magnetic interactions between particles (Figure 6.3e) [*Roberts et al.,* 2000]. High-temperature measurements conducted on strongly magnetic iron sulphide nodules that were manually extracted from the bulk sediment undergo a steep drop in magnetization between 150°C and 300°C, with thermal alteration to form magnetite above 400°C (Figure 6.3f). The heating curve decreases sharply at ~320°C, which likely indicates the presence of monoclinic pyrrhotite (T_c = 320°C), before falling to near-zero magnetizations at 350°C (Figure 6.3f). Mineral alteration at higher temperatures probably results from trace amounts of clay minerals or pyrite altering to form magnetite [e.g., *Linssen,* 1988; *Dekkers,* 1990; *Horng et al.,* 1998; *Dinarès-Turell and Dekkers,* 1999; *Sagnotti and Winkler,* 1999]. Thermal demagnetization of a 3-axis IRM indicates a sharp decrease of magnetizaton between

140°C and 300°C for all three components before reaching near-zero values at ~340°C (Figure 6.3g). The maximum unblocking temperature and range of coercivities suggest that monoclinic pyrrhotite is present [*Lowrie,* 1990]. Finally, XRD data from an iron sulphide nodule sample, analyzed prior to heating, contain strong pyrrhotite (Po) peaks (Figure 6.3h). Additional peaks for pyrite (P), quartz (Q), clays (C), and feldspar (F) are identified. There is no evidence for magnetite or greigite at these sites.

Higher in the studied sequence, a relatively soft magnetization component (<50 mT) is isolated with a stable ChRM direction similar to the pyrrhotite-bearing sites described above (Figure 6.4a). ZFC and FC curves separate at 30-40 K (Figure 6.4b) and there is a small anomaly in the derivative, which suggests that pyrrhotite may be present [*Dekkers et al.,* 1989; *Rochette et al.,* 1990]. Hysteresis loops from bulk samples yield coercivities that are intermediate between the magnetite- and pyrrhotite-bearing sites (Figure 6.4c). The nature of the magnetic mineral assemblage is more clearly apparent in FORC diagrams (Figure 6.4d), where contours close around a SD peak at H_c = 25-30 mT, with a small SP peak about the origin of the plot similar to that for the magnetite-bearing sample at site C2500 (Figure 6.2e). Comparison of the FORC diagrams in Figures 6.2e and 6.4d highlights some important differences. Equivalent contours extend to higher coercivities (e.g., 70 mT compared to 60 mT) and the vertical spread is somewhat greater in Figure 5.4d. Both observations suggest that a magnetic mineral in addition to a broad range of magnetite grain sizes exists at this site. The high-temperature magnetization of the bulk sediment is characterized by a steep decrease between 300°C and 400°C and alteration to form magnetite occurs above 400°C (Figure 6.4e), which is typical of iron sulphide-bearing sediments [*Roberts,* 1995b; *Dekkers,* 1990]. The hard IRM component reduces to zero at around 300°C, while thermal demagnetization of the intermediate and soft IRM components indicates a steep decrease between 160 and 340°C before decaying more slowly to zero at 550-600°C (Figure 6.4f). FORC distributions that are smeared towards higher coercivities, sharp decreases in magnetization at around 300-400°C, interactions between magnetic particles, and

persistence of a magnetic component up to 580°C, suggest a mixed magnetic mineral assemblage where magnetite and pyrrhotite coexist. The ChRM is probably carried by pyrrhotite (because of directional agreement with other pyrrhotite-bearing sites as described below). As is the case for the magnetite-only sites, the magnetite is likely to be present in a wide range of sizes from SP to MD sizes. The presence of a MD magnetite fraction could also explain the lack of a clear separation between ZFC and FC curves at temperatures below 120 K [*Moskowitz et al.*, 1993].

The stratigraphic relationship between the analyzed sites is shown in Figure 6.1, with a summary of the magnetic minerals identified at each site. Hysteresis ratios from each site are plotted in Figure 6.5. Samples containing pyrrhotite yield mostly SD-like data ($M_r/M_s > 0.5$, $H_{cr}/H_c \approx 1.5$), while magnetite-bearing samples tend towards values of $M_r/M_s \approx 0.2$ and $H_{cr}/H_c \approx 2.5$-3.0. Data from samples with a mixed magnetic mineral assemblage plot along a mixing line between the magnetite and pyrrhotite end-members (Figure 6.5). This is consistent with the rock magnetic observations described above.

6.4.2. Paleomagnetism

Analysis of paleomagnetic directions was carried out before and after correction for bedding tilt. Normal polarity directions are associated with samples containing pyrrhotite (Figure 6.3a,b) and stable reversed polarity ChRM directions are found in samples containing magnetite (Figure 6.2a,b). In pre-tilt (*in situ*) coordinates, the mean direction for the magnetite-only samples is: $D = 215.4°$, $I = -59.9°$, with $\alpha_{95} = 5.8°$ (Table 6.1). The mean *in situ* direction for the pyrrhotite-bearing samples is: $D = 26.2°$, $I = 67.9°$, with $\alpha_{95} = 3.7°$ (Figure 6.6a; Table 6.1). Low-coercivity magnetic overprints, identified in all of the magnetite-bearing samples and in some of the mixed pyrrhotite + magnetite samples, have a mean pre-tilt direction of: $D = 348.5°$, $I = 70.0°$, with $\alpha_{95} = 7.2°$ (Figure 6.6b; Table 6.1). This direction is similar to the present-day field direction at the locality (IGRF, $D = 349.5°$, $I = 61.2°$ [*Tauxe*, 1998]). After applying a full tilt correction (21°W/182°) to the ChRM data, the mean directions for each group are not

antipodal and therefore fail a reversals test [*Tauxe,* 1998]. Pyrrhotite-bearing samples plot about a mean of: D = 333.4°, I = 65.7°, with α_{95} = 3.1° (Table 6.1). The magnetite samples are indistinguishable from the expected geocentric axial dipole (GAD) direction for a Miocene reversed polarity field at the site latitude [*Weaver et al.,* 2003]: D = 179.7°, I = -66.2°, with α_{95} = 4.0° (Figure 6.6c; Table 6.1). The normal polarity paleomagnetic data from the pyrrhotite-bearing samples are neither consistent with an expected GAD direction nor with the present-day field direction. The pyrrhotite data only become antipodal to the fully corrected magnetite direction at 40% untilting. After this partial unfolding, the pyrrhotite directions align with the expected GAD field direction, with: D = 358.7°, I = 68.0°, and α_{95} = 3.1° (Figure 6.6d; Table 6.1).

6.4.3. Electron Microscopy

Polished thin sections from samples containing pyrrhotite, magnetite and mixtures of both minerals were analyzed using a SEM with EDS. Ferrimagnetic iron sulphides are usually associated with pyrite in sediments deposited under anoxic conditions [*Sweeney and Kaplan,* 1973; *Berner,* 1984]. Pyrite and pyrrhotite can be distinguished under the SEM because pyrrhotite has a greater molecular mass and should therefore appear brighter than pyrite in backscattered electron images. In addition, EDS spectra indicate a significantly larger difference between iron and sulphur peaks for pyrite than for pyrrhotite (Figure 6.7a,b).

Pyrite is abundant in all samples. It is most easily identified in polished sections as round framboids that consist of aggregates of small crystals. Isolated pyrite framboids occur in the sediment matrix, but usually they appear in clusters (Figure 6.7c,d). The larger framboids are about 10 μm in diameter. In pyrrhotite-bearing samples, clustered pyrite framboids are usually separated from each other (Figure 6.7c). Pyrrhotite sometimes occurs as growths into micro-cracks in the matrix, often in the vicinity of pyrite framboid aggregates (Figure 6.7c). In magnetite-only samples, the interstices

between framboids are filled with aggregates of pyrite crystals (Figure 6.7d); no magnetic iron sulphides were observed.

The main mode of occurrence of pyrrhotite in the pyrrhotite-bearing samples is in iron sulphide nodules. These nodules (up to about 2 mm) have variable shape and occur with distinctive halos surrounding them (Figure 6.7e). At higher magnifications, the nodules have a fibrous or spiky exterior surface, comprising a dense mass of randomly oriented fine acicular laths (Figure 6.7f). SEM-EDS analyses consistently indicate a pyrrhotite composition, which corroborate XRD analyses on the same nodules (Figure 6.3h). Similar fibrous laths have been reported for other occurrences of pyrrhotite in sediments [*Reynolds et al.,* 1993; *Dinarès-Turell and Dekkers,* 1999]. In addition, pyrite is found in the nodules, but it tends to occur as larger grains in contrast to its framboidal appearance elsewhere in the sediment matrix.

Nodular masses of pyrrhotite laths and pyrite seem to occur in variable contexts (Figure 6.8a,b). In one case, pyrite can be identified as tightly clustered laths along the edge of a large feldspar crystal. They are oriented at a high angle to the feldspar surface and extend up to 15 μm from this surface. There is an apparent boundary in the matrix, beyond which the needles consist of pyrrhotite. The pyrrhotite crystals appear to be randomly oriented and become progressively less dense with distance from the feldspar crystal edge (Figure 6.8a).

In another case, pyrite and acicular pyrrhotite are found around the edges, and in patches within a mass of silica (Figure 6.8b). Pyrite is also found as a smooth tabular area toward the edge of the silica mass, whereas pyrrhotite occurs as a mesh of interlocking needles and also along the (001) cleavage of mica grains in peripheral regions of the silica mass (Figure 6.8c).

Fine magnetite particles are not evident in the nodular pyrrhotite-bearing samples. In the magnetite-bearing samples, magnetite particles are difficult to detect because of their small (sub-micron) size. In the sample containing pyrrhotite and magnetite, the magnetite occurs as small interstitial grains between feldspar crystals within felsic

volcanic clasts (Figure 6.8d). Small amounts of titanium are usually present in the magnetite (Figure 6.8e).

6.5. Discussion

6.5.1. Paleomagnetic Evidence for a Synfolding Magnetization in Pyrrhotite

Tectonically corrected ChRM data from sites with normal polarity (pyrrhotite samples) and reversed polarity (magnetite-only samples) have mean directions that are not antipodal and the data consequently fail a reversals test (Figure 5.6c). The mean declination of the normal polarity overprints is in good agreement with the present-day field direction (IGRF, $D = 349.5°$, $I = 61.2°$ [*Tauxe,* 1998]), although the inclination of the overprint is steeper than the IGRF direction. The directional precision of the overprint may have been affected by the later exposure of samples to laboratory fields. The overprint (Figure 6.6b) is probably a viscous remanent magnetization that resides in fine magnetite particles near the SP/SD grain-size boundary, as indicated by the presence of a secondary peak near the origin of FORC diagrams (Figure 6.2e, 6.4d). The pre-tilt corrected normal polarity pyrrhotite component has a direction that is different from the overprint, with a clockwise-deflected declination of 26.2° (Figure 6.6a). Clearly, the normal polarity ChRM associated with pyrrhotite cannot have originated from remagnetization in the present-day field. When data from magnetite-bearing sites are corrected for stratal tilt, a reversed polarity direction that is consistent with a GAD field at the site latitude is obtained (Figure 6.6c). It is therefore clear that the pyrrhotite ChRM data are anomalous: they neither record a prefolding GAD direction nor a post-folding present-day field direction. Differential unfolding of data from the two groups of sites, with the magnetite data fully unfolded and the pyrrhotite data subjected to 40% unfolding, reveals antipodal directions (Figure 6.6d). The resultant mean directions are consistent with the expected time-averaged GAD field for the site latitude ($D = 0°$, $I = 65°$) [*Weaver et al.,* 2003]. The data suggest that a CRM has been acquired by the

pyrrhotite, which post-dates the magnetite ChRM directions, and which appears to be a synfolding magnetization.

6.5.2. Micro-Textural Evidence for the Timing of Nodular Iron Sulphide Formation

Different textures of iron sulphides in the Okhta River samples give clues about the timing of their formation. Groups of pyrite framboids with clear spaces between them suggest a relatively early stage of formation [c.f. *Wilkin and Barnes,* 1997]. Groups of pyrite framboids are found in all of the studied sites (Figure 6.7c,d). In the magnetite-bearing sediments, interstitial voids are filled by polyframboidal pyrite aggregates (Figure 6.7d) [*Love,* 1971]. This process requires abundant sulphate for ongoing pyritization. No ferrimagnetic iron sulphides are evident in the magnetite-bearing samples. Thus, although the magnetite-bearing site has clearly undergone early diagenetic sulphidization, these reactions have neither led to the complete dissolution of magnetite nor to the preservation of magnetic iron sulphides.

While early diagenetic pyrite framboids are ubiquitous in all of the sites analyzed here, late diagenetic magnetizations are only observed in samples containing iron sulphide nodules (Figures 6.7e,f, 6.8). Non-framboidal pyrite crystals are present within these nodules (Figure 6.8a,b). The nodules, which dominantly consist of acicular pyrrhotite laths, are well-defined within the sediment matrix (Figure 6.7e) and do not display any preferred orientation. The morphology of the non-framboidal elongate pyrite is similar to the pyrrhotite (Figure 6.8a), which suggests that pyrite has locally replaced pyrrhotite. Furthermore, the acicular pyrrhotite crystals appear to have random orientations and do not show any signs of deformation around the edges of nodules due to sediment compaction. These observations suggest that the nodules formed after sediment compaction [*Sellés-Martínez,* 1996].

Fluid flow is likely to be associated with the formation of the nodules. The nodules usually have halos around them which define regions where diagenetic fluid/mineral interactions may have taken place (Figures 6.7e, 6.8a,b). This is

particularly apparent in Figure 6.8a, where a small iron sulphide nodule is asymmetrically developed on one side of a feldspar grain. The morphology of the feldspar crystal appears to have controlled the nodule shape and the distribution of iron sulphides, which would be possible by restricting or deviating a sulphidic fluid around it. It is conceivable that the feldspar crystal provided an impermeable barrier to the fluid which was forced to flow around the grain, and that the fluid migrated down a localized fluid pressure gradient caused by a dilating micro-crack at the feldspar-matrix interface. Pyrrhotite then nucleated on the feldspar surface to form lath-like or acicular crystals, later to be replaced by pyrite (Figure 6.8a). Since these crystals are at a high angle to the feldspar surface, it suggests face-controlled growth into a dilating micro-crack rather than growth by replacement. Less sulphidic fluid appears to have permeated further to the right of the boundary, to produce acicular pyrrhotite crystals in the adjacent matrix. A halo has formed to the right of the feldspar crystal and seems to mark the limits of possible sulphidic fluid migration and the associated distribution of pyrrhotite. Another nodule has silica in its core and within the alteration halo below the nodule (Figure 6.8b). The nodule is dominated by pyrrhotite laths toward the outside, with some larger pyrite crystals toward the centre. In the cases shown in Figure 6.8a,b, there are chemical iron sulphide gradients associated with the nodules, which may be linked with fluid flow. The halo textures seem to be diagnostic of the presence of a diagenetic fluid and it seems that differences in chemical gradients for iron and sulphur have resulted in different iron sulphide products (pyrite or pyrrhotite), which have a determining control on the magnetization of the sediment.

The overall micro-textural evidence from pyrrhotite nodules (especially randomly oriented laths) suggests a late diagenetic formation that post-dates sediment compaction. All of the samples that contain pyrrhotite, as indicated by rock magnetic and XRD analyses, also contain nodules that can be identified in hand specimen and using SEM observations. Magnetostatic interactions between particles, as suggested by the vertical

spread in FORC distributions (Figure 6.3e), are consistent with microscopic evidence for the closely intergrown nature of the pyrrhotite laths in the iron sulphide nodules.

At site C1879, where magnetite and pyrrhotite co-exist (Figure 6.1; Table 6.1), magnetite occurs as abundant submicron interstitial grains within (>40 μm) clasts of felsic volcanic rock (Figure 6.8d), which are relatively common in samples from this site. They appear to be randomly oriented, which probably explains why the magnetite does not appear to be paleomagnetically significant at this site and why the ChRM is dominated by pyrrhotite.

6.5.3. Implications for Paleomagnetism

Chemical remagnetization of sediments associated with late diagenetic iron sulphide minerals is being increasingly documented [*Reynolds et al.,* 1994; *Thompson and Cameron,* 1995; *Florindo and Sagnotti,* 1995; *Horng et al.,* 1998; *Richter et al.,* 1998; *Dinarès-Turell and Dekkers,* 1999; *Xu et al.,* 1998; *Jiang et al.,* 2001]. Our data suggest that the magnetization in the studied sediments was acquired during folding and that a tectonically-driven fluid migration event has altered the redox conditions to enable late diagenetic growth of pyrrhotite. Tightly-clustered remanence directions from the pyrrhotite-bearing sites suggests that the pyrrhotite formed within a relatively short period of time, which is consistent with a CRM due to a fluid-activated event of limited duration. It is only possible to speculate about the source of fluid that allowed the chemical reaction to occur. Late diagenetic magnetizations carried by iron sulphide minerals could be linked to numerous processes including the migration of hydrocarbons, gas hydrates, hydrothermal fluids, or release of trapped pore waters [*Machel and Burton,* 1991; *Reynolds et al.,* 1991; *Housen and Musgrave,* 1996; *Urbat et al.,* 2000]. Alternatively, slow reactions in sulphate-limited environments might enable late diagenetic formation of magnetic iron sulphide phases [*Jiang et al.,* 2001]. Climatic or regional tectonic forcing can also alter the redox conditions in sedimentary basins, which may allow authigenic iron sulphides to form. It is clear that great care is needed to assess

the origin of the magnetic remanence in order to establish a reliable timing for magnetizations carried by magnetic iron sulphide minerals.

Late diagenetic (synfolding) acquisition of a CRM in pyrrhotite has been demonstrated in this study and suggests that the assumption of early diagenetic remanence acquisition in magnetic iron sulphide-bearing sediments may not be appropriate for studies of short-term geomagnetic field behaviour such as secular variation or geomagnetic polarity transitions [e.g., *Linssen,* 1988; *Tric et al.,* 1991]. In addition to fine-scale field behaviour, the magnetic polarity record of a sedimentary sequence can be compromised by late CRM acquisition, as has recently been documented in several cases [*Florindo and Sagnotti,* 1995; *Thompson and Cameron,* 1995; *Horng et al.,* 1998; *Richter et al.,* 1998; *Dinarès-Turell and Dekkers,* 1999]. It should be noted, however, that in one case where greigite and pyrrhotite are both present, the greigite usually carried a late diagenetic signal whereas the pyrrhotite carried a syn-depositional signal [*Horng et al.,* 1998].

Depending on the timing of remanence acquisition, an iron sulphide CRM could also be difficult to interpret in tectonic studies. In cases where there have been multiple phases of deformation, lack of knowledge of the exact timing of remanence acquisition could prove particularly confusing. In particular, careful consideration should be given to the formation processes of the magnetic iron sulphide to ensure that geomagnetic secular variation can be properly averaged. Field tests are of paramount importance to evaluate whether a magnetic iron sulphide carries a primary CRM (e.g., fold test, reversals test, conglomerate test).

6.6. Conclusions

Paleomagnetic data from a marine mudstone sequence sampled at Okhta River, Sakhalin, suggest that the magnetization is a synfolding CRM carried by pyrrhotite. Rock magnetic and XRD results confirm the presence of pyrrhotite and SEM analyses indicate that the pyrrhotite dominantly occurs in nodules in the studied samples. The nodules

consist of pyrrhotite laths that have no preferred orientation and which show no evidence of deformation during sediment compaction. This suggests that the nodules formed after sediment compaction. Halos around the nodules suggest that fluids have played an important part in the formation of the pyrrhotite nodules. Together, the paleomagnetic, rock magnetic, and micro-textural evidence suggests that pyrrhotite formed during late diagenesis in association with a tectonically driven fluid migration event.

The documented late diagenetic magnetizations carried by pyrrhotite do not give a reliable syn-depositional paleomagnetic signal, which is required for detailed studies of geomagnetic field behaviour. Geological, environmental and oceanographic events are also likely to be misinterpreted from polarity records based on a CRM carried by magnetic iron sulphide minerals unless the timing of remanence acquisition can be accurately constrained. In tectonic studies where the deformation is multiphase and complex, it is critical that the mean paleomagnetic direction represents a time-averaged direction that predates deformation. It is clear from this study that a great deal of care must be taken to establish the timing of remanence acquisition in studies of magnetic iron sulphide-bearing sediments.

Acknowledgements

Fieldwork in Sakhalin was carried out as part of a Cambridge Arctic Shelf Programme research project. RW gratefully acknowledges financial support from a UK NERC PhD studentship and APR acknowledges support from the Royal Society of London. We thank Mike Jackson for his assistance during visits to the Institute for Rock Magnetism, Minnesota, Vladimir Galversen, Pavel Kovtunovich, Zhenia Rasshchepkina, and Valeriy Gorbachov for their support in the field, and Lidiya Fot'yanova, Rachel Flecker, David Macdonald, and Eric Blanc for other support. We thank Arlo Weil, Donald Peacor, and Fabio Florindo for constructive reviews that helped to improve the manuscript.

Table 6.1. Paleomagnetic data from Okhta River, Sakhalin

Sample	*In situ*		100% untilted		40% untilted		Error	*In situ*	
	Dec. (°)	Inc. (°)	Dec. (°)	Inc. (°)	Dec. (°)	Inc. (°)	MAD (°)	Dec. (°)	Inc. (°)
Magnetite									
C2500/2	227.2	-57.6	189.9	-67.6	-	-	3.3	329.8	80.7
C2500/3	229.4	-58.2	191.3	-68.8	-	-	3.9	0.0	65.7
C2500/4	234.7	-60.5	192.2	-72.3	-	-	2.5	330.1	77.8
C2501/2	224.3	-55.5	190.2	-64.9	-	-	5.5	27.6	72.6
C2501/3	212.6	-59.8	172.8	-64.0	-	-	4.9	339.7	70.3
C2501/4	217.5	-57.4	180.8	-63.9	-	-	7.0	3.6	63.7
C2502/1	177.0	-63.4	175.4	-70.4	-	-	22.8	294.9	54.8
C2502/3	204.4	-62.2	162.6	-62.8	-	-	10.1	-	-
C2502/4	203.6	-55.6	171.1	-57.7	-	-	16.2	346.1	73.9
Mean	215.4	-59.9	179.7	-66.2					
α_{95}	5.8		4.0						
Magnetite and pyrrhotite									
C1879/1	39.1	62.8	350.7	67.8	359.2	68.2	2.6	348.2	60.6
C1879/2	35.4	63.4	348.4	67.4	9.3	65.7	2.1	351.6	62.5
C1879/3	38.3	62.7	349.8	66.9	14.9	66.2	0.6	21.7	64.5
C1879/4	18.3	69.8	321.7	61.9	337.1	59.7	6.1	-	-
Mean								348.5	70.0
α_{95}								7.2	
Pyrrhotite									
C1876/1	42.0	75.0	322.7	72.5	4.9	76.5	4.3	-	-
C1876/2	23.3	60.9	330.0	63.9	351.0	69.4	10.3	-	-
C1876/3	39.2	72.7	326.5	67.3	357.1	71.6	5.5	-	-
C1877/1	14.9	67.1	332.2	60.3	354.9	65.8	10.0	-	-
C1877/3	2.1	78.3	315.6	66.0	7.3	71.1	4.7	-	-
C1877/4	25.1	72.0	329.3	68.0	0.4	69.1	3.6	-	-
C1878/1	29.9	64.1	343.2	65.9	11.0	67.0	7.9	-	-
C1878/2	9.8	60.6	334.9	56.8	353.3	59.9	6.2	-	-
C1878/3	17.4	68.2	328.1	64.4	351.1	69.6	7.1	-	-
Mean	26.2	67.9	333.4	65.7	358.7	68.0			
α_{95}	3.7		3.1		3.1				

Bedding: 21°W/182°; MAD: Maximum angular deviation for analysed vector components; α_{95}: 95% confidence limit for the mean paleomagnetic direction. The mean pyrrhotite direction includes magnetite and pyrrhotite data.

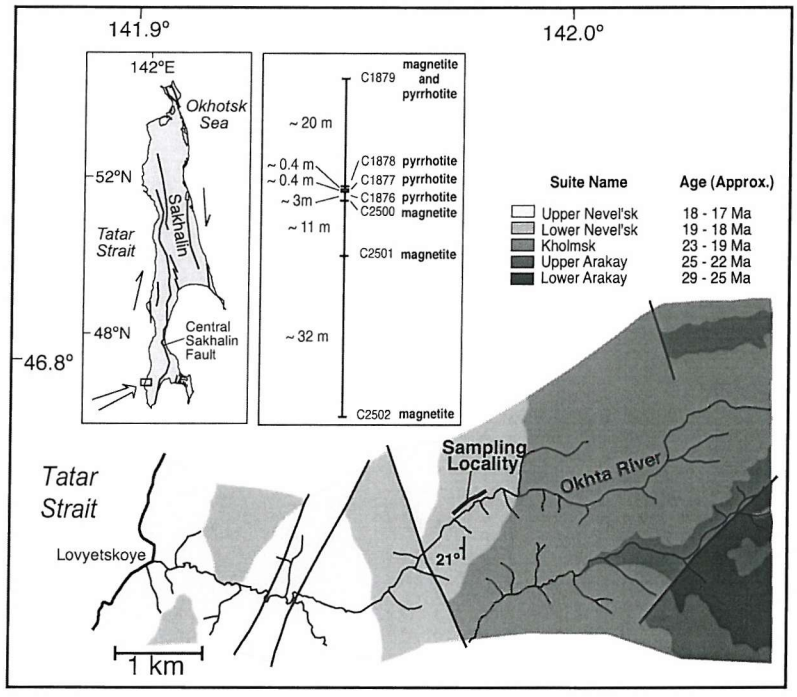

Figure 6.1. Location map of Okhta River, SW Sakhalin, with simplified geological map, summary stratigraphic section for the sampled interval, and magnetic mineralogy at each sampled site. Approximate ages and mapped geological units are from an unpublished map provided by V. Galversen, Sakhalin Geological Expedition.

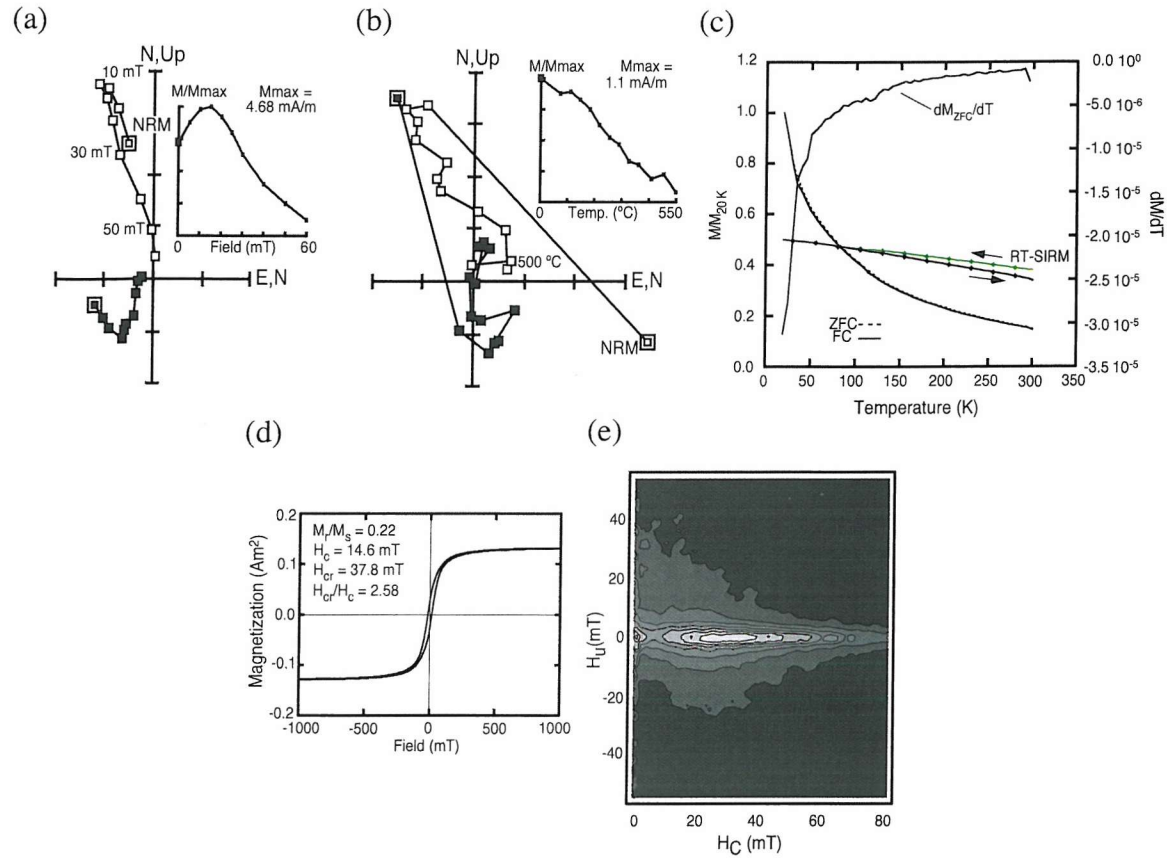

Figure 6.2. Representative rock magnetic data for sites C2500-C2502. Typical vector component diagrams for (a) AF demagnetization (sample C2500/3), and (b) thermal demagnetization (sample C2502/1). Open symbols indicate paleomagnetic inclinations and solid symbols indicate paleomagnetic declinations. The inset graph shows the decay of magnetization during stepwise demagnetization. (c) Normalized low-temperature ZFC, FC, and RT-SIRM curves (sample C2500/4). The first derivative of the ZFC curve is also plotted. The derivative is calculated by the method of adjacent points. (d) Hysteresis loop with associated hysteresis parameters (sample C2500/3). (e) FORC diagram (sample C2500/3). The FORC distribution is defined as the mixed second derivative of the magnetiztion with respect to the reversal field, H_a, and the field point being evaluated, H_b, along the FORC. H_u is defined as $(H_a+H_b)/2$, and the microscopic coercive force, H_c, is defined as $(H_b-H_a)/2$.

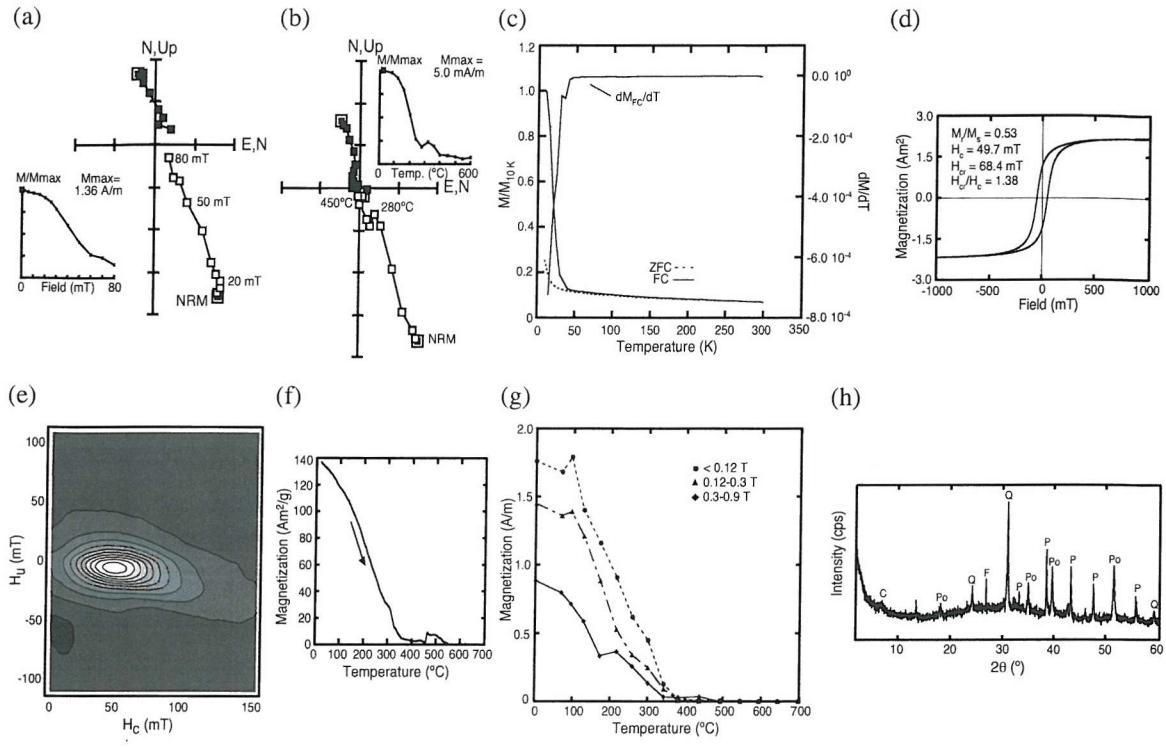

Figure 6.3. Representative rock magnetic and mineralogical data for sites C1876-C1878. Typical vector component diagrams for (a) AF demagnetization (sample C1877/1), and (b) thermal demagnetization (sample C1876/4). Symbols are the same as in Figure 6.2. (c) Normalized low-temperature ZFC and FC curves (sample C1877/4). Derivatives are calculated as described in Figure 6.2. (d) Hysteresis loop with associated hysteresis parameters (sample C1877/1). (e) FORC diagram (sample C1877/1). Definitions are as described in Figure 6.2. (f) High-temperature thermomagnetic curve from extracted iron sulphide nodule (sample C1877/1). (g) Thermal demagnetization of 3-axis IRM (sample C1877/1). (h) XRD analysis for a manually extracted iron sulphide nodule prior to heating. C = clay, Po = pyrrhotite, Q = quartz, F = feldspar, and P = pyrite.

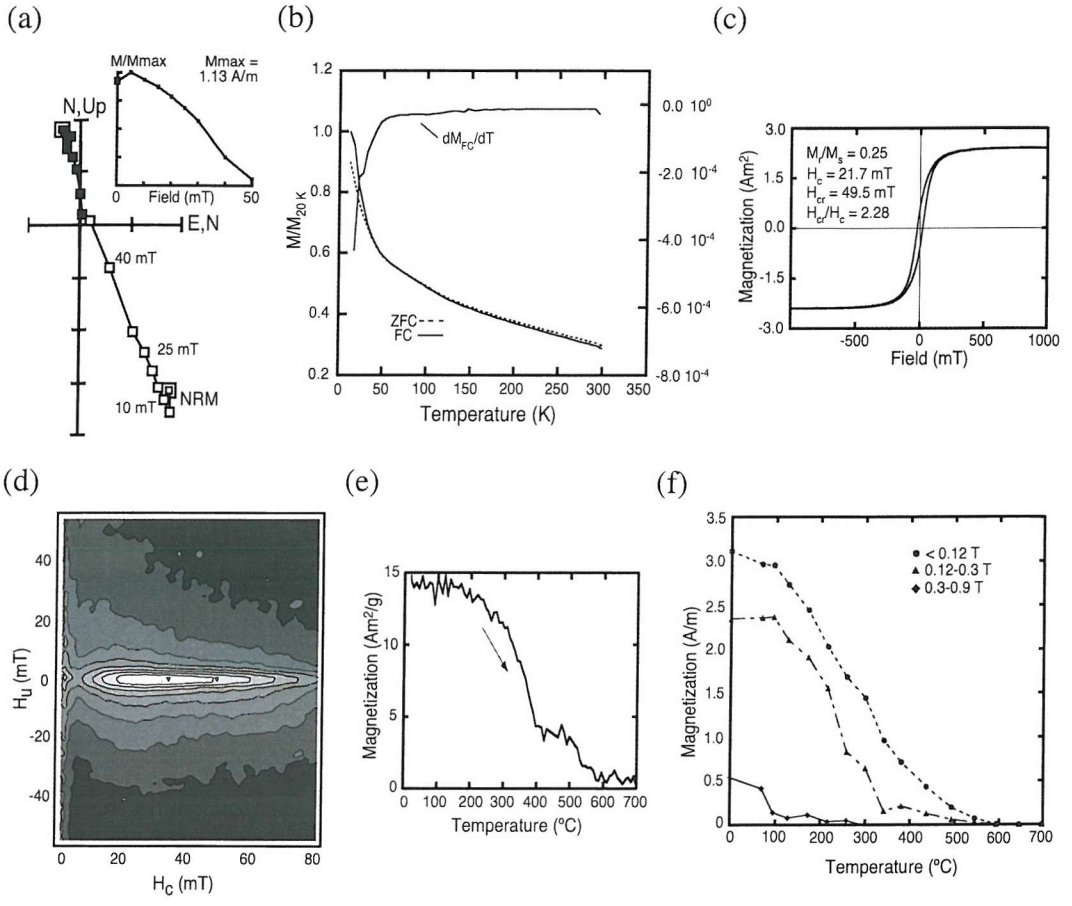

Figure 6.4. Representative rock magnetic data for site C1879. (a) Vector component diagram for AF demagnetization (sample C1879/3). Symbols are the same as in Figure 6.2. (b) Normalized low-temperature ZFC and FC curves (sample C1879/3). Derivative is calculated as described in Figure 6.2. (c) Hysteresis loop with associated hysteresis parameters (sample C1879/1). (d) FORC diagram (sample C1879/1). Definitions are as described in Figure 6.2. (e) High-temperature thermomagnetic curve (sample C1879/3). (f) Thermal demagnetization of 3-axis IRM (sample C1879/1).

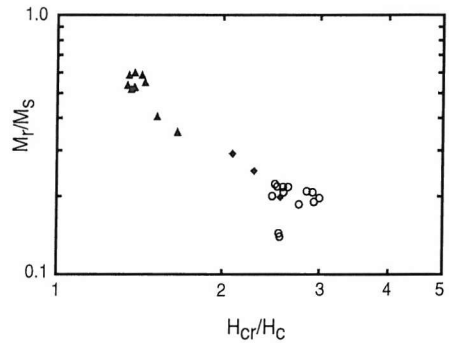

Figure 6.5. Hysteresis parameters (M_r/M_s vs. H_{cr}/H_c) for sites from Okhta River. Open circles indicate magnetite-bearing samples, solid diamonds indicate samples containing pyrrhotite and magnetite, and solid triangles indicate samples containing pyrrhotite.

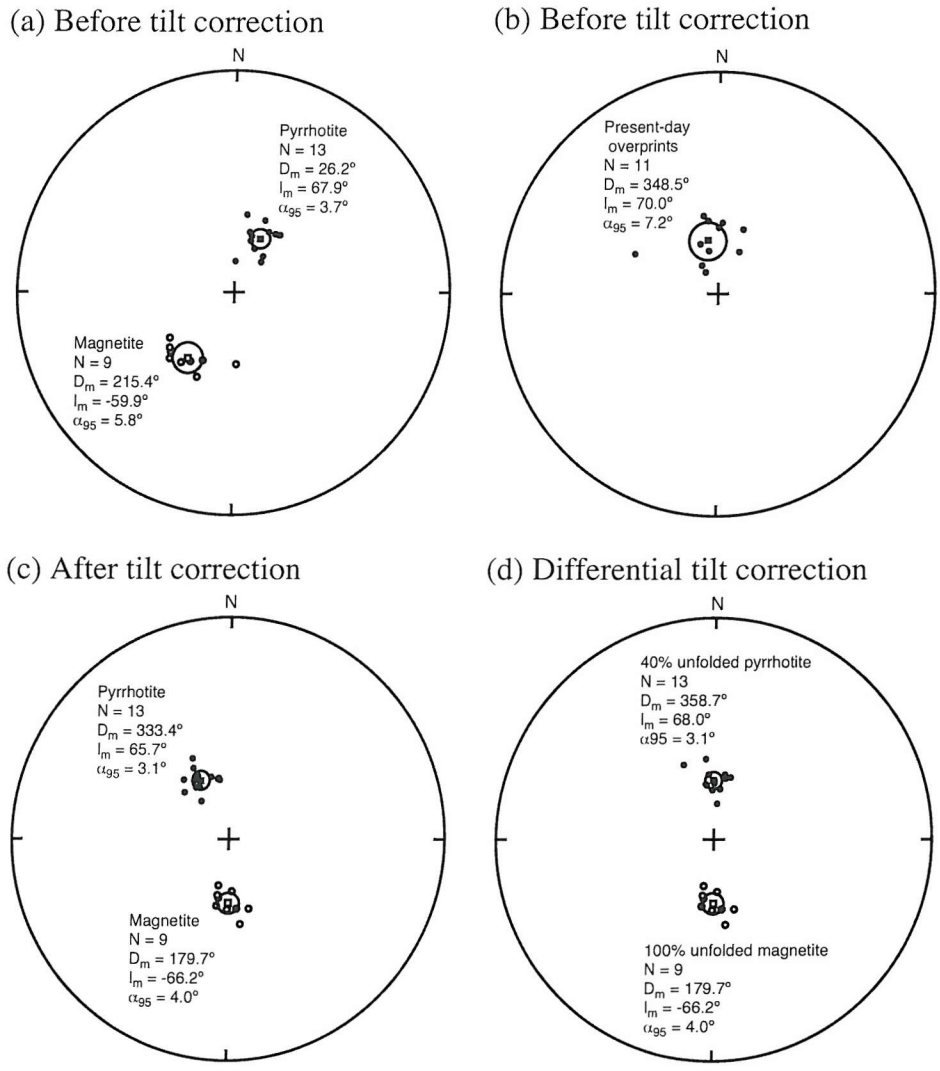

Figure 6.6. Equal-area stereographic projections (lower hemisphere) of paleomagnetic data with mean directions indicated by a square. Solid symbols indicate normal polarity and open symbols indicate reversed polarity. The mean paleomagnetic directions are accompanied by 95% confidence ellipses.

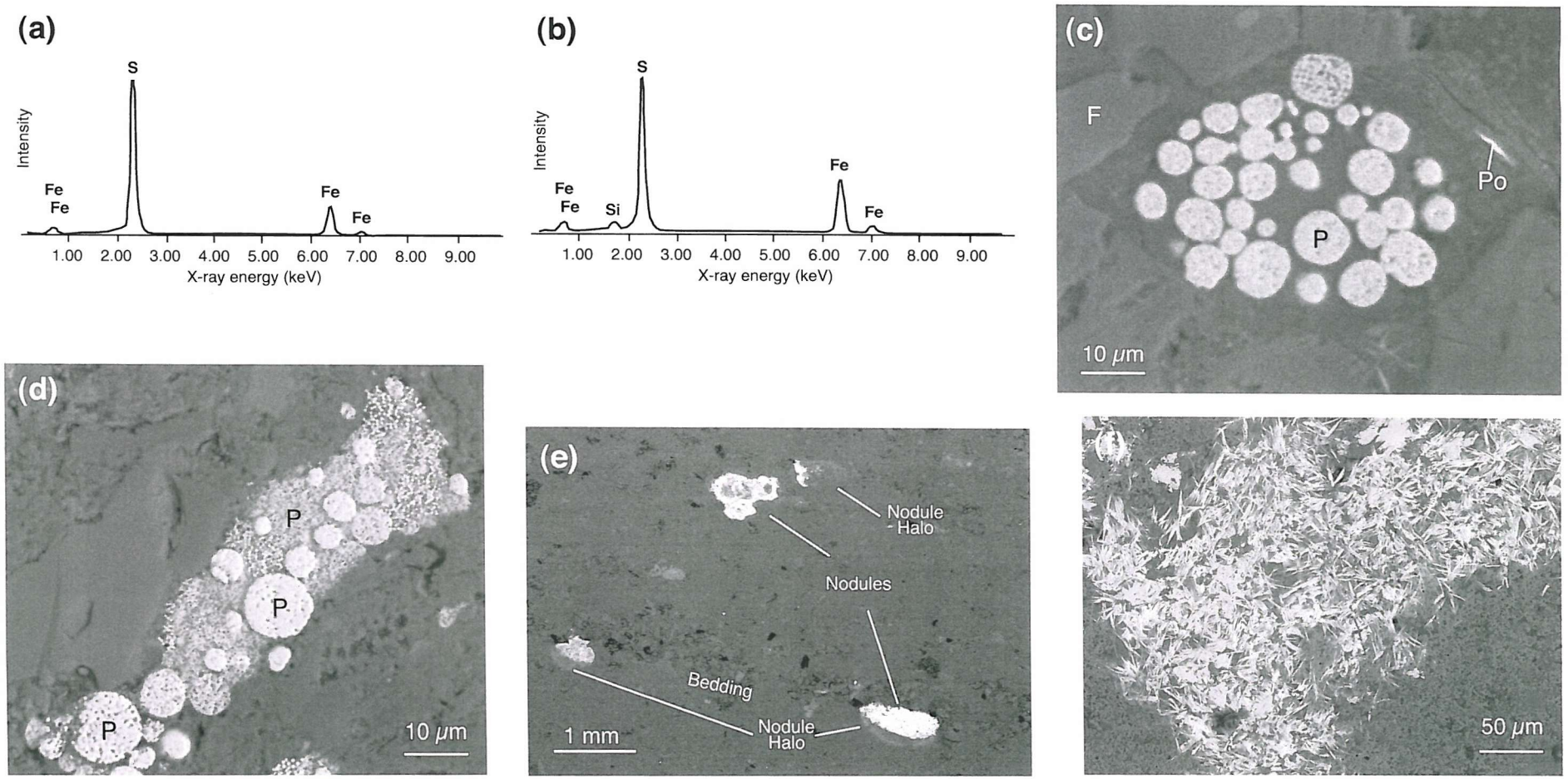

Figure 6.7. X-ray energy-dispersive spectra for (a) pyrite and (b) pyrrhotite. Backscattered electron micrographs for (c) spherical pyrite framboids (P) arranged in groups on the surface and around the edges of detrital silicate minerals. Pyrrhotite (Po) is identified in the cleavage of a mica grain (sample C1979/1). (d) Polyframboidal pyrite (P) aggregate where later growth of pyrite appears to have occurred between larger framboids (sample C2501/3). (e) Overview of iron sulphide nodules in the overall context of the sediment matrix (sample C1877/1). (f) Higher magnification of a typical iron sulphide nodule consisting of pyrrhotite laths with no preferred orientations (sample C1878/3).

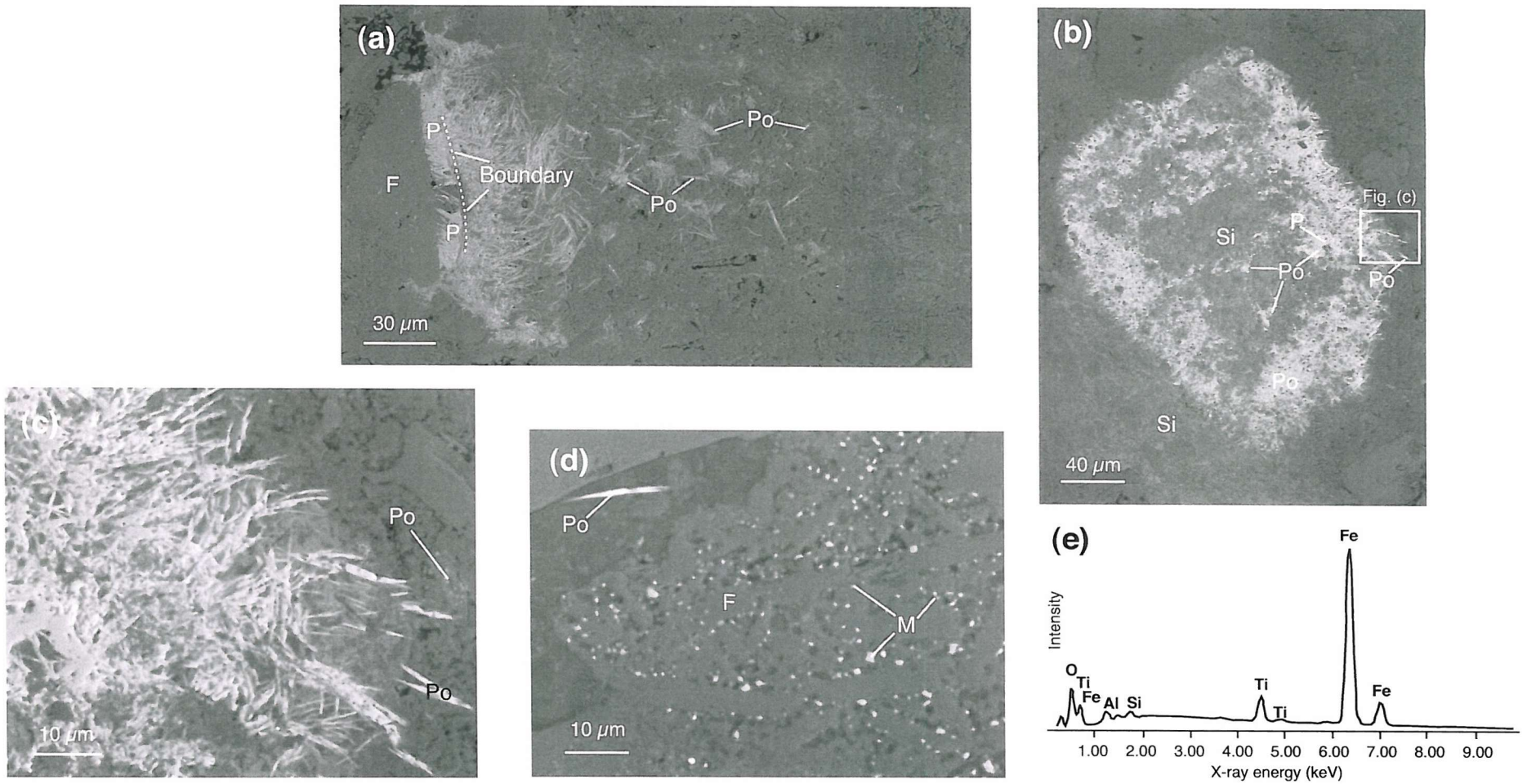

Figure 6.8. Backscattered electron micrographs. (a) Pyrrhotite nodule with a halo in the shadow of a feldspar (F) grain. Pyrite (P) is identified close to the right-hand grain boundary. Away from the boundary, pyrrhotite (Po) is dominant in fibrous laths (sample C1877/1). (b) Acicular pyrrhotite (Po) exists around the edges of a mass of silica (Si). Larger crystals of pyrite (P) are found in the centre of the nodule (sample C1877/1). (c) High-magnification reveals the presence of small pyrrhotite (Po) grains along micro-cleavage planes in mica grains close to large nodules (sample C1877/1). (d) Submicron magnetite particles (M) occur within large detrital feldspar grains (sample C1879/1). (e) EDS of (Ti-) magnetite particles within feldspar grains.

7

Summary and Conclusions

7.1. Summary

7.1.1 Regional Tectonic Evolution

Sakhalin is located along the western margin of the Okhotsk Sea in a tectonically complex region on the NW Pacific margin. Details of the plate interactions and tectonic evolution from the Late Cretaceous to the present day are unclear. Regional geodynamic research has focused primarily on the Japan region following recent drilling of the Japan Sea back-arc basin [e.g., *Tamaki et al.,* 1992; *Jolivet et al.,* 1994]. Extensive deep-sea drilling has not been carried out in the Okhotsk Sea and Kuril Basin. As a result, regional geodynamic models have been proposed that are based primarily on constraints from Japan and the Japan Sea, which do not take into account deformation to the north in Sakhalin and the Okhotsk Sea [*Otofuji et al.,* 1991; *Jolivet et al.,* 1994; *Altis,* 1999]. *Worrall et al.* [1996] suggested that the Eocene India-Eurasia collision could have been responsible for a significant part of the deformation observed in northeast Asia. This contradicts geological data from other marginal Tertiary basins such as the Bohai Basin, China [*Allen et al.,* 1998]. A local-scale tectonic study of Sakhalin and Hokkaido by *Fournier et al.* [1994] indicated that Neogene counterclockwise rotations may be expected in northeast Sakhalin. Fault-set data were used to infer paleostress directions from south Sakhalin and Hokkaido, but these directions were inconsistent, which suggests that vertical-axis rotations had affected the rocks [*Fournier et al.,* 1994]. They pointed out that paleomagnetic data would be required to constrain this model. A small-scale paleomagnetic study of Tertiary sediments was carried out by *Takeuchi et al.* [1999], which was focused on south Sakhalin and Hokkaido. They proposed a domino model for clockwise vertical-axis rotation, but no evidence was documented regarding the expected field structures. The present paleomagnetic study was conducted to improve our understanding of the evolution of Sakhalin.

7.1.2. Paleomagnetism

Reliable paleomagnetic data were obtained from mid-Paleocene to late Miocene marine mudstones and siltstones at 9 localities from Sakhalin. Inclination data were compared with the APWPs for the North American, Eurasian, and Pacific Plates. AMS and remanence anisotropy data indicate that the inclinations have been shallowed as a result of post-depositional sediment compaction. After correction for inclination shallowing, it appears that the sampled rocks have remained near the present-day latitude since the mid-Paleocene, which suggests that the geodynamic evolution has not been controlled by Pacific Plate motion. It is not possible to determine whether the paleomagnetic data agree best with Eurasian or North American Plate motions. Unfortunately, relevant paleomagnetic reference poles do not exist from the Okhotsk Sea Plate or the Amurian Plate.

Comparison of the paleomagnetic declination data with the APWP's of the North American and Eurasian plates indicate different phases of clockwise vertical-axis rotation. Data from west and southwest Sakhalin indicate a rapid clockwise rotation phase of about 40° in the mid-Miocene that may have been associated with the opening of the Japan Sea, Tatar Strait, and Kuril Basin. Declination data indicate about 20° of clockwise vertical-axis rotation of localities in east Sakhalin in the late Miocene, which might have been associated with subsequent cessation of opening of the Kuril Basin.

It is likely that right-lateral transpression along N-S-trending strike-slip faults accommodated the rotational deformation [e.g., *Fournier et al.,* 1994]. Clockwise vertical-axis rotation appears to have occurred from around the mid-late Eocene, which suggests that strike-slip tectonics had replaced the ancient E-W-directed subduction phase. This is consistent with paleomagnetic data from a Late Cretaceous exotic terrane that accreted against southeast Sakhalin in the mid-Eocene [*Bazhenov et al.,* 2001]. The consistency of the declination data from east Sakhalin suggests that this region deformed as a coherent structural domain. Clockwise deflected declinations are in conflict with expected counterclockwise rotations in a tectonic model for east Sakhalin proposed by

Fournier et al. [1994]. Variable declinations in southwest Sakhalin suggest that the deformation was complex. This indicates that the kinematic domino model proposed by *Takeuchi et al.* [1999] is overly simplistic, despite a consistent sense of rotation. Other structural domains may be identified with future paleomagnetic sampling. Such work is necessary before it is possible to provide a robust model to account for vertical-axis rotations in Sakhalin.

7.1.3. Tectonic Transport

AMS was measured successfully for samples from Late Cretaceous to late Miocene rocks at 22 localities including 8 of those which yielded reliable paleomagnetic data. Low bulk susceptibility values indicate that paramagnetic and diamagnetic matrix minerals dominate the AMS fabrics. The observed magnetic fabrics have k_{min} axes that are perpendicular to bedding as expected for sedimentary fabrics. The fabrics also have clustered k_{max} axes in the bedding plane. The fabrics are regionally consistent after correction for vertical-axis rotations and indicate the direction of net tectonic transport. Domains were defined over which the net tectonic transport directions were observed to be consistent. The data are consistent with a regional geodynamic model, in which Sakhalin is located at the boundary of the Northern Honshu Plate, Amurian Plate, and Okhotsk Sea Plate [*Seno,* 1985; *Takahashi et al.,* 1999]. In southwest Sakhalin the transport direction has remained constant around N035°E from the mid-Paleocene. The Miocene direction in east Sakhalin is around N040°E. This is consistent with the observed clockwise vertical-axis rotations being accommodated by right-lateral faulting on N-S-trending strike-slip faults. In west Sakhalin, a regionally consistent direction of around N080°E is observed from the Oligocene, before a ~25° clockwise vertical-axis rotation phase occurred in the mid-Miocene. The E-W-directed k_{int} axes may be due to local stress and strain effects associated with opening of the Tatar Strait.

7.1.3. Remagnetization

Paleomagnetic data provide evidence of a normal and reversed polarity ChRM in samples from adjacent sites in a Miocene mudstone sequence at Okhta River, southern Sakhalin. After full tilt correction, the reversed polarity data coincide with the expected GAD field direction for the locality. The normal polarity data are antipodal to the reversed polarity data only after 40% untilting, which suggests that the normal polarity ChRM constitutes a post-early Miocene synfolding magnetization. Rock magnetic measurements indicate that the normal polarity ChRM is carried by pyrrhotite. In the reversed polarity samples, magnetite is the remanence carrying mineral. The microtexture of the pyrrhotite was investigated by using an electron microscope. Pyrrhotite occurs primarily as randomly oriented laths within iron sulphide nodules. The random orientation of the pyrrhotite laths, lack of compaction of the nodules, and alteration halos around the nodules indicate that the nodules formed after sediment compaction and that fluids played an important part in their formation. The paleomagnetic, rock magnetic and micro-textural observations suggest that the pyrrhotite formed during late diagenesis in association with a tectonically driven fluid migration event.

Paleomagnetic data from other localities in Sakhalin suggest that remagnetization is widespread (see Appendix A). It is possible that plate-scale Miocene tectonic events observed both in the reliable paleomagnetic data and in the AMS data sets could be associated with activation of the fluids and regional remagnetization. This possibility is being tested with ongoing studies.

7.2. Conclusions

7.2.1. Plate Tectonic Evolution

Paleomagnetic results from sedimentary rocks indicate that Sakhalin has remained near present-day latitudes since the mid-Paleocene, which suggests that a Tertiary evolution in association with the Pacific Plate is unlikely. The data from

Sakhalin agree within error of the North American and Eurasian APWPs. It remains possible that Sakhalin could have evolved with the Okhotsk Sea Plate, but paleomagnetic reference poles do not exist for this plate.

The spatial distribution of ancient net tectonic transport directions in Sakhalin is consistent with a suggested present-day plate geometry where the boundary of the Amurian Plate, Okhtosk Sea Plate, and the Northern Honshu Plate transects Sakhalin [*Seno et al.*, 1985; *Takahashi et al.*, 1999].

It is likely that the opening of the Kuril Basin and the Tatar Strait Basin adjacent to Sakhalin is linked with discrete rapid phases of Miocene clockwise rotational deformation, which are evident in the paleomagnetic and AMS results. Miocene fluid-controlled remagnetization in southern Sakhalin may be associated with such events.

7.2.2. Transition from Subduction to Strike-slip Tectonics

NE-SW-directed horizontal compressive stress orientations observed in east and southwest Sakhalin are consistent with right-lateral transpression along N-S-trending faults, which accommodated Miocene phases of clockwise vertical-axis crustal rotation. Clockwise vertical-axis rotation had commenced by the late Eocene, which suggests that a transition from the ancient E-W-directed subduction regime had occurred by this time. The exact timing is uncertain and a clear kinematic mechanism was not apparent from the paleomagnetic data or from the AMS data.

7.2.3. Structural Domains and Rotational Mechanism

On the basis of consistent paleomagnetic declinations, east Sakhalin can be regarded as a discrete structural domain that has deformed uniformly. This is supported by regionally consistent AMS lineations from Miocene rocks. Clockwise rotation in the late Miocene contradicts the tectonic model of *Fournier et al.* [1994], which predicts counterclockwise rotation in the Neogene.

Rotational deformation in west and southwest Sakhalin appears to have been considerably more complex. No obvious structural domains were identified, but AMS data suggest that deformation in west and southwest Sakhalin may have occurred in the presence of a stress field that yielded a consistent direction of tectonic transport. Rotation of 100-km-scale crustal blocks, as suggested by *Takeuchi et al.* [1999], does not appear to represent a realistic explanation for the deformation. Further paleomagnetic data are required to be able to establish the kinematic mechanisms that led to the vertical-axis rotations.

7.3. Future Work

In order to eventually obtain a reasonable understanding of the regional geodynamics and kinematics, the role of the Okhotsk Sea Plate must be established. The nature of the lithosphere beneath the Okhosk Sea Plate is not known. The strength of the lithosphere has important implications for the extent and style of crustal deformation. It is likely that the presence and motion of the Okhotsk Sea Plate has had a significant influence on the rotational deformation observed in Sakhalin and on the style of opening of marginal basins, such as the Magadan Basin, Derugin Basin, Tatar Strait Basin, and Kuril Basin.

Geophysical work has so far been restricted to a few low-resolution seismic studies and the analysis of dredged sea floor samples. Sea floor spreading magnetic anomalies do not appear to exist in the Okhotsk Sea. An extensive program involving different geophysical and direct geological methods is required to provide new evidence concerning the past and present role of the Okhotsk Sea Plate.

7.3.1. Sea Floor Drilling

Sea floor drilling of the Okhotsk Sea should provide important data of several types. 1) Petrological data can provide information on the thermal history of the crust, the strength of the lithosphere, and the affinity of the lithosphere (i.e. oceanic vs.

continental). 2) The age of the crust can be established from deep crustal rocks. 3) Paleomagnetic measurements of basement rocks can provide constraints on the paleolatitude of the Okhotsk Sea Plate during formation of the crustal rocks of the plate. Future drilling technologies may allow cores to be reliably oriented, in which case the motion of the Okhotsk Sea may be established, and an APWP for the Okhotsk Sea Plate may be obtainable. Until then, paleomagnetic investigation of localities on the margin the Okhotsk Sea, e.g., Magadan, Sakhalin, west Kamchatka, and the Kuril islands may be used to constrain the Okhotsk Sea APWP.

7.3.2. Paleomagnetic Investigations

Acquisition of extensive paleomagnetic data from ancient allochtonous rocks in the Sikhote Al'in-Sakhalin-Okhotsk region would help to differentiate between different subduction and accretion episodes by enabling comparison of terrane trajectories. This would allow the timing of block accretion events to be established. In turn, this would provide temporal constraints on how long the Okhotsk Sea Plate has been in existence.

Paleomagnetic studies of more recent rocks (Oligocene and younger) may reflect motion of a relatively rigid Okhotsk Sea Plate. It is clear that rotational deformation has played a significant part in the geodynamic development of Sakhalin. It has not been possible to fully constrain the spatial extent of the rotational deformation. Further paleomagnetic sampling of sedimentary rocks would enable this to be achieved. Paleomagnetic sampling of Paleogene sequences in Sakhalin would be useful to more accurately determine the timing of the onset of rotational deformation. Sampling of Neogene rocks along E-W transects would also reveal systematic differences in the amount of rotation. In zones of plastic deformation, an exponential decrease in the amount of rotation should occur away from the bounding faults of the shear zone.

7.3.3. Geophysical Surveys

Seismic reflection surveys targeted at deep crustal structures should be carried out. Seismic reflection data can be used to establish the depth to the moho for different parts of the Okhotsk Sea. The structure of the crust of the main sedimentary basins is important for determining the mechanisms of basin rifting. Gravity and magnetic surveys data could also help to discriminate between different types of crustal rocks.

8

References

8. References

Allen, P. A., and J. R. Allen, *Basin Analysis*, 451 pp., Blackwell Sciences, 1990.

Allen, M. B., D. I. M. Macdonald, Z. Xun, S. J. Vincent, and C. Brouet-Menzies, Transtensional deformation in the evolution of the Bohai Basin, northern China, in *Continental Transpressional and Transtensional Tectonics*, R. E. Holdsworth, R. A. Strachan, and J. F. Dewey (Eds.), *Geol. Soc. London Spec. Publ., 135,* 215-229, 1998.

Altis, S., Interpretations of a Middle Miocene and late Quaternary steady dextral transpression in SW Japan and the opening tectonics for the Japan Sea, *Tectonophysics, 302*, 257-285, 1999.

Altis, S., Tectonic stress state in NE Japan as part of the Okhotsk plate, *Tectonophysics, 339,* 311-329, 2001.

Antipov, M. P., V. M. Kovylin, and V. P. Filat'yev, Sedimentary cover of deepwater basins of Tatar Strait and the northern part of the Sea of Japan, *Int. Geol. Rev., 22,* 1327-1334, 1980.

Arason, P., and S. Levi, Models of inclination shallowing during sediment compaction, *J. Geophys. Res., 95*, 4481-4499, 1990.

Arefiev, S., E. Rogozhin, R. Tatevossian, L. Rivera, and A. Cisternas, The Neftegorsk (Sakhalin Island) 1995 earthquake: A rare interplate event, *Geophys. J. Int.,* 143, 595-607, 2000.

Aubourg, C., P. Rochette, J.-F. Stéphan, M. Popoff, and C. Chabert-Pelline, The magnetic fabric of weakly deformed Late Jurassic shales from the southern subalpines chains (French Alps): Evidence for SW-directed tectonic transport direction, *Tectonophysics, 307,* 15-31, 1999.

Averbruch, O., D. Frizon de Lamotte, and C. Kissel, Magnetic fabric as a structural indicator of the deformation path within a fold-thrust structure: A test case from the Corbières (NE Pyrenees, France), *J. Struct. Geol., 14,* 461-474, 1992.

Banerjee, S. K., J. King, and J. Marvin, A rapid method for magnetic granulometry with applictions to environmental studies, *Geophys. Res. Lett., 8,* 333-336, 1981.

Baranov, B. V., and E. I. Pristavakina, The structure of the Okhotsk Sea and the development of its sedimentary basin, in *CASP Russian and Arctic Studies, 671,* R. Flecker (Ed.), 114 pp., unpublished, 1997.

Baranov, B. V., K. A. Dozorova, B. Y. Karp, and V. A. Karnaukh, Geometry of the Kuril Basin opening, *Dokl. Akad. Nauk, 367,* 751-753, 1997.

Baranov, B. V., R. Werner, K. A. Hoernle, I. B. Tsoy, P. Van den Bogaard, and I. A. Tararin, Evidence for compressionally induced high subsidence rates in the Kurile Basin (Okhotsk Sea), *Tectonophysics, 350,* 63-97, 2002.

Barton, C. E., Revision of international geomagnetic reference field released, *EOS Trans., 77,* 153-154, 1996.

Bayasgalan, A., J. Jackson, J.-F. Ritz, and S. Carretier, Field examples of strike-slip fault terminations in Mongolia and their tectonic significance, *Tectonics, 18,* 394-411, 1999.

Bazhenov, M. L., M. V. Alexutin, G. E. Bondarenko, and S. D. Sokolov, Mesozoic paleomagnetism of the Taigonos Peninsula, the Sea of Okhotsk: Implications to kinematics of continental and oceanic plates, *Earth Planet Sci. Lett., 173,* 113-127, 1999.

Bazhenov, M. L., A. E. Zharov, N. M. Levashova, K. Kodama, N. Y. Bragin, P. I. Fedorov, L. G. Bragina, and S. M. Lyapunov, Paleomagnetism of a Late Cretaceous island arc complex from South Sakhalin, East Asia: Convergent boundaries far away from the Asian continental margin?, *J. Geophys. Res., 106,* 19193-19205, 2001.

Bazhenova, O. K., B. A. Sokolov, and D. I. M. Macdonald, The geology and hydrocarbon potential of the Mid-Amur Basin, in *CASP Arctic and Russian Series, 630,* 122 pp., unpublished, 1995.

Beck, M. E., Block rotations in continental crust: Examples from western North America, in *Paleomagnetic Rotations and Continental Deformation*, C. Kissel and C. Laj (Eds.), pp. 1-16, Kluwer Academic Publishing, 1989.

Berner, R. A., Sedimentary pyrite formation, *Am. J. Sci., 268,* 1-23, 1970.

Berner, R. A., Sedimentary pyrite formation: An update, *Geochim. Cosmochim. Acta, 48,* 605-615, 1984.

Besse, J., and V. Courtillot, Revised and synthetic apparent polar wander paths of the African, Eurasian, North American and Indian Plates, and true polar wander since 200 Ma, *J. Geophys. Res., 96,* 4029-4050, 1991.

Blow, R. A., and N. Hamilton, Effect of compaction on the acquisition of a detrital remanent magnetization in fine-grained sediments, *Geophys. J. R. Astr. Soc., 52,* 13-23, 1978.

Borradaile, G. J., Magnetic susceptibility, petrofabrics and strain, *Tectonophysics, 156,* 1-20, 1988.

Borradaile, G. J., Correlation of strain with anisotropy of magnetic susceptibility (AMS), *Pure Appl. Geophys., 135,* 15-29, 1991.

Borradaile, G.J., and B. Henry, Tectonic applications of magnetic susceptibility and its anisotropy, *Earth Sci. Rev., 42,* 49-93, 1997.

Butler, R. F., *Paleomagnetism: Magnetic domains to geologic terranes,* Blackwell Sciences (electronic edition), 238 pp., 1992.

Channell, J. E. T., and C. McCabe, Comparison of magnetic hysteresis parameters of unremagnetized and remagnetized limestones, *J. Geophys. Res., 99,* 4613-4623, 1994.

Day, R., M. D. Fuller, and V. A. Schmidt, Hysteresis properties of titanomagnetites: grain size and composition dependence, *Phys. Earth Planet. Inter., 13,* 260-266, 1977.

Debiche, M. G., A. Cox and D. Engebretson, The motions of allochtonous terranes across the North Pacific basin, *Geol. Soc. Am. Sp. Pap., 207,* 49 pp., 1987.

Dekkers, M. J., Magnetic properties of natural pyrrhotite. I. Behaviour of initial susceptibility and saturation-magnetization-related rockmagnetic parameters in a grainsize-dependent framework, *Phys. Earth Planet. Inter., 52,* 376-393, 1988.

Dekkers, M. J., Magnetic monitoring of pyrrhotite alteration during thermal demagnetization, *Geophys. Res. Lett., 17,* 779-782, 1990.

Dekkers, M. J., J.-L. Mattéi, G. Fillion, and P. Rochette, Grain-size dependence of the magnetic behaviour of pyrrhotite during its low-temperature transition at 34 K, *Geophys. Res. Lett., 16,* 855-858, 1989.

DeMets, C., A test of present-day plate geometries for northeast Asia and Japan, *J. Geophys. Res., 97,* 17627-17635, 1992a.

DeMets, C., Oblique convergence and deformation along the Kuril and Japan trenches, *J. Geophys. Res., 97,* 17615-17625, 1992b.

Dickinson, W. R., Kinematics of transrotational tectonism in the California Transverse Ranges and its contribution to cumulative slip along the San Andreas transform fault system, *Geol. Soc. Am. Spec. Pap., 305,* 46 pp., 1996.

Dinarès-Turell, J., and M. J. Dekkers, Diagenesis and remanence acquisition in the Lower Pliocene Trubi marls at Punta di Maiata (southern Sicily): Paleomagnetic and rock magnetic observations, in *Palaeomagnetism and diagenesis in sediments,* D. H. Tarling and P. Turner (Eds.), *Geol. Soc. London Spec. Publ., 151,* 53-69, 1999.

Dunlop, D. J., On the use of Zijderveld vector diagrams in multicomponent paleomagnetic samples, *Phys. Earth Planet. Inter., 20,* 12-24, 1979.

Dunlop, D. J., Magnetism in rocks, *J. Geophys. Res., 100,* 2161-2174, 1995.

Dunlop, D. J., and Ö. Özdemir, *Rock magnetism:Fundamentals and frontiers,* Cambridge University Press, 573 pp., 1997.

Engebretson, D. C., A. Cox, and R. G. Gordon, Relative motions between oceanic plates of the Pacific Basin, *J. Geophys. Res., 89,* 10291-10310, 1984.

England, P, and J. Jackson, Active deformation of the continents, *Ann. Rev. Earth Planet. Sci., 17,* 197-226, 1989.

England, P, and R. E. Wells, Neogene rotations and quasicontinuous deformation of the Pacific northwest continental margin, *Geology, 19,* 978-981, 1991.

Fisher, N. I., T. Lewis, and B. J. J. Embleton, *Statistical Analysis of Spherical Data,* Cambridge University Press, 1987.

Fisher, R. A., Dispersion on a sphere, *Proc. R. Soc. London, 217,* 295-305, 1953.

Flecker, R., and D. I. M. Macdonald, New analytical results from Sakhalin, *in CASP Arctic and Russian Studies, 668,* 66 pp., unpublished, 1997.

Flecker, R., and D. I. M. Macdonald, Field observations from the southeast coast of the Schmidt Peninsula, Sakhalin, in *CASP Arctic and Russian Studies, 685,* 164 pp., unpublished, 1998.

Flecker, R., and D. I. M. Macdonald, Cenozoic evolution of the Tatar Strait, Russian far east and its relationships to the opening of the Sea of Japan, *Basin Research,* 2002, in press.

Flecker, R., D. I. M. Macdonald, and L. G. Voronova, Interpretation of field observations on the Tertiary rocks of Sakhalin made during the 1997 field season, in *CASP Arctic and Russian Studies, 674,* 326 pp., unpublished, 1998.

Florindo, F., and L. Sagnotti, Palaeomagnetism and rock magnetism in the upper Pliocene Valle Ricca (Rome, Italy) section, *Geophys. J. Int., 123,* 340-354, 1995.

Fot'yanova, L. M., M. Y. Serova, V. G. Galversen, A. E. Zharov, N. M. Grokhotova, and V. P. Tuzov, Key section of the Paleogene deposits of the Kril'on Peninsula (south Sakhalin, Kitosiya River) (in Russian), *Strat. Geol. Correl., 9,* 58-76, 2001.

Fournier, M., L. Jolivet, P. Huchon, K. F. Sergeyev, and L. S. Oscorbin, Neogene strike-slip faulting in Sakhalin and the Japan Sea opening, *J. Geophys. Res., 99,* 2701-2725, 1994.

Fuller, M. D., Magnetic anisotropy and paleomagnetism, *J. Geophys. Res., 68,* 293-309, 1963.

Fuller, M., R. Haston, and E. Schmidtke, Paleomagnetism in SE Asia: Sinistral shear between Philippine Sea plate and Asia, in *Paleomagnetic rotations and continental deformation,* C. Kissel and C. Laj (Eds.), pp. 411-430, NATO Series 254, 1989.

Garfunkel, Z., Regional deformation by block translation and rotation, in *Paleomagnetic rotations and continental deformation,* C. Kissel and C. Laj (Eds.), pp. 181-208, NATO Serires 254, 1989.

Garrels, R. M., and C. L. Christ, *Solutions, Minerals and Equilibria,* Harper and Row, New York, 450 pp., 1965.

Gladenkov, Y. B., Neogene stratigraphy of northeast Asia (Kamchatka, Sakhalin, in *Pacific Neogene datum planes,* N. Ikebe and R. Tsuchi (Eds.), pp. 235-243, Univ. Tokyo Press, 1988.

Gorbatov, A., S. Widiyantoro, Y. Fukao, and E. Gordeev, Signature of remnant slabs in the North Pacific from P-wave tomography, *Geophys. J. Int., 142,* 27-36, 2000.

Gordon, R. G., and R. Van der Voo, Mean paleomagnetic poles for the major continents and the Pacific Plate, in *A Handbook of Geophysical Constants*, T. J. Ahrens (Ed.), pp. 225-239, AGU Reference Shelf 1, 1995.

Hallam, D. F., and B. A. Maher, A record of reversed polarity carried by the iron sulphide greigite in British early Pleistocene sediments, *Earth Planet. Sci Lett., 121,* 71-80, 1994.

Hamilton, N., and A. I. Rees, The use of magnetic fabric in paleocurrent estimation, *Paleogeophysics,* pp. 446-464, 1970.

Haq, B. U., J. Hardenbol, and P. R. Vail, Chronology of fluctuating sea levels since the Triassic, *Science, 235*, 1156-1167, 1987.

Heki, K., S. Miyazaki, H. Takahashi, M. Kasahara, F. Kimata, S. Miura, N. F. Vasilenko, A. Ivashchenko, and K.-D. An, The Amurian Plate motion and current plate kinematics in eastern Asia, *J. Geophys. Res., 104,* 29147-19155, 1999.

Hext, G., The estimation of second-order tensors, with related tests and designs, *Biometrika, 50,* 353-357, 1963.

Hodych, J. P., and S. Bijaksana, Can remanence anisotropy detect paleomagnetic inclination shallowing due to compaction?, *J. Geophys. Res., 98,* 22429-22441, 1993.

Hodych, J. P., and K. L. Buchan, Early Silurian palaeolatitude of the Springdale Group redbeds of central Newfoundland: A paleomagnetic determination with a remanence anisotropy test for inclination error, *Geophys. J. Int., 117,* 640-652, 1994.

Hodych, J. P., S. Bijaksana, and R. Patzold, Using magnetic anisotropy to correct for paleomagnetic inclination shallowing in some magnetite-bearing deep-sea turbidites and limestones, *Tectonophysics, 307,* 191-205, 1999.

Hoffman, K. A., and R. Day, Separation of multicomponent NRM: A general method, *Earth Planet. Sci. Lett., 40,* 433-438, 1978.

Hornafius, J. S., Neogene tectonic rotation of the Santa Ynez Range, Western Transverse Ranges, California, suggested by paleomagnetic investigation of the Monterey Formation, *J. Geophys. Res., 90,* 12503-12522, 1985.

Hornafius, J. S., B. P. Luyendyk, R. R. Terres, and M. J. Kamerling, Timing and extent of Neogene tectonic rotation in the western Transverse Ranges, California, *Geol. Soc. Am. Bull., 97,* 1476-1487, 1986.

Horng, C.-S., M. Torii, K.-S. Shea, and S.-J. Kao, Inconsistent magnetic polarities between greigite- and pyrrhotite/magnetite-bearing marine sediments from the Tsailiao-chi section, southwestern Taiwan, *Earth Planet. Sci. Lett., 164,* 467-481, 1998.

Housen, B. A., and R. J. Musgrave, Rock-magnetic signature of gas hydrates in accretionary prism sediments, *Earth Planet. Sci. Lett., 139,* 509-519, 1996.

Housen, B. A., B. A. Van der Pluijm, and E. J. Essene, Plastic behavior of magnetite and high strains observed from magnetic fabrics in the Parry Sound shear zone, Ontario Grenville Province, *J. Struct. Geol., 17,* 265-278, 1995.

Housen, B. A., S. K. Banerjee, and B. M. Moskowitz, Low-temperature magnetic properties of siderite and magnetite in marine sediments, *Geophys. Res. Lett., 23,* 2843-2846, 1996.

Hrouda, F., and S. Kahan, The magnetic fabric relationship between sedimentary and basement nappes in the High Tatra Mountains, N. Slovakia, *J. Struct. Geol., 13,* 431-442, 1991.

Hyden, F., R. Flecker, and D. I. M. Macdonald, Initial provenance results from Sakhalin, in *CASP Arctic and Russian Studies, 667*, 60 pp., unpublished, 1997.

Ikeda, Y., R. J. Stern, H. Kagami, and C.-H. Sun, Pb, Nd, and Sr isotopic constraints on the origin of Miocene basaltic rocks from northeast Hokkaido, Japan: Implications for opening of the Kurile back-arc basin, *Island Arc, 9,* 161-172, 2000.

Ingle Jr., J. C., Origin of Neogene diatomites around the north Pacific rim, in *The Monterey Formation and Related Siliceous Rocks of California*, SEPM, pp. 159-179, 1981.

Ingle Jr., J. C., Subsidence of the Japan Sea: Stratigraphic evidence from ODP sites and onshore sections, *Proc. ODP Sci. Res., 127-128*, 1197-1218, 1992.

Ivashchenko, A. I., C. U. Kim, L. S. Oscorbin, L. N. Poplavskaya, A. A. Poplavskiy, R. N. Burymskaya, T. G. Mikhailova, N. F. Vasilenko, and M. I. Streltsov, The Neftegorsk, Sakhalin Island, earthquake of 27 May 1995, *Island Arc, 6*, 288-302, 1997.

Jackson, J. A., Active normal faulting and crustal extension, in *Continental Extensional Tectonics,* M. P. Coward et al. (Eds.), *Geol. Soc. London Spec. Publ., 28,* 3-17, 1987.

Jackson, J. A., and D. McKenzie, Relations between seismicity and paleomagnetic rotations in zones of distributed continental deformation, in *Paleomagnetic rotations and continental deformation,* C. Kissel and C. Laj (Eds.), pp. 33-42, NATO Series 254, 1989.

Jackson, J. A., and P. Molnar, Active faulting and block rotations in the western Transverse Ranges, California, *J. Geophys. Res., 95,* 22073-22087, 1990.

Jackson, M., Diagenetic sources of stable remanence in remagnetized Paleozoic cratonic carbonates: A rock magnetic study, *J. Geophys. Res., 95,* 2753-2761, 1990.

Jackson, M., Anisotropy of magnetic remanence: A brief overview of mineralogical sources, physical origins, and geological applications, and comparison with susceptibility anisotropy, *Pure Appl. Geophys., 136,* 1-27, 1991.

Jackson, M., W. Gruber, J. Marvin, and S. K. Banerjee, Partial anhysteretic remanence and its anisotropy: Applications and grainsize-dependence, *Geophys. Res. Lett., 15,* 440-443, 1988.

Jackson, M. J., S. K. Banerjee, J. A. Marvin, R. Lu, and W. Gruber, Detrital remanence, inclination errors, and anhysteretic remanence anisotropy: Quantitative model and experimental results, *Geophys. Res. Lett.,* 104, 95-103, 1991.

Jelinek, V., *The statistical thory of measureing anisotropy of magnetic susceptibility of roakc and its application,* Brno, Geophysika, pp. 1-88, 1976.

Jelinek, V., Statistical processing of anisotropy of magnetic susceptibility measured on groups of specimens, *Studia Geophys. Geod., 22,* 50-62, 1978.

Jelinek, V., Characterization of the magnetic fabric of rocks, *Tectonophysics, 79,* T63-T67, 1981.

Jiang, W.-T., C.-S. Horng, A. P. Roberts, and D. R. Peacor, Contradictory magnetic polarities in sediments and variable timing of neoformation of authigenic greigite, *Earth Planet. Sci. Lett., 193,* 1-12, 2001.

Jolivet, L., and K. Tamaki, Neogene kinematics in the Japan Sea region and volcanic activity of the northeast Japan arc, *Proc. ODP Sci. Res., 127-128,* 1311-1331, 1992.

Jolivet, L., P. Davy, and P. Cobbold, Right-lateral shear along the northwest Pacific margin and the India-Eurasia collision, *Tectonics, 9,* 1409-1419, 1990.

Jolivet, L., P. Huchon, J. P. Brun, X. Le Pichon, N. Chamot-Rooke, and J. C. Thomas, Arc deformation and marginal basin opening: Japan Sea as a case study, *J. Geophys. Res., 96,* 4367-4384, 1991.

Jolivet, L., M. Fournier, P. Huchon, V. S. Rozhdestvenskiy, K. F. Sergeyev, and L. S. Oscorbin, Cenozoic intracontinental dextral motion in the Okhotsk-Japan Sea region, *Tectonics, 11,* 968-977, 1992.

Jolivet, L., K. Tamaki, and M. Fournier, Japan Sea, opening history and mechanism: A synthesis, *J. Geophys. Res., 99,* 22237-22259, 1994.

Jolivet, L., H. Shibuya, and M. Fournier, Paleomagnetic rotations and the Japan Sea opening, in *Active Margins and Marginal Basins of the Western Pacific*, B. Taylor and J. Natland (Eds.), *AGU Geophys. Monogr., 88,* 355-369, 1995.

Kalcheva, V., P. Nozharov, M. Kovacheva, and V. Shopov, Paleomagnetic research on Black Sea Quaternary sediments, *Phys. Earth Planet. Inter., 63,* 113-120, 1990.

Kamerling, M. J., and B. P. Luyendyk, Paleomagnetism and Neogene tectonics of the Northern Channel Islands, California, *J. Geophys. Res., 90,* 12485-12502, 1985.

Kent, J. T., The Fisher-Bingham distribution on the sphere, *J. R. Statist. Soc. B, 44,* 71-80, 1982.

Kharakhinov, V. V., S. D. Gal'tsev-Bezyuk, and A. A. Tereshchenkov, Faults of Sakhalin, *Geol. Pac. Ocean, 3,* 355-373, 1985.

Kimura, G., Oblique subduction and collision: Forearc tectonics of the Kuril arc, *Geology, 14*, 404-407, 1986.

Kimura, G., The latest Cretaceous-early Paleogene rapid growth of accretionary complex and exhumation of high pressure series metamorphic rocks in northwestern Pacific margin, *J. Geophys. Res., 99*, 22147-22164, 1994.

Kimura, G., and K. Tamaki, Collision, rotation, and back-arc spreading in the region of the Okhotsk and Japan seas, *Tectonics, 5,* 389-401, 1986.

Kimura, G., S. Miyashita, and S. Miyasaka, Collision Tectonics in Hokkaido and Sakhalin, in *Accretion Tectonics in the Circum-Pacific Regions*, M. Hashimoto and S. Uyeda (Eds.), pp. 123-134, Terra Scientific Publishing Company, Tokyo, 1983.

Kimura, G., V. S. Rozhdestvenskiy, K. Okamura, O. Melnikov, and M. Okamura, Mode of mixture of oceanic fragments and terrigenous trench fill in an accretionary complex: Example from southern Sakhalin, *Tectonophysics, 202,* 361-374, 1992a.

Kimura, G., M. Sakakibara, H. Ofuka, H. Ishizuka, S. Miyashita, M. Okamura, O. A. Melinikov, and V. Lushchenko, A deep section of accretionary complex: Susunai Complex in Sakhalin Island, Northwest Pacific Margin, *Island Arc, 1,* 166-175, 1992b.

Kinimani, K., and Y. Kontani, Mesozoic Arc-Trench Systems in Hokkaido, Japan, in *Accretion Tectonics in the Circum-Pacific Regions*, M. Hashimoto and S. Uyeda (Eds.), pp. 107-122, Terra Scientific Publishing Company, Tokyo, 1983.

Kirschvink, J. L., The least-squares line and plane and the analysis of palaeomagnetic data, *Geophys. J. R. Astr. Soc., 62*, 699-718, 1980.

Kissel, C., and C. Laj, The Tertiary geodynamic evolution of the Aegean arc: A paleomagnetic reconstruction, *Tectonophysics, 146*, 183-201, 1988.

Kissel, C., E. Barrier, C. Laj, and T.-Q. Lee, Magnetic fabric in "undeformed" marine clays from compressional zones, *Tectonics, 5,* 769-781, 1986.

Knight, M., and G. Walker, Magma flow directions in dikes of the Koolau Complex, Oahu, determined from magnetic fabric studies, *J. Geophys. Res., 93,* 4301-4319, 1988.

Kodama, K., H. Maeda, Y. Shigeta, T. Kase, and T. Takeuchi, Magnetostratigraphy of upper Cretaceous strata in south Sakhalin, Russian far east, *Cret. Res., 21,* 469-478, 2000.

Kodama, K. P., A successful rock magnetic technique for correcting paleomagnetic inclination shallowing: Case study of the Nacimiento Formation, New Mexico, *J. Geophys. Res., 102*, 5193-5205, 1997.

Kravchinsky, V. A., J.-P. Cogné, W. P. Harbert, and M. I. Kuzmin, Evolution of the Mongol-Okhotsk Ocean as constrained by new palaeomagnetic data from the Mongol-Okhotsk suture zone, Siberia, *Geophys. J. Int., 148,* 34-57, 2002.

Lagroix, F., and S. K. Banerjee, Paleowind directions from the magnetic fabric of loess profiles in central Alaska, *Earth Planet. Sci. Lett., 195,* 99-112, 2002.

Lallemand, S., and L. Jolivet, Japan Sea – a pull-apart basin, *Earth Planet. Sci. Lett., 76,* 375-389, 1986.

Lamb, S., A model for tectonic rotations about a vertical axis, *Earth Planet. Sci. Lett., 84,* 75-86, 1987.

Lamb, S., Vertical axis rotation in the Bolivian orocline, South America 1. Paleomagnetic analysis of Cretaceous and Cenozoic rocks, *J. Geophys. Res., 106,* 26605-26632, 2001.

Lee, T.-Q., C. Kissel, C. Laj, C.-S. Horng, and Y.-T. Lue, Magnetic fabric analysis of the Plio-Pleistocene sedimentary formations of the Coastal Range of Taiwan, *Earth Planet. Sci. Lett., 98,* 23-32, 1990.

Levashova, N. M., M. L. Bazhenov, and M. N. Shapiro, Late Cretaceous paleomagnetism of the East Ranges island arc complex, Kamchatka: Implications for terrane movements and kinematics of the northwest Pacific, *J. Geophys. Res., 102*, 24843-24857, 1997.

Levashova, N. M., M. N. Shapiro, and M. L. Bazhenov, Late Cretaceous paleomagnetic data from the Median Range of Kamchatka, Russia: Tectonic implications, *Earth Planet. Sci. Lett., 163*, 235-246, 1998.

Lindquist, S. J., The north Sakhalin Neogene total petroleum system of eastern Russia, *USGS open file report (online edition), 99-50-O,* 18 pp., 2000.

Linssen, J. H., Preliminary results of a study of four successive sedimentary geomagnetic reversal records from the Mediterranean (Upper Thvera, Lower and Upper Sidufjall, and Lower Nunivak), *Phys. Earth Planet. Inter., 52*, 207-231, 1988.

Little, T. A., and A. P. Roberts, Distribution and mechanism of Neogene to present-day vertical axis rotations, Pacific-Australian plate boundary zone, South Island, New Zealand, *J. Geophys. Res., 102*, 20447-20468, 1997.

Lonsdale, P., Paleogene history of the Kula plate: offshore evidence and onshore implications, *Geol. Soc. Am. Bull., 100,* 733-754, 1988.

Love, L. G., Early diagenetic polyframboidal pyrite, primary and redeposited, from the Wenlockian Denbigh Grit group, Conway, north Wales, U.K., *J. Sed. Pet., 41,* 1038-1044, 1971.

Lowrie, W., Identification of ferromagnetic minerals in a rock by coercivity and unblocking temperature properties, *Geophys. Res. Lett.,* 17, 159-162, 1990.

Luyendyk, B. P., A model for Neogene crustal rotations, transtension, and transpression in southern California, *Geol. Soc. Am. Bull., 103,* 1528-1536, 1991.

Luyendyk, B. P., and J. S. Hornafius, Neogene crustal rotations, fault slip, and basin development in southern California, in *Cenozoic Basin Development of Coastal California,* R. V. Ingersoll and G. S. Ernst (Eds.), pp. 259-283, Prentice-Hall, 1987.

Luyendyk, B. P., M. J. Kamerling, and R. R. Terres, Geometric model for Neogene crustal rotations in southern California, *Geol. Soc. Am. Bull., 91*, 211-217, 1980.

Luyendyk, B. P., M. J. Kamerling, R. R. Terres, and J. S. Hornafius, Simple shear of Southern California during Neogene time suggested by paleomagnetic declinations, *J. Geophys. Res., 90*, 12454-12466, 1985.

Maeda, J., Opening of the Kuril Basin deduced from the magmatic history of central Hokkaido, north Japan, *Tectonophysics, 174,* 235-255, 1990.

Macdonald, D. I. M., and R. Flecker, Preliminary report on the Tertiary palaeofacies of Sakhalin and factors controlling sediment distribution, in *CASP Arctic and Russian Studies, 675*, 32 pp., unpublished, 1998.

Machel, H. G., and E. A. Burton, Causes and spatial distribution of anomalous magnetization in hydrocarbon seepage environments, *Am. Assoc. Petr. Geol. Bull., 75,* 1864-1876, 1991.

Maggi, A., J. A. Jackson, D. McKenzie, and K. Priestley, Earthquake focal depths, effective elastic thickness, and the strength of the continental lithosphere, *Geology, 28,* 495-498, 2000.

Maruyama, S., and T. Seno, Orogeny and relative plate motions: Example of the Japanese islands, *Tectonophysics, 127,* 305-329, 1986.

Mary, C., S. Iaccarino, V. Courtillot, J. Besse, and D. M. Aïssaoui, Magnetostratigraphy of Pliocene sediments from the Stirone River (Po Valley), *Geophys. J. Int., 112,* 359-380, 1993.

Mattei, M., L. Sagnotti, C. Faccenna, and R. Funicello, Magnetic fabric of weakly deformed clay-rich sediments in the Italian peninsula: Relationship with compressional and extensional tectonics, *Tectonophysics, 271,* 107-122, 1997.

McCabe, C., and R. D. Elmore, The occurrence and origin of late Paleozoic remagnetization in the sedimentary rocks of North America, *Rev. Geophys., 27,* 471-494, 1989.

McElhinny, M. W., *Palaeomagnetism and Plate Tectonics,* Cambridge University Press, 356 pp., 1973.

McKenzie, D., and J. Jackson, The relationship between strain rates, crustal thickening, paleomagnetism, finite strain and fault movements within a deforming zone, *Earth Planet. Sci. Lett., 65,* 182-202, 1983.

McKenzie, D., and J. Jackson, A block model of distributed deformation by faulting, *J. Geol. Soc. London, 143,* 349-353, 1986.

McKenzie, D., and J. Jackson, The kinematics and dynamics of distributed deformation, in *Paleomagnetic rotations and continental deformation*, C. Kissel and C. Laj (Eds.), pp. 17-31, NATO Series 254, 1989.

Menner, V. V., Y. P. Baranova, and L. S. Zhidkova, Neogene of the northeastern USSR (Kolyma Region, Kamchatka and Sakhalin), in *Proceedings of the first international congress of Pacific Neogene stratigraphy*, T. Saito and H. Ujiie (Eds.), pp. 82-88, Tokyo, 1977.

Molnar, P., Continental tectonics in the aftermath of plate tectonics, *Nature, 335,* 131-137, 1988.

Molnar, P., and J. Stock, Relative motions of hotspots in the Pacific, Atlantic and Indian Oceans since late Cretaceous time, *Nature, 327,* 587-591, 1987.

Molnar, P., and P. Tapponnier, Relation of the tectonics of eastern China to the India-Eurasia collision: Application of slip-line field theory to large-scale continental tectonics, *Geology, 5,* 212-216, 1977.

Moskowitz, B. M., R. B. Frankel, and D. A. Bazylinski, Rock magnetic criteria for the detection of biogenic magnetite, *Earth Planet. Sci. Lett., 120,* 283-300, 1993.

Moskowitz, B. M., M. Jackson, and C. Kissel, Low-temperature magnetic behavior of titanomagnetites, *Earth Planet. Sci. Lett., 157,* 141-149, 1998.

Nakamura, K., and S. Uyeda, Stress-gradient in arc-back arc regions and plate subduction, *J. Geophys. Res., 85,* 6419-6428, 1980.

Natal'in, B., History and modes of Mesozoic accretion in Southeastern Russia, *Island Arc, 2,* 15-34, 1993.

Néel, L., Some theoretical aspects of rock magnetism, *Adv. Phys., 4,* 191-242, 1955.

Nelson, M. R., and C. H. Jones, Paleomagnetism and crustal rotations along a shear zone, Las Vegas Range, southern Nevada, *Tectonics, 6,* 13-33, 1987.

Niitsuma, N., and F. Akiba, Neogene tectonic evolution and plate subduction in the Japanese island arcs, in *Formation of Active Ocean Margins*, N. Nasu et al. (Eds.), pp. 75-108, Terra Scientific Publishing Company, Tokyo, 1985.

Northrup, C.J., L. H. Royden, and B. C. Burchfiel, Motion of the Pacific plate relative to Eurasia and its potential relation to Cenozoic extension along the eastern margin of Eurasia, Geology 23, 719-722, 1995.

Norton, I. O., Plate motions in the North Pacific: The 43 Ma nonevent, *Tectonics, 14*, 1080-1094, 1995.

Nur, A., H. Ron, and O. Scotti, Mechanics of distributed fault and block rotation, in *Paleomagnetic rotations and continental deformation*, C. Kissel and C. Laj (Eds.), pp. 209-228, NATO Series 254, 1989.

Okamura, S., Y. A. Martynov, K. Furuyama, and K. Nagao, K-Ar ages of the basaltic rocks from far east Russia: Constraints on the tectono-magmatism associated with the Japan Sea opening, *Island Arc, 7*, 271-282, 1998.

Otofuji, Y., Large tectonic movement of the Japan Arc in late Cenozoic times inferred from paleomagnetism: Review and synthesis, *Island Arc, 5*, 229-249, 1996.

Otofuji, Y., T. Matsuda, and S. Nohda, Opening mode of the Japan Sea inferred from palaeomagnetism of the Japan Arc, *Nature, 317*, 603-604, 1985.

Otofuji, Y., T. Itaya, and T. Matsuda, Rapid rotation of southwest Japan – palaeomagnetism and K-Ar ages of Miocene volcanic rocks of southwest Japan, *Geophys. J. Int., 105*, 397-405, 1991.

Otofuji, Y., A. Kambara, T. Matsuda, and S. Nohda, Counterclockwise rotation of Northeast Japan: Paleomagnetic evidence for regional extent and timing of rotation, *Earth Planet. Sci. Lett., 121*, 503-518, 1994.

Özdemir, Ö., D. J. Dunlop, and B. M. Moskowitz, The effect of oxidation on the Verwey transition in magnetite, *Geophys. Res. Lett., 20,* 1671-1674, 1993.

Parés, J. M., B. A. Van der Pluijm, and J. Dinarès-Turell, Evolution of magnetic fabrics during incipient deformation of mudrocks (Pyrenees, northern Spain), *Tectonophysics, 307,* 1-14, 1999.

Parfenov, L.M., B. A. Natal'in, I. P. Voyanova, L. I. Popenko, Tectonic evolution of active continental margins along the northwestern margin of the Pacific Ocean (in Russian), Geotectonics 17, 466-477, 1981.

Parfenov, L. M., and B. A. Natal'in, Mesozoic tectonic evolution of northeastern Asia, *Tectonophysics, 127,* 291-304, 1986.

Pechersky, D. M., M. N. Shapiro, and Z. V. Sharonova, Palaeomagnetic study of the eastern Kamchatka Cretaceous-Palaeocene island arc: New evidence concerning palaeosubduction zone absolute motion, *Geophys. J. Int., 130,* 606-622, 1997.

Peltzer, G., and P. Tapponnier, Formation and evolution of strike-slip faults, rifts, and basins during the India-Asia collision: An experimental approach, *J. Geophys. Res., 93,* 15085-15117, 1988.

Pike, C. R., A. P. Roberts, and K. L. Verosub, Characterizing interactions in fine magnetic particle systems using first order reversal curves, *J. Appl. Phys., 85,* 6660-6667, 1999.

Pike, C. R., A. P. Roberts, and K. L. Verosub, First-order reversal curve diagrams and thermal relaxation effects in magnetic particles, *Geophys. J. Int., 145,* 721-730, 2001.

Piper, J. D. A., O. Tatar, and H. Gürsoy, Deformational behaviour of continental lithosphere deduced from block rotations across the North Anatolian fault zone in Turkey, *Earth Planet. Sci. Lett., 150,* 191-203, 1997.

Platt, J. P., Dynamics of orogenic wedges and the uplift of high-pressure metamorphic rocks, *Geol. Soc. Am. Bull., 97,* 1037-1053, 1986.

Ramsay, J. G., and R. J. Lisle, *The techniques of modern structural geology. Volume 3: Applications of continuum mechanics in structural geology,* 1061 pp., Academic Press, 2000.

Rees, A. I., and W. A. Woodall, The magnetic fabric of some laboratory-deposited sediments, *Earth Planet. Sci. Lett., 25,* 121-130, 1975.

Reynolds, R. L., R. S. Fishman, and M. R. Hudson, Sources of aeromagnetic anomalies over Cement oil field (Alaska), and the Wyoming-Idaho-Utah thrust belt, *Geophysics, 56,* 606-617, 1991.

Reynolds, R. L., M. B. Goldhaber, and M. L. Tuttle, Sulphidization and magnetization above hydrocarbon reservoirs, in: *Applications of paleomagnetism to sedimentary geology,* D. J. Aïssaoui, D. F. McNeil, and N. F. Hurley (Eds.), SEPM Spec. Publ., 49, 167-179, 1993.

Reynolds, R. L., M. L. Tuttle, C. A. Rice, N. S. Fishman, J. A. Karachewski, and D. M. Sherman, Magnetization and geochemistry of greigite-bearing Cretaceous strata, North Slope Basin, Alaska, Am. J. Sci., 294, 485-528, 1994.

Richards, M. A., and C. Lithgow-Bertelloni, Plate motion changes, the Hawaiian-Emperor bend, and apparent success and failure of geodynamic models, *Earth Planet. Sci. Lett., 137,* 19-27, 1996.

Richter, C., and B. A. Van der Pluijm, Separation of paramagnetic and ferrimagnetic susceptibilities using low temperature magnetic susceptibilities and comparison with high field methods, *Phys. Earth Planet. Inter., 82,* 113-123, 1994.

Richter, C., A. P. Roberts, J. S. Stoner, L. D. Benning, and C.T. Chi, Magnetostratigraphy of Pliocene-Pleistocene sediments from the eastern Mediterranean Sea, *Proc. ODP, Sci. Res., 160,* 61-74, 1998.

Rikhter, A.V., The structure, age and structural setting of the metamorphic rocks of Sakhalin (in Russian), Geotectonics 6, 55-65, 1984.

Riegel, S. A., K. Fujita, B. M. Koz'min, V. S. Imaev, and D. B. Cook, Extrusion tectonics of the Okhotsk Plate, northeast Asia, *Geophys. Res. Lett., 20,* 607-610, 1993.

Rikhter, A. V., The structure, age and structural setting of the metamorphic rocks of Sakhalin (in Russian), *Geotektonica, 6,* 55-65, 1984.

Roberts, A. P., Tectonic rotation about the termination of a major strike-slip fault, Marlborough fault system, New Zealand, *Geophys. Res. Lett., 22,* 187-190, 1995a.

Roberts, A. P., Magnetic properties of sedimentary greigite (Fe_3S_4), *Earth Planet. Sci. Lett., 134,* 227-236, 1995b.

Roberts, A. P., and G. M. Turner, Diagenetic formation of ferrimagnetic iron sulphide minerals in rapidly deposited marine sediments, South Island, New Zealand, *Earth Planet. Sci. Lett., 115,* 257-273, 1993.

Roberts, A. P., Y. Cui, and K. L. Verosub, Wasp-waisted hysteresis loops: Mineral magnetic characteristics and discrimination of components in mixed magnetic systems, *J. Geophys. Res., 100,* 17909,17924, 1995.

Roberts, A. P., R. L. Reynolds, K. L. Verosub, and D. P. Adam, Environmental magnetic implications of greigite (Fe_3S_4) formation in a 3 m.y. lake sediment record from Butte Valley, northern California, *Geophys. Res. Lett., 23,* 2859-2862, 1996.

Roberts, A. P., C. R. Pike, and K. L. Verosub, First-order reversal curve diagrams: A new tool for characterizing the magnetic properties of natural samples, *J. Geophys. Res., 105,* 28461-28475, 2000.

Rochette, P., Magnetic susceptibility of the rock matrix related to magnetic fabric studies, *J. Struct. Geol., 9,* 1015-1020, 1987.

Rochette, P., G. Fillion, J.-L. Mattéi, and M. J. Dekkers, Magnetic transition at 30-34 Kelvin in pyrrhotite: Insight into a widespread occurrence of this mineral in rocks, *Earth Planet. Sci. Lett., 98,* 319-328, 1990.

Rochette, P., M. Jackson, and C. Aubourg, Rock magnetism and the interpretation of anisotropy of magnetic susceptibility, *Rev. Geophys., 30,* 209-226, 1992.

Ron, H., R. Freund, Z. Garfunkel, and A. Nur, Block rotation by strike-slip faulting: Structural and paleomagnetic evidence, *J. Geophys. Res., 89,* 6256-6270, 1984.

Rozhdestvenskiy, V. S., The role of wrench-faults in the structure of Sakhalin, *Geotectonics, 16,* 323-332, 1982.

Sagnotti, L., and A. Winkler, Rock magnetism and palaeomagnetism of greigite-bearing mudstones in the Italian peninsula, *Earth Planet. Sci. Lett., 165,* 67-80, 1999.

Sagnotti, L., C. Faccenna, R. Funicello, and M. Mattei, Magnetic fabric and structural setting of Plio-Pleistocene clayey units in an extensional regime: The Tyrrhenian margin of central Italy, *J. Struct. Geol., 16,* 1243-1257, 1994.

Sagnotti, L., A. Winkler, P. Montone, L. Di Bella, F. Florindo, M. T. Mariucci, F. Marra, L. Alfonsi, and A. Frepoli, Magnetic anisotropy of Plio-Pleistocene sediments from the Adriatic margin of the northern Apennines (Italy): Implications for the time-space evolution of the stress field, *Tectonophysics, 311,* 139-153,1999.

San'kov, V., J. Déverchère, Y. Gaudemer, F. Houdry, and A. Filippov, Geometry and rate of faulting in the North Baikal Rift, Siberia, *Tectonics, 19,* 707-722, 2000.

Savostin, L., L. Zonenshain, and B. Baranov, Geology and plate tectonics of the Sea of Okhotsk, in *Geodynamics of the western Pacific-Indonesian region,* T. W. C. Hilde and S. Uyeda (Eds.), *AGU Geodynamic Series, 11,* 189-221, Washington, D. C., 1983.

Sellés-Martínez, J., Concretion morphology, classification and genesis, *Earth Sci. Rev., 41,* 177-210, 1996.

Seno, T., Is northern Honshu a microplate?, *Tectonophysics, 115,* 177-196, 1985.

Seno, T., T. Sakurai, and S. Stein, Can the Okhotsk plate be distinguished from the North American plate?, *J. Geophys. Res., 101*, 11305-11315, 1996.

Serova, M. Y., and L. M. Fot'yanova, Paleogene-Neogene boundary in heterofacieal deposits of Sakhalin and Kamchatka, in *Monographic proceedings of IGCP-114 International workshop on Pacific Neogene biostratigraphy*, N. Ikebe (Ed.), pp. 135-136, 1981.

Sheriff, R. E., and L. P. Geldart, *Exploration Seismology (2nd ed.)*, 592 pp., Cambridge University Press, 1995.

Snowball, I. F., Magnetic hysteresis properties of greigite (Fe_3S_4) and a new occurrence in Holocene sediments from Swedish Lappland, *Phys. Earth Planet. Inter., 68,* 32-40, 1991.

Snowball, I. F., and R. Thompson, A stable chemical remanence in Holocene sediments, *J. Geophys. Res., 95,* 4471-4479, 1990.

Sonder, L. J., and P. C. England, Vertical averages of rheology of the continental lithosphere: Relation to thin sheet parameters, *Earth Planet. Sci. Lett., 77,* 81-90, 1986.

Sonder, L. J., P. C. England, and G. A. Houseman, Continuum calculations of continental deformation in transcurrent environments, *J. Geophys. Res., 91,* 4797-4810, 1986.

Stumm, W., and J. J. Morgan, *Aquatic Chemistry (2nd ed.),* 780 pp., Wiley and Sons,.1981.

Sweeney, R. E., and I. R. Kaplan, Pyrite framboid formation: Laboratory synthesis and marine sediments, *Econ. Geol., 68,* 618-634, 1973.

Takahashi, H., M. Kasahara, F. Kimata, S. Miura, K. Heki, T. Seno, T. Kato, N. Vasilenko, A. Ivashchenko, V. Bahtiarov, V. Levin, E. Gordeev, F. Korchagin, and M. Gerasimenko, Velocity field of around the Sea of Okhotsk and Sea of Japan regions determined from a new continuous GPS network data, *Geophys. Res. Lett., 26,* 2533-2536, 1999.

Takeuchi, T., K-Ar ages of the Tertiary volcanic rocks in South Sakhalin and their tectonic significance (in Japanese), *J. Geol. Soc. Japan, 103,* 67-79, 1997.

Takeuchi, T., K. Kodama, and T. Ozawa, Paleomagnetic evidence for block rotations in central Hokkaido-south Sakhalin, Northeast Asia, *Earth Planet. Sci. Lett., 169,* 7-21, 1999.

Tamaki, K., K. Suyehiro, J. Allan, J. C. Ingle, and K. Pisciotto, Tectonic synthesis and implications of Japan Sea ODP drilling, *Proc. ODP Sci. Res., 127-128,* 1333-1350, 1992.

Tan, X., and K. P. Kodama, Compaction-corrected inclinations from southern California Cretaceous marine sedimentary rocks indicate no paleolatitudinal offset for the Peninsular Ranges terrane, *J. Geophys. Res., 103*, 27169-27192, 1998.

Tapponnier, P., and P. Molnar, Slip-line field theory and large-scale continental tectonics, *Nature, 264,* 319-324,1976.

Tapponnier, P., and P. Molnar, Active faulting and tectonics in China, *J. Geophys. Res., 82,* 2905-2930, 1977.

Tapponnier, P., and P. Molnar, Active faulting and Cenozoic tectonics of the Tien Shan, Mongolia, and Baykal regions, *J. Geophys. Res., 84,* 3425-3459, 1979.

Tapponnier, P., G. Peltzer, A. Y. Le Dain, R. Armijo, and P. Cobbold, Propagating extrusion tectonics in Asia: New insights from simple experiments with plasticine, *Geology, 10*, 611-616, 1982.

Tapponnier, P., G. Peltzer, and R. Armijo, On the mechanics of the collision between India and Asia, in *Collision tectonics*, M. P. Coward and A. C. Ries (Eds.), *Geol. Soc. London. Spec. Publ., 19,* 115-157, 1986.

Tarduno, J. A., and R. D. Cottrell, Paleomagnetic evidence for motion of the Hawaiian hotspot during formation of the Emperor seamounts, *Earth Planet. Sci. Lett., 153*, 171-180, 1997.

Tauxe, L., *Paleomagnetic Principles and Practice,* Kluwer Academic, 299 pp., 1998.

Tauxe, L., and G. Watson, The fold test: An eigen analysis approach, *Earth Planet. Sci. Lett., 122*, 331-341, 1994.

Tauxe, L., C. G. Constable, L. Stokking, and C. Badgley, Use of anisotropy to determine the origin of characteristic remanence in the Siwalik red beds of northern Pakistan, *J. Geophys. Res., 95*, 4391-4404, 1990.

Tauxe, L., N. Kylstra, and C. Constable, Bootstrap statistics for paleomagnetic data, *J. Geophys. Res., 96*, 11723-11740, 1991.

Tauxe, L., T. Mullender, and T. Pick, Potbellies, wasp-waists, and superparamagnetism in magnetic hysteresis, *J. Geophys. Res., 101,* 571-583, 1996.

Taymaz, T., J. Jackson, and D. McKenzie, Active tectonics of the north and central Aegean Sea, *Geophys. J. Int., 106,* 433-490, 1991.

Thompson, R., and T. J. D. Cameron, Palaeomagnetic study of Cenozoic sediments in North Sea boreholes: An example of a magnetostratigraphic conundrum in a hydrocarbon-producing area, in *Palaeomagnetic applications in hydrocarbon exploration,* P. Turner and A. Turner (Eds.), *Geol. Soc. London Spec. Publ., 98,* 223-236, 1995.

Torii, M., K. Fukuma, C.-S. Horng, and T.-Q. Lee, Magnetic discrimination of pyrrhotite- and greigite-bearing sediment samples, *Geophys. Res. Lett., 23,* 1813-1816, 1996.

Townsend, D. B., and T. A. Little, Pliocene-Quaternary deformation and mechanisms of near-surface strain close to the eastern tip of the Clarence Fault, northeast Marlborough, *N. Z. J. Geol. Geophys., 41,* 401-417, 1998.

Tric, E., C. Laj, C. Jehanno, J.-P. Valet, C. Kissel, A. Mazaud, and S. Iaccarino, High-resolution record of the Upper Olduvai transition from Po Valley (Italy) sediments: Support for dipolar transition geometry?, *Phys. Earth Planet. Inter., 65,* 319-336, 1991.

Twiss, R. J., and E. M. Moores, *Structural Geology*, Freeman and Co., New York, 532 pp., 1992.

Urbat, M., M. J. Dekkers, and K. Krumsiek, Discharge of hydrothermal fluids through sediment at the Escanaba Trough, Gorda Ridge (ODP Leg 169): Assessing the effects on the rock magnetic signal, *Earth Planet. Sci. Lett., 176,* 481-494, 2000.

Uyeda, S., Subduction zones: An introduction to comparative subductology, *Tectonophysics, 81,* 133-159, 1982.

Van der Voo, R., *Paleomagnetism of the Atlantic, Tethys and Iapetus oceans,* Cambridge Univesity Press, 411 pp., 1993.

Van der Voo, R., W. Spakman, and H. Bijwaard, Mesozoic subducted slabs under Siberia, *Nature, 397,* 246-249, 1999.

Varnavskiy, V.G., A. K. Sedykh, and V. I. Rybalko, The Paleogene and Neogene of Priamur'ye and Primor'ye (in Russian), Far Eastern Division, Russian Academy of Sciences, Vladivostok, 183 pp., 1990.

Vereshchagin, V. N., Geological map of Sakhalin, *Ministry of geology of the USSR*, 1969.

Verosub, K. L., Depositional and post-depositional processes in the magnetization of sediments, *Rev. Geophys. Space Phys., 15,* 129-143, 1977.

Verosub, K. L., and A. P. Roberts, Environmental magnetism: Past, present, and future, *J. Geophys. Res., 100,* 2175-2192, 1995.

Voronova, L., and J. Wardell, The Paleogene and Neogene Geology of Sakhalin, in *CASP Soviet Arctic Stratigraphic Series, 499*, 150 pp., unpublished, 1991.

Watson, G. S., A test for randomness, *Mon. Not. Roy. Astr. Soc., 7*, 160-161, 1956.

Watson, M. P., A. B. Hayward, D. N. Parkinson, and Zh. M. Zhang, Plate tectonic history, basin development and petroleum source rock deposition onshore China, *Marine Petrol. Geol., 4*, 205-225, 1987.

Weaver, R., A. P. Roberts, and A. J. Barker, A late diagenetic (synfolding) magnetization carried by pyrrhotite: Implications for paleomagnetic studies from magnetic iron sulphide-bearing sediments, *Earth Planet. Sci. Lett.,* 200, 371-386, 2002.

Weaver, R., A. P. Roberts, R. Flecker, D. I. M. Macdonald, and L. M. Fot'yanova, Geodynamic implications of paleomagnetic data from Tertiary sediments in Sakhalin, Russia (NW Pacific), *J. Geophys. Res.,* 108, 2066, doi: 10.1029/ 2001JB001226, 2003.

Wilkin, R. T., and H. L. Barnes, Formation processes of framboidal pyrite, *Geochim. Cosmochim. Acta, 61,* 323-339, 1997.

Worrall, D. M., V. Krugliak, F. Kunst, and V. Kuznetsov, Tertiary tectonics of the Sea of Okhotsk, Russia: Far-field effects of the India-Eurasia collision, *Tectonics, 15*, 813-826, 1996.

Xu, W., R. Van der Voo, and D. Peacor, Electron microscopic and rock magnetic study of remagnetized Leadville carbonates, central Colorado, *Tectonophysics, 296,* 333-362, 1998.

Yin, A., and M. T. Harrison, Geologic evolution of the Himalayan-Tibeten orogen, *Ann. Rev. Earth Planet. Sci., 28,* 211-280, 2000.

Zhidkova, L. S., and B. A. Sal'nikov, Reference section of Paleogene-Neogene deposits of south-east Sakhalin (Makarov section), *VNIGRI*, St. Petersburg, 1992.

Zijderveld, J. D. A., A.C. demagnetization of rocks: Analysis of results, in *Methods in Palaeomagnetism,* D. W. Collinson, K. M. Creer, and S. K. Runcorn (Eds.), Elevier, Amsterdam, pp. 254-286, 1967.

Zonenshain, L. P., and L. A. Savostin, Geodynamics of the Baikal rift zone and plate tectonics of Asia, *Tectonophysics, 76,* 1-45, 1981.

Zonenshain, L. P., and M. I. Kuzmin, *Paleogeodynamics. The Plate Tectonic Evolution of the Earth (English ed.),* V. G. Kazmin, W. Harbert, and B. M. Page (Eds.), American Geophysical Union, Washington, D. C., 218 pp., 1997.

Zonenshain, L. P., M. V. Kononov, and L. A. Savostin, Pacific and Kula/Eurasia relative motions during the last 130 Ma and their bearing on orogenesis in northeast Asia, in *Circum-Pacific orogenic belts and evolution of the Pacific Ocean basin,* J. W. H. Monger and J. Franchteau (Eds.), *AGU Geodynamic Series, 18,* 29-47, Washington, D. C. 1987.

Zonenshain, L. P., M. I. Kuz'min, and L. V. Natapov, Geology of the USSR: A plate tectonic synthesis, in *AGU Geodynamic Series, 21,* B. M. Page (Ed.), 242 pp., Washington, D. C., 1990.

Zyabrev, V.S., Mesozoic geological evolution of the West Sakhalin Trough, in *CASP Arctic and Russian Series, 635,* D. I. M. Macdonald and J. C. Stewart (Eds.), 182 pp., unpublished, 1996.

Zyabrev, V.S., and N. Y. Bragin, Deep water terrigenous sedimentation in the West Sakhalin Trough, *Dokl. Akad. Nauk SSSR, 292*, 168-171, 1987.

Appendix A

A1. Paleomagnetic Data from Remagnetized Localities

Paleomagnetically stable, normal polarity ChRMs, which have probably resulted from remagnetization, were observed at 9 localities in Sakhalin (Table A1.1; Figure B1.2). Close agreement of the paleomagnetic mean directions before tilt correction (geographic coordinates) with either the present-day internationl geomagnetic reference field (IGRF) or the expected (Bruhns Chron) geocentric axial dipole (GAD) field suggests that remagnetization has occurred (Table A1.1). Tilt-corrected directions are often in disagreement with unremagnetized paleomagnetic directions obtained from samples collected elsewhere in Sakhalin.

A1.1.Korsakov

The uncorrected data from Korsakov have a mean direction of D_m = 350.0°, I_m = 57.7°, with η_{95} = 3.0° and ζ_{95} = 6.4° (Figure A1.1), which is in excellent agreement with the present-day field direction (Table A1.1). The mean paleomagnetic direction is different from the expected GAD field at the 95% significance level [*Tauxe,* 1998]. In stratigraphic coordinates, two separate groups of paleomagnetic directions are observed (Figure A1.1b). The two groups correspond to samples from each limb of a tight anticline. This observation provides strong evidence for remagnetization at this locality.

A1.2. Tunaicha Coast

A paleomagnetic mean direction of D_m = 2.9°, I_m = 70.5°, with α_{95} = 6.2°, in geographic coordinates is similar to the IGRF or GAD field (Figure A1.2, Table A1.1). Statistical comparison of the directions [c.f. *Tauxe,* 1998] indicates that the uncorrected mean paleomagnetic direction is significantly different from the IGRF direction, but that it cannot be distinguished from the expected GAD field direction. The tilt-corrected paleomagnetic direction indicates ~60° of counterclockwise deflection of the declination from the expected GAD direction. Significant counterclockwise-deflected declinations

have not been observed elsewhere in Sakhalin, which, along with better clustering of directions that are indistinguishable from the expected GAD direction prior to tilt-correction, supports the interpretation these rocks have been remagnetized.

A1.3. Ilinskiy Coast

Uncorrected ChRM directions from the Ilinskiy Coast cluster tightly with D_m = 356.4°, I_m = 65.5°, and α_{95} = 2.8° (Figure A1.3). The mean direction is in excellent agreement with the GAD field (Table A1.1). The tilt-corrected direction is anomalously shallow relative to Miocene data from elsewhere in Sakhalin (Figure A1.3b, Table 3.2). Only normal polarity directions were obtained from the samples, which were collected at 1-2 m intervals over a 30-m-thick late Miocene stratigraphic sequence. The evidence suggests that samples were remagnetized after folding.

A1.4. Kormovaya River

Paleomagnetic data from Kormovaya River (in geographic coordinates) cannot be distinguished from either the IGRF or the GAD field at the 95% significance level (Table A1.1). The uncorrected mean direction is D_m = 7.7°, I_m = 61.8°, with η_{95} = 6.3° and ζ_{95} = 9.7° (Figure A1.4). The tilt-corrected mean direction has a larger uncertainty than the uncorrected direction and it has a significantly shallower inclination than the Miocene GAD field observed elsewhere in Sakhalin (Figure A1.4b, Table 3.2).

A1.5. Shakhtnaya River

Analysis of ChRM directions in geographic coordinates suggests that mid-late Miocene rocks from Shakhtnaya River have been remagnetized in the present-day field (Table A1.1). The paleomagnetic mean direction (before tilt correction), D_m = 354.7°, I_m = 58.3°, with η_{95} = 3.8° and ζ_{95} = 7.6° (Figure A1.5a), is not significantly different from the GAD field, but agreement with the IGRF is much better (Table A1.1) [*Tauxe,* 1998].

The tilt-corrected direction has an anomalously shallow inclination value (Figure A1.5b). These observations suggest that the samples from Shakhtnaya River are remagnetized.

A1.6. Chamgu River

The mean paleomagnetic direction obtained before tilt correction from the mid-Miocene Khuzin Suite at Chamgu River is $D_m = 343.1°$, $I_m = 70.2°$, with $\eta_{95} = 2.4°$ and $\zeta_{95} = 3.6°$ (Figure A1.6). At the 95% significance level, the mean direction is consistent with either the IGRF or the GAD field, but agreement is better with the GAD field (Table A1.1). The tilt-corrected direction is $D_m = 7.0°$, $I_m = 68.7°$, with $\eta_{95} = 2.4°$ and $\zeta_{95} = 3.5°$ (Figure A1.6b). Because of the shallow dip of the sampled beds, it is difficult to determine whether the tilt-corrected direction represents a primary magnetic signal. However, tightly clustered normal polarity directions ($\eta_{95} = 2.4°$ and $\zeta_{95} = 3.5°$) suggest that remagnetization might have occurred after folding.

A1.7. North Piltun

Mudstone samples from North Piltun a uniformly dipping sequence and yield paleomagnetic data with a mean direction that indicates remagnetizaiton due to either the IGRF or a GAD field at the site latitude (Figure A1.7, Table A1.1). The mean direction before tilt correction is $D_m = 346.1°$, $I_m = 66.5°$, with $\eta_{95} = 5.9°$ and $\zeta_{95} = 7.8°$. The tilt-corrected direction ($D_m = 68.9°$) is incompatible with paleomagnetic data from elsewhere in Sakhalin (Table 4.2).

A mud dyke, which intruded the overlying sands of the Nutovsk Suite, yielded similar paleomagnetic data with a mean direction in geographic coordinates of $D_m = 334.4°$, $I_m = 62.1°$, with $\alpha_{95} = 6.7°$ (Figure A1.8). The dyke is interpreted to have intruded as a result of recent earthquake activity. At North Piltun, the overall statistical agreement is best with the IGRF direction (Table A1.1). Remagnetization of sediments in this region is probably related to recent earthquakes.

A1.8. Sabo-Nogliki Quarry

Late Miocene mudstones of the Nutovsk Suite reveal a paleomagnetic mean direction before tilt correction of D_m = 355.0°, I_m = 62.0°, with η_{95} = 4.0° and ζ_{95} = 8.6° (Figure A1.9). This direction agrees well with the IGRF direction and can be discriminated from the GAD field direction at the 95% significance level (Table A1.1) [*Tauxe,* 1998]. The tilt-corrected inclination value is shallower than the expected GAD field direction and the dispersion around the mean is greater than in geographic coordinates (Figure A1.9). Remagnetization appears to have occurred in the present-day geomagnetic field.

A1.9. Summary

Paleomagnetic data demonstrate that remagnetization has probably taken place at the above-described 9 localities in Sakhalin. Post-folding remagnetization in the presence of the IGRF appears to have affected lower Nutovsk Suite mudstones, probably in association with local deformation due to recent earthquakes. At Korsakov and Ilinskiy Coast, a post-folding remagnetization in a GAD field (probably Brunhes Chron) is likely. At the remaining localities it was not possible to determine whether the post-folding paleomagnetic directions were acquired due to exposure in the present-day geomagnetic field or to a time-averaged normal polarity GAD field.

Improved constraints on the timing of the remagnetization may be possible in future by obtaining samples from sites with contrasting bedding attitudes in order to carry out field tests. The acquisition mechanisms for the observed secondary magnetizations may be established through detailed rock magnetic measurements and mineralogical work. Such work was beyond the scope of the present study, which was aimed at using reliable paleomagnetic directions to decipher the regional tectonic history.

Table A1.1. Remagnetized paleomagnetic data from Tertiary rocks, Sakhalin

Locality	Age	Suite Name	Average Bedding Dip (°)/Strike (°)	Lat.	Long.	Pol.	n	D_m	I_m	α_{95}	k	Fshr?	η_{95}	ζ_{95}	D_m	I_m	α_{95}	k	Fshr?	η_{95}	ζ_{95}	IGRF field* D	IGRF field* I	GAD** I
	(Ma)			(°)	(°)			(°)	(°)	(°)			(°)	(°)	(°)	(°)	(°)			(°)	(°)	(°)	(°)	(°)
								Geographic coordinates							*Stratigraphic coordinates*									
Korsakov	22-18	Kholmsk		46.6	142.8	N	22	350.0	57.7	-	37	No	3.0	6.4	-	-	-	-	-	-	-	349.8	60.7	64.7
			60 NW 202	46.6	142.8	N	7	-	-	-	-	-	-	-	309.6	22.2	4.5	181	Yes	-	-	349.8	60.7	64.7
			80 NW/226***	46.6	142.8	N	15	-	-	-	-	-	-	-	114.0	23.3	4.4	77	Yes	-	-	349.8	60.7	64.7
Tunaicha Coast	22-18	Kholmsk	30 W/163	46.9	143.2	N	7	2.9	70.5	6.2	94	Yes	-	-	302.8	61.9	8.3	54	Yes	-	-	349.8	61	64.9
Il'inskiy Coast	15-9	Kurasiy	36 NE/317	47.9	142.1	N	26	356.4	65.5	2.8	105	Yes	-	-	23.4	34.7	2.8	105	Yes	-	-	349.3	62.1	65.7
Kormovaya River	14-6	Kurasiy-L. Maruyam	65 E/357	48.7	142.7	N	19	7.7	61.8	-	16	No	6.3	9.7	49.7	40.1	10.5	11	Yes	-	-	349.1	62.8	66.3
Shakhtnaya River	17-8	Sertunay-Kurasiy	65 E/005	48.8	142.8	N	25	354.7	58.3	-	24	No	3.8	7.6	54.2	24.4	4.8	37	Yes	-	-	349.1	62.9	66.4
Chamgu River	13-8	Khuzin	10 NE/348	50.9	143.5	N	36	343.1	70.2	-	61	No	2.4	3.6	7.0	68.7	-	64	No	2.4	3.5	348.6	64.7	67.9
North Piltun	11-5	Lower Nutovsk	34 SE/030	52.8	143.1	N	15	346.1	66.5	-	28	No	5.9	7.8	68.9	67.3	-	32	No	5.8	7.3	347.9	66.5	69.2
North Piltun Mud Dyke	11-5	Lower Nutovsk	34 SE/030	52.8	143.1	N	12	334.4	62.1	6.7	44	Yes	-	-	39.2	71.4	7.3	37	Yes	-	-	347.9	66.5	69.2
Sabo-Nogliki Quarry	11-5	Lower Nutovsk	36 E/009	53.1	143.0	N	13	355.0	62.0	-	34	No	4.0	8.6	27.2	47.7	9.1	22	Yes	-	-	347.8	66.8	69.4

* Determined from the revised IGRF model for the period 1995-2000 [*Barton*, 1996].

** The unrotated geocentric axial dipole (GAD) declination is D = 0° or D = 180°.

*** Overturned bedding.

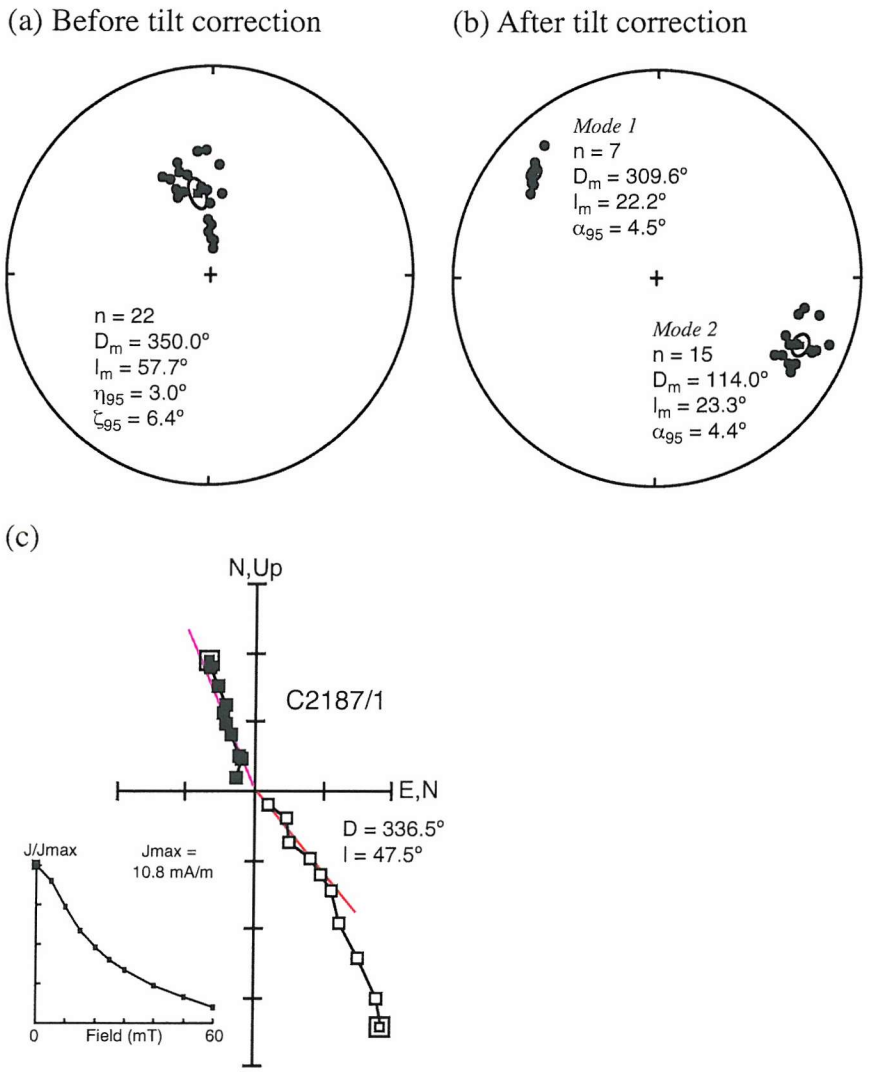

Figure A1.1. Paleomagnetic data from the Kholmsk suite, Korsakov, Sakhalin. Equal area stereographic projections (lower hemisphere) show the mean (solid square) paleomagnetic direction: (a) before tilt correction, and (b) after tilt correction. (D_m = mean declination; I_m = mean inclination; n = number of stably magnetized samples). Ellipses represent the 95% confidence limits defined by α_{95} [*Fisher,* 1953] or by η_{95} and ζ_{95} [*Tauxe et al.,* 1991]. Solid symbols indicate lower hemisphere projections (normal polarity). (c) Vector component plot for a representative sample (C2187/1) before tilt correction. Lines represent the best-fit to the ChRM vector [*Kirschvink,* 1980]. Data are projected onto the vertical plane (open symbols = inclinations) and the horizontal plane (solid symbols = declinations).

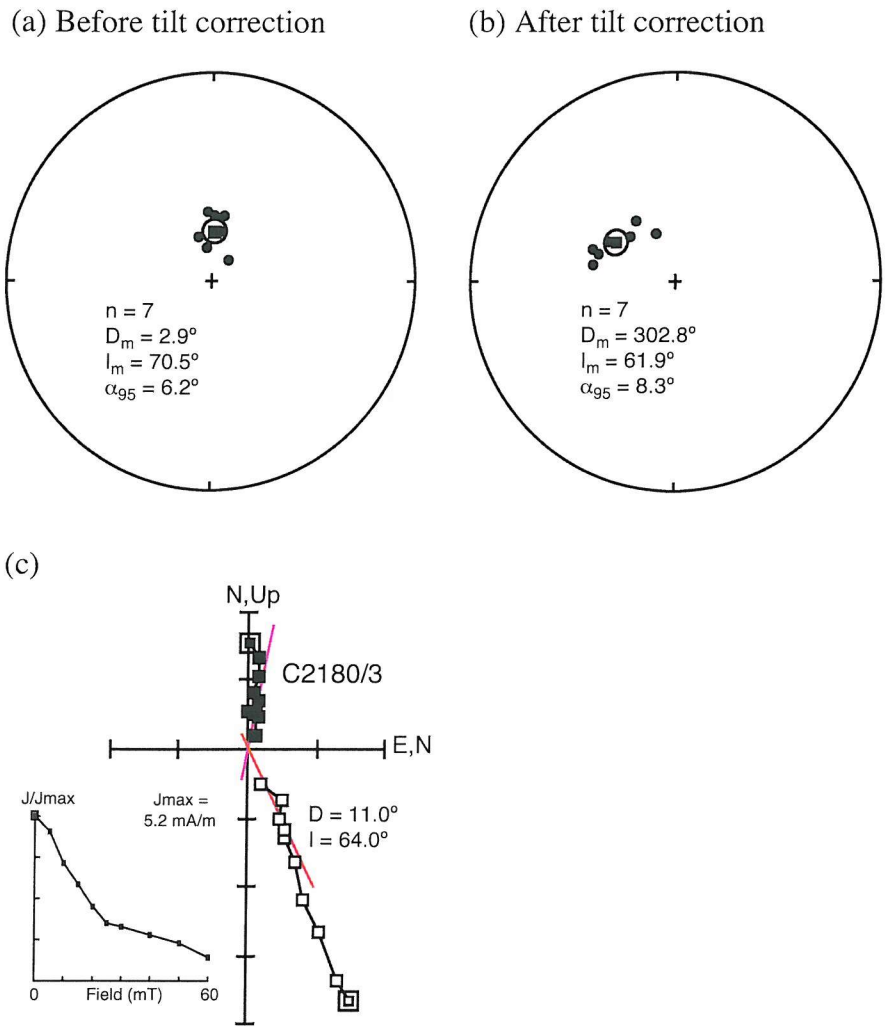

Figure A1.2. Paleomagnetic data from the Kholmsk suite, Tunaicha, Sakhalin. Equal area stereographic projections (lower hemisphere) show the mean paleomagnetic direction: (a) before tilt correction, and (b) after tilt correction. (c) Vector component plot for a representative sample (C2180/3). Conventions are the same as used in Figure A1.1.

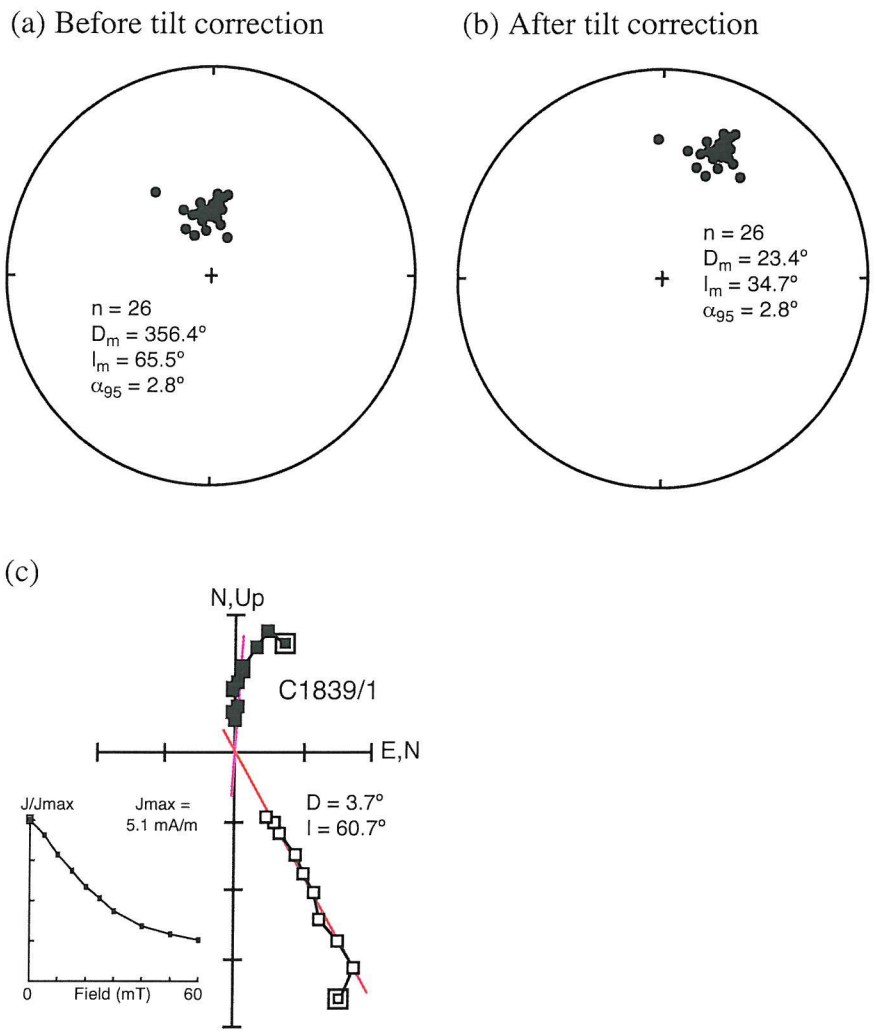

Figure A1.3. Paleomagnetic data from the Kurasiy suite, Il'inskiy, Sakhalin. Equal area stereographic projections (lower hemisphere) show the mean paleomagnetic direction: (a) before tilt correction, and (b) after tilt correction. (c) Vector component plot for a representative sample (C1839/1). Conventions are the same as used in Figure A1.1.

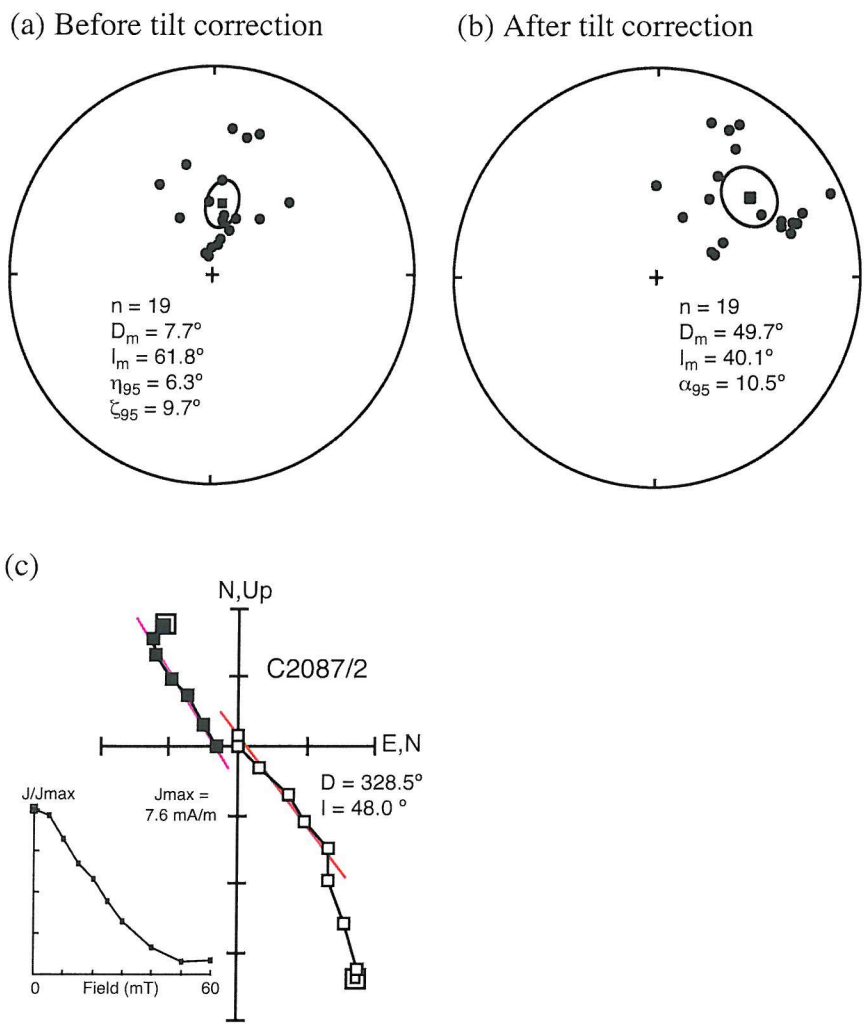

Figure A1.4. Paleomagnetic data from the Kurasiy suite to the lower Maruyama suite, Kormovaya River, Sakhalin. Equal area stereographic projections (lower hemisphere) show the mean paleomagnetic direction: (a) before tilt correction, and (b) after tilt correction. (c) Vector component plot for a representative sample (C2087/2). Conventions are the same as used in Figure A1.1.

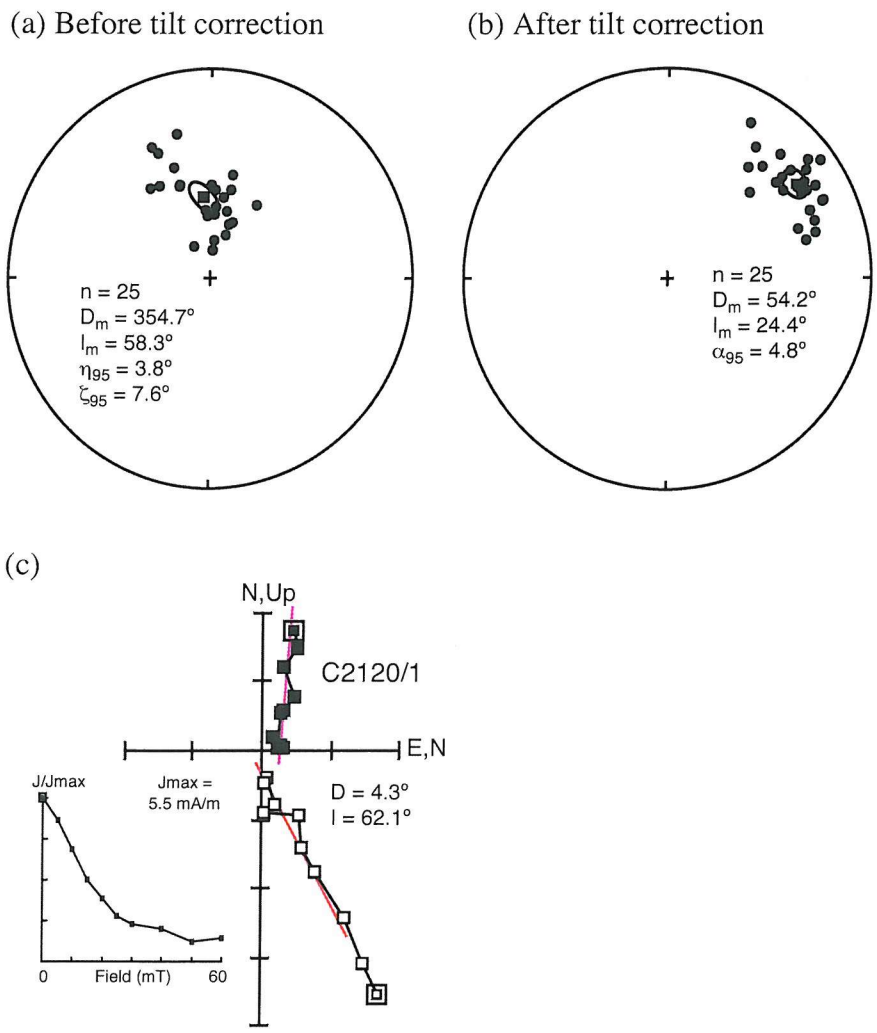

Figure A1.5. Paleomagnetic data from the Sertunay suite to the Kurasiy suite, Shakhtnaya River, Sakhalin. Equal area stereographic projections (lower hemisphere) show the mean paleomagnetic direction: (a) before tilt correction, and (b) after tilt correction. (c) Vector component plot for a representative sample (C2120/1). Conventions are the same as used in Figure A1.1.

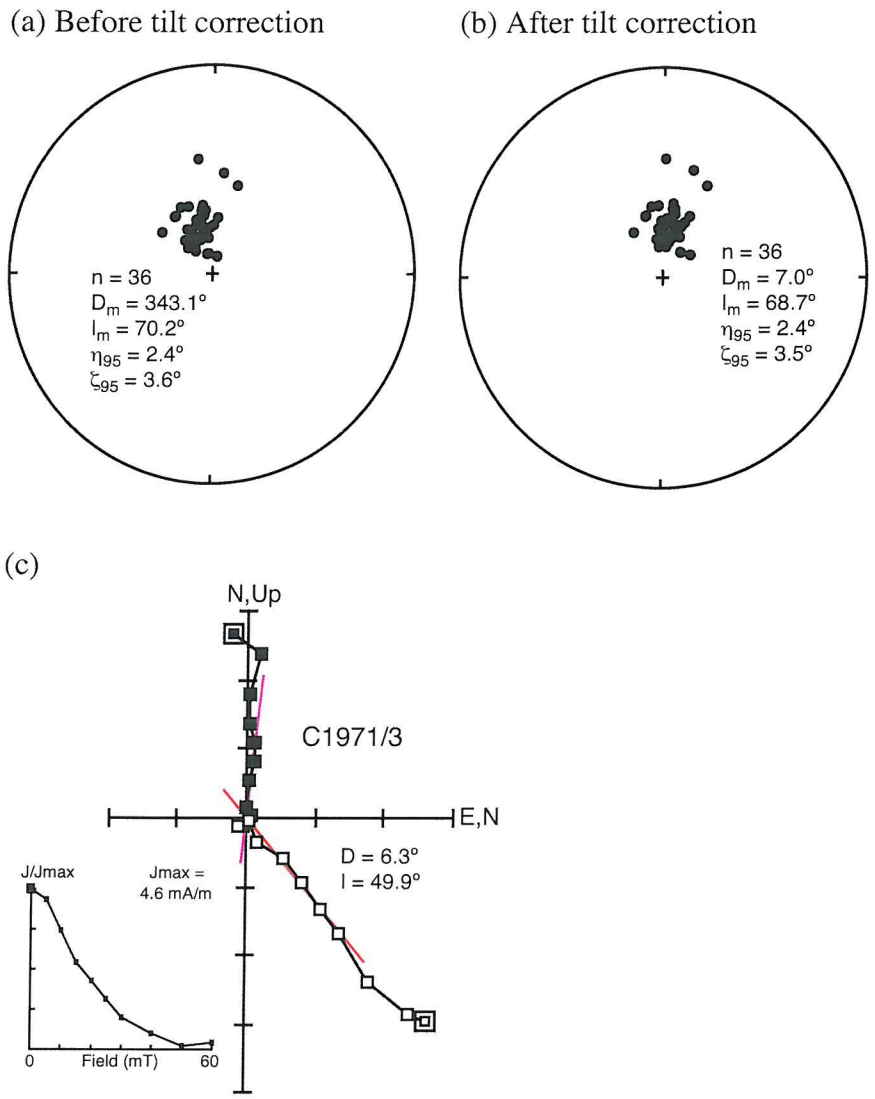

Figure A1.6. Paleomagnetic data from the Khuzin suite, Chamgu, Sakhalin. Equal area stereographic projections (lower hemisphere) show the mean paleomagnetic direction: (a) before tilt correction, and (b) after tilt correction. (c) Vector component plot for a representative sample (C1971/3). Conventions are the same as used in Figure A1.1.

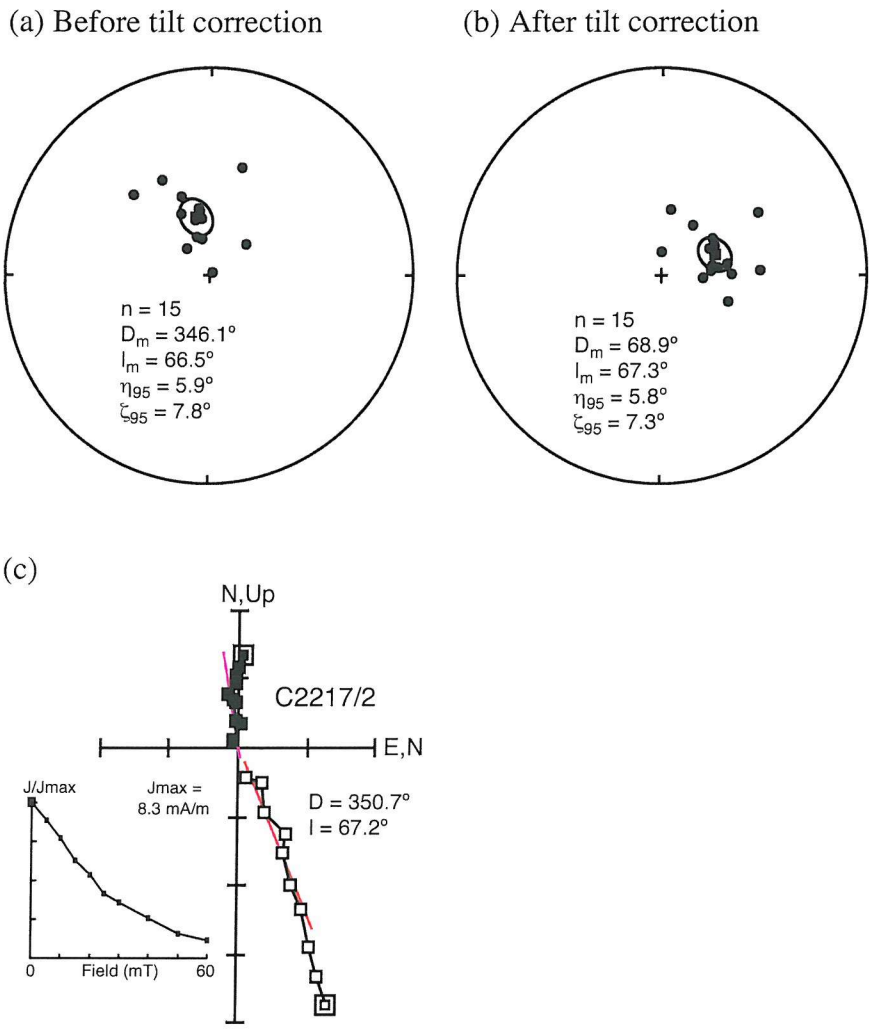

Figure A1.7. Paleomagnetic data from the lower Nutovsk suite, North Piltun, Sakhalin. Equal area stereographic projections (lower hemisphere) show the mean paleomagnetic direction: (a) before tilt correction, and (b) after tilt correction. (c) Vector component plot for a representative sample (C2217/2). Conventions are the same as used in Figure A1.1.

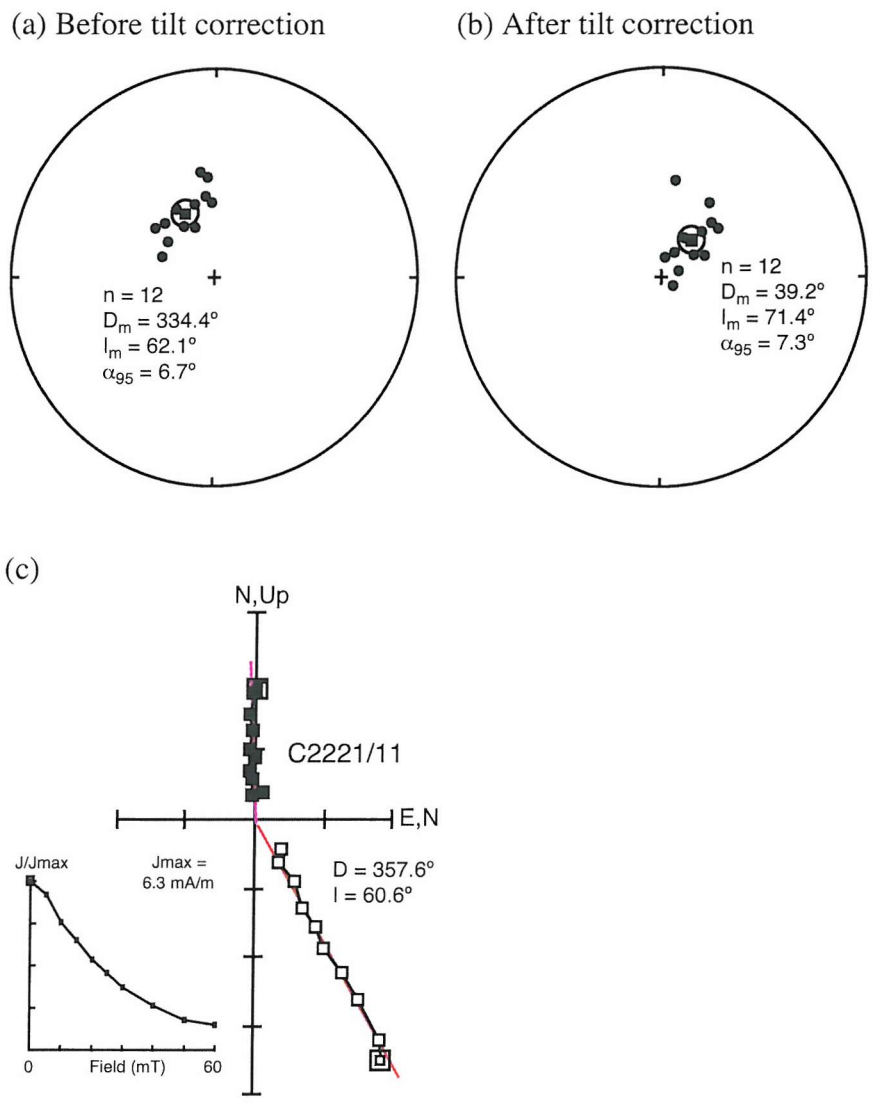

Figure A1.8. Paleomagnetic data from a mud dyke in the lower Nutovsk suite, North Piltun, Sakhalin. Equal area stereographic projections (lower hemisphere) show the mean paleomagnetic direction: (a) before tilt correction, and (b) after tilt correction. (c) Vector component plot for a representative sample (C2221/11). Conventions are the same as used in Figure A1.1.

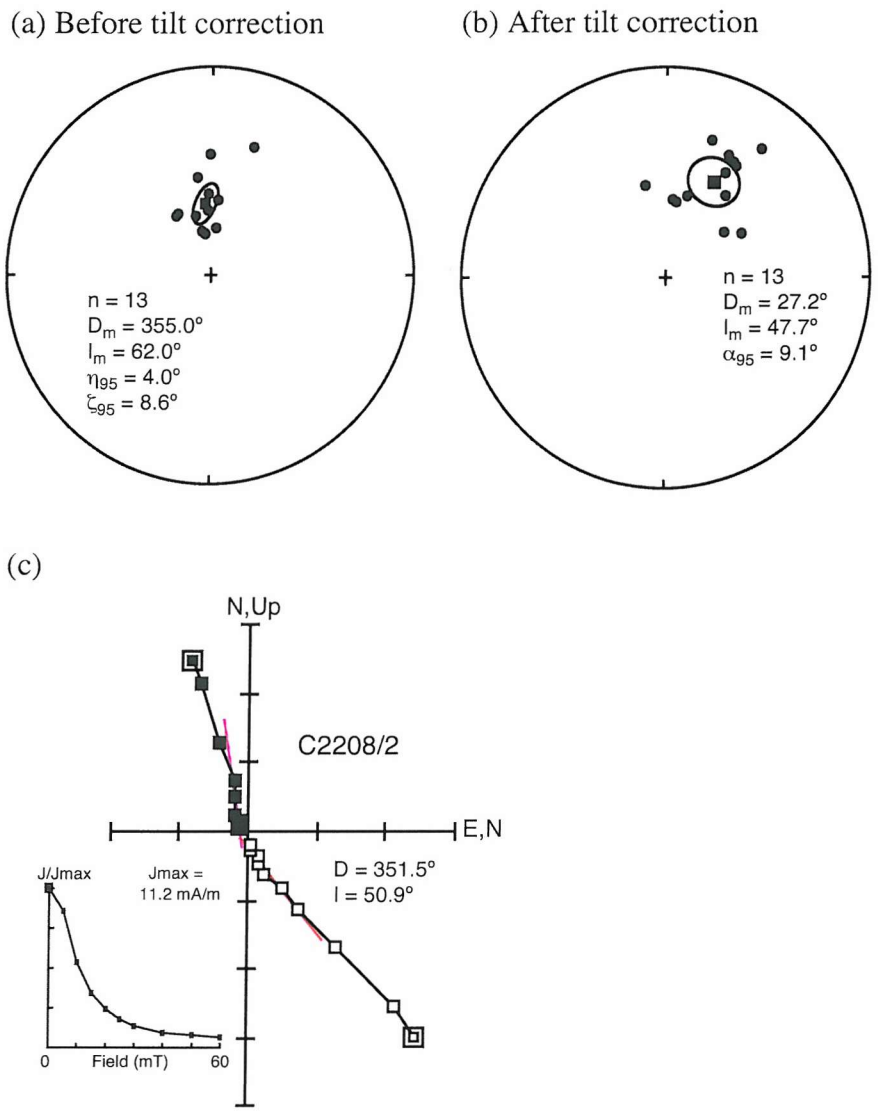

Figure A1.9. Paleomagnetic data from the Nutovsk suite, Sabo and Nogliki quarry, Sakhalin. Equal area stereographic projections (lower hemisphere) show the mean paleomagnetic direction: (a) before tilt correction, and (b) after tilt correction. (c) Vector component plot for a representative sample (C2208/2). Conventions are the same as used in Figure A1.1.

Appendix B

B1. Unstable Paleomagnetic Data

Paleomagnetic samples from 8 localities in Sakhalin failed to yield useful paleomagnetic data because they are either dominated by multi-domain (MD) magnetic minerals or have low NRM intensity values. For the purpose of reference, the typical paleomagnetic behaviour is shown in Figure B1.1. Figure B1.2 shows the stable, remagnetized, and unstable paleomagnetic sampling localities in Sakhalin. Table B1.1 gives details of the paleomagnetic stability and lithology of the sampling localities in Sakhalin.

Table B1.1. Lithology and NRM characteristics of paleomagnetic sampling localities in Sakhalin

Locality	Lat. (°)	Long. (°)	Suite	Age (Ma)	Lithology and Environment	Sample Colour	Average Bedding Dip (°)/Strike(°)	NRM Stability	ChRM polarity
SOUTH SAKHALIN									
Kitosiya River	46.4	141.9	Sinegorian Beds	64-60	lagoonal/brackish mudstone and siltstone, intermitt ‹ marine sandstone , coal	brown-grey	31 W/187	stable	R+N
Kamenitskiy Stream	46.6	141.9	Kurasiy	15-9	marine very fine silty sandstone and siliceous siltst o carbonate concretions	dark blue-grey	52 W/150°	unstable	undefined
Korsakov	46.6	142.8	Kholmsk	22-18	shallow marine siliceous siltstone, mudstone, an c sandstone with silt/mud laminations	mid-grey and green grey	80 NW/176	remagnetized	N
Okhta River	46.9	142.0	Lower Nevel'sk	21-17	marine mudstone and siltstone, volcanic clasts commo n	mid-grey	50 W/158	stable	R
Okhta River	46.9	142.0	Lower Nevel'sk	21-17	marine mudstone and siltstone, volcanic clasts com r some iron su lphide nodules	mid-grey	50 W/158	remagnetized, CRM	N
Tunaicha Coast	46.9	143.1	Kholmsk	22-18	marine siliceous mudstone	grey	30 W/163	remagnetized	N
Yar/Vladimirovka River	47.1	142.3	Kholmsk	23-15	marine mudstone, siltstone, sandstone, volcanicla s and con glomerate	mid-grey	70 SE/020 to 80 NW/204	stable	R+N
Kholmsk Pass	47.1	142.1	Takaraday, Arakay, Kholmsk	33-23	marine mudstone, siltstone, sandstone, volcanicla s and con glomerate	mid-grey matrix with sand-size dark clast s	28 W/158 to 2 SE/040	stable	N
Il'inskiy Coast	47.9	142.1	Kurasiy	15-9	marine siliceous mudstone, opoka, and porcellani t laminations , carbonate concretions	pink-grey with darker laminations	36 NE/317	remagnetized	N
Lesavaya River	48.6	142.6	Gastellovsk	33-27	marine siltstone	grey	67 E/001	unstable	undefined
Kormovaya River	48.7	142.7	Kurasiy-L. Maruyam	14-6	marine mudstone and muddy sandstone	brown and brown-grey	65 E/355	remagnetized	N
Shakhtnaya River	48.8	142.8	Sertunay-Kurasiy	17-8	marine mudstone	grey and brown-grey	65 E/005	remagnetized	N
Shakhtnaya River	48.8	142.8	Krasnoyarkov Volcanics	84-66	basalt granular sill/dyke intrusive, some tuffaceous clasts	dark grey to black	sub-horizontal	unconstrained*	variable
CENTRAL SAKHALIN									
Onnay River	49.6	142.2	Takaraday, Arakay	30-22	marine siliceous mudstone, siltstone, sandstone, a conglomerate	dark grey to black	40 W/193 to 80 W/193	stable	N
Malaya Orlovka River	49.7	142.7	Nutov	11-2	marine/deltaic siltstone and sandstone, shell beds	light brown-grey	76 NE/330 to 22 SW/114	stable	R
Bolshaya Orlovka River	49.7	142.7	Upper Due	20-17	lagoonal/brackish siltstone, marine sandstone, carb o and coal	light brown-grey	29 S/029	unstable	undefined
Avgustovka River	49.7	142.2	Krasnopol'ev, Gennoyshi	40-22	marine siltstone	dark grey	45 W/184	unstable	undefined
Dvoynoye River	50.1	143.7	Lyukamen	47-41	marine mudstone and sandstone, often clayey	mid blue-grey	15 N/215	stable	R
Aleksandrovsk-Due Coast	50.8	142.1	Krasnoyarkov	84-66	shale, fine sandstone laminae	very dark grey to black	51 SW/026	unstable	undefined
Aleksandrovsk-Due Coast	50.8	142.2	Gennoyshi-Upper Due	27-17	marine mudstone, some diffuse sand laminations	dark grey	50 NE/328	unstable	undefined

Continued on next page

Table B1.1. *Continued*

Aleksandrovsk-Due Coast	50.8	142.2	Khoyndzho Volcanics	22-20	dolerite dykes and sills intruded into the Gennoys countr y rock , tuffs , and volcaniclastic sandstone	dark grey	50 NE/328	unconstrained*	variable
Chamgu River	50.9	143.5	Lower Borsk	24-20	marine siliceous mudtone	dark grey	48 W/175	stable	R
Chamgu River	50.9	143.5	Khuzin	13-8	marine siliceeous sandy mudstone, diatomite	light grey	10 NE/348	remagnetized	N
Kongi River	51.1	143.4	Upper Borsk	11-5	marine siltstone	dark grey	48 W/175	stable	R
North Aleksandrovsk	51.2	142.2	Sertunay, Okobykay	17-11	marine deltaic sandstone, sandy mudstone and siltstone	brown-grey	22 SW/158	unconstrained*	variable
NORTH SAKHALIN									
North Piltun	52.8	143.1	Lower Nutov	11-5	marine deltaic sandstone and mudstone	brown-grey	34 SE/030	remagnetized	N
North Piltun Mud Dyke	52.8	143.1	Lower Nutov	11-5	locally-sourced mud dyke intruding Nutov sandstone	brown-grey	34 SE/030	remagnetized	N
Sabo-Nogliki Quarry	53.1	143.0	Lower Nutov	11-5	marine deltaic sandstone, mudstone lenses	brown-grey	36 E/009	remagnetized	N
SE Schmidt Peninusula	54.0	142.9	Pil'sk	16-12	marine sandstone, siliceous mudstone (opoka and porcellanite), intruded sand d ykes and sills	pale yellow-grey	36 NE/322	unstable	undefined
NE Schmidt Peninusula	54.2	142.2	Tonin	74-68	marine mudstone, fine silt/mud laminations	grey-dark grey	41 E/350	unstable	undefined

*Samples were both stable and unstable. Stable data could not be used to determine a statistically meaningful mean paleomagnetic direction.

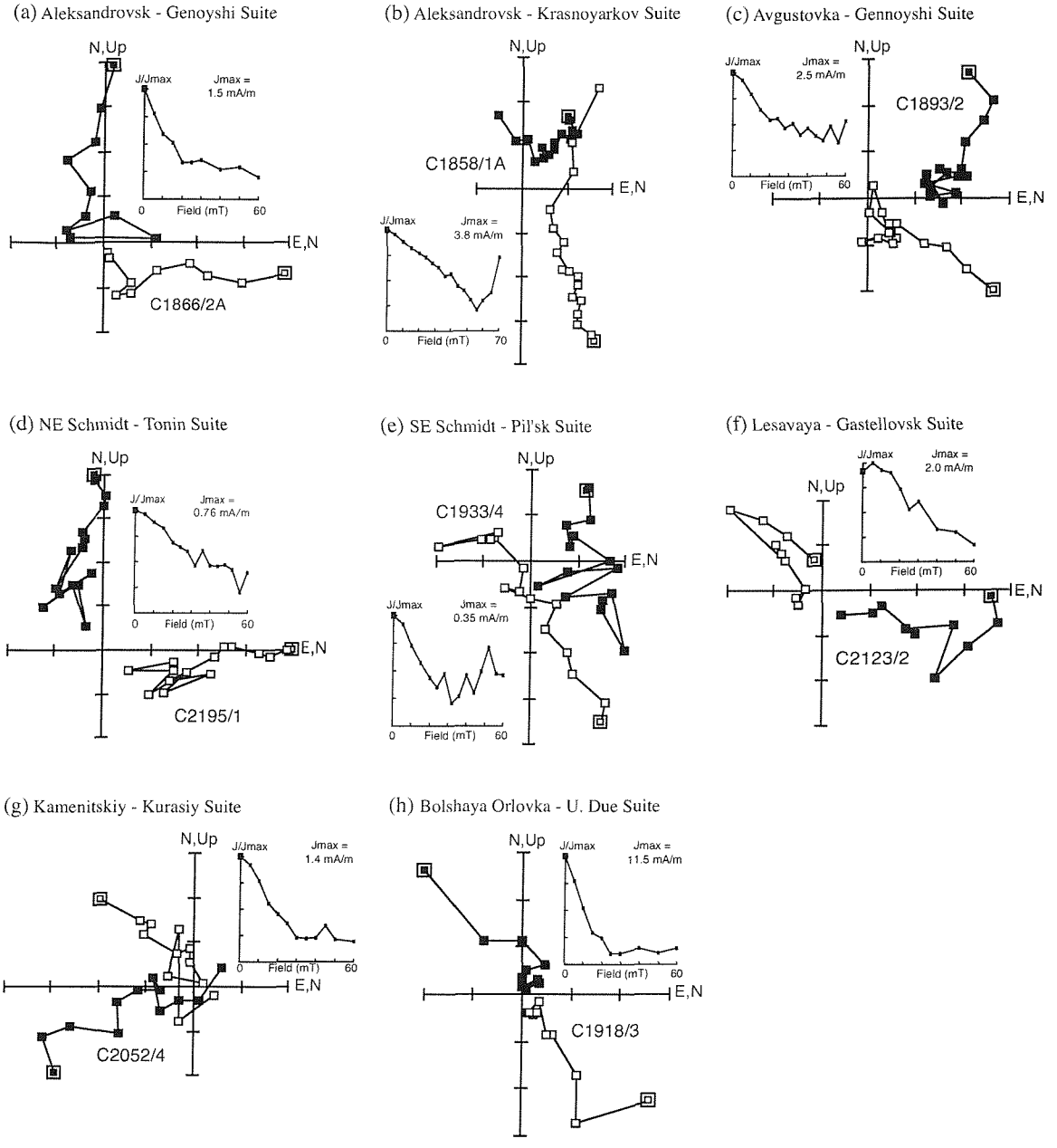

Figure B1.1. Vector component plots for samples displaying unstable paleomagnetic behaviour from different localities in Sakhalin.

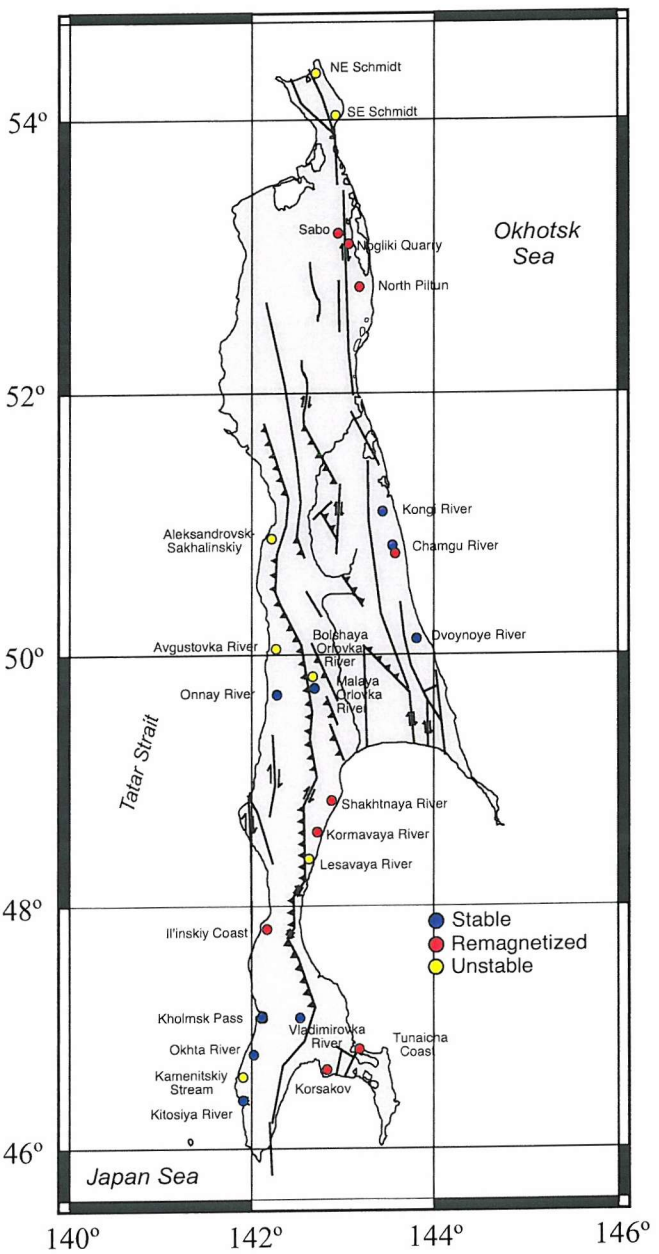

Figure B1.2. Paleomagnetic sampling localities in Sakhalin. Different localities are colour coded according to whether the samples were paleomagnetically stable, unstable, or remagnetized.